Universidade de Aveiro Departamento de Física
2016

Carina de Lurdes Bastos Lopes

# Avaliação de Risco de Inundação na Ria de Aveiro em Cenários Atuais e Futuros

# Flood Risk Assessment in Ria de Aveiro Under Present and Future Scenarios

**Universidade de Aveiro** Departamento de Física
2016

**Universidade do Porto** Faculdade de Ciências

**Universidade do Minho** Departamento de Física

Carina de Lurdes Bastos Lopes

# Avaliação de Risco de Inundação na Ria de Aveiro em Cenários Atuais e Futuros

# Flood Risk Assessment in Ria de Aveiro Under Present and Future Scenarios

Dissertação apresentada à Universidade de Aveiro para cumprimento dos requisitos necessários à obtenção do grau de Doutor em Física, realizada sob a orientação científica do Doutor João Miguel Sequeira Silva Dias, Professor do Departamento de Física da Universidade de Aveiro, do Doutor Paulo Manuel Cruz Alves da Silva, Professor do Departamento de Física da Universidade de Aveiro e da Doutora Maria de Fátima Lopes Alves, Professora do Departamento de Ambiente e Ordenamento da Universidade de Aveiro

A autora foi financiada pela Fundação para a Ciência e Tecnologia (FCT), através da bolsa de Doutoramento com a referência SFRH/BD/78345/2011, no âmbito do Quadro de Referência Estratégico Nacional (QREN) e do Programa Operacional de Potencial Humano (POPH), comparticipado pelo Fundo Europeu e por fundos nacionais do Ministério da Educação e Ciência (MEC). Este trabalho foi desenvolvido no âmbito do projeto ADAPTARia: Modelação das Alterações Climáticas no Litoral da Ria de Aveiro - Estratégias de Adaptação para Cheias Costeiras e Fluviais (PTDC/MAR/107939/2008) com o apoio financeiro da Fundação para a Ciência e Tecnologia - FCT.

**o júri**

presidente

**Doutor José Carlos da Silva Neves**
Professor Catedrático do Departamento de Eletrónica, Telecomunicações e Informática da Universidade de Aveiro

vogais

**Doutor Alexandre Manuel de Oliveira Soares Tavares**
Professor Auxiliar com Agregação da Faculdade de Ciências e Tecnologia da Universidade de Coimbra

**Doutor André Bustorff Fortunato**
Investigador Principal com Habilitação do Laboratório Nacional de Engenharia Civil

**Doutor José Luís da Silva Pinho**
Professor Auxiliar do Departamento de Engenharia Civil da Universidade do Minho

**Doutor José Fortes do Nascimento Lopes**
Professor Auxiliar do Departamento de Física da Universidade de Aveiro

**Doutor João Miguel Sequeira Silva Dias**
Professor Auxiliar com Agregação do Departamento de Física da Universidade de Aveiro

**Acknowledgements**

This dissertation could not have been completed without the great support that I have received from so many people along its realization.

Firstly, I would like to express my sincere gratitude to my supervisors. The continuous support, patience and encouragement of Prof. João Miguel Dias were absolutely determinant during this journey. Also, the support and suggestions of Prof. Paulo Silva and Prof. Fátima Alves were fundamental to the success of this multidisciplinary study.

Besides my supervisors, I would like to thank to André Fortunato for his support on the numerical models implementation and application. He was always available to clarify my doubts.

I would like to thank Luís Bandeira from Polis Litoral Ria de Aveiro for sharing information related with the Polis activities and works. Also thank Magalhães Crespo from DRAP Centro for sharing his knowledge and to provide access to relevant documentation related with Baixo Vouga Lagunar region.

I want acknowledge Administração do Porto de Aveiro and Sociedade Polis Ria de Aveiro for the topographic, bathymetric and hydrographic data used in this study. Also thank the ADAPTARia and LAGOONS project teams for the wave and discharge data. I would also thank Ines Alvarez from the University of Vigo to provide the wave data of Puertos del Estado.

I thank my laboratory colleagues, members and former members of NMEC (Estuarine and Coastal Modelling Division), for their availability and for all the fun we have had in the last years. In particular, I am grateful to Sandra Plecha for the explanations and technical support during the MORSYS2D implementation. Also, a special thanks to Magda Sousa and Ana Picado for the constructive suggestions, and also for their patience and encouragement during difficult moments.

Finally, I would like to thank my friends and my family, specially my parents for all the support and love. I thank also my daughter and Luís for their patience, understanding and encouragement. All of them contributed to my mental well-being, which was crucial during this journey.

**palavras-chave** inundação, Ria de Aveiro, modelação numérica, alterações climáticas, perigosidade de inundação, risco de inundação, medidas de adaptação

**Resumo**

As inundações são uma das maiores ameaças às regiões costeiras, afetando milhões de pessoas, atividades socioeconómicas e ecossistemas. As lagunas costeiras, como a Ria de Aveiro, são sistemas de baixo relevo marginal, particularmente ameaçados por inundações, que enfrentam permanentes mudanças motivadas por fatores naturais e antropogénicos. Consequentemente, o presente estudo tem como objetivo principal avaliar o risco de inundação para eventos de origem oceânica, fluvial e combinada na Ria de Aveiro em cenários presentes e futuros. É também objetivo deste trabalho propor e avaliar a eficiência de medidas estruturais na mitigação do risco de inundação. Para alcançar estes objetivos foi aplicada a metodologia Fonte - Percurso - Recetor, uma abordagem multidisciplinar que compreendeu a realização dos seguintes passos: 1) caracterização dos agentes forçadores de cheias (oceânicos e fluviais) através de análises estatísticas; 2) implementação, calibração e aplicação de modelos hidro/morfodinâmicos para identificação do percurso e extensão de inundação; 3) avaliação dos danos causados pelas inundações, através da identificação dos elementos socioeconómicos e ecológicos expostos ao perigo de inundação e do cálculo do risco combinando a probabilidade com os efeitos adversos das inundações nos elementos expostos. Adicionalmente avaliou-se a eficiência de barreiras de inundação e de alterações na geometria da área central da laguna na mitigação do risco de inundação. Os resultados evidenciam que as inundações de origem oceânica são consequência de elevações significativas no nível do mar induzidas por sobre-elevações de origem meteorológica (>0.4 m) e níveis de maré elevados (>3.3 m), os quais aumentaram na Ria de Aveiro nas últimas décadas em resposta ao aprofundamento generalizado da laguna motivado por dragagens nos canais principais. Estas alterações morfológicas aumentaram o prisma de maré, as correntes de maré e a extensão de inundação, aumentando a ameaça de inundações de origem oceânica. Estas ameaçam aglomerados populacionais e atividades económicas (principalmente agricultura, indústria e comércio) localizadas ao longo das margens dos canais principais e ainda habitats localizados na área central da laguna. As inundações de origem fluvial ocorrem em condições atmosféricas adversas e ameaçam as regiões adjacentes à foz dos rios, causando danos em pequenos aglomerados populacionais e atividades económicas (quase exclusivamente agricultura). Além das regiões de influência oceânica e fluvial, os eventos de origem combinada afetam particularmente as áreas adjacentes às zonas de transição, uma vez que aí a drenagem é dificultada pela sobre-elevação do nível do mar. Apesar das incertezas relacionadas com a infuência de atividades antropogénicas na geomorfologia da laguna, prevê-se uma intensificação/redução do risco de inundação de origem oceânica/fluvial em cenários futuros, como consequência do aumento do nível do mar/diminuição das descargas fluviais previstas para a região. Finalmente, este trabalho demonstrou o potencial da modelação hidrodinâmica para simular a eficiência de medidas estruturais na mitigação do risco de inundação, e consequentemente no suporte ao processo de tomada de decisão subjacente à gestão do risco de inundação.

**keywords** inundation, Ria de Aveiro, numerical modelling, climate changes, flood hazard, flood risk, adaptation measures

**Abstract**

Floods are a major threat to coastal regions, affecting millions of people, socio-economic activities and natural ecosystems. Ria de Aveiro is a coastal lagoon, particularly threatened by floods, facing permanent changes motivated by both natural and anthropogenic factors. Consequently, the main aim of this study is to assess flood risk for floods of oceanic, fluvial and combined origin in Ria de Aveiro under present and future scenarios. This study also aims to propose and evaluate the effectiveness of structural measures on flood risk mitigation. These goals were achieved by applying the methodology Source - Pathway - Receptor, which is a multidisciplinary approach that comprised the following steps: 1) characterization of flooding drivers (oceanic and fluvial) through statistical analysis; 2) implementation, calibration and application of hydro/morphodynamic models to identify the flooding pathway and the flood extent; 3) assessment of flood damage by identifying the socio-economic and ecological assets exposed to flood hazard and determining flood risk by combining the probability and the adverse effects of flood events on assets. In addition, the effectiveness of flood barriers and changes in the lagoon central area geometry on flood risk mitigation was assessed. Results highlight that oceanic floods are consequence of significant sea levels induced by storm surge events (>0.4 m) and high tidal levels (>3.3 m), which increased in the last decades due to the general lagoon deepening motivated by dredging activities. These morphological changes increased the tidal prism, the tidal currents and the flood extent, increasing the threat to floods of oceanic origin. These endanger settlements and economic activities (mainly, agriculture, industry and commerce) located along the lagoon main channels margins as well as habitats in the lagoon central area. Floods of fluvial origin occur during adverse weather conditions, and endanger the rivers mouth adjacent regions causing damage in restricted settlements, economic activities (almost only agriculture) and farmland habitats. Besides the areas dominated by oceanic and fluvial forcing, the events of combined origin also affect the margins adjacent to the transition zones, once the flood water drainage is hindered by high sea levels. Although the uncertainties associated to the influence of anthropogenic actions on the lagoon geomorphology, it is predicted an/a increase/decrease of flood risk for events of oceanic/fluvial origin under future scenarios, as consequence of mean sea level rise/river discharges reduction predicted for the region. Finally, this work demonstrated the potential of hydrodynamic modelling for simulate the effectiveness of structural measures on flood risk mitigation, and consequently in supporting the decision making process underlying the flood risk management.

# Publications and communications in the context of this dissertation

Several publications in peer reviewed journals and presentations at international and national conferences resulted from the research developed in this thesis. The publications were used as basis for several chapters of this thesis (marked in bold in the list bellow).

**Papers in international journals indexed in Web of Science:**

- Lopes C.L., Azevedo A., Dias J.M (2013) Flooding assessment under sea level rise scenarios: Ria de Aveiro case study. *Journal of Coastal Research.* SI65, 766-771. (**Chapters 4, 7**)

- Lopes C.L, Plecha S., Silva P.A., Dias J.M. (2013) Influence of morphological changes in a lagoon flooding extension: case study of Ria de Aveiro (Portugal). *Journal of Coastal Research.* SI65, 1158-1163. (**Chapter 6**)

- Picado A. , Lopes C.L, Mendes R., Vaz N., Dias J.M. (2013) Storm surge impact in the hydrodynamics of a tidal lagoon: the case of Ria de Aveiro. *Journal of Coastal Research.* SI65, 796-801. (**Chapter 3**)

- Lopes C.L., Dias J.M. (2014) Influence of mean sea level rise on tidal dynamics of the Ria de Aveiro lagoon, Portugal. *Journal of Coastal Research.* SI70, 574-579. (**Chapters 4, 5**)

- Lopes C.L., Dias J.M. (2015) Assessment of flood hazard during extreme sea levels in a tidally dominated lagoon. *Natural Hazards*.77(2), 1345-1364. (**Chapters 3, 4, 7**)

- Lopes C.L., Dias J.M. (2015) Tidal dynamics in a changing lagoon: Flooding or not flooding the marginal regions. *Estuarine, Coastal and Shelf Science*. 167, Part A, 14-24. (**Chapters 4, 5**)

**Book Chapters:**

- Plecha S., Lopes C., Bruneau N., Ribeiro N., Silva P.A., Fortunato A., Dias J.M. (2012) Influence of the Wave Regime in Coastal Sediment Budget: Present and Future Scenarios. In: Lynett, P., Smith, J.M. (EDS.), 33$^{rd}$ Conference on Coastal Engineering 2012. 978-0-9896611-1-9.

- Dias, J.M., Lopes, C.L., Silva, P.A., Fortunato, A.B. (2013) Previsão de Inundação Marginal Lagunar. In: Dias, J.M., Alves, F.L. (EDS.), Risco de Cheia e Estratégias de Adaptação para a Zona Costeira e Lagunar da Ria de Aveiro. 17-21. 978-989-8481-24-5.

- Dias, J.M., Rocha, A. Fortunato, A.B., Lopes, C.L., Rodrigues, T., Ribeiro, N.A. (2013) Características dos Agentes Forçadores de Cheias. In: Dias, J.M., Alves, F.L. (EDS.), Risco de Cheia e Estratégias de Adaptação para a Zona Costeira e Lagunar da Ria de Aveiro. 11-16. 978-989-8481-24-5.

**Other publications:**

- Lopes C.L., Alvarez, I., Dias J.M. (2014) Ria de Aveiro marginal flooding: dependence on oceanic and fluvial drivers and on morphological evolution. *Revista Avances en Ciencias de la Tierra (ACT)*, 5, 23-31.

**Conference abstracts, proceedings and communications:**

- Plecha, S., Lopes, C.L., Bruneau, N., Ribeiro, N.A., Silva, P.A., Fortunato, A.B., Dias, J.M. (2012) Influence of the wave regime in coastal sediment budget: Present and future scenarios. *33rd International Conference on Coastal Engineering 2012 (ICCE 2012)*, 01-06/07/2012, Santander, Spain.

- Lopes C.L, Plecha S., Silva P.A., Dias J.M. (2013) Influence of morphological changes in a lagoon flooding extension: case study of Ria de Aveiro (Portugal). *12th International Coastal Symposium (ICS 2013)*, 08-12/04/2013, Plymouth, UK.

- Lopes C.L., Azevedo A., Dias J.M. (2013) Flooding assessment under sea level rise scenarios: Ria de Aveiro case study. *12th International Coastal Symposium (ICS 2013)*, 08-12/04/2013, Plymouth, UK.

- Picado A. , Lopes C.L, Mendes R., Vaz N., Dias J.M. (2013) Storm surge impact in the hydrodynamics of a tidal lagoon: the case of Ria de Aveiro. *12th International Coastal Symposium (ICS 2013)*, 08-12/04/2013, Plymouth, UK.

- Lopes C.L., Plecha, S., Silva, P.A., Azevedo, A., Dias J.M. (2013) Implicações de variações morfológicas e de subida do nível médio do mar na extensão de cheia da Ria de Aveiro. *2ª Conferência sobre Morfodinâmica Estuarina e Costeira (MEC 2013)*, 09-10/05/2013, Aveiro, Portugal.

- Lopes C.L., Dias J.M. (2014) Influence of mean sea level rise on tidal dynamics of the Ria de Aveiro lagoon, Portugal. *13th International Coastal Symposium (ICS 2014)*, 13-18/04/2014, Durban, South Africa.

- Lopes C.L., Silva, P.A., Dias J.M. (2014) Inundação marginal da Ria de Aveiro: dependência dos forçamentos marinhos e fluviais e da evolução morfológica. *Encontro de Oceanografia (APOCEAN)*, 21-22/03/2014, Nazaré, Portugal.

- Lopes C.L., Dias J.M. (2014) Tidal dynamics in a changing lagoon: Flooding or not flooding the marginal regions. *ECSA 54 - Coastal Systems Under Change: Tuning Assessment and Management Tools*, 12-16/05/2014, Sesimbra, Portugal.

- Lopes C.L., Alves, F.L., Dias J.M. (2015) Avaliação do risco de inundações de origem oceânica na Ria de Aveiro. *VIII Congresso sobre Planeamento e Gestão das Zonas Costeiras dos Países de Expressão Portuguesa* , 14-16/10/2015, Aveiro, Portugal.

# Contents

# List of figures

# List of tables

# List of symbols

| | |
|---|---|
| $A_{M_4}$ | Amplitude of $M_4$ constituent |
| $A_{M_2}$ | Amplitude of $M_2$ constituent |
| $A_r$ | Amplitude ratio |
| $b$ | Velocity power |
| $C$ | Wave phase velocity |
| $C_f$ | Potential adverse consequences of flood events |
| $CC$ | Correlation coefficient |
| $C_D$ | Drag coefficient |
| $C_g$ | Wave group velocity |
| $C_u$ | Courant number |
| $c_{Hs}$ | Correlation coefficient of significant wave height |
| $c_T$ | Correlation coefficient of wave period |
| $c_\theta$ | Correlation coefficient of wave direction |
| $c_x, c_y$ | Wave propagation speed in eastward and northward directions |
| $c_\theta$, $c_{sigma}$ | Wave propagation speed in spectral space |
| $D$ | Flood depth |
| $D_f$ | Flood damage |
| $D_r$ | Relative flood damage |
| $d$ | Deviation between each year and the perfect adjustment |
| $d_{50}$ | Sediment grain size |
| $E$ | Wave energy |
| $ECC$ | Eccentricity of $M_2$ tidal ellipses |

| | |
|---|---|
| $E_f$ | Exposure to floods |
| $f$ | Coriolis parameter |
| $g$ | Gravity |
| $H$ | Total water depth |
| $\overline{H}$ | Annual average hazard |
| $H_s$ | Significant wave height |
| $h$ | Depth |
| $IR$ | Tidal prism increase ratio |
| $N$ | Wave action density |
| $NSD_o$ | Normalized standard deviation observed |
| $NSD_p$ | Normalized standard deviation predicted |
| $n$ | Manning coefficient |
| $P$ | Probability |
| $P(A_i)$ | Probability of an astronomic level |
| $P(R_i)$ | Probability of a residual level |
| $P(A_i \cap R_i)$ | Probability of a residual level occur simultaneously with a astronomic level |
| $Q$ | Sediment flux |
| $Q^*$ | Tide averaged transport |
| $Q_*^i$ | Sediment flux integrated over a time step |
| $R$ | Flood risk |
| $\overline{R}$ | Annual average risk |
| $RMSD$ | Root mean square difference |
| $RMSE$ | Root mean square error |
| $S$ | Wave energy source term |
| $SEMA$ | Semi-major axis of $M_2$ tidal ellipses |
| $S_f$ | Susceptibility to be damaged |
| $Skill$ | Skill score |

| | |
|---|---|
| $S_{xx}$, $S_{yx}$, $S_{yy}$, $S_{xy}$ | Wave radiation stresses |
| $T$ | Wave period |
| $TP$ | Tidal prism |
| $t$ | Time |
| $U$ | Depth averaged velocity in the eastward direction |
| $u$ | Magnitude of velocity |
| $V$ | Depth averaged velocity in the northward direction |
| $V_f$ | Value of assets |
| $x$ | Eastward direction |
| $y$ | Northward direction |
| $\alpha$ | Wave angle to the $x$ axis |
| $\Delta Error$ | Percentage of $RMSE$ relative to the mean local amplitude |
| $\Delta H^i$ | Bottom variation over a time step |
| $\epsilon$ | Horizontal eddy viscosity |
| $\eta$ | Surface water elevation |
| $\eta_o$ | Observed sea surface elevation |
| $\eta_p$ | Predicted sea surface elevation |
| $\theta$ | Wave direction |
| $\theta_{M_4}$ | Phase of $M_4$ constituent |
| $\theta_{M_2}$ | Phase of $M_2$ constituent |
| $\lambda$ | Sediment porosity |
| $\nu$ | Artificial diffusion |
| $\rho$ | Water density |
| $\sigma$ | Wave frequency |
| $\tau_{Sx}$ | Surface stress in eastward direction |
| $\tau_{Sy}$ | Surface stress in northward direction |
| $\tau_x$ | Bottom stress in eastward direction |
| $\tau_y$ | Bottom stress in northward direction |
| $\varphi$ | Relative phase |

# List of acronyms

| | |
|---|---|
| **ACW** | Anticlockwise |
| **AOGCM** | Atmosphere Ocean General Circulation Model |
| **APA** | Aveiro Harbour Administration |
| **AW** | Ackers and White |
| **BGRI** | Geographic Base for the Referencing of Information |
| **BVL** | Baixo Vouga Lagunar |
| **CDF** | Cumulative Distribution Function |
| **CLC** | Corine Land Cover |
| **CMIP5** | Coupled Model Intercomparison Project Phase 5 |
| **CIRA** | Aveiro Region Intermunicipal Community |
| **CW** | Clockwise |
| **DGT** | Directorate General for Territory |
| **DEFRA** | Department for Environment Food and Rural Affairs |
| **ESL** | Extreme Sea Level |
| **EXCIMAP** | European Exchange Circle on Flood Mapping |
| **FEMA** | Federal Emergency Management Agency |
| **GEV** | Generalized Extreme Value |
| **GIS** | Geographic Information Systems |
| **GPD** | Generalized Pareto Distribution |
| **GVA** | Gross Value Added |
| **ICDC** | Integrated Climate Data Center |
| **ICNF** | Institute for the Conservation of Nature and Forest |

| | |
|---|---|
| **IH** | Hydrographic Institute |
| **INE** | Statistics Portugal |
| **IPCC** | Intergovernmental Panel on Climate Change |
| **MCA** | Multi-Criteria Analysis |
| **MHWS** | Mean High Water Springs |
| **MSLR** | Mean Sea Level Rise |
| **NUTS** | Nomenclature of Units for Territorial Statistics |
| **NR** | Natural Reserve |
| **O2FM** | Oceanic forcing for 2 years return period combined with mean fluvial discharges |
| **O10FM** | Oceanic forcing for 10 years return period combined with mean fluvial discharges |
| **O25FM** | Oceanic forcing for 25 years return period combined with mean fluvial discharges |
| **O50FM** | Oceanic forcing for 50 years return period combined with mean fluvial discharges |
| **O100FM** | Oceanic forcing for 100 years return period combined with mean fluvial discharges |
| **OMF2** | Oceanic forcing for mean tide combined with fluvial discharges for 2 years return period |
| **OMF10** | Oceanic forcing for mean tide combined with fluvial discharges for 10 years return period |
| **OMF25** | Oceanic forcing for mean tide combined with fluvial discharges for 25 years return period |
| **OMF50** | Oceanic forcing for mean tide combined with fluvial discharges for 50 years return period |
| **OMF100** | Oceanic forcing for mean tide combined with fluvial discharges for 100 years return period |
| **O2F2** | Oceanic forcing for 2 years return period combined with fluvial discharges for 2 years return period |
| **O10F2** | Oceanic forcing for 10 years return period combined with fluvial discharges for 2 years return period |

| | |
|---|---|
| **O25F2** | Oceanic forcing for 25 years return period combined with fluvial discharges for 2 years return period |
| **O50F2** | Oceanic forcing for 50 years return period combined with fluvial discharges for 2 years return period |
| **O2F10** | Oceanic forcing for 2 years return period combined with fluvial discharges for 10 years return period |
| **O10F10** | Oceanic forcing for 10 years return period combined with fluvial discharges for 10 years return period |
| **O2F25** | Oceanic forcing for 2 years return period combined with fluvial discharges for 25 years return period |
| **O2F50** | Oceanic forcing for 2 years return period combined with fluvial discharges for 50 years return period |
| **Polis** | Polis Litoral Ria de Aveiro |
| **RCP** | Representative Concentration Pathway |
| **RNAP** | National Network of Protected Areas |
| **SCI** | Site of Community Importance |
| **SNAC** | National System of Classified Areas |
| **SPA** | Special Protection Area |
| **SPR** | Source-Pathway-Receptor |
| **SRES** | Special Report on Emissions Scenarios |
| **SSE** | Sea Surface Elevation |
| **ZH** | Chart Datum |

# Chapter 1

# Introduction

## 1.1 Motivation

Floods are one of the most widely distributed of all natural hazards across Europe, threatening millions of people, livelihoods/goods, and ecosystems. As a natural hazard, floods cannot be avoided, but their consequences can be prevented and mitigated. It is known that the anthropogenic action is contributing to increase the adverse impacts of extreme floods, once the number of people and economic assets located in flood hazard zones has increased. Attending these issues, in 2007, the European Union approved the European Directive (2007/60/EC) on the assessment and management of flood risk. This directive intends to reduce and to manage the risks that floods pose to human health, environment, cultural heritage and economic activities. In this way, the directive requires Member States to map the flood extent and flood risk in all water courses and coastlines as well as to establish flood risk management plans focused on the prevention of flood damage, on the protection of endangered areas and on the preparedness in case of flood events.

Low-lying coastal regions are particularly endangered by flood events, presenting high flood risk, once are generally located in these regions strategic urban centres densely populated. Indeed, McGranahan et al. [2007] estimated that 10% of the worlds population lives in low-lying coastal regions (contiguous area along the coast that is less than 10 m above the mean sea level). Also, according the Statistical Office of

the European Communities (Eurostat) 40.8% of the EU-27 population lived in coastal regions in 2011 [Collet and Engelbert, 2013].

Coastal lagoons are an example of low-lying coastal areas threatened by both natural and anthropogenic factors [Nicholls et al., 1999; Jonkman and Vrijling, 2008; FitzGerald et al., 2008]. Besides its socio-economic value, they provide also excellent conditions for biological production, supporting consequently many valuable species and ecosystem services [Alongi, 1998; Perez-Ruzafa et al., 2013]. The flow within a coastal lagoon is determined by the exchanges between the lagoon and the ocean, by the interaction with the atmosphere and by the discharge of its tributaries. Consequently, its dynamics is constantly modified by changes on its drivers and on its geomorphological features induced by both natural and anthropogenic factors [Oliveira et al., 2006; Picado et al., 2010; Zhang et al., 2010; Jewell et al., 2012; Lopes et al., 2013a,b; Gao et al., 2014; Li et al., 2014; Song et al., 2013]. Duck and da Silva [2012] described that the artificialization and regulation of inlets, the construction of port areas and terminals, the dredging operations and the construction of tanks for aquaculture are some common examples of human induced geomorphological changes occurring in several coastal lagoons worldwide, such as Ria de Aveiro, Venice, Vistula, Ria Formosa and Tuzla Lake lagoons.

Besides the increase of anthropogenic pressures in these systems it is expected that the natural drivers will be also modified as result of climate changes [Anthony et al., 2009; Wong et al., 2014]. Indeed, IPCC [2013] found that the predicted increase of greenhouse gases in the atmosphere will change the sea level patterns and the hydrological cycle. The global mean sea level rise (MSLR) motivated by the sea water thermal expansion and glacier melting is a very likely consequence of air temperature increase predicted for the end of 21$^{st}$ century [IPCC, 2013]. With lower confidence IPCC [2013] also forecasts changes in freshwater inputs and in storminess patterns. However, more studies on the assessment of regional and local changes are needed once these factors present high spatial variability [Wong et al., 2014]. According to Nicholls et al. [2011] and Wong et al. [2014], the predicted drivers changes will impact the redistribution of sediments, the partitioning of habitats, the salinity distribution, the tidal range and the submergence periods within estuaries and lagoons. Moreover, in

response to the anticipated increase of natural hazards it is expected a growing number of man made coastal protection structures. Thus, the landward migration may be restricted due to human occupation and intervention [Wong et al., 2014]. Indeed, flood protection structures already exist in several coastal areas. The River Thames barrier gates in UK, various dikes around the Netherlands coastal region and mobile gates in the Venice lagoon inlets are just some examples of coastal protection works.

As summary of future evolution of coastal lagoons, Wong et al. [2014] study highlights that the human and climate related drivers changes will affect the functioning and services of lagoons. However, the impacts can not be evaluated at a global scale once the main drivers act at a local scale, highlighting the importance of local studies.

The Ria de Aveiro is a coastal lagoon with a very complex geometry, located on the northwest Portuguese coast (Figure 1.1). According the Nomenclature of Units for Territorial Statistics (NUTS) the Ria de Aveiro region is part of the Centro (NUTSII) region of Portugal (NUTSI). It is constituted by eight municipalities, seven of them (Ovar, Estarreja, Murtosa, Albergaria-a-Velha, Ílhavo and Vagos) are inserted in the Baixo Vouga region (NUTSIII), while Mira is part of Baixo Mondego region (NUTSIII).

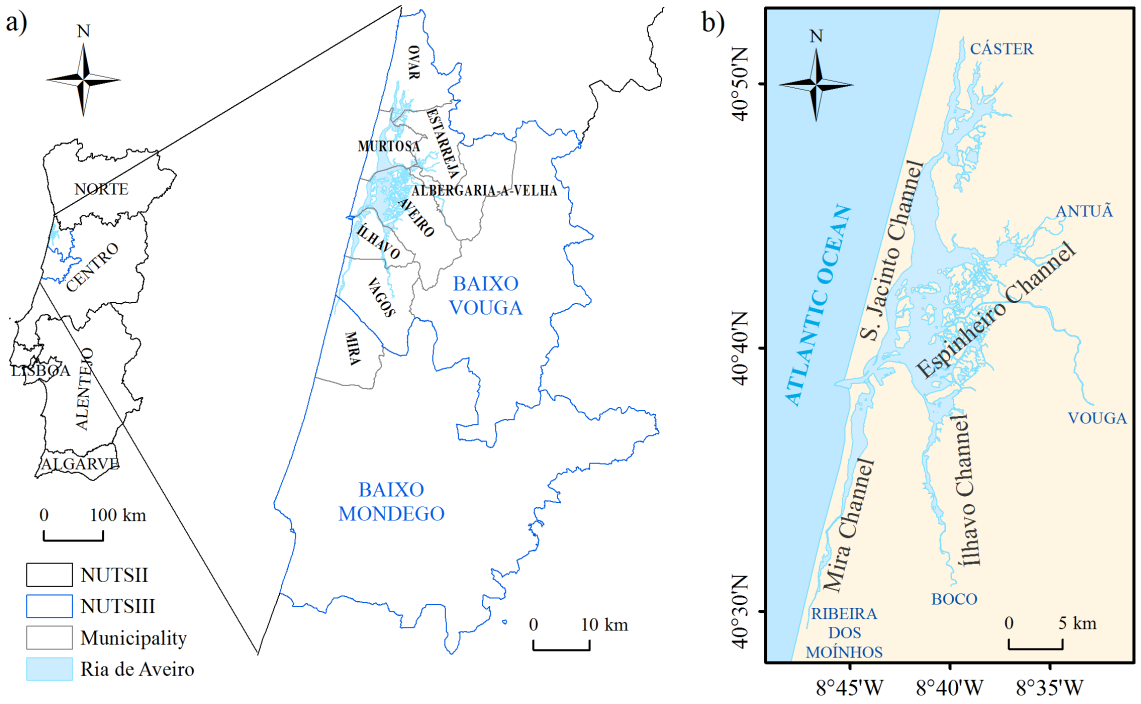


Figure 1.1: a) Ria de Aveiro region showing the territorial units boundaries. b) Ria de Aveiro main channels and tributaries.

The lagoon presents four main channels Mira, S. Jacinto, Ílhavo and Espinheiro and connects with the Atlantic Ocean through a single artificial inlet built in 1808. The lagoon presents five main tributaries. The Vouga river flow is the main source of freshwater to the lagoon (2/3 of the total freshwater) and inflows at the Espinheiro channel [Dias, 2001]. The Boco, Ribeira dos Moinhos, Cáster and Antuã rivers inflow also at the lagoon, but their discharge is significantly lower than Vouga river discharge. Ria de Aveiro is considered a flood prone region given the low altitude and flat topography of its marginal lands. Flood events occur in this region when high sea levels or high river discharges occur. The hugest flood events occur during adverse weather conditions when high river discharges coincide with high sea levels originated by both high tides and storm surge events. The lagoon hydrodynamics is essentially ruled by oceanic forcing and extremely dependent on its morphology [Araújo et al., 2008; Plecha, 2011; Lopes et al., 2011, 2013b]. Particularly, the deepening of the entrance channel and of its four main channels promoted an increase on the oceanic influence, increasing among others the tidal prism and threatening even more the flooding of the marginal regions. Indeed, several regions located at the lagoon margins, among others agricultural fields, are nowadays threatened by the enlargement of the lagoon area induced by larger high tides.

Although its importance, floods in the Ria de Aveiro region were not studied in detail before the beginning of this research in 2010. Therefore this work intends to fill the gap of knowledge related with floods in Ria de Aveiro region. It is important to highlight that it is performed in the frame of the research project ADAPTARia: Climate Change Modelling on Ria de Aveiro Littoral - Adaptation Strategy for Coastal and Fluvial Flooding (`http://climetua.fis.ua.pt/legacy/adaptaria/index.html`), that held between 2010 and 2013. Consequently, by one hand, the present work benefited from the involvement of a multidisciplinary team, which provided critical analyses and also data needed for this research. On the other hand, most of the results of this research reverted to the ADAPTARia project.

## 1.2 Aims

Attending the concerns referred in previous section, the main aim of this work is to assess flood risk for events of oceanic, fluvial and combined origin in Ria de Aveiro region under present and future scenarios. Additionally, this study intends to propose and evaluate the effectiveness of structural measures on flood risk mitigation. Besides this, the present work aims to:

- Investigate the occurrence and the effects of past flood events reported in the media;
- Characterize the Ria de Aveiro driving forces for the present and future climates, by statistically analysing hydrographic and oceanic data;
- Implement, calibrate and validate the hydrodynamic model ELCIRC to study flooding events in the Ria de Aveiro area, to guaranty that it reproduces accurately the flow propagation within the lagoon in these conditions;
- Apply the morphodynamic model MORSYS2D to the inlet region, to study the influence of climate changes on the inlet morphologic evolution;
- Characterize the tidal propagation within the lagoon, considering alterations on both forcing drivers and geomorphological configuration;
- Understand the processes controlling the lagoon morphology and to quantify its effects on the lagoon flood extent evolution;
- Evaluate the dependence of the lagoon flood extent on the magnitude of the oceanic and fluvial driving forces;
- Assess flood hazard for events of oceanic, fluvial and combined origin under present and future climates;
- Identify socio-economic and ecological assets exposed to flood hazard;
- Assess and map flood risk for events of oceanic, fluvial and combined origin under present and future climates;

- Propose and evaluate the effectiveness of structural measures on flood risk mitigation.

To achieve these goals the conceptual model Source−Pathway−Receptor (SPR) proposed by Holdgate [1979] was applied. This conceptual model requires a multidisciplinary approach, that integrates statistical analysis, hydrodynamic and morphodynamic modelling and GIS (Geographic Information Systems) techniques. Synthetically this approach comprises the characterization of: a) flooding drivers, by statistically analysing observed/predicted hydrographic and oceanic data; b) the flow propagation within the floodplain through hydrodynamic/morphodynamic modelling; and c) the negative consequences of floods on assets at risk by spatially intersecting the modelled flood extent with socio-economic and ecological data of the floodplain.

## 1.3 Literature review

### 1.3.1 Flood risk assessment

According to the Floods Directive (2007/60/EC), flood is the temporary covering by water of land normally uncovered. Floods may occur when a water body (e.g. river, estuary, lagoon, etc.) exceeds the total capacity and the water overflows inundating the marginal lands. There are many factors that cause the excess of water within the water bodies, that are often associated to adverse weather conditions. Concerning estuaries and coastal lagoons, flood events occur when sea levels are high (oceanic origin), or when river discharges are high (fluvial origin), or even when high sea levels and high discharges are coincident (combined origin) [Maskell et al., 2014; Yang et al., 2015].

Flood risk is also defined in the Floods Directive (2007/60/EC) as a combination of the probability of a flood event and of the potential adverse consequences for human health, the environment, cultural heritage and economic activity associated with a flood event.

The conceptual model SPR was developed in the scope of environmental pollution analysis where it was used to study the movement of a pollutant from a source, through a pathway to a receptor [Holdgate, 1979]. According to Schanze [2006],

flood risk can be assessed within the conceptual model SPR as a casual chain ranging from the characterization of flood drivers (source) to the delimitation of inundation extent (pathway) and the physical impacts on assets at risk (receptors). In this context, this model was used to assess flood risk, among others, under the scope of the projects FLOODsite (`http://www.floodsite.net/`), XtremRisk (`https://www.tu-braunschweig.de/lwi/hyku/xtremrisk`) and THESEUS (`http://www.theseusproject.eu/`). Within the FLOODsite project, Gouldby and Samuels [2005] defined:

**Source** - as the origin of a hazard (e.g. high river discharges, storm surges, high tides, etc.);

**Pathway** - the route that a hazard takes to reach receptors (e.g. floodplain, estuary, channel, etc.);

**Receptor** - the entity that may be harmed (e.g. population, economic activities, habitats, etc.).

#### 1.3.1.1 Sources of flooding

Given that in coastal lagoon systems floods occur during high sea level and/or high river discharge conditions, there is a great effort by the scientific community to define accurately extreme sea levels and discharges. Generally, its characterization is supported on the statistics of extremes [Büchele et al., 2006; Oumeraci et al., 2015; Thieken et al., 2015; Wahl et al., 2015]. Therefore extreme sea levels and discharges are often determined by adjusting measured sea levels and flows to probability distributions, and then extrapolating them for different return periods. This methodology was applied by Chan [1983] to estimate extreme sea levels, however this author found uncertainties in the results that are attributed to interactions between storm surges and astronomic tides. Considering that extreme sea levels can be assumed as a combination of the mean sea level, storm surge and tides (by ignoring the effect due to oceanic wind generated waves), its estimation is most of the time supported on joint probability analysis (e.g. Hawkes [2008] and Liu et al. [2010]). This approach is recommended on flood analysis among others by the FLOODsite integrated project

(http://www.floodsite.net/), the Department for Environment Food and Rural Affairs of UK (DEFRA) (http://www.defra.gov.uk/) and the Federal Emergency Management Agency of USA (FEMA) (http://www.fema.gov/).

Joint probability methods are also used to determine the probability of simultaneous occurrence of storm surge, tides and discharges extremes [Kew et al., 2013; Xu et al., 2014; Zheng et al., 2014; Klerk et al., 2015]. Indeed, the occurrence of a given inland water level may result from a number of combinations of high sea levels (combination of tides and storm surges) and high fluvial flows. Although complex, its determination is extremely important once the most dangerous flood events occur under these circumstances.

It is very likely that climate changes will change coastal systems flood drivers worldwide [IPCC, 2014]. However, the integration of climate projections of the 4$^{\text{th}}$ and 5$^{\text{th}}$ Intergovernmental Panel on Climate Change (IPCC) reports on local studies is complex. First, the estimations are global and hide the spatial variability of climate variables. Secondly, the estimations are supported on the output of Atmosphere Ocean General Circulation Models (AOGCM) that have a coarse resolution, often inadequate for local studies. These issues are surpassed through spatial downscaling techniques, that can be categorized into dynamical and statistical types [Tabor and Williams, 2010; Schoof et al., 2010]. Statistical downscaling, establishes a statistical relationship between predicted large scale variables and observed local variables at a particular site [Hertig and Jacobeit, 2008; Fasbender and Ouarda, 2010; Schoof et al., 2010]. In dynamical downscaling, the output variables of AOGCM are used to feed regional numerical models with higher spatial resolution, which able to simulate local conditions in greater detail. This method was applied successfully worldwide among others by Castro et al. [2005] and Giorgi et al. [2009]. Particularly Giorgi et al. [2009], through the EURO-CORDEX initiative, provide regional climate projections for Europe within the timeline of the 5$^{\text{th}}$ IPCC report. As the regional climate models can not simulate some flood drivers, such as river flow and waves, the global and/or regional projections are commonly used to feed watershed [Fowler and Kilsby, 2007] and wave models [Andrade et al., 2007; Casas-Prat and Sierra, 2013; Shimura et al., 2015].

#### 1.3.1.2 Pathway of flooding

Ideally, tidal gauge data can be used to quantify the flood extent and depth in estuarine and coastal lagoon systems. However, often the tidal gauge records are scarce and space and time limited disabling a detailed and rigorous flood mapping. Remote sensing techniques are being used to fill the gap of observed flood marks in order to map in detail the flood extent [Ramsey III et al., 2011; Jung et al., 2014; Ticehurst et al., 2014; Pedrozo-Acuña et al., 2015]. Ticehurst et al. [2014] found that remote sensing provides reliable results in medium to large flooding events at basin scales. Moreover, in the scope of this research, were not found studies addressing the flood extent in tidal dominated lagoons through remote sensing techniques.

The limitations of both methods described before are frequently overcome using numerical models [Peng et al., 2004; Rego and Li, 2010; Gallien et al., 2011; Condon and Sheng, 2012; Fortunato et al., 2013; Bertin et al., 2014; Bhaskaran et al., 2014; Yasuda et al., 2014]. The models require observed data to calibrate and/or validate the predicted flood extent, but once calibrated for a given location they provide detailed flood mapping. Moreover, the models are able to simulate flood propagation under both present and future climates, being considered important tools to support coastal management decisions [Plate, 2002; Tsihrintzis et al., 2007; Balica et al., 2013].

There is a huge variety of open source numerical models able to reproduce the flooding pathway within coastal systems. The guidelines present in the Asselman et al. [2009] study, highlight that the numerical model should be appropriate to describe as reliable as possible the geomorphologic patterns and the dominant physical processes of the coastal system under study. Hydrodynamic models have been applied worldwide to study inundation in coastal systems [Peng et al., 2004; Purvis et al., 2008; Sheng et al., 2010; Kuhn et al., 2011]. Hydrodynamic models using unstructured grids are being used to describe the flow within complex morphological lagoons, like Ria de Aveiro [Dias et al., 2009; Rego and Li, 2010; Umgiesser et al., 2014]. Various data inputs are required in order to set-up, calibrate and validate this kind of model. Detailed topographic and bathymetric data is required to describe the system geomorphology. Also, hydrographic data for use as boundary condition and to assess model accuracy is necessary. Hosseinipour et al. [2012] found that the accurate representation of site

conditions (e.g. bathymetry, topography, geometry) is an essential step towards a precise flood extent mapping.

In dynamic sedimentary environments, the use of morphodynamic models is also recommended to account for the morphological changes, that affect water levels and the flood propagation [Asselman et al., 2009]. Moreover, Reeve et al. [2007] highlighted that the knowledge of the influence of coastal systems morphology on flood risk is determinant to implement appropriate management strategies. Although important, the use of these models for inundation purposes is not common, given its complexity and computational cost. Also, they require detailed sediment data, that often are not available.

#### 1.3.1.3 Receptors of flooding

The floods propagate within the floodplain inundating, among others, roads, buildings, habitats and agricultural fields. The identification of assets at risk and the evaluation of the negative consequences of floods on assets is a fundamental step towards flood risk management [Meyer et al., 2009]. The assets at risk are identified, after the determination of flood extent, through GIS based techniques [Büchele et al., 2006; Meyer et al., 2009; Burzel et al., 2015]. The damage induced on assets can be categorised firstly in direct and indirect and secondly in tangible and intangible (Table 1.1) [Meyer and Messner, 2005; Messner and Meyer, 2006; Jonkman et al., 2008; Merz et al., 2010]. According these works, direct damages result from the physical contact of flood water on assets, while indirect damages occur outside the floodplain and are caused by the disruption of physical and economic linkages located within the floodplain. The difference between tangible and intangible damages is that the first can be specified in monetary terms, while the second has no monetary value. Table 1.1 reflects the wide range of floods damage effects on assets, revealing the complexity that evolves flood damage assessment. In order to reduce the complexity of damage evaluation, most of the flood risk assessment studies focus on the assessment of direct damages [Merz et al., 2004; Jonkman et al., 2008; Meyer et al., 2009; de Moel and Aerts, 2011; Scheuer et al., 2011]. Among this, the studies by Merz et al. [2004], Jonkman et al. [2008] and de Moel and Aerts [2011] emphasize only the direct economic damages.

Table 1.1: Categorization of flood damage.

| | Tangible | Intangible |
|---|---|---|
| Direct | • Buildings<br>• Vehicles<br>• Roads<br>• Agricultural and Industrial Units | • Fatalities<br>• Health<br>• Ecological Losses |
| Indirect | • Companies located outside the floodplain | • Societal Disruptions<br>• Psychological Traumas |

Otherwise, Meyer et al. [2009] and Scheuer et al. [2011] assessed spatial flood risk by evaluating risk on socio-economic and environmental assets and then integrating all individual risks through a multi-criteria analysis (MCA). Within MCA approach, the global flood risk is obtained by summing each individual risk, which was previously weighted according its relevance. Meyer et al. [2009] highlighted the importance of MCA on flood risk assessment presenting an alternative to the complex monetary evaluation and internalisation of intangible consequences. Also, this approach can be combined with GIS and provide detailed flood risk mapping.

### 1.3.2 Ria de Aveiro

Ria de Aveiro has been extensively studied during the last 20 years, in a wide variety of scientific areas from physics, chemistry, geology, biology, environment and territorial planning. As this study focus on flood risk assessment the literature research is focused on hydrodynamic and morphodynamic models applications and on flood risk assessment studies. The Ria de Aveiro hydrodynamic processes were studied through several hydrodynamic model applications. The first applications used the structured grid model SIMSYS2D [Dias et al., 2000; Lopes et al., 2001; Dias et al., 2003; Dias and Lopes, 2006]. These works addressed essentially processes related to tidal dynamics. More recently, still using structured grids, the MOHID model was applied by Vaz et al. [2009] to study the stratification within the lagoon.

Oliveira et al. [2006] applied for the first time an unstructured grid model (MORSYS2D) to Ria de Aveiro, which was developed to study the inlet region morphodynamics. This model was applied later by Plecha [2011] to investigate which processes influence the sedimentary dynamics of the inlet region. This author found that the inlet morphodynamic is driven by tides and waves. Also, Lopes et al. [2011] applied this model to investigate the influence of MSLR on the inlet morphodynamics. They found an intensification of sedimentary fluxes and of the sedimentation rates under MSLR conditions.

The unstructured grid developed by Oliveira et al. [2006] was improved by Picado et al. [2010], and used to run the hydrodynamic model ELCIRC. These authors incorporated in the former grid the complex web of small channels located in the lagoon central area and studied in detail the tidal changes induced by the flooding of abandoned salt pans. They found an intensification of the tidal currents, tidal prism and tidal asymmetry associated to the flooded area increase. Vaz [2012] used this implementation coupled with the wave model SWAN to study the influence of waves on the lagoon inlet hydrodynamics. This study found that the inlet currents and sea levels are driven by tidal forcing, and the waves can present only moderate relevance during high wave activity events. The unstructured grid model SELFE was applied recently by Azevedo [2010], Rodrigues [2012], Fortunato et al. [2013] and Tomas et al. [2014]. Azevedo [2010] used the SELFE model within the transport and oil weathering model VOILS to study the evolution of an hypothetical oil spill in the lagoon inlet. Rodrigues [2012] used the SELFE model within the ecological model ECO-SELFE to investigate the water quality and ecological dynamics of Ria de Aveiro lagoon. Fortunato et al. [2013] assessed inundation in Ria de Aveiro region, for different extreme sea levels (obtained from synthetic water levels) and MSLR scenarios. These authors found that the lagoon flooded area and the maximum water levels increase for higher sea levels. Tomas et al. [2014] investigated the uncertainties in the modelling of salinity fields in the Ria de Aveiro lagoon associated with the estimation of river flow discharges. More recently, the Delft3D-Flow and Delft3D-WAQ models were applied to Ria de Aveiro lagoon by Silva et al. [2013] and Hesse et al. [2015] to investigate the physical drivers

controlling the turbidity and the water quality within the lagoon under present and future scenarios, respectively.

Flood risk in the overall Ria de Aveiro region was previously studied under the scope of SECUR-Ria project [Coelho et al., 2007] in order to support municipal safety plans for the Ria de Aveiro region municipalities. A flood risk map was developed based on the inventory and survey of flood marks. Evidences of flood events in the overall marginal area were found, which are exacerbated in the regions adjacent to the mouth of main rivers, where the fluvial drainage is hindered by tidal action.

Later, Lemos [2008] investigated the risk of Aveiro municipality to several natural and anthropogenic hazards, among which inundation. This author identified the parishes most damaged by flooding events, by intersecting the maximum flood extent of SECUR-RIA project, with road network and buildings of the region. This study revealed that all the parishes that include channels of Ria de Aveiro are affected by flooding events. Among these, the parishes located within the Aveiro town present the highest flood risk.

Recently, Dias and Alves [2013] and Dias et al. [2014], assessed flood risk in the Ria de Aveiro region and adjacent coastal area for both present and future climates. These works, performed under the scope of ADAPTARia project, integrate climate scenarios and hydrodynamic modelling applications developed in the present work. Accordingly, several climate scenarios combining sea levels and fluvial discharges were designed and used to feed hydrodynamic simulations. The predicted flood extents were intersected with a vulnerability chart that categorizes 4 classes (residual, low, moderate and high), according the classification of Corine Land Cover (CLC) of 2006 [EEA, 2007]. A flood risk matrix that combines flood probability (low, medium, high) and vulnerability of the territory (residual, low, medium and high) classes was constructed and the flood risk was categorized as residual, low, medium, high and extreme. Following this methodology, it was found that the agricultural fields located in the riverine regions present medium flood risk, while the agricultural fields located in the lagoon marginal areas present high flood risk. Also, the extension of urban flood area tends to increase under climate change conditions, considering the predicted MSLR for the region.

## 1.4 Structure of this work

This dissertation was divided in 10 chapters. Chapter 1 presents the introduction, where the motivations, general objectives, a general literature review and the structure of the work are described. This is followed by Chapter 2, where a characterization of the Ria de Aveiro region is presented, highlighting hydrodynamic, geomorphological, socio-economic and environmental aspects and the historical background of flooding events. In Chapter 3 the sources of flooding events are investigated by characterizing the Ria de Aveiro driving forces under present and future climate conditions. The results obtained in this chapter provides the necessary information to characterize the flood propagation through hydrodynamic and morphodynamic modelling (Chapters 4 to 9). In Chapter 4 the hydrodynamic model ELCIRC and the morphodynamic model MORSYS2D are described. Also, in this Chapter, the ability of ELCIRC model to reproduce the tidal and storm surge propagation is investigated. In Chapter 5 the hydrodynamic model ELCIRC is used to study tidal propagation within Ria de Aveiro. The tidal modifications between 1987 and 2012 motivated by the main channels deepening are described, as well as tidal modifications expected for the future as consequence of MSLR and consequent construction of flood protection barriers in threatened regions. Chapter 6 investigates the dependence of the lagoon flooding patterns on the morphology. Firstly, the hydrodynamic model ELCIRC is applied to find changes in the lagoon flooding patterns motivated by past geomorphological changes. Secondly, the morphodynamic model MORSYS2D is applied to the inlet region in order to investigate if climate changes will change the inlet morphodynamics. In Chapter 7, the ELCIRC model is used to study the sensitivity of the lagoon flooded area and extent to flooding drivers changes. Chapter 8 focus on Ria de Averio region flood hazard and flood risk assessments for events of oceanic, fluvial and combined origin, under both present and future climates. In this context, the model ELCIRC was applied for several scenarios combining sea levels and river discharges. Numerical results are used to construct flood depth, probability and hazard maps. Moreover, the socio-economic and ecological receptors are identified and flood risk is assessed following the European Floods Directive. Chapter 9 proposes and investigates some structural

measures on flood risk reduction. The effectiveness of these measures is investigated by comparing the risk before and after its implementation. Finally, Chapter 10 presents the main conclusions of this dissertation and suggestions for further work.

# Chapter 2

# Characterization of Ria de Aveiro

## 2.1 Hydrodynamics and morphological aspects

The Ria de Aveiro is a shallow coastal lagoon that presents a very complex geometry (Figure 2.1). Besides the four main channels (Mira, S. Jacinto, Ílhavo and Espinheiro), the lagoon presents a complex web of shallow and narrow channels and is characterized by large areas of mud flats and salt marshes. It is 45 km long and 10 km wide and currently covers an area of 89.2 $km^2$ at spring tide which is reduced to 64.9 $km^2$ at neap tide [Lopes et al., 2013a]. The Vouga River's mean flow is 80 $m^3/s$ [Génio et al., 2008] and represents the main source of freshwater to the lagoon (2/3 of the total freshwater) and inflows into the Espinheiro channel [Dias, 2001]. The Boco, Ribeira dos Moínhos, Cáster and Antuã Rivers also drain into the lagoon, but their mean discharges (5 $m^3/s$, 10 $m^3/s$, 5 $m^3/s$ and 20 $m^3/s$ [Génio et al., 2008], respectively) are significantly lower than that from Vouga River. The total mean river discharge of $1.8\times10^6$ $m^3$ during a tidal cycle [Moreira et al., 1993] is considerably lower than the tidal prism at the lagoon mouth. Lopes et al. [2013b], using the most recent bathymetry, determined tidal prisms of $65.8\times10^6$ $m^3$ and $139.7\times10^6$ $m^3$, for neap and spring tides, respectively.

The lagoon hydrodynamics is dominated by the tide, which is semi-diurnal with a small diurnal pattern [Dias, 2001]. The lagoon is ebb dominant at the mouth and flood dominant at the upper parts [Dias, 2001; Oliveira et al., 2006; Picado et al., 2010]. In this way, the lagoon presents a tendency to export sediments to the ocean [Oliveira et al., 2006]. The lagoon can be considered as vertically homogeneous, except

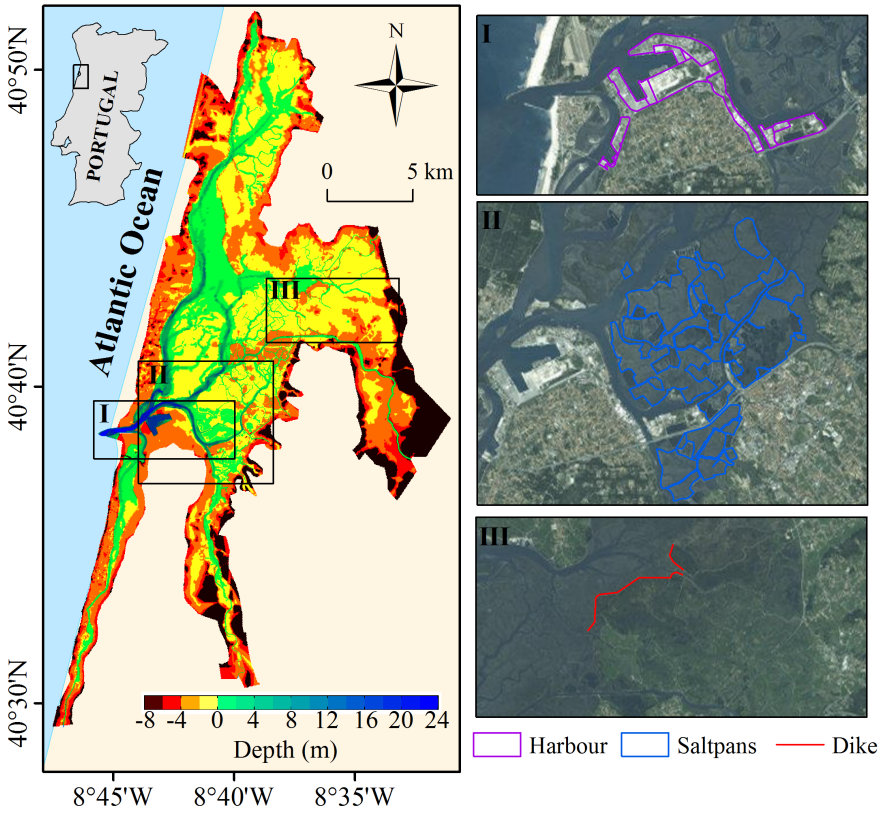


Figure 2.1: Location, topography and bathymetry of Ria de Aveiro region. Detail of: I) Aveiro harbour area; II) Saltpans existent in the central area; III) Baixo Vouga Lagunar (BVL) dike.

occasionally when freshwater inflows are high, and the upper parts of the lagoon can present vertical stratification [Dias et al., 2000; Vaz et al., 2009]. The influence of wind stress on lagoon water levels is small when compared with tidal action [Dias, 2001]. Recently, Fortunato et al. [2013], assessed analytically and numerically the effect of wind stress on the lagoon water levels during storm surge events. Under these circumstances, those authors found that winds induce water over elevations typically lower than 0.05 m, which is considerably lower than the tidal elevations. The waves play also a minor role on the lagoon hydrodynamics when compared with the tides [Vaz, 2012]. Vaz [2012] found that only the waves with significant height higher than 4 m may induce sea surface over elevations of approximately 0.2 m at the inlet, which is considerably lower than tidal elevations.

The human action affected directly the natural geomorphological evolution of the lagoon and these remain still evident on the actual geomorphological behaviour. The most remarkable work was the construction of a fixed inlet in 1808 (Figure 2.1 I)

that deeply changed the hydrodynamics of the system, resulting in changing the flow circulation from river dominated to tidal dominated [da Silva and Duck, 2001]. After the opening of the permanent connection with the ocean (1808) numerous saltpans were constructed (Figure 2.1 II) over the intertidal flats in the lagoon central area for salt production [da Silva and Duck, 2001].

Over the last 30 years the lagoon suffered other man induced geomorphological changes, namely extensions on the inlet breakwaters in 1987 and 2012, regular dredging activities in the inlet channel and in the lagoon main channels and the natural destruction of saltpans walls motivated by the abandonment of its exploitation [Plecha, 2011; Lopes et al., 2013b].

The bathymetric changes between 1987 and 2012 were quantified in the scope of this research by analysing the bathymetric data recorded within this period. Data collected in four surveys (Table 2.1) were made available by the Portuguese Hydrographic Institute (IH), Aveiro Harbour Administration (APA) and Polis Litoral Ria de Aveiro (Polis). To perform a comparative analysis between bathymetric changes of consecutive surveys, the collected data was interpolated using the ACE/gredit tool (Oregon Health and Science University), to a triangular grid developed in the frame of this work, which features will be described in Chapter 4. The depth difference between bathymetric data collected in 1987, 2001, 2011 and 2012 was computed (Figure 2.2).

In general the lagoon experienced mostly a deepening of its main channels over the time, keeping its geometry unchanged. The inlet channel depth increased after the extension of northern breakwater in 1987, as depicted in the Figure 2.2a. Between 1987 and 2001 the deepening of the inlet channel achieved 10 m in some areas. Figure

Table 2.1: Details of bathymetric surveys.

| Survey | Entity | Extension |
|---|---|---|
| 1987 | IH | Overall lagoon area |
| 2001 | APA | Channels adjacent the Aveiro harbour |
| 2011 | Polis | Channels adjacent the Aveiro harbour and four main channels |
| 2012 | APA | Channels adjacent the Aveiro harbour |

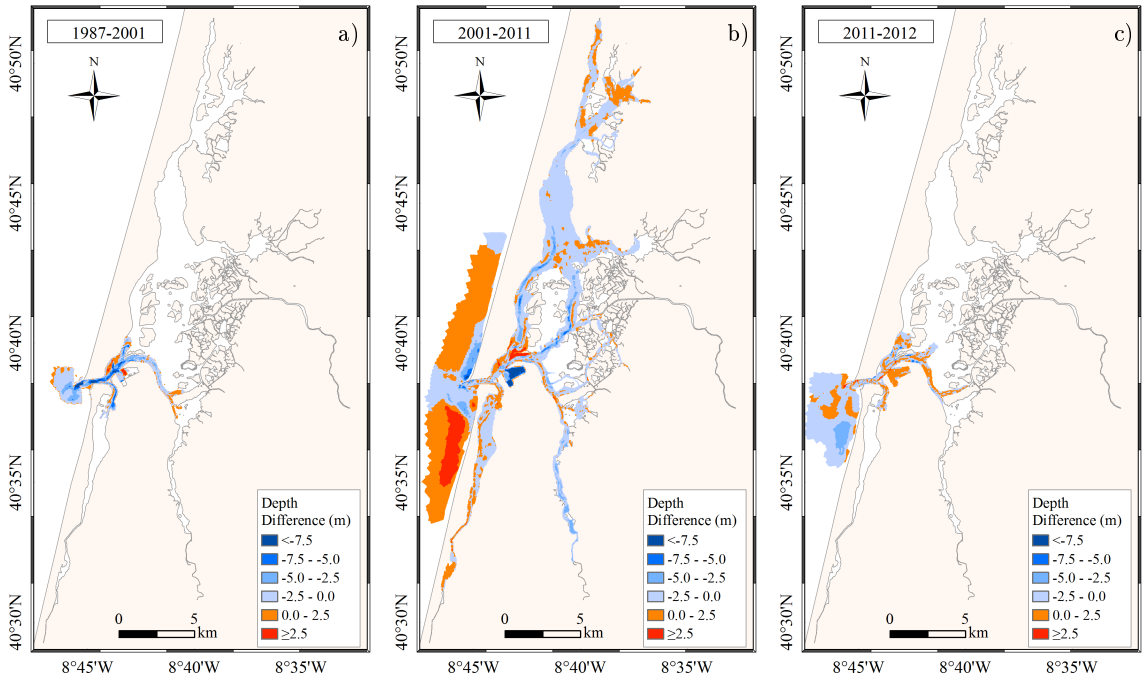


Figure 2.2: Depth difference (m) between: a) 1987 and 2001 bathymetries; b) 2001 and 2011 bathymetries; c) 2011 and 2012 bathymetries.

2.2b evidences a deepening of lagoon main channels and the enlargement of the Aveiro harbour, which was the only geometric change found, but considered of minor relevance. Deepening at the Mira channel was lower than 3 m, while at the lower reaches of S. Jacinto and Espinheiro channels can achieve 8 m. In the upper reaches of S. Jacinto, Mira and Ílhavo channels a depth decrease is also evident. Furthermore, a mean deepening of 2 m in inlet region was found. Between 2011 and 2012 (see Figure 2.2c) main bathymetric changes are restricted to the inlet and revealed a deepening of the inlet channel of 2 m. Additionally, the lower reaches of Ílhavo channel had also experienced a slight deposition. It is believed that the depth changes found are due to both natural and anthropogenic factors. Indeed, Plecha [2011] found that the inlet channel deepening was motivated by the new inlet configuration, which changed the sediment dynamics, and by regular dredging operations performed in the late eighties and early nineties. Moreover, the lagoon main channels deepening was driven by several dredging operations carried out between 1996 and 1999, in order to provide conditions for navigability [Marinheiro, 2008].

As the lagoon becomes deeper along the last years, the tidal wave amplitude increased and its propagation along the lagoon channels became faster. By analysing

tidal gauge data, Araújo et al. [2008] found that in average the amplitude of $M_2$ constituent increased 24.5 cm from 1987/88 to 2002/03 [Araújo et al., 2008]. Contrarily the $M_2$ average phase decreased approximately 17.41°. As consequence, actually, several marginal regions, among others agricultural fields, are threatened by the advance of sea waters. One of the lagoons marginal regions most affected by salt water intrusion is the Baixo Vouga Lagunar (BVL) (see Figure 2.1 III). In the eighties some interventions were made to block this salt water intrusion, namely the design and construction of a dike that would protect most of the agricultural fields existing in this region. However, only a fraction of this dike was build, and since then there are no evidences of dike breach or overtopping. Consequently, at the unprotected areas of BVL are still reported some occurrences of saltwater intrusion during high sea levels.

The inlet region accesses the Aveiro harbour (see Figure 2.1 I) and therefore its average depth (15 m relative the chart datum (ZH)) is higher than the average depth of the remaining lagoon (1 m (ZH)). Plecha [2011] studied in detail through morphodynamic modelling the processes controlling the hydro/morphodynamics of the inlet region. This author found that tidal currents determine the sediment fluxes and consequently the bathymetric changes at the inner channel, while the influence of the oceanic wave regime is restricted to the lagoon mouth and adjacent shoreline. Also, the residual sedimentary fluxes at the entrance channel are mostly directed offshore and significantly lower than those observed at the nearshore area, evidencing the lagoon capacity to export sediments. Regarding the sedimentation rates, were identified preferential areas for erosion and deposition, however the entrance channel tend to be globally filled by sediments.

## 2.2 Environmental aspects

The Ria de Aveiro hydrodynamic conditions provides the establishment of numerous species, presenting in this way several habitats with high biodiversity. Attending their high biodiversity and the need to preserve species of flora and fauna existing in this ecosystem, the Ria de Aveiro integrates the National System of Classified Areas (SNAC). The SNAC was structured by Decree-Law No. 142/2008 of 24 July,

being constituted by the National Network of Protected Areas (RNAP), the Natura 2000 classified areas and other areas classified under international commitments of the Portuguese State. According this, the Ria de Aveiro territory received three distinct classifications (Figure 2.3a). Under the Birds Directive (79/409/EEC) it is classified as Special Protection Area (SPA) given the high importance of this region for the shelter, feeding and reproduction of many species of birds. Furthermore, it was recently classified as a Site of Community Importance (SCI) (Resolution of the Council of Ministers No. 45/2014, of 8 July) once it provides access to the mouth of the rivers used by diadromous migratory species for reproduction. In addition, a part of the region (995.77 ha) located between the Atlantic Ocean and the S. Jacinto channel is classified as Natural Reserve (NR) of S. Jacinto Dunes (Decree-Law No. 41/79 of 6 March; Decree-Law No 46/97 of 17 November; Decree-Law No. 24/2004 of 12 July). This region is very sensitive due to its sandy composition and at the same time provides the establishment of valuable species of fauna and flora.

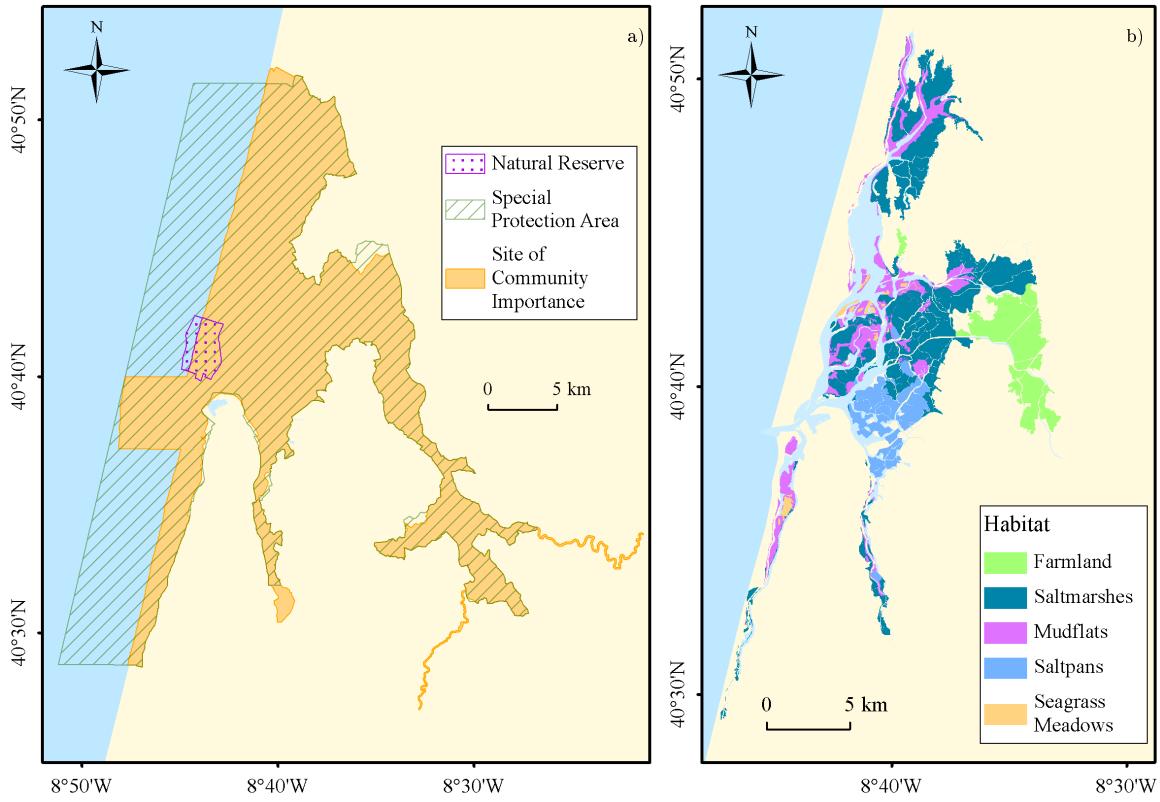


Figure 2.3: Charts of Ria de Aveiro showing, a) the classified areas; and b) the distribution of the main habitats (Source: AMBIECO [2011]).

Regarding their ecological importance should be highlighted saltmarshes, mudflats, seagrass meadows, saltpans and farmland habitats [AMBIECO, 2011; LAGOONS, 2011; Sousa et al., 2013] (Figure 2.3b). LAGOONS [2011] identified saltmarshes, mudflats and seagrass meadows as key habitats regarding the local ecological importance, which plays a crucial role on the equilibrium of the overall Ria de Aveiro ecosystem.

Saltmarshes are colonized by halophyte plants and their ecosystem services include primary productivity, nutrient cycling, protection against tidal action and provide habitat and nursery areas for several species of fish. Regarding seagrass meadows, they are colonized essentially by *Zostera noltii* and its presence is restricted to Mira and S. Jacinto channels. da Silva and Duck [2001], da Silva et al. [2004] and Azevedo et al. [2013] reported a decline of seagrass meadows associated with an increase of tidal currents and water column height that changed the sediment and turbidity distributions. Particularly, at the upper reaches of S. Jacinto channel the area covered by seagrasses of *Zostera noltii* species decreased from 8 $km^2$ in 1984 [da Silva et al., 2004] to 0.431 $km^2$ in 2010 [Cunha et al., 2013]. Despite its general decline, seagrasses present important ecological services, including high primary production, carbon and nutrient cycling, sediment stabilization, protection against erosion and habitat and nursery areas for fish species.

The mudflats are colonized by microphytobenthos and support high densities of macroinvertebrate species (among others molluscs, polychaetes and crustaceans). Their ecosystem services include high biological productivity, source of feeding for several birds, protection against erosion and nutrient cycling [LAGOONS, 2011].

Saltpans play a crucial role in the ecological equilibrium of the ecosystem Ria de Aveiro, once they are used as refuge, feeding and breeding areas for resident and migratory species of aquatic birds, most of them included in the Birds Directive (79/409/EEC) [Rodrigues et al., 2011]. Rodrigues et al. [2011] highlight that the degradation of these structures caused important modifications in the whole Ria de Aveiro ecosystem, changing its fauna and flora. Particularly, the rise of lagoon water levels leads to habitat loss and turns more difficult the establishment of aquatic birds.

The farmland habitats are present essentially in the BVL area and are characterized

by small farmland fields surrounded by living hedges and water ditches (bocage landscape). It is considered an agroecosystem managed by farmers, where the human activities are in full harmony with nature [Sousa et al., 2015; Andresen et al., 2001]. This area presents high biodiversity sustained by herbaceous stratum, both natural and seeded. The current insight is related with the equilibrium between agriculture and nature which can be disrupted by saltwater intrusion [García et al., 2012]. Indeed, the BVL region is under pressure from the rising sea water level caused by climate change affecting the maintenance of agricultural fields. García et al. [2012] found that bocage landscape tends to disappear together with its unique natural values (flora and fauna).

## 2.3 Socioeconomic aspects

The Ria de Aveiro supports a range of natural services and goods favourable to the establishment of human communities and consequent development of economic activities. The predominant land uses in the Ria de Aveiro municipalities (Figure 2.4a) are forestry and agriculture, occupying approximately 52% and 26% of total area, respectively. The artificial surfaces represent approximately 13% of the whole area and are used for residential, industrial and commercial purposes. Actually, the Ria de Aveiro plays a crucial role in the regional and national economy, directly contributing to more than 12% of the total gross value added (GVA)(gross production value less the cost intermediate consumption) of the Baixo Vouga NUTSIII region [PLRA, 2011a]. The Aveiro harbour is a key factor to the economy of Baixo Vouga NUTSIII region, playing a crucial role in supplying services to several industrial sectors, such as the ceramics, chemical, metallurgy, wood derivatives, agricultural, food and construction industries [APA, 2014]. According the PLRA [2011a], the services activities are predominant in the Ria de Aveiro region representing approximately 61% of the total GVA. The industry, including energy and construction activities represent 37% of the total GVA, while agriculture, hunting, forestry, fishing and aquaculture represent only 2% of total GVA [PLRA, 2011a]. Despite its minor importance to the global economy, the agriculture, fishing and aquaculture activities are important resources to

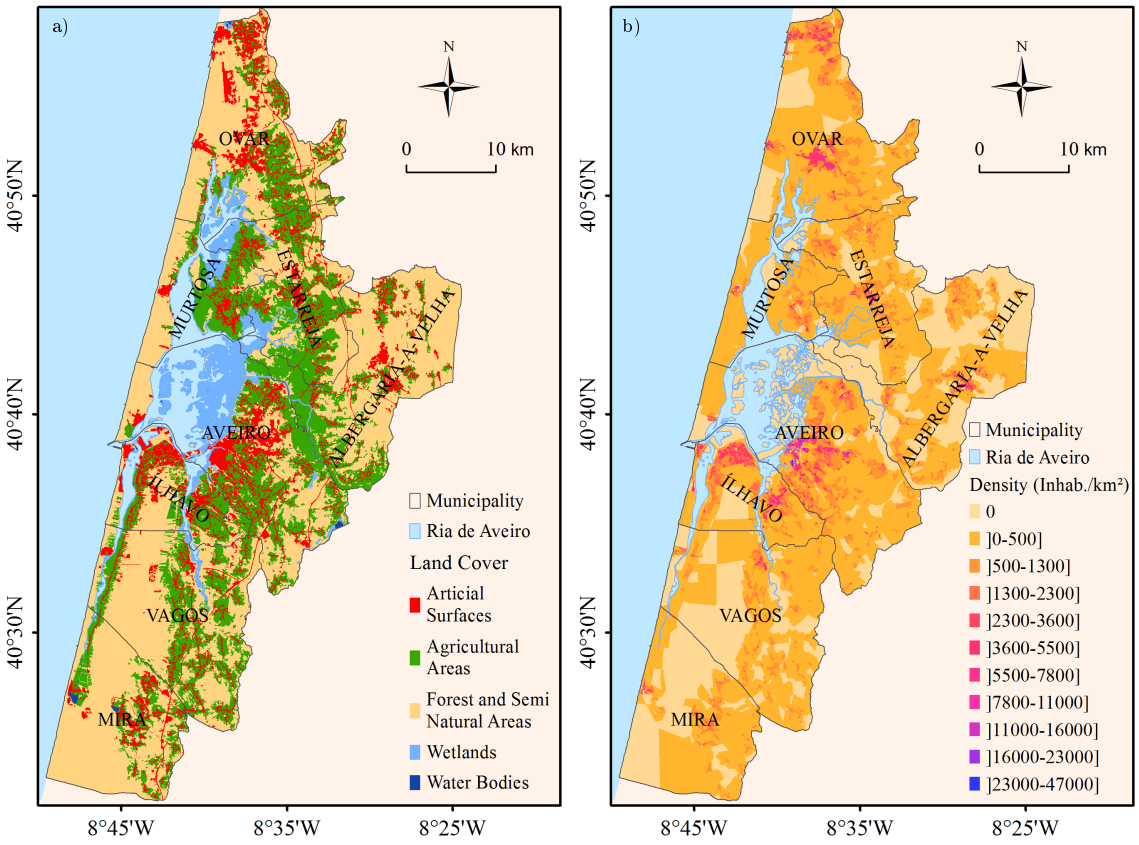


Figure 2.4: Charts of Ria de Aveiro showing: a) the land cover; and b) the population density (Inhabitants/km$^2$).

the sustainability of local communities. Artisanal activities, such as salt production, shellfish collecting, bait digging and recreational fishing, together with sport activities, such as kitesurf, surf and sailing, contribute to the local tourism growth and are therefore also important to the local communities.

According the PLRA [2011a] the total resident population in the Ria de Aveiro municipalities in 2009 was 274 789. From the population census performed in 2011 by the Statistics Portugal (INE), was found that the total resident population in these municipalities decreased 1.5%, to 270 596 inhabitants. The Aveiro municipality is the most populated one, with 78 450 inhabitants, followed by Ovar (55 398), Ílhavo (38 598), Estarreja (26 997), Albergaria-a-Velha (25 252), Vagos (22 851), Mira (12 465) and Murtosa (10 585). The census 2011 data was disaggregated at local scale using the Geographic Base for the Referencing of Information (BGRI), in order to localize the settlements (Figure 2.4b). According this, the largest population density areas

are coincident with the most developed urban areas, and are located close the lagoon central area margins in the Aveiro and Ílhavo municipalities.

## 2.4 Ria de Aveiro past floods

The Ria de Aveiro is considered a flood prone region given the low altitude and flat topography of its marginal lands. Most of the flooding events occur during adverse weather conditions associated to the existence of a low pressure localized in the NW of the Iberian Peninsula. In these circumstances, heavy rainfall induces high river discharges while the low pressure causes storm surges in the Portuguese coast.

Details of past flood events (until 2005) were investigated under the scope of SECUR-Ria project [Coelho et al., 2007]. Supported on the inventory of past events through questionnaires elaborated on local communities, a flood extent polygon was determined (Figure 2.5). According this, the critical areas correspond to the margins of the lagoon close the mouth of its tributaries. Regular episodes of seawater flooding during spring tide conditions were also identified in the lagoon margins of Ovar, Murtosa, Estarreja and Ílhavo municipalities (red stars Figure 2.5).

In the scope of the present work an inventory of flood events was made by consulting newspapers, videos available online and surveying sites during adverse weather conditions. The flood marks (purple diamonds of Figure 2.5) evidence the occurrence of flood events in Ovar, Murtosa, Estarreja, Albergaria-a-Velha, Aveiro and Ílhavo municipalities. This research highlighted a flood event occurred in $27^{\text{th}}$ February 2010 caused by the storm Xynthia. This storm was developed in the Atlantic Ocean and originated storm surges and coastal inundations in the NW coast of Iberian Peninsula and Bay of Biscay [Bertin et al., 2012]. According the local and national media, this storm threatened the NW Portuguese coast, inundating roads, agricultural fields, residential, commercial and industrial buildings. Within Ria de Aveiro region, this storm caused inundation in the S. Jacinto channel margins, which was recorded in S. Jacinto (AV2), Torreira (MU1) and Marinha (O2) localities (Figures 2.6a, 2.6b and 2.6c, respectively).

Another inundation episode occurred during the summer season, in August 2009,

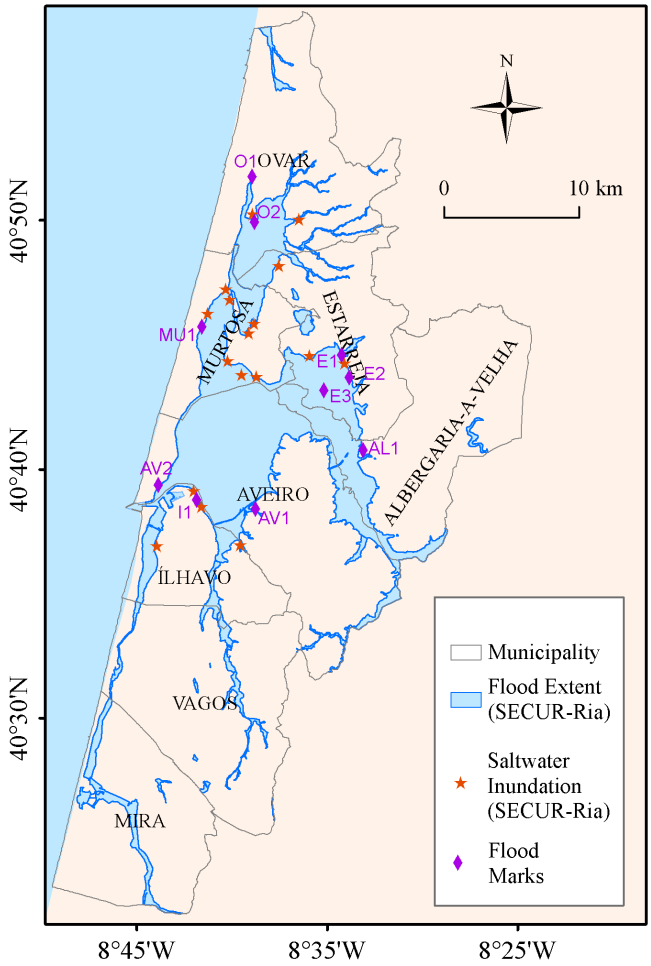


Figure 2.5: Ria de Aveiro maximum flood extent surveyed (Source: Coelho et al. [2007]), indicating flood marks.

in the Marinha locality (O2) during equinoctial tides. According local and national media, approximately 200 ha of agricultural fields were inundated by saltwater and tonnes of corn were lost (in Público: `http://www.publico.pt/local-porto/jornal/agua-salgada-esta-a-dizimar-campos-de-milho-em-ovar-17506454`). Still in S. Jacinto channel, an episode occurred in May 2015 in the marina of Carregal (O1) was highlighted in the media. This event caused damage in the marina area, however this area was recently improved (rising its elevation) in the framework of Polis Litoral Ria de Aveiro activities (`www.polisriadeaveiro.pt/`).

Inundation events affecting the marginal areas of Vouga and Antuã rivers mouths are the most documented situation within the Ria de Aveiro region. Figure 2.7 shows the inundation in four distinct locations during the January 2014 flood event. The agricultural fields located in this area are flooded almost every year during winter,


Figure 2.6: Inundation caused by the storm Xynthia in: a) S. Jacinto (AV2) (www.bombeirosnovos.pt/node/107); b) Torreira (MU1) (www.antorreira.org/cms2/index.php?option=com_content&view=article&id=158:temporal-na-ria&catid=15:marina&Itemid=10); c) Marinha (OV2) (www.ovar.pcp.pt/local/actividade/439-pcp-alerta-camara-para-situacao-de-emergencia-na-marinha).

when river discharges are high. The water level in the Antuã and Vouga rivers increase and overflow the margins inundating an extensive area characterized by flat topography. These events cause damage mainly on agriculture, but under more severe events traffic disruptions and the inundation of residential areas may occur. Moreover, situations of livestock losses are documented when the river level rises suddenly.

The rupture of embankments adjacent to the river channels is another important consequence of high discharges. Almost every year it is necessary to repair the disruptions in order to prevent the salinization of agricultural fields when the rivers discharges decrease. Indeed, if the disruptions occur in spring tide conditions, repairs will not be completed in time to avoid saltwater intrusion. This issue had already been reported in several local and national newspapers, consequently there is a rising tendency to abandon the cultivation of farmlands, thereby weakening the agroecosystem equilibrium discussed before.


Figure 2.7: Inundation caused by high river discharges (January 2014) in: a) Angeja (AL1); b) Estarreja (E1); c) Ladeira (E2); d) Canelas (E3).

The flood events in the Aveiro town (AV1) have been also highlighted in several media, once it is the most important urban centre of the Ria de Aveiro region. The Aveiro town is a district capital characterized among others by tourism, commerce and services activities. The down town is crossed by narrow channels that were overflowed several times during its history, causing damages around. In order to control the flow within the city channels, a system of sluices and flood gates at the city entrance came into operation at 23 November of 1985 (in Diário de Aveiro 25$^{th}$ November 1985). Besides the flood control, this system also aims to maintain the channels with a minimum water level during low tides. Since its installation the flood events decreased considerably, however they may still occur when heavy rainfall coincides with spring tide. In this condition the sluices and flood gates are closed to prevent the entrance of ocean water, however the rain water remains trapped causing inundation. The floods that occurred in October 1999 and April 2008 are examples of this problem (Figure 2.8).

Another critical point is Gafanha da Nazaré (I1), where flood events occur when sea levels are high (Figure 2.9). It is a small city located close the lagoon entrance that


Figure 2.8: Inundation in the Aveiro down town (AV1) in October 1999 (in Campeão das Províncias 28$^{th}$ October 1999).


Figure 2.9: Inundations in Gafanha da Nazaré (I1): a) September 2014 (in Diário de Aveiro); b) January 2013 (in `http://mclvieira.blogspot.pt/2013/01/mau-tempo-em-aveiro-19-01-2013.html`).

contains fish berths of Aveiro harbour, which are surrounded by diverse industries of fish processing. Here, during equinoctial tides (Figure 2.9a), the lagoon water invades the area adjacent to industrial fishing units. Moreover, this area suffers inundation when high tides coincide with storm surge events (Figure 2.9b).

# Chapter 3

# Characterization of driving forces

## 3.1 Introduction

The characterization of flood drivers is the first step towards a precise flood risk assessment [Domeneghetti et al., 2013]. To identify the driving forces within a coastal lagoon and to determinate its magnitude and respective probability is fundamental for flood risk analysis.

According to Kjerfve [1994], the water level within a coastal lagoon is determined by oceanic and fluvial drivers. The fluvial drivers account the input of freshwater flows, while oceanic drivers include water oscillations driven by tides, storm surges, wind waves and mean sea level. Ideally, the forcing are characterized through the analysis of long records of river discharges and sea surface levels. As long series of observed data are not always available, watershed and oceanic data models are often used to fill periods of data failures or even the inexistence of data [Loukas and Vasiliades, 2014].

With the exception of tides, all of these drivers are affected by atmospheric factors. Attending this, climate changes can potentially affect coastal lagoon driving forces and consequently its hydrodynamics [Anthony et al., 2009; Wang et al., 2014]. Moreover, there is an extended consensus among the scientific community that the global mean sea level is rising in response to the increase of green house gases concentration in the atmosphere. However, the mean sea level is not changing uniformly around the world, as both tide gauge and satellite data confirm [Church and White, 2006, 2011; IPCC, 2007]. Indeed, in some regions, the sea level rates are higher than the global

mean, while in other regions the sea level is decreasing. Attending this, it is crucial to understand the local mean sea level variability in assessing the risk of flooding in a particular coastal region.

It is very likely that the MSLR will change the tidal characteristics and sedimentary processes within coastal lagoons and estuaries [Nicholls, 2011; Wong et al., 2014]. Attending this, the impacts of climate changes within these systems should account not only the driving forces changes but also future morphological changes.

Attending these concerns, the main aim of this chapter is to characterize the Ria de Aveiro hydrodynamic and morphodynamic driving forces. The magnitude and probability of oceanic and fluvial drivers will be investigated for both the present and future climates. The results of this research will provide estimates of oceanic and fluvial variables to input as boundary conditions in hydrodynamic and morphodynamic numerical models applications.

## 3.2 Methodology

According the literature review, the Ria de Aveiro hydrodynamics and morphodynamics are determined by both oceanic (tides, storm surges, wind generated waves and mean sea level) and fluvial (river discharges) drivers [Dias, 2001; Araújo, 2005]. In this chapter the oceanic and fluvial drivers will be characterized for both present and future climates, by analysing observed and modelled data.

### 3.2.1 Tides and storm surges

The tides were assessed by analysing the hourly sea surface elevation (SSE) data recorded at the inlet (8.75°W; 40.64°N) tidal gauge between 1976 and 2013 (Figure 3.1). Some interruptions were found along the 38 years of data (Figure 3.2), namely the inexistence of data over 2006, 2008, 2009 and 2011. Also, the record of 2013 presents the highest number of failures; about 59% of the hourly sea levels were not recorded. The hourly sea levels were used to determine the tidal constants by applying harmonic analysis using the t_tide package [Pawlowicz et al., 2002]. The interannual variability


Figure 3.1: Location and details of inlet tidal gauge.

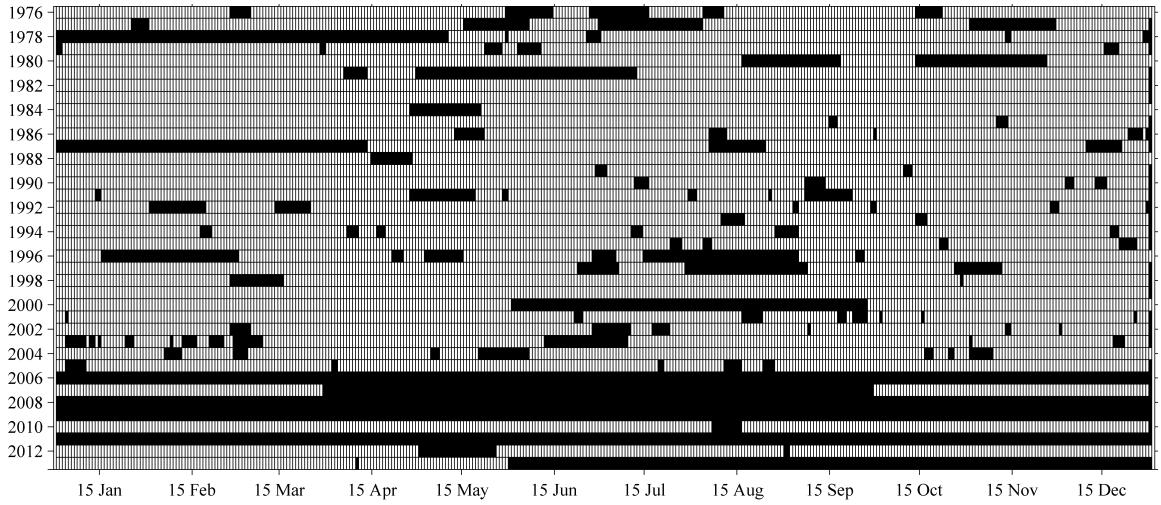


Figure 3.2: Tidal gauge record gaps (represented by black squares).

of amplitude and phase of $M_2$ and $M_4$ constituents was analysed, once its importance on the lagoon hydrodynamics [Dias, 2001].

Also, the tidal constants of 2012 were used to reconstruct hourly astronomic levels over a year, in order to determine the tidal range and the maximum level of typical neap, mean and spring tides. The 2012 harmonic constants were chosen for two reasons. First, it is important to choose recent tidal constants once, as will be explained further, the tidal constants changed considerably between 1976 and 2013 at the lagoon mouth. Secondly, because the SSE record of 2012 year has one of the lowest percentage of failures (approximately 7%) over the last 10 years of records.

Considering that tidal propagation depends on the coastal morphology, tidal constants can be modified in the future as consequence of MSLR [Pickering et al., 2012; Ward et al., 2012]. This issue has not been studied yet for the Portuguese coast. However, Woodworth [2010] analysed tidal gauge data recorded in the $20^{th}$ century and did not find evidences of significant changes in the main harmonic constants in

Europe. Accordingly, it is considered that the tidal conditions at the lagoon mouth are identical for both present and future climates.

Regarding storm surges, they were characterized by analysing the residual levels obtained from the inlet tidal gauge record, between 1976 and 2013. The annual tidal constants previously determined were used to construct astronomic series through harmonic synthesis, using the t_tide package [Pawlowicz et al., 2002]. Then, the residual levels were computed as the difference between observed and synthesized astronomic levels. It is assumed that the residual signal is a response of atmospheric pressure oscillations, once the wind generated waves play a minor role on the establishment of SSE [Vaz, 2012]. The storm surge events were identified considering that the residual levels higher than 3 standard deviations of residual series are storm surge events, as recommended by Pugh [1987].

The storm surge maximum annual peaks were identified and adjusted to a Generalized Extreme Value (GEV) distribution in order to determine the storm surge height for return periods of 2, 10, 25, 50 and 100 years. In this analysis only the annual maxima observed between 1976 and 2005 were considered, due to the inexistence of data in the years 2006, 2008, 2009 and 2011. Indeed, successive annual maximum levels are required to determine return periods through this method.

As storm surges are generated by atmospheric low pressures, climate changes can induce modifications in storm surge patterns. Rodrigues [2011], studied the cyclonic activity over the North Atlantic region for both present and future climates, by using the climate data of $4^{th}$ IPCC report. By comparing the present and future climates this author found a slight reduction in the intensity of cyclones, accompanied by a northward displacement during the winter. However, as stated in that work, these changes are not statistical significant, evidencing no substantial changes in the cyclonic activity over the North Atlantic region in the future, relative to the present. Marcos et al. [2011] used the climate data of $4^{th}$ IPCC report to feed an oceanic baratropic model, and studied storm surges in the Mediterranean Sea and in the Atlantic Iberian coasts during the $21^{st}$ century. They found that storm surges frequency and magnitude tends to decrease for future climate, relative to the present. Particularly, a slight attenuation, between 3 and 4 cm, for storm surge levels of 50 years return period in the

Portuguese coast was found. Attending the conclusions of these studies, in the present work is considered that the future storm surges regime will be identical to the present.

#### 3.2.1.1 Simultaneous occurrence of tides and storm surges

The simultaneous occurrence of storm surge and high tidal levels is extremely important in flood risk assessment, once the flood extent and the consequent damage caused during storm surge events depends on both tidal and storm surge levels. Indeed, the same storm surge event has different impacts in the coastal zone if occurs in neap or spring tide conditions. Considering this, the SSE recorded at the inlet tidal gauge, the storm surge height and the tidal level were investigated during three distinct storm surge events. These were then related with the flooding events described in the previous chapter.

#### 3.2.1.2 Extreme sea levels

Extreme sea levels can be considered as a combination of the mean sea level, storm surge, and tides (ignoring the effect due to oceanic wind-generated waves). Therefore, its estimation is often supported on joint probability analysis (e.g. Hawkes [2008] and Liu et al. [2010]. The joint probability approach was applied to the SSE inlet record and extreme sea levels for 2, 10, 25, 50 and 100 years return periods were determined.

### 3.2.2 Mean sea level

The present mean sea level was characterized by analysing the inlet tidal gauge data between 1976 and 2013. The annual mean sea levels, determined through harmonic analysis, were used to investigate the interannual variability of mean sea level over this period.

As previously discussed, the MSLR is a very likely consequence of climate changes. Extrapolating the tendency observed in the Cascais tidal gauge, Antunes and Taborda [2009] projected a rise of 0.47 m with a 95% confidence interval between 0.19 and 0.75 m in the year 2100 relative to 1990 mean sea level. Lopes et al. [2011], studied the mean sea level under climate change conditions in the Portuguese coast by analysing

the output of the AOGCM, GISS-ER, in the eight nearest points of Portugal. They found that the mean sea level at the end of the 21$^{st}$ century will increase between 0.28 m and 0.42 m, relative to the present, corresponding to the B1 and A2 SRES published in the 4$^{th}$ IPCC report [IPCC, 2007].

As the global MSLR estimates (0.37-0.82 m during 2081-2100) reported in the 5$^{th}$ IPCC report [IPCC, 2013] are higher than the ones (0.18-0.59 m during 2071-2100) presented in the 4$^{th}$ report [IPCC, 2007], the future mean sea level changes at the Portuguese coast were revaluated here by analysing the models output that support the global estimates of the 5$^{th}$ IPCC report.

Sea levels derived from the Coupled Model Intercomparison Project Phase 5 (CMIP5) models and provided by Integrated Climate Data Center (ICDC) of the University of Hamburg (`http://icdc.zmaw.de/1/daten/ocean/ar5-slr.html`), were used. The data has $1° \times 1°$ resolution and corresponds to the 2081-2100 mean minus 1980-2005 mean of the ensemble of 21 CMIP5 AOGCM. The total mean sea level change account for long-term changes in Greenland dynamic ice and surface mass balance, Antarctic dynamic ice and surface mass balance, glaciers, dynamic sea surface height, global thermosteric sea surface height anomaly, the inverse barometer effect from the atmosphere, land water storage and glacial isostatic adjustment.

This data was used to assess the sea level change in the Portuguese coast, for four Representative Concentration Pathway (RCP) scenarios derived under the scope of 5$^{th}$ IPCC report.

### 3.2.3 Waves

Despite its minor importance on the lagoon hydrodynamics, the wind generated waves can be important on the sedimentary processes that occur at the inlet region. Therefore, present and future oceanic wave regimes were characterized in the Aveiro coastal region, by analysing the output of the WW3 model [Tolman, 2009], previously validated for the North East Atlantic Ocean [Dodet et al., 2010]. Predicted data, instead of observed data, was used to characterize the present oceanic wave regime given the lack of wave monitoring offshore Ria de Aveiro. Indeed, the buoys of Leixões (9.09°W; 41.20°N) and Figueira da Foz (9.15°W; 40.19°N) (Figure 3.3) present the wave

records nearest to the Ria de Aveiro inlet. However, these records are not available for free, present several interruptions (since some days to several months) and are relatively short for climate analysis (Leixões - 1993 to present; Figueira da Foz - 1984 to 1996).

The WW3 configuration was applied by Ribeiro et al. [2012] using the wind data outputted by the climate model ECHAM5MPI-OM [Marsland et al., 2003; Roeckner et al., 2003] in order to characterize the present and future oceanic wave regimes. The present oceanic wave regime data corresponds to the 20C3M ($20^{th}$ century) case over 1971-2000, while the future climate corresponds to the SRES A2 over 2071-2100 [IPCC, 2007]. This implementation was validated by comparing the WW3 oceanic wave regimes forced by 20C3M or by re-analyses NCEP wind data between 1971 and 2000. Also, the mean wave parameters derived from WW3 model were compared with that recorded in Leixões, Figueira da Foz and Sines (1993 - 1995 [Ribeiro et al., 2012].

The mean wave parameters (period, significant height and direction) of WW3 in the nearest point of the Ria de Aveiro inlet (41°N, 10°W) (Figure 3.3), that were made available through the ADAPTARia project (`http://climetua.fis.ua.pt/legacy/adaptaria/`), were statistically analysed, taking the objective to provide the boundary conditions to the morphodynamic model. As the model needs time series of wave

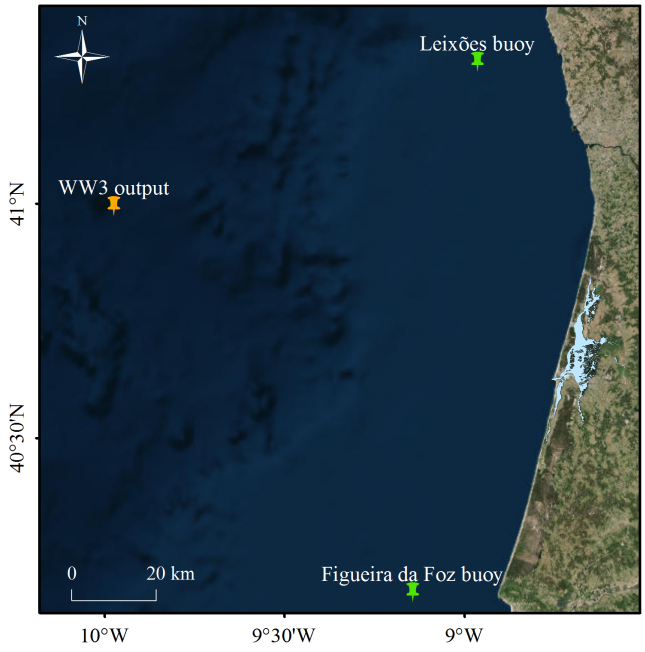


Figure 3.3: Location of points where there is wave data.

parameters, the representative year of each climate was determined by comparing the 30 years data with each year data of the respective climate.

### 3.2.4 Fluvial discharges

Concerning fluvial drivers, as there is no continuous monitoring of discharges inflowing at the lagoon, predicted discharges outputted by the watershed models SWAT [Arnold et al., 1993] and SWIM [Krysanova et al., 1989] at the five main tributaries were statistically analysed. These models were calibrated and validated, and Nash-Sutcliffe coefficients of the order of 0.7 were obtained for both implementations [Dias et al., 2013a; Stefanova et al., 2015]. The present climate discharges were simulated over 1931-2010 and 1981-2010 for SWAT and SWIM, respectively, when fed with observed precipitation. Concerning future climate, the models were fed with ECHAM5MPI-OM precipitation under scenario SRES A2 over 2071-2100. SWAT and SWIM data were made available through ADAPTARia (`http://climetua.fis.ua.pt/legacy/adaptaria/`) and LAGOONS (`http://lagoons.biologiaatua.net/`) projects, respectively.

The daily mean discharges predicted by SWAT and SWIM models were used to determine the peak discharges for 2, 10, 25, 50 and 100 years return periods, for each one of the five tributaries considered in this study, for both present and future climates.

## 3.3 Results and discussion

### 3.3.1 Tides and storm surges

A first analysis of the record highlights that the tides are semi-diurnal with a small diurnal pattern. Also, the fortnightly spring/neap tide cycle is evidenced on elevations registered at the lagoon inlet, generating tidal ranges between 0.46 m at neap tide and 3.52 m at spring tide.

The annual amplitude and phase of $M_2$ and $M_4$ constituents is represented in Figures 3.4 and 3.5, respectively. The results highlight that the amplitude of $M_2$ constituent increased over this period at a rate of 2.8 mm/year while its phase decreased

$0.04^o$/year. An opposite behaviour was found for $M_4$ constituent amplitude, once it is observed a slight decrease of the amplitude and a phase decrease at a rate of $0.9^o$/year. The amplitude of $M_2$ constituent ranged from 0.86 m in 1979 to 0.97 m in 2000. The maximum and minimum values of $M_2$ phase were $83^o$ and $76^o$, observed in 1980 and 2003, respectively. The $M_4$ amplitude ranged from 0.03 m in 1984 to 0.05 m in 1976. Concerning the $M_4$ phase the minimum value observed was $242^o$ in 2013, while the maximum value observed was $291^o$ in 1979. It is important to highlight that the highest variations on the amplitude of the $M_2$ constituent occurred between 1983 and

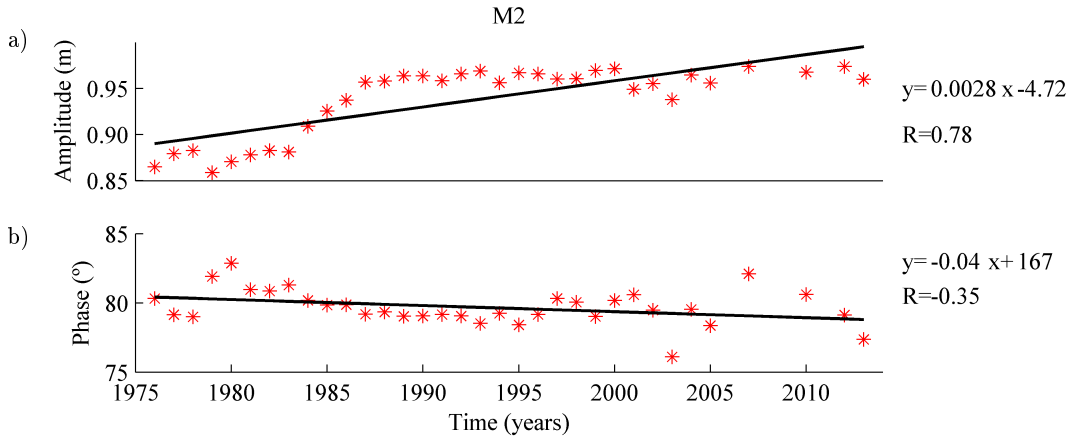


Figure 3.4: Interannual variability of: a) amplitude (m) and b) phase ($^o$) of the $M_2$ constituent.

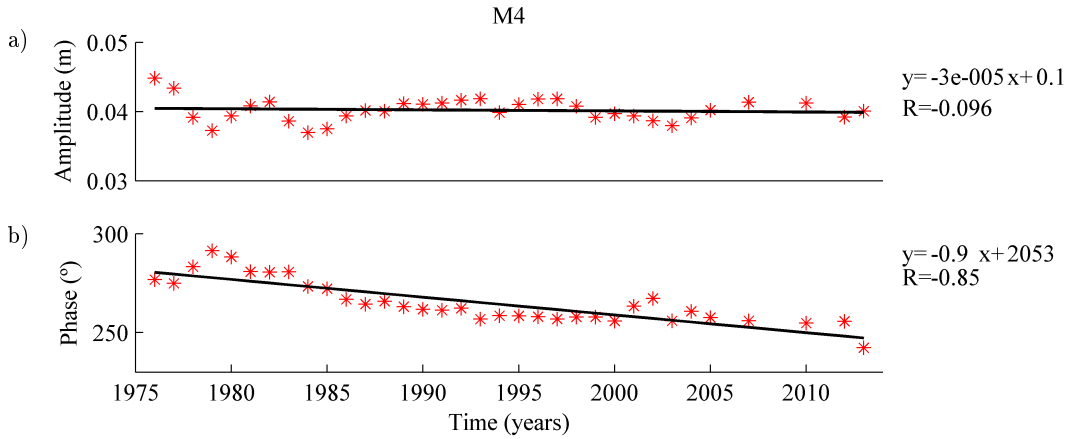


Figure 3.5: Interannual variability of: a) amplitude (m) and b) phase ($^o$) of the $M_4$ constituent.

1987 that coincides with the first extension of the lagoon northern breakwater. Also, it is observed that the $M_2$ amplitude suffered minor changes from 1989 to 2013.

The tidal constants of 2012 were used to reconstruct hourly astronomic levels over a year, in order to determine the tidal range and the maximum level of typical neap, mean and spring tides (Table 3.1). The results highlight that the maximum levels at the lagoon entrance range between 2.8 and 3.6 m, depending on the tidal condition.

The residual levels were computed and used to identify storm surge events (3 standard deviations). Considering the procedure described previously, 208 peaks higher than 0.32 m (3 standard deviations) were found within 1976 and 2013 at the lagoon entrance. The highest storm surge recorded had 1.09 m height and occurred on 30 December of 1981, and the mean height of storm surge peaks is 0.43 m.

The storm surge maximum annual peaks were identified (Figure 3.6a) and adjusted to a GEV distribution (Figure 3.6b). The empirical cumulative distribution function (CDF) was computed according to Kaplan and Meier [1958], while the theoretical distributions were determined by calculating the likely location, scale and shape parameters. The CDF curve represents the likely CDF, while the 5% and 95% curves represent the CDF limit for a confidence interval of 90%. Once the empirical CDF is within the limit curves (Figure 3.6b) it is concluded that the storm surge annual maximums fit to a GEV distribution at a confidence level of 90%. Attending this, the likely distribution was used to determine return periods of storm surge events. By definition, the return period of an event is the period of time estimated for an event to be equalled or exceeded. Results suggest storm surges heights of 0.58 m, 0.84 m, 0.97 m, 1.08 m and 1.17 m for the return periods of 2, 10, 25, 50 and 100 years, respectively.

Table 3.1: Tidal range (m) and maximum level (m) (ZH), of typical tides.

| | Tidal Range (m) | Maximum Level (m) |
|---|---|---|
| Neap Tide | 1.2 | 2.8 |
| Mean Tide | 2.1 | 3.0 |
| Spring Tide | 2.9 | 3.6 |

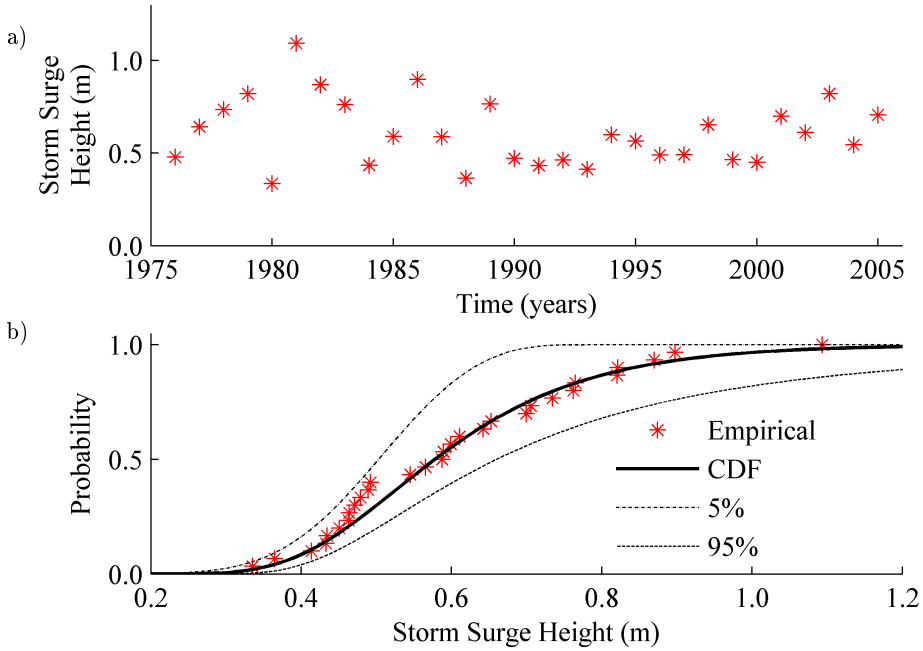


Figure 3.6: a) Annual maximum storm surge height (m); b) Cumulative distribution functions, empirical and theoretical (CDF, 5% and 95%).

#### 3.3.1.1 Simultaneous occurrence of tides and storm surges

Figure 3.7 represents the observed SSE, the residual and the tidal levels during three distinct storm surge events. The first case refers to an event occurred between 16 and 17 February 1986, which storm surge peak height reached 0.9 m. Although is one of the most intense recorded, this occurred in neap tide conditions causing a maximum level of 3.4 m, which is lower than the sea level reached during a typical spring tide (see Table 3.1). The second case corresponds to an event occurred between 23 and 25 October 1999. This storm surge achieved 0.47 m height, and occurred in spring tide conditions, causing a maximum sea level of 3.76 m. As demonstrated in the previous section this event caused inundation in the downtown of Aveiro (Figure 2.8). The last situation analysed corresponds to a storm surge event occurred on February 2010, which maximum storm surge peak reached 0.6 m. This storm occurred in intermediate tide causing a maximum sea level of 4.01 m. As shown in the previous section, this storm caused inundation along the S. Jacinto channel margins (Figure 2.6). In this way this analysis proved that the consequences of a storm surge event on the Ria de Aveiro highly depends on the tidal condition.

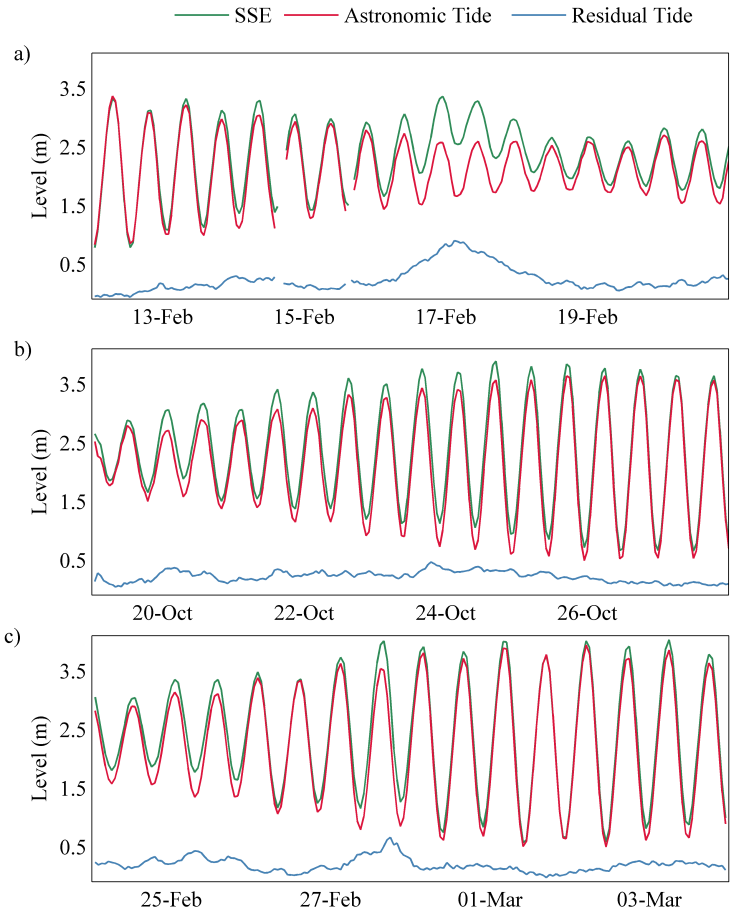


Figure 3.7: SSE (m), astronomic and residual levels (m) between: a) 12$^{th}$ and 20$^{th}$ February 1986; b) 19$^{th}$ and 27$^{th}$ October 1999; c) 24$^{th}$ February and 3$^{rd}$ March 2010.

#### 3.3.1.2 Extreme sea levels

The joint probability approach was applied to the tidal gauge record in order to estimate extreme sea levels at the lagoon mouth. The first step consists in determining the probability of residual and tidal levels independently. Concerning the tidal probabilities, they can be determined from short periods of data once the tidal forcing is well known from the astronomy [Pugh, 2004]. Attending this, the harmonic constants of 2012 were used to predict the astronomic levels over 18.6 years, that corresponds to the 5$^{th}$ component of lunar nodal cycle as recommended by Pugh [2004]. In this study, it is assumed that extreme sea levels occur when tidal level is higher than 3.3 m, which corresponds to the mean high water springs (MHWS), as recommended by Pugh [2004]. Attending this, the tidal levels equal or higher than

3.3 m were grouped in intervals of 0.01 m, and the probability of occurrence of each interval was computed (Figure 3.8a).

The residual series were then examined to determine the probability of occurrence of storm surge height, which was obtained analysing the peaks over a threshold value. Several threshold levels between 0.33 m and 0.50 m were used to compute extreme sea levels and results were compared to the annual maxima observed. This sensitivity test showed that 0.45 m threshold level produces the more coherent results and therefore was considered in this analysis. The empirical CDF was computed by the method presented by Kaplan and Meier [1958]. Then, the parameters of the likely Generalized Pareto Distribution (GPD) were computed as well as the lower and the upper limits at a confidence level of 90% in order to investigate the adjustment between empirical and GPD distribution (Figure 3.8b).

The results evidence that empirical CDF is statistically similar to the GPD distribution at a confidence level of 90%, once the empirical CDF are comprised between the upper (95%) and lower (5%) limit curves of the GPD distribution. Given that the correlation coefficient between tides and storm surges is -0.0015 for Ria de Aveiro tidal gauge [Fortunato et al., 2013], the probability of a residual level $R_i$ to occur simultaneously with an astronomical level $A_i$ is given by equation 3.1:

$$P(A_i \cap R_i) = P(A_i)P(R_i) \tag{3.1}$$

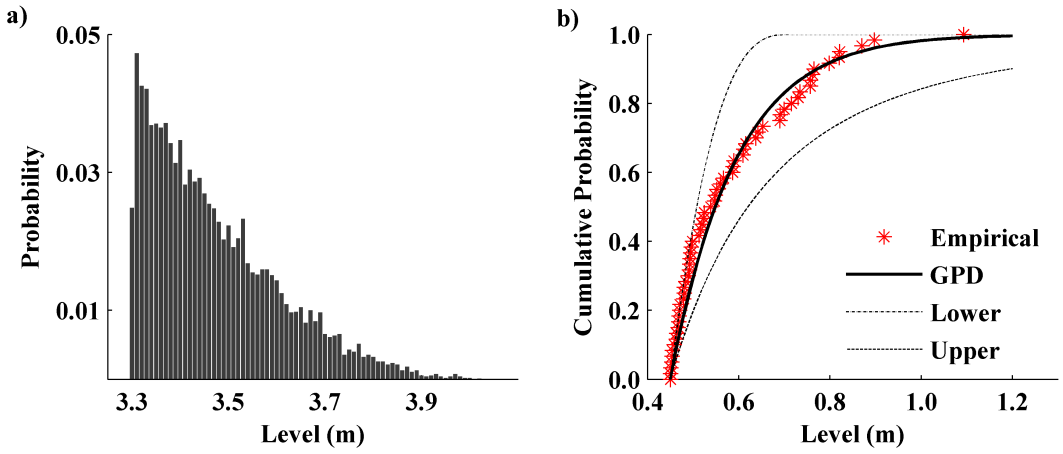


Figure 3.8: a) Probability of tidal astronomic levels. b) Empirical and theoretical cumulative distribution functions (GPD, 5% and 95%) for storm surge levels.

Where $P(R_i)$ , is the probability of a residual level of magnitude $R_i$ and $P(A_i)$ is the probability of an astronomical level of magnitude $A_i$.

Following this methodology, maximum levels between 3.85 m and 4.56 m were computed (Table 3.2), evidencing a difference of 0.71 m between 2 and 100 years return period estimates. This difference is in agreement with the observations, once the maximum range between the measured surge heights is 0.77 m (maximum 1.09 m and minimum 0.32 m).

Fortunato et al. [2013] proposed a different methodology to estimate extreme sea levels by generating synthetically elevation series resulting from the combination of annual tide and annual residual series. Those authors obtained for the Ria de Aveiro inlet tidal gauge maximum levels of 4.20, 4.41 and 4.48 m for 10, 50 and 100 years return periods (Table 3.2). The estimates obtained here from joint probability analysis are slightly higher than those presented by Fortunato et al. [2013], with the larger differences found for the highest return periods. Indeed, the difference between estimates is 3 cm and 8 cm for 10 and 100 years return periods, respectively.

### 3.3.2 Mean sea level

The annual mean sea levels at the lagoon entrance obtained through harmonic analysis are represented in Figure 3.9. The mean sea levels range between 2.02 m (ZH) in 2000 and 2.20 m (ZH) in 2013. These results highlight that the mean sea level increased at a rate of 2.2 mm/year, that is slightly higher than the rate of 1.15 mm/year obtained by Araújo [2005] when analysing the inlet tidal gauge record between 1976 and 2003. This trend is in agreement with that observed for Cascais and Lagos tidal gauges. Dias and Taborda [1988] estimated a relative sea level rise at a rate of 1.5±0.2 mm/year at Lagos between 1908 and 1987 and 1.3±0.1 mm/year at Cascais between

Table 3.2: Extreme sea levels (m) relative the ZH.

| Return Period (years) | 2 | 10 | 25 | 50 | 100 |
|---|---|---|---|---|---|
| Joint Analysis | 3.85 | 4.23 | 4.37 | 4.47 | 4.56 |
| Fortunato et al. [2013] | - | 4.20 | 4.32 | 4.41 | 4.48 |

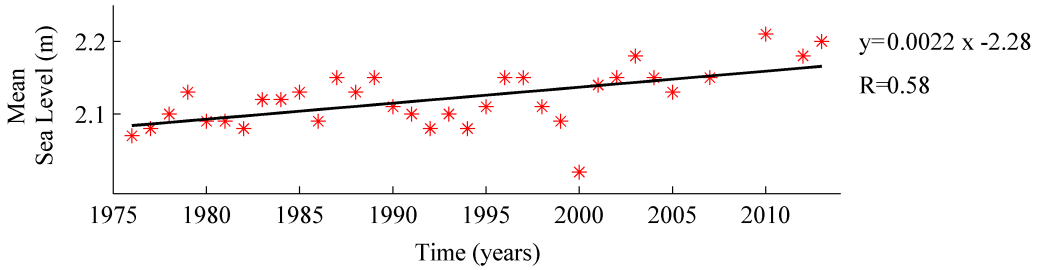


Figure 3.9: Interannual variability of mean sea level (m).

1882 and 1987. More recently, Antunes and Taborda [2009] found an acceleration of the relative sea level rise rate during 1977-2000 at Cascais and have estimated for this period a rate of 2.1±0.1 mm/year. Conversely, a decrease rate of 0.70±0.27 mm/year was found by Araújo et al. [2013] when analysing the Leixões record between 1906 and 2008.

The mean sea level changes for the end of the 21$^{st}$ century were estimated for the Portuguese coast, by analysing the models output that supported the global estimates of the 5$^{th}$ IPCC report. Figure 3.10 presents the total mean sea level change during 2081-2100 relative to the present mean sea level (1986-2005), for the four RCP scenarios. For all scenarios a rise in mean sea level was observed for the whole region.

The sea level change anomaly (difference between each grid point represented in Figure 3.10 and the mean value over these points) was computed (Figure 3.11), confirming that the spatial variability of sea level change close the Portuguese coast is very weak. The highest anomalies do not exceed 0.04 m, representing a maximum of 6% of the mean sea level change. According this, the mean sea level change at the Portuguese coast can be considered as the mean value of the grid points under analysis.

Figure 3.12 presents the local and the global mean sea level change for each RCP scenario. Results point for a MSLR of 0.40 m, 0.47 m, 0.48 m and 0.63 m for scenarios RCP 2.6, RCP 4.5, RCP 6.0 and RCP 8.5, respectively. The results also show that both global and local mean sea level change estimates are quite similar, however the uncertainty of local projections is considerably higher than the global estimates. In summary, the projections obtained here point for a rise in the order of 0.45 m, for RCP 2.6, RCP 4.5 and RCP 6.0 and a most pessimist one of 0.63 m, for RCP 8.5. It can therefore be concluded that the local projections obtained now are broadly similar

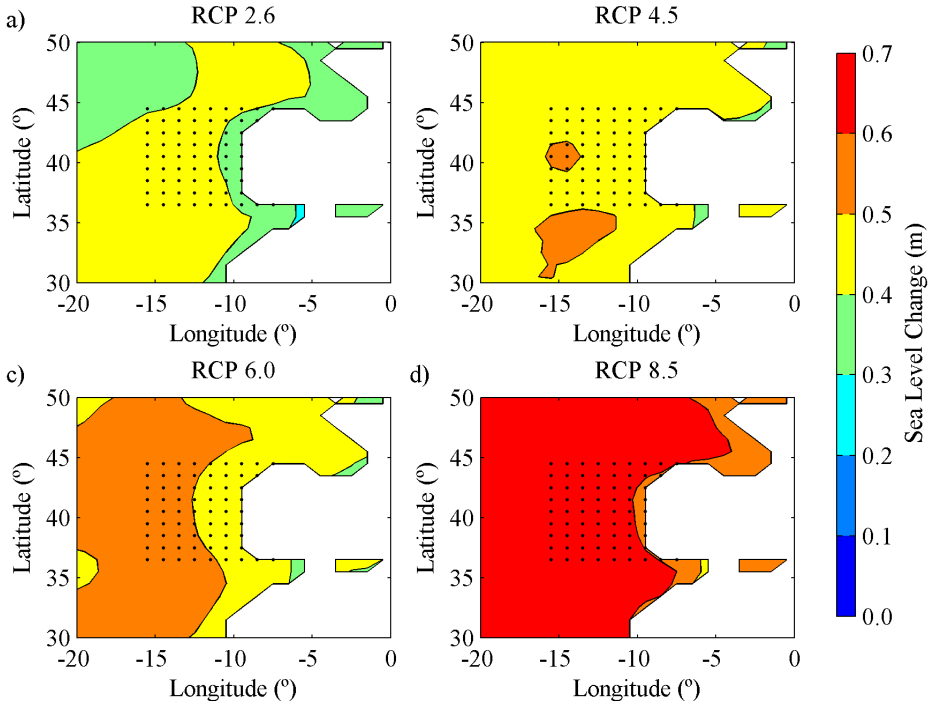


Figure 3.10: Sea level change (m) around the Portuguese coast during 2081-2100, relative the 1986-2005 for: a) RCP 2.6, b) RCP 4.5, c) RCP 6.0 and d) RCP 8.5.

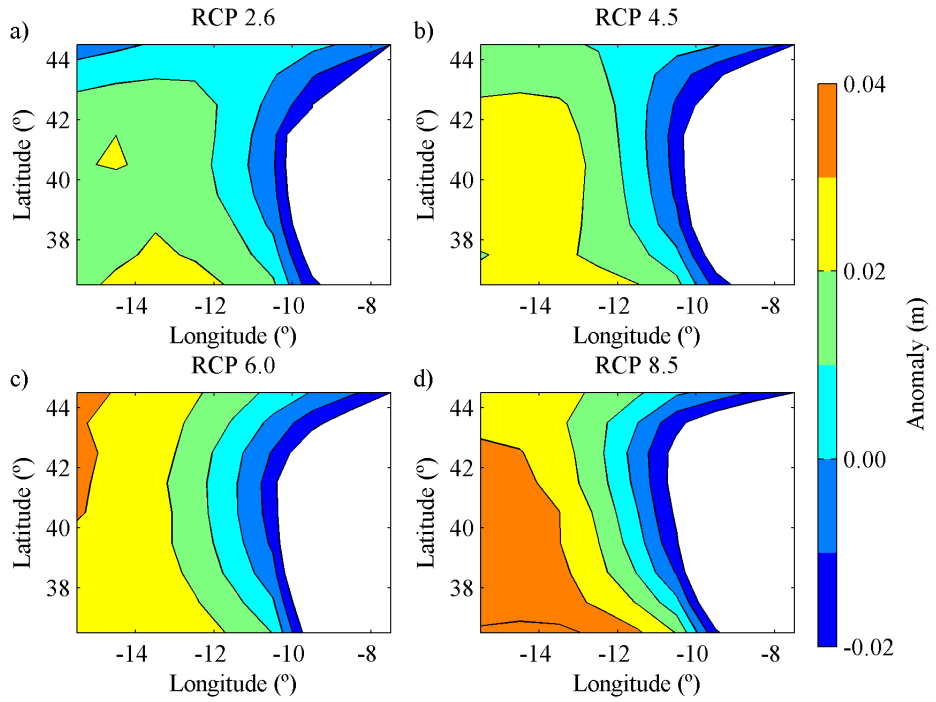


Figure 3.11: Sea level change anomaly (m) around the Portuguese coast during 2081-2100, relative the 1986-2005 for: a) RCP 2.6, b) RCP 4.5, c) RCP 6.0 and d) RCP 8.5.

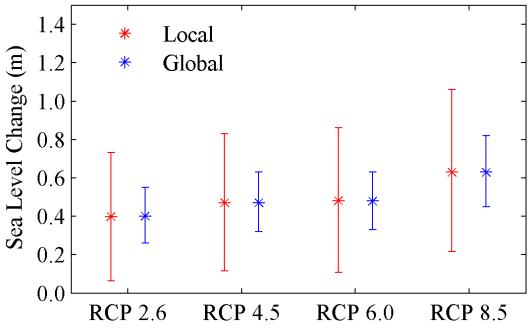


Figure 3.12: Local an global sea level change (m) estimates under RCP 2.6, RCP 4.5, RCP 6.0 and RCP 8.5.

to the 0.42 m projection obtained by Lopes et al. [2011] using the 4$^{th}$ IPCC report. Attending this, and to be coherent with the other forcing changes considered in this study (that are supported on the 4$^{th}$ IPCC report), it is assumed hereafter the 0.42 m local projection.

### 3.3.3 Waves

The oceanic wave regime representative of present and future climates was determined following the steps below. Initially, the wave period, the wave height and the wave direction were grouped in classes and the percentage of occurrence was determined for the 30 years data and for each year. After that, the correlation coefficient between each year and the respective climate was computed for each parameter frequency distribution (Figures 3.13a and 3.13b). The correlation coefficients are higher than 0.84, revealing a good correlation between a single year and the respective climate. However, the three wave parameters should be compared simultaneously in order to determine the year representative of each climate. Considering that the perfect adjustment between a year and the respective climate matches a correlation coefficient of 1 for the three parameters, the deviation ($d$) between each year and the perfect adjustment was computed through the equation 3.2:

$$d = \sqrt{(1 - c_{H_s})^2 + (1 - c_T)^2 + (1 - c_\theta)^2} \tag{3.2}$$

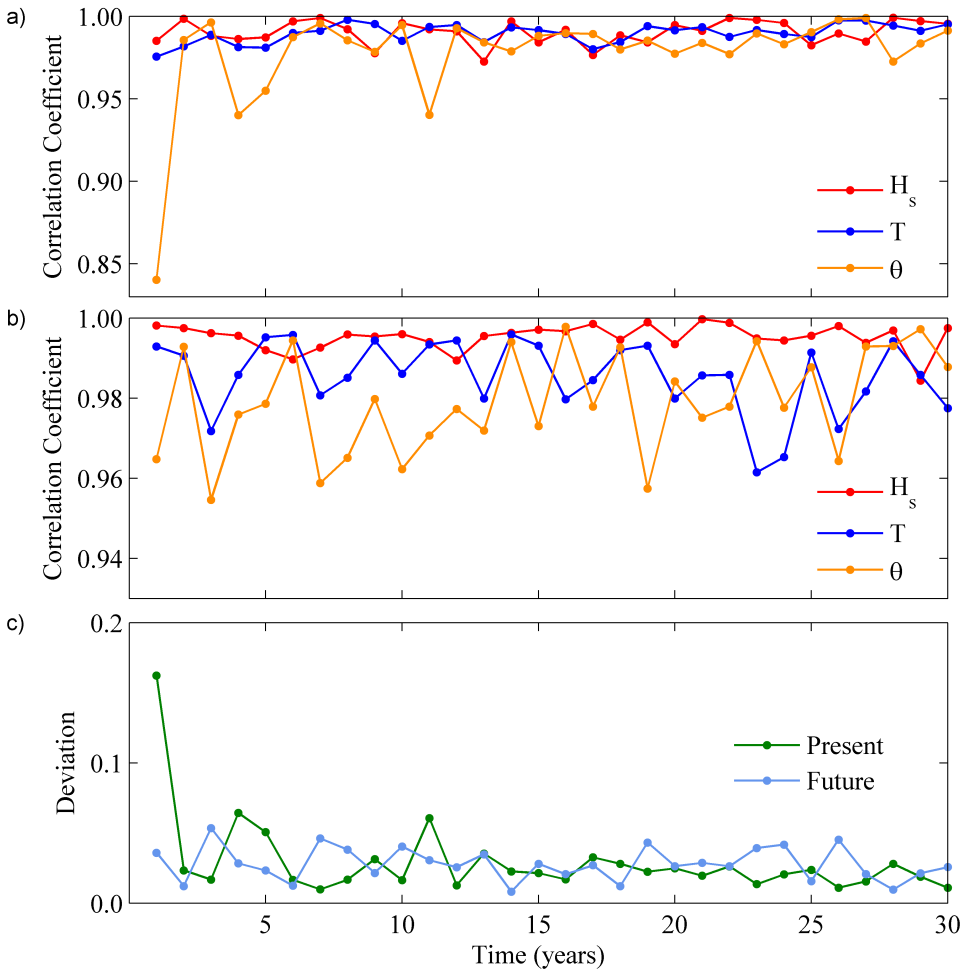


Figure 3.13: Correlation coefficient of significant wave height ($H_s$), wave period ($T$) and wave direction ($\theta$) between each year and 30 years for: a) Present climate; b) Future climate. c) Deviation between each year and the perfect adjustment for present and future climates.

where $c_{H_s}$, $c_T$ and $c_\theta$ are the correlation coefficients of significant wave height, wave period and wave direction, respectively. The deviation values for each climate are presented in the Figure 3.13c). The years 1977 and 2084 present the lowest deviations, 0.01 and 0.008 respectively, being considered representatives of each climate. Also, the deviation between the 1977 and 2084 climates is 0.0674, which is considerably higher than the deviations obtained previously. In this way, it is concluded that the analysis performed here is adequate to determine the representative year of the present and future wave regimes.

Once the 1977 and 2084 years are considered representative of the present and future

wave regimes, the distribution of significant wave height, wave direction and wave period of the years 1977 and 2084 were analysed (Figure 3.14) in order to characterize each climate. For the present climate, 38.5% of waves present a significant height between 0.5 m and 1.5 m. The classes 1.5-2.5 m, 2.5-3.5 m and 3.5-4.5 m present an occurrence of 35.3%, 15% and 7.9%, respectively. The occurrence of waves higher than 4.5 m height is 3.0%. Concerning the period, approximately 54% of the waves have period between 7 and 10 s. The occurrence of waves with period lower than 7 s and higher than 10 s is 22.5% and 23.5%, respectively. The waves arrive predominantly from the NW and NNW directions, presenting 34.1% and 32.1% of the occurrences, respectively. These results are in agreement with Coelho [2005] and Vaz [2012], that

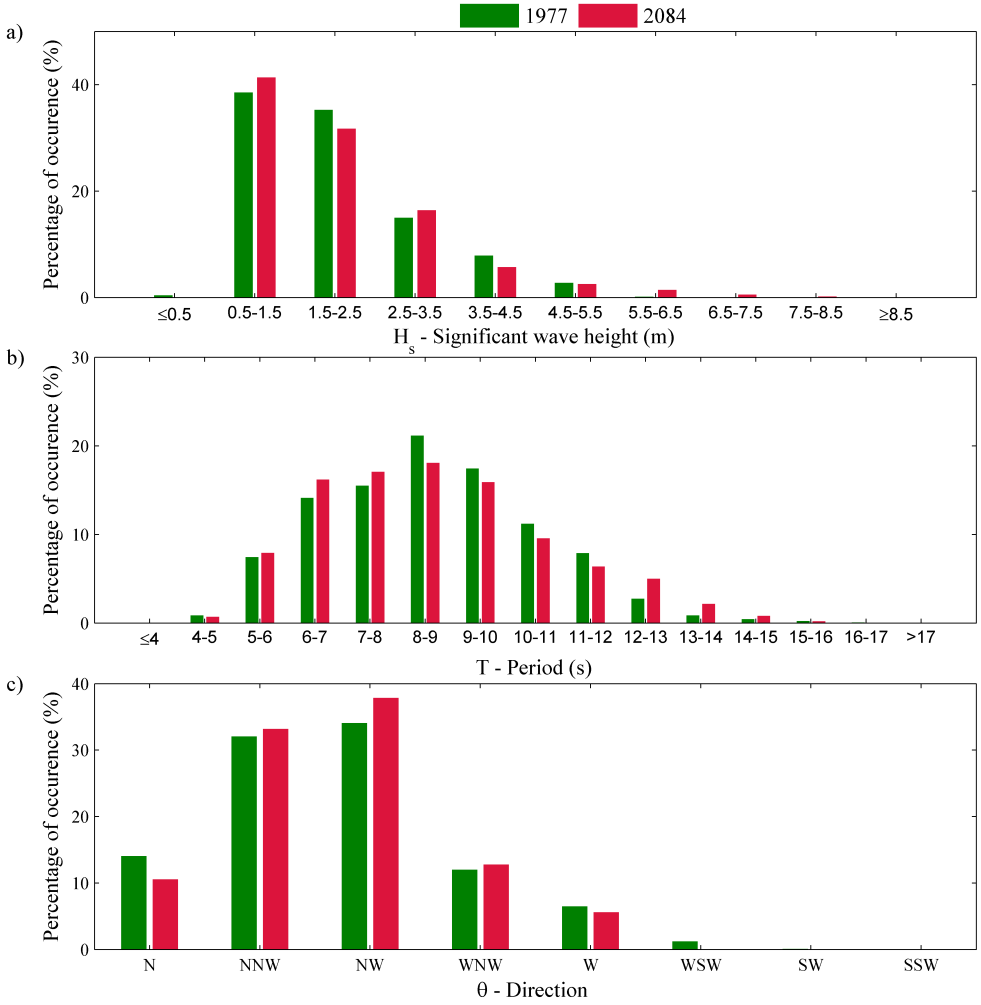


Figure 3.14: Percentage of occurrence of: a) significant wave height ($H_s$); b) wave period ($T$) and c) wave direction ($\theta$).

characterized the wave regime statistically analysing the wave data recorded at the buoys of Leixões between 1993 and 2003 and Figueira da Foz between 1984 and 1996, respectively. The major difference found is related with the wave direction. Indeed, this study evidenced that approximately 14% of the waves propagate from N, while the previous studies were not identified waves propagating from N. This disagreement can be a limitation of the wave model or can be related with the coastline configuration and the different geographic position of data under analysis. Indeed, the WW3 point is located offshore the buoys and therefore is exposed to the waves propagating from N direction (see Figure 3.3).

To distinguish the oceanic wave regimes of 1977 and 2084, the difference between the percentage of occurrence of 2084 and 1977 wave parameters was computed (Figure 3.15). Several differences between the distribution of wave heights were found, however was undetected any remarkable tendency of change. Concerning the wave period, the results evidence that the percentage of occurrence of waves with periods between $]8-12]$ s decreases 7.5% in the future, while waves with periods $\leq 8$ s and $> 12$ s increase 4% and 3.8%, respectively. Regarding the direction, and ignoring the northward waves (once they can result from model limitations), a decrease of waves propagating from W and WSW was found. To compensate this decrease a large number of waves propagating from NNW, NW and WNW are expected in the future, indicating a clockwise rotation of future wave regime.

Figure 3.16 represents the wave period in function of the wave height and the wave direction in function of the wave height for each wave regime. This evidences higher percentage of waves with higher period and significant height for the future, relative to the present climate. Also, higher percentage of waves of NW/high significant height for the future climate are predicted.

These results are in agreement with Andrade et al. [2006] and Dodet et al. [2010] works. Andrade et al. [2006] applied the wave model MAR3G to the Atlantic Ocean and found for the Portuguese coast only minor changes in the wave significant height and a clockwise rotation between 5° to 15° in the future wave regime direction, relative to the present. Recently, Dodet et al. [2010] analysed past trends in time series of wave parameters in the North-East Atlantic Ocean between 1953 and 2009. They found a

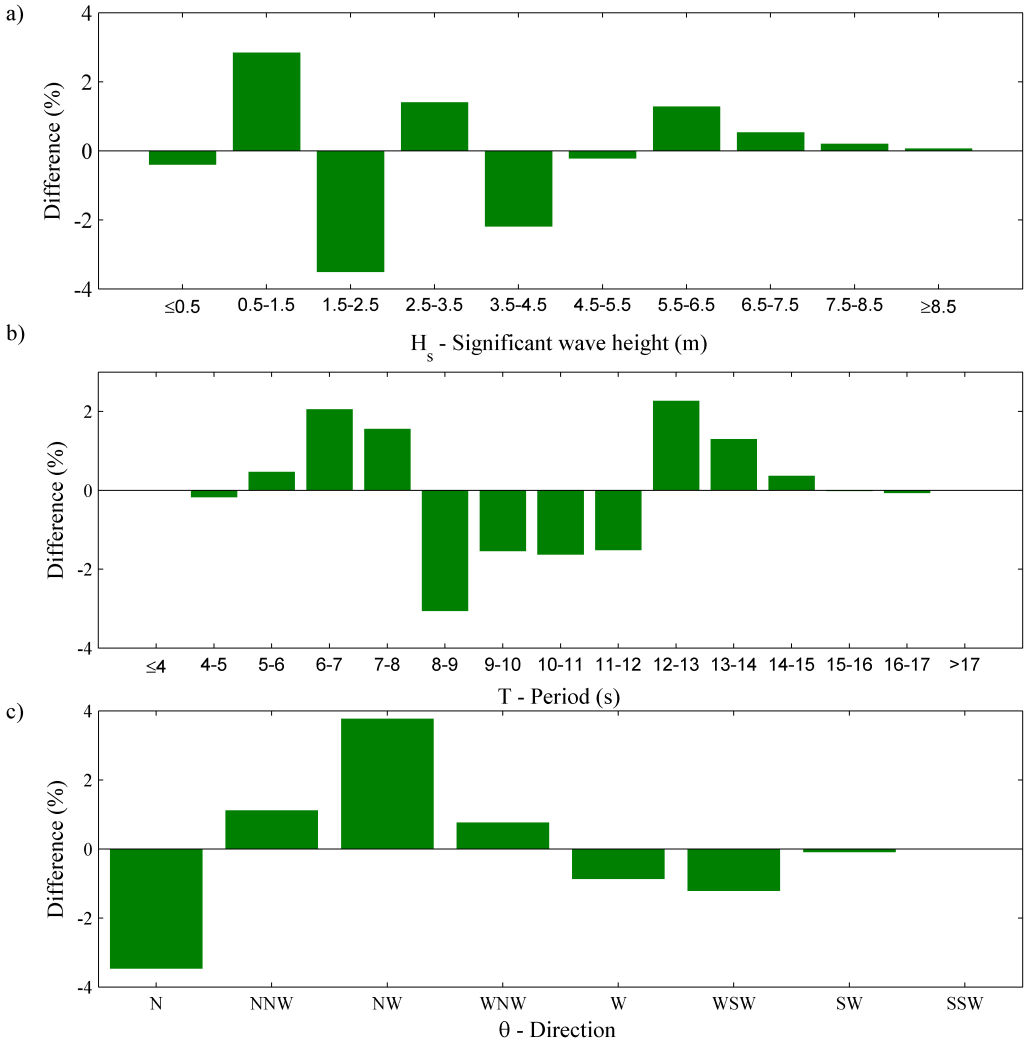


Figure 3.15: Difference between future and present climates of: a) significant wave height; b) wave period and c) wave direction.

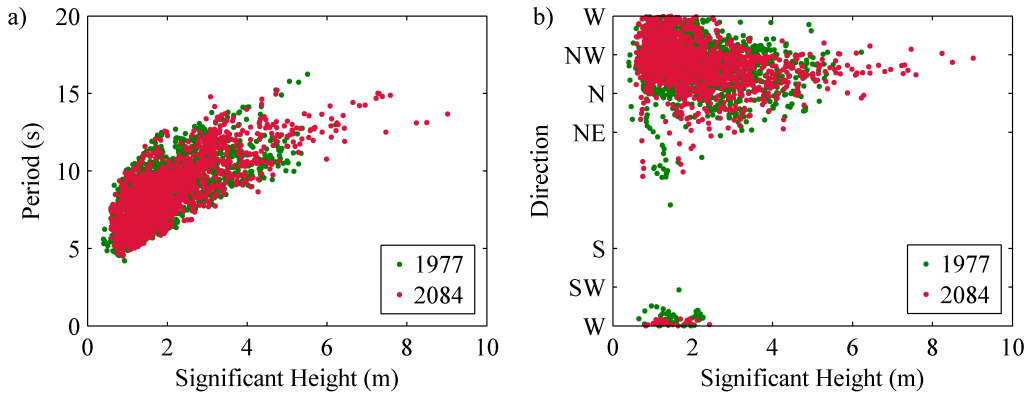


Figure 3.16: a) Wave period in function of significant wave height; b) Wave direction in function of significant wave height.

negligible increase in significant wave height (≈0.002 m/year) and a clockwise rotation of the winter waves of about 0.05°/year and of summer waves of 0.002°/year.

### 3.3.4 Fluvial discharges

The daily mean discharges predicted by SWAT and SWIM models over 1931-2010 and 1981-2010, respectively, when forced with observed precipitation were used to calculate the peak discharge for 2, 10, 25, 50 and 100 years return periods, for each one of the five tributaries. For each database, the annual maximum discharges were identified and the respective empirical CDF was determined through Kaplan and Meier [1958]. Also, the annual maximum discharges were fitted to GEV, Gamma, Log-n, Exponential, Gumbel and Weibull distributions. The best distribution fit was determined by performing a chi-square goodness-of-fit test, Kolmogorov-Smirnov goodness-of-fit hypothesis test and by computing the deviation between the empirical and the theoretical distributions.

The best fit distribution was used to estimate the peak discharge (Table 3.3). Results highlight that Vouga discharge is considerably higher than the other tributary discharges. Oppositely, the Boco discharge is the lowest source of freshwater into the lagoon.

It is clear that the two databases generate very different peak discharges. Indeed, the SWIM peak discharges are lower than the SWAT discharges for all tributaries. Moreover, in some cases, the SWAT estimates are more than twice the SWIM discharges. The underestimation of SWIM peak discharges had already been found by Stefanova et al. [2015].

In summary, the peak discharge projections present great variability and it is almost impossible to determine the best database available given the inexistence of permanent monitoring of fluvial discharges into the lagoon. Despite this, the PLRA [2011b] estimated peak discharges at the 5 main tributaries (Table 3.3), by using observed precipitation data. Accordingly, the maximum annual precipitation was fit to statistical distributions and derived in river discharge, by using an hydrologic modelling system. Again, it is evident the great variability between the PLRA [2011b] estimates and those obtained here. Even so, SWAT estimations fit better to the PLRA [2011b] estimations

Table 3.3: Peak discharge ($m^3/s$) for the present climate at the Ria de Aveiro tributaries.

| | | 2 | 10 | 25 | 50 | 100 |
|---|---|---|---|---|---|---|
| Vouga | SWAT | 797 | 1302 | 1559 | 1750 | 1943 |
| | SWIM | 264 | 368 | 413 | 444 | 473 |
| | PLRA [2011b] | 374 | 1050 | - | 1845 | 2241 |
| Antuã | SWAT | 106 | 173 | 203 | 225 | 245 |
| | SWIM | 36 | 49 | 54 | 58 | 61 |
| | PLRA [2011b] | 89 | 185 | - | 276 | 318 |
| Cáster | SWAT | 47 | 78 | 94 | 106 | 118 |
| | SWIM | 13 | 18 | 19 | 20 | 21 |
| | PLRA [2011b] | 69 | 137 | - | 200 | 227 |
| Boco | SWAT | 33 | 63 | 81 | 94 | 108 |
| | SWIM | 12 | 18 | 19 | 21 | 22 |
| | PLRA [2011b] | 12 | 36 | - | 64 | 77 |
| Ribeira dos Moínhos | SWAT | 113 | 221 | 283 | 331 | 381 |
| | SWIM | 26 | 37 | 42 | 45 | 49 |
| | PLRA [2011b] | 26 | 80 | - | 139 | 167 |

for Vouga and Antuã, which are the most important sources of freshwater into the lagoon.

Therefore, it is considered that the SWAT discharges are more reliable than the SWIM discharges. Moreover, this study aims to assess flood risk under high river discharges, and SWIM model underestimates the high peak discharges [Stefanova et al., 2015].

In this way, only the SWAT output was analysed for the future climate (2071-2100). Making a similar statistical analysis peak discharges for 2, 10, 25, 50 and 100 years return periods were obtained, for the future climate (Table 3.4). Results highlight that the peak discharges tend to decrease under climate change conditions. Particularly, for the Vouga river, it is expected a reduction between 24% and 40% in peak discharges. The decrease rates expected for the remaining tributaries range between 55% and 70%.

The results obtained here are in agreement with Cunha et al. [2006]. Those authors found a reduction by 50% in the Vouga discharges during winter, considering the SRES A2. Contrarily, considering the scenario B2, they found and a tendency to increase Vouga discharges by 20%.

## 3.4 Conclusions

This chapter presented a characterization of Ria de Aveiro driving forcing for present and future climates. This research revealed that tides are the forcing that drives highest sea level variations (between 0.46 m and 3.52 m). Also, the tide experienced significant modifications between 1976 and 2013. The amplitude of $M_2$ constituent increased at a rate of 2.8 mm/year between 1976 and 2013.

The analysis of the storm surge events revealed that the average height is 0.43 m, however the most extreme events can reach more than 1 m height. Moreover, the most intense storm surge events do not always induce extreme sea levels, once extreme sea levels depend also on the tidal level. The joint probability analysis between tides and storm surges highlighted that extreme sea levels at the lagoon entrance range from 3.85 to 4.56 m, for return periods of 2 and 100 years, respectively.

Also, were not found significant evidences that climate changes will modify tidal and storm surge levels in the Ria de Aveiro adjacent coast.

The mean sea level analysis evidenced an increase at a rate of 2.2 mm/year between 1976 and 2013 at the lagoon mouth. It is very likely that mean sea level will rise in the Portuguese coast under climate change conditions. The results evidence that the

Table 3.4: Peak discharge ($m^3/s$) for the future climate at Ria de Aveiro tributaries.

| | 2 | 10 | 25 | 50 | 100 |
|---|---|---|---|---|---|
| Vouga | 494 | 955 | 1175 | 1333 | 1485 |
| Antuã | 39 | 73 | 88 | 100 | 110 |
| Cáster | 17 | 32 | 39 | 44 | 49 |
| Boco | 8 | 19 | 25 | 31 | 37 |
| Ribeira dos Moínhos | 33 | 73 | 98 | 119 | 141 |

local mean sea level change derived from the data of 5$^{th}$ IPCC report (0.45 m) is quite similar to the local estimate obtained by Lopes et al. [2011] taking into account data of the 4$^{th}$ IPCC report (0.42 m).

The wind generated waves play a minor contribution to lagoon water levels, however they can be important factors driving the inlet morphodynamics. The waves arrive predominantly from NW and NNW directions with significant height ranging between 0.5 and 2.5 m. It was found a clockwise rotation of wave regime under climate change conditions, which can modify the inlet morphodynamics.

Regarding fluvial discharges, the Vouga and Antuã rivers present the highest peak discharges inflowing the lagoon. It was found that the Vouga peak discharge range between 797 $m^3/s$ and 1943 $m^3/s$, for 2 and 100 years return periods, respectively. Also, the peak river discharges tend to decrease under climate change conditions, with higher rates for the smaller tributaries.

# Chapter 4

# Numerical models

## 4.1 Introduction

The hydrodynamic models simulate the water flow in coastal environments, solving the fluids physics laws through computational numerical techniques. The use of these models has increased over the years, once their ability to describe the physical processes affecting coastal hazards. Often, the hydrodynamic models are coupled to other models (e.g. atmospheric, sediment transport, ecological, oil weathering, etc.) to predict coastal hazards, such inundation caused during storms, silting and erosion, eutrophication and dispersion of oils and pollutants. Nowadays, they are recognized as important tools on supporting the management of coastal areas [Plate, 2002; Neves, 2007; Balica et al., 2013].

The use of numerical models to study inundation in coastal systems is increasing, to fill the insufficient monitoring and to provide detailed flood mapping, essential to support flood risk management.

This chapter describes the numerical models used to reproduce the lagoon hydrodynamics (ELCIRC) and the inlet morphodynamics (MORSYS2D). Besides the general description, details of models set up, calibration and validation are presented.

## 4.2 ELCIRC model

The hydrodynamic model ELCIRC uses a finite-volume/ finite difference Eulerian-Lagrangian algorithm to solve the shallow waters equations, in order to realistically address a wide range of physical processes [Zhang et al., 2004]. In this study the ELCIRC model was applied to the Ria de Aveiro lagoon in barotropic mode and with a single vertical layer, once Ria de Aveiro can be considered vertically homogeneous. In this case, the model solves the depth-integrated momentum and conservation of mass equations:

$$\frac{\partial \eta}{\partial t} + \frac{\partial [HU]}{\partial x} + \frac{\partial [HV]}{\partial y} = 0 \tag{4.1}$$

$$\frac{\partial U}{\partial t} + U\frac{\partial U}{\partial x} + V\frac{\partial U}{\partial y} = fV - g\frac{\partial \eta}{\partial x} - \frac{\tau_x}{\rho} + \epsilon\left(\frac{\partial^2 U}{\partial x^2} + \frac{\partial^2 U}{\partial y^2}\right) \tag{4.2}$$

$$\frac{\partial V}{\partial t} + U\frac{\partial V}{\partial x} + V\frac{\partial V}{\partial y} = -fU - g\frac{\partial \eta}{\partial y} - \frac{\tau_y}{\rho} + \epsilon\left(\frac{\partial^2 V}{\partial x^2} + \frac{\partial^2 V}{\partial y^2}\right) \tag{4.3}$$

Where $H$ is the total water depth, $\eta$ is the surface water elevation, $U$ and $V$ are the depth averaged velocity components in the $x$ (eastward) and $y$ (northward) directions, $t$ is the time, $f$ is the Coriolis parameter, $g$ is the acceleration of gravity, $\rho$ is the water density, $\epsilon$ is the horizontal eddy viscosity and $\tau_x$ and $\tau_y$ are the bottom stress in $x$ and $y$ directions, respectively, given by:

$$\tau_x = \rho C_D \sqrt{U^2 + V^2} U \tag{4.4}$$

$$\tau_y = \rho C_D \sqrt{U^2 + V^2} V \tag{4.5}$$

Where, $C_D$ is the drag coefficient, which is computed by:

$$C_D = g^2 n H^{-\frac{1}{3}} \tag{4.6}$$

Where $n$ is the Manning coefficient. The Eulerian-Lagrangian method avoids potential

instability problems once allows Courant numbers ($C_u$) higher than the unity:

$$C_u = 2u\frac{\Delta t}{\Delta x} \tag{4.7}$$

Where, $\Delta t$ is the time step, $\Delta x$ the element-size and $u$ the magnitude of velocity. The numerical algorithm is volume conservative and incorporates wetting and drying in order to represent accurately the hydrodynamics of intertidal areas and marginal areas during inundation events. After computing the surface water elevation the nodes are dry if $H < 0.01$ m.

The ELCIRC uses unstructured grids in the horizontal, with combinations of triangles and quadrangles. Unstructured grids provide much better representation of complex boundaries such as coastlines and areas around islands than do conventional regular grids and also provide the opportunity to concentrate mesh resolution in areas of interest. This feature is particularly important in describing the hydrodynamics of geomorphological complex estuarine systems that present irregular coastlines and/or strong bathymetry variations. Furthermore, these grids are particularly accurate to simulate the flood extension, and are therefore being used in flood mapping studies. Several applications aiming to study inundation using unstructured grids were found for UNTRIM, FVCOM, TINFLOOD, SELFE and ELCIRC models [Shen et al., 2006a,b; Gong et al., 2009; Kuiry et al., 2010; Bertin et al., 2012; Fortunato et al., 2013; Wang et al., 2014; Chen et al., 2015; Guerreiro et al., 2015].

### 4.2.1 Ria de Aveiro implementation

#### 4.2.1.1 Numerical grid

The ELCIRC application used in this study was developed from a previous implementation for Ria de Aveiro by Picado et al. [2010]. This was improved by including in the former numerical grid a larger area of intertidal regions, the lagoon margins and the existing protection structures, as well as refining some channels (Figure 4.1a). The intertidal regions were constructed manually due to the difficulty to link channels of reduced width to the surroundings. In these zones the mesh is irregular,

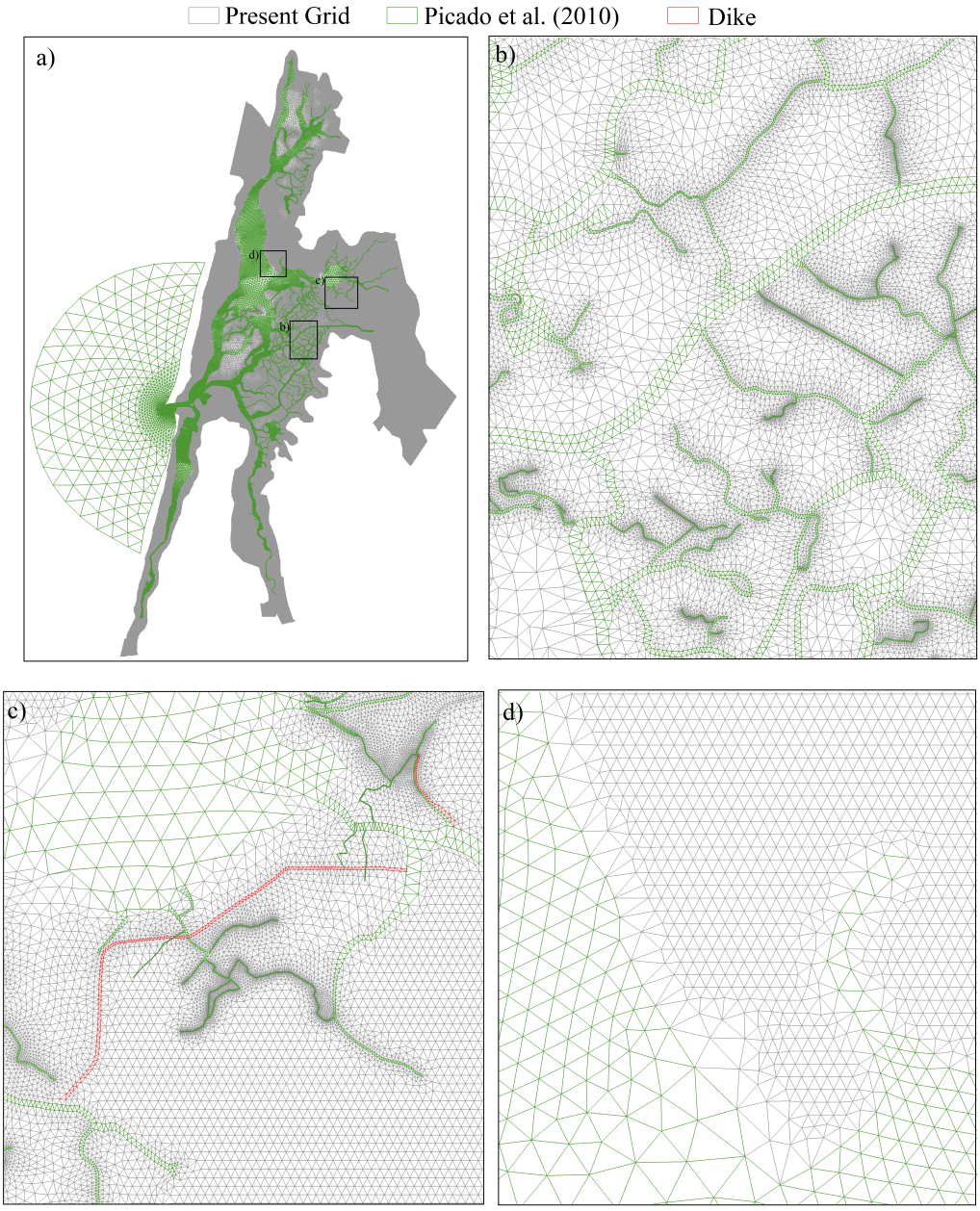


Figure 4.1: ELCIRC numerical grid for Ria de Aveiro: a) Entire domain; b) Detail of intertidal areas; c) Detail of BVL dike; d) Detail of marginal areas.

increasing its resolution toward the lagoon channels (Figure 4.1b). The BVL dike was also included (Figure 4.1c), given its importance on controlling the saltwater intrusion in the BVL region. Furthermore, the main rivers which drain in the lagoon were extended to the limit of tidal influence. The margins were constructed automatically linking the channels to a regular mesh which consists in isosceles triangles (Figure 4.1d). The present configuration presents 219722 nodes and 437912 elements, while the mesh

grid developed by Picado et al. [2010] presents 71996 nodes and 94352 elements. The final horizontal grid resolution is variable. At the continental shelf ranges from 100 m at the lagoon mouth to 1400 m offshore. A finer grid is implemented at the lagoon main channels, which resolution ranges from 10 to 120 m. Furthermore, the resolution at the narrowest channels can achieve 1 or 2 m. The resolution of lagoon margins was set almost constant, approximately 50 m.

#### 4.2.1.2 Field data

A hydrodynamic model requires detailed topo-hydrographic data of the study area in order to build the digital terrain model, as well as SSE data measured along the time at different stations to calibrate and validate the model. Figure 4.2a presents the spatial extension of the topo-bathymetric surveys available for this work.

Concerning the topography the surveys include:

- lagoon adjacent regions data obtained in 1987/88 by the IH, with vertical accuracy of 1 m;

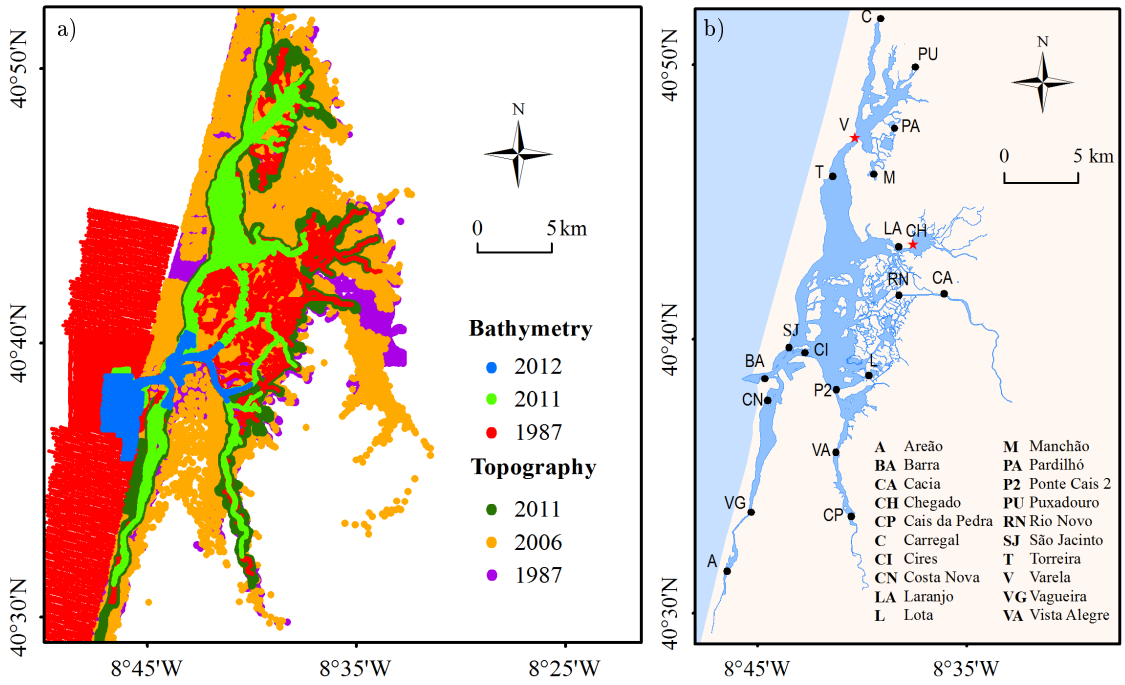


Figure 4.2: a) Topo-bathymetric data used to construct the digital elevation model of Ria de Aveiro; b) Location of lagoon water level stations (stations represented by black dots were used in the model calibration).

- lagoon adjacent regions data obtained in 2006 by the Intermunicipality Community for Ria de Aveiro (CIRA), with vertical accuracy of 0.1 m and horizontal resolution ranging from 50 to 300 m;
- main channels margins data obtained in 2011 by Polis, with horizontal resolution varying from 10 to 100 m;

Regarding bathymetry, data from several bathymetric surveys are available:

- A general lagoon survey performed in 1987 by IH;
- Inlet region and lagoon main channels survey, performed in 2011 by Polis;
- Inlet region survey performed in 2012 by APA.

Concerning SSE, there is available data at the stations represented in Figure 4.2b, that were collected in:

- 1987/88 at 18 stations (A, BA, CA, CP, C, CI, CN, LA, L, M, PA, P2, PU, RN, SJ, T, VG, VA), recorded over 30 to 50 days;
- 2002/03 at 18 stations (BA, CA, CP, C, CI, CN, LA, L, M, PA, P2, PU, RN, SJ, T, V, VG, VA), recorded over 30 days to 9 months;
- 2012 at 6 stations (BA, CH, RN, V, VG, and VA), recorded over 9 months;
- 2013 at 7 stations (BA, CH, CN, RN, V, VG, and VA), recorded over 12 months;

Given the important geomorphological changes occurred between 1987 and 2012 (described in Chapter 2), there was a need to construct different numerical domains in order to simulate the hydrodynamic conditions generated by different geomorphological configurations. Details of numerical domains will be defined in the next sections, as well as the hydrographic data used to calibrate and validate the model.

### 4.2.2 Model calibration

The model calibration consists of using site specific information from a period of time and to adjust model free parameters in the governing equations (e.g. bottom

friction coefficient) in order to obtain the best agreement possible between measured data and model predictions for state variables [Hayter and Gailani, 2014]. Attending this, and considering the topo-hydrographic data available, the model calibration was made using the most recent data available.

#### 4.2.2.1 Methodology

As there are no recent topo-bathymetric data covering the entire region under research, the digital terrain model was constructed by aggregating data from different surveys, using the more recent data whenever there was overlapping of surveyed areas. Accordingly, the numerical bathymetry used corresponds to the bathymetry surveyed in 2011, except at the inner and narrow channels and at the continental shelf, where the only available bathymetric data are from 1987 (Figure 4.2a). At the inlet region the bathymetric data collected in 2012, was taken into account (Figure 4.2a). Regarding topography, all the data collected in 2011 and 2006 was aggregated and used, while the 1987/88 data was used only in restricted areas to fill some gaps. The numerical digital terrain model is represented in Figure 4.3, where it is evident the shallow bathymetry for most of the channels and the flat topography of the marginal areas.

Regarding SSE, the data measured in 1987/88 was discarded for calibration, once the numerical bathymetry used considers updates that changed considerably the bathymetry surveyed in 1987. Among the more recent SSE surveys, the one performed in 2002/03 covers most of the lagoon area, while SSE of 2012 and 2013 concerns only restricted areas. Therefore, it was decided to perform model calibration with 2002/03 data. As discussed in Chapter 2, the major bathymetric changes occurred before the hydrographic campaigns of 2002/03, in the eighties after the extension of the northern breakwater and in the nineties motivated by dredging operations carried out in the lagoon main channels. Therefore, it is assumed that the numerical configuration constructed here is closer to the lagoon configuration in 2002/03.

To reproduce the 2002/03 periods where SSE data were available the model was forced at the oceanic boundary by eleven harmonic constituents ($M_{Sf}$, $O_1$, $K_1$, $Q_1$,$N_2$, $M_2$, $S_2$, $M_4$, $MN_4$, $MS_4$ and $M_6$) taken from the regional model developed by Fortunato et al. [2002] and adopts the local mean sea level determined for the Barra tide gauge

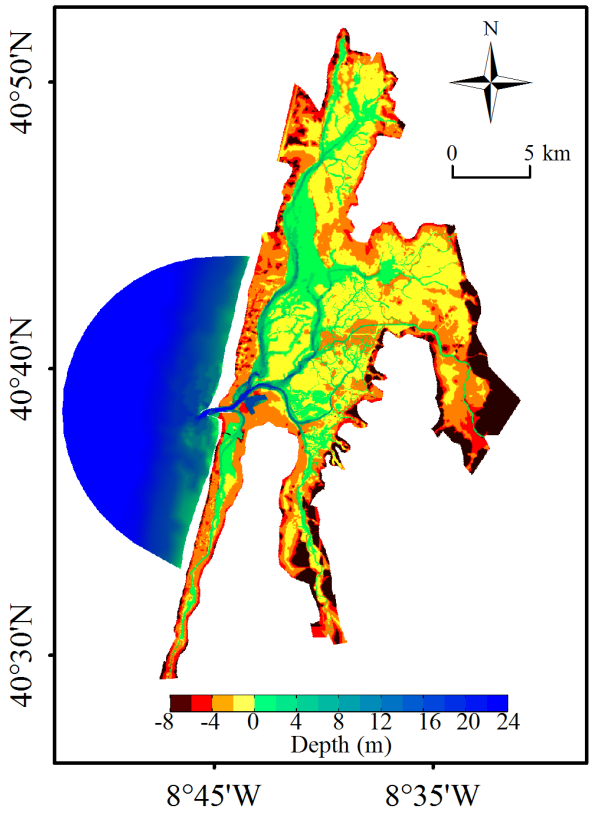


Figure 4.3: Ria de Aveiro digital terrain model.

for the present, following Picado et al. [2010]. The freshwater input was set constant during the simulation and mean fluvial discharges were attributed according to Génio et al. [2008] for the five lagoon tributaries (80 $m^3/s$, 20 $m^3/s$, 5 $m^3/s$, 10 $m^3/s$ and 5 $m^3/s$ for Vouga, Antuã, Boco, Ribeira dos Moínhos and Cáster, respectively). The wind effects were neglected, considering its minor importance in the establishment of lagoon water levels comparing to tidal forcing [Dias, 2001; Fortunato et al., 2013].

A large number of simulations were performed to improve the model accuracy in reproducing the tidal propagation in Ria de Aveiro, by comparing model predictions and 2002/03 observations of SSE, and changing the Manning coefficients, which define the bottom friction. It was considered that the Manning coefficient is dependent on lagoon channels depth, as followed in Dias and Lopes [2006] and Picado et al. [2010] studies. Therefore, the Manning coefficients established by Picado et al. [2010] for the lagoon channels were modified (Table 4.1), in order to guarantee that model predictions reproduce accurately the field data. At the lagoon margins the Manning coefficients

Table 4.1: Manning coefficients for the lagoon channels as function of depth ($h$).

| Depth (m) | Manning Coefficient |
|---|---|
| $-1.0 \leq h < -0.5$ | 0.028 |
| $-0.5 \leq h < 0.0$ | 0.026 |
| $0.0 \leq h < 0.5$ | 0.024 |
| $0.5 \leq h < 1.0$ | 0.022 |
| $1.0 \leq h < 3.0$ | 0.018 |
| $3.0 \leq h < 6.0$ | 0.016 |
| $6.0 \leq h < 10.0$ | 0.015 |
| $h \geq 10$ | 0.014 |

are dependent on Corine Land Cover data set of 2006 [EEA, 2007] (Figure 4.4), and were attributed according to Bunya et al. [2010] study (Table 4.2).

The eddy viscosity was neglected, as the horizontal grid resolution is considered sufficient to resolve the relevant scales, as suggested by Picado et al. [2010]. The model was running for 30 days with a time step of 90 s, following the Picado et al. [2010] study.

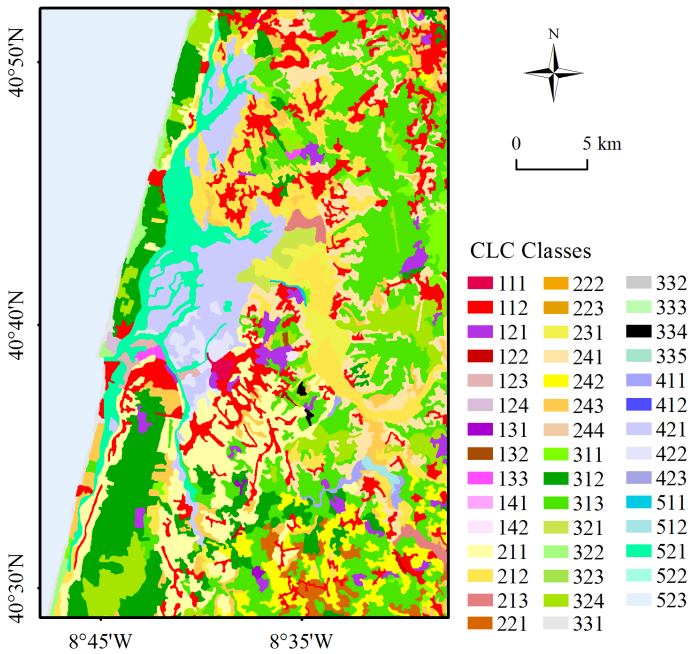


Figure 4.4: CORINE Land Cover classes for Ria de Aveiro adjacent area.

Table 4.2: Manning coefficients for marginal areas as function of CORINE Land Cover.

| CLC | Manning Coefficient | CLC | Manning Coefficient |
|---|---|---|---|
| 111 | 0.1205 | 242 | 0.0375 |
| 112 | 0.1200 | 243 | 0.0375 |
| 121 | 0.0850 | 311 | 0.1600 |
| 122 | 0.0850 | 312 | 0.1700 |
| 123 | 0.0850 | 313 | 0.1650 |
| 124 | 0.0850 | 321 | 0.0350 |
| 132 | 0.0400 | 322 | 0.0700 |
| 133 | 0.0900 | 324 | 0.0700 |
| 142 | 0.0600 | 331 | 0.0400 |
| 211 | 0.0375 | 334 | 0.0400 |
| 212 | 0.0375 | 411 | 0.0450 |
| 213 | 0.0350 | 422 | 0.0350 |
| 231 | 0.0400 | 511 | 0.0225 |
| 241 | 0.0375 | 521 | 0.0225 |

The ability of ELCIRC model to reproduce the propagation of the tidal wave along Ria de Aveiro was first evaluated visually, by comparing the predicted and observed time series of SSE. The low frequency signal was removed from both observed and predicted datasets, using a cut-off frequency of 0.0000093 Hz (30 h).

Model accuracy was quantified by computing for each station the root mean square error ($RMSE$) and predictive $Skill$ values, following equations 4.8 and 4.9, respectively:

$$RMSE = \sqrt{\frac{1}{N}\sum_{i=1}^{N}\left(\eta_{o_i} - \eta_{p_i}\right)^2} \tag{4.8}$$

$$Skill = 1 - \frac{\sum_{i=1}^{N}\left|\eta_{p_i} - \eta_{o_i}\right|^2}{\sum_{i=1}^{N}\left[\left|\eta_{p_i} - \overline{\eta_o}\right| + \left|\eta_{o_i} - \overline{\eta_o}\right|\right]^2} \tag{4.9}$$

$N$ is the length of SSE datasets, $\eta_o$ and $\eta_p$ are the observed and predicted SSE. The

over-bar represents the time average. Also, the percentage of $RMSE$ relative to the mean local amplitude was assessed ($\Delta Error$).

The adjustment between observed and predicted elevations was also quantified through Taylor diagrams. Besides the SSE data measured in 2002/03, this analysis includes the SSE data collected in 2012 and 2013 campaigns in order to prove that the model reproduces accurately the most recent SSE data. As discussed previously, the configuration Taylor [2001] constructed a theory based on the cosines law and developed a diagram that provides a concise statistical summary of how well observed patterns match in a model. This diagram has been used recently to assess the performance of hydrodynamic models [Venkatram, 2008; Mendicino and Senatore, 2013]. The Taylor diagrams depict the normalized standard deviations observed and predicted ($NSD_o$ and $NSD_p$, respectively), the root-mean-square differences ($RMSD$), and the correlation coefficients ($CC$) between predicted and observed SSE, that were computed following equations 4.10, 4.11, 4.12 and 4.13:

$$NSD_o = \sqrt{\frac{\sum_{i=1}^{N} (\eta_{o_i} - \overline{\eta_o})}{N}} \tag{4.10}$$

$$NSD_p = \sqrt{\frac{\sum_{i=1}^{N} (\eta_{p_i} - \overline{\eta_p})}{N}} \tag{4.11}$$

$$RMSD = \sqrt{\frac{\sum_{i=1}^{N} \left[(\eta_{p_i} - \overline{\eta_p}) - (\eta_{o_i} - \overline{\eta_o})\right]^2}{N}} \tag{4.12}$$

$$CC = \frac{\sum_{i=1}^{N} \left[(\eta_{p_i} - \overline{\eta_p})\,(\eta_{o_i} - \overline{\eta_o})\right]}{N \times NSD_o \times NSD_p} \tag{4.13}$$

#### 4.2.2.2 Results and discussion

The Manning values established by Picado et al. [2010] were locally adjusted until the model outputs agreed satisfactorily with the field data. Figure 4.5 presents the best fit between predicted and observed SSE, during a day at the overall stations. The graphs evidence a good agreement between predictions and observations for all stations, as the predicted tidal wave (amplitude and phase) presents a pattern similar

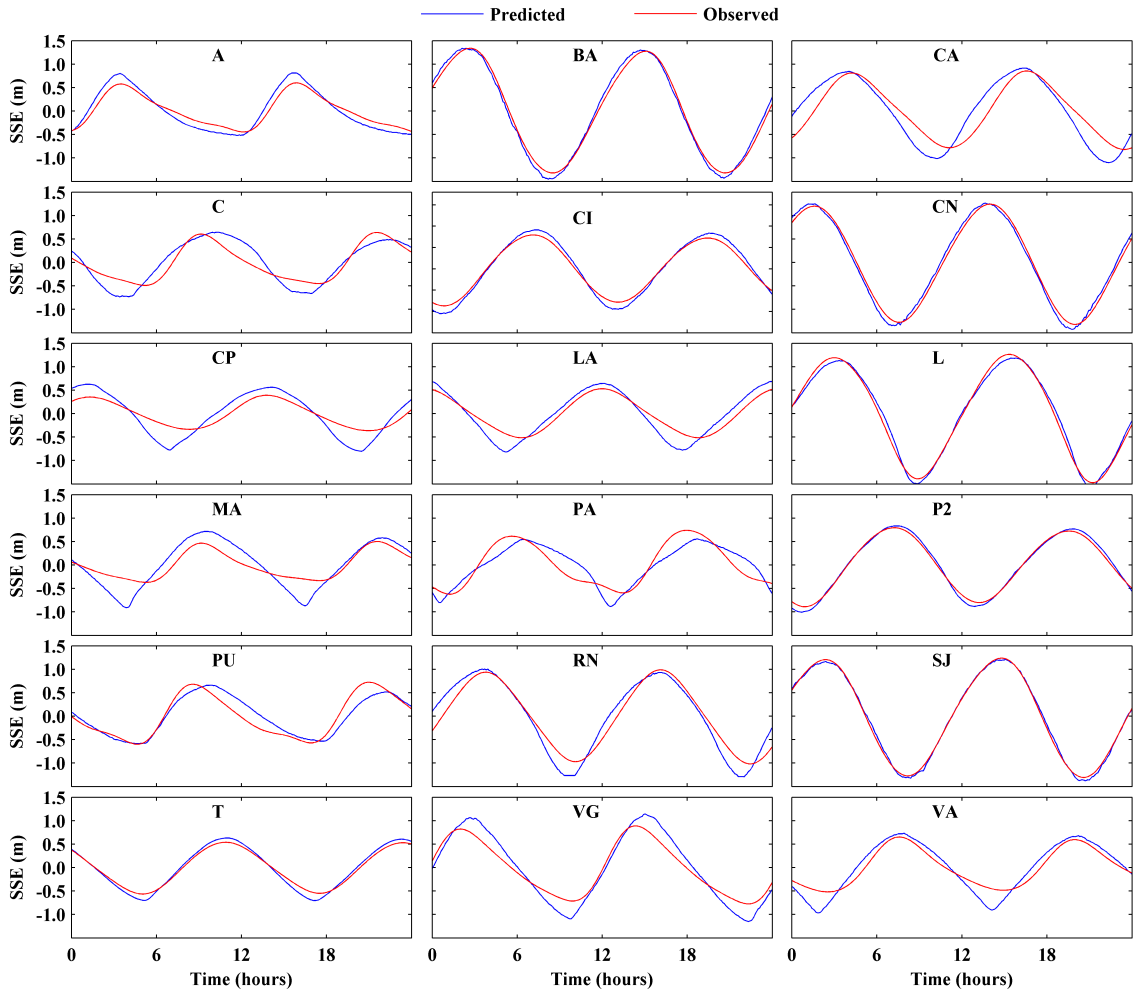


Figure 4.5: Observed and predicted tidal levels in 2002/03 stations (represented in Figure 4.2).

to that of the observed wave. Also, it is evident that the model accuracy decreases upstream.

Table 4.3 presents the $RMSE$, the $Skill$ and the $\Delta Error$ for all stations. It is evident once again the good agreement between model predictions and observations. $RMSE$ values range from 7 cm at the inlet (BA) to 32 cm at Manchão (M) (head of S. Jacinto channel). $RMSE$ values lower than 10 cm are found at the lower reaches of the main channels at BA, CN, L, P2, SJ and T stations. Further upstream the $RMSE$ values are higher, denoting that tidal propagation errors increase from the lagoon mouth to the channels heads.

Concerning the $\Delta Error$, Dias et al. [2009] stated that if percentages are lower than 5% of the local amplitude, the agreement between model results and observations

Table 4.3: *RMSE* (m), $\Delta Error$ (%) and *Skill* values for the lagoon stations represented in Figure 4.2

| Station | *RMSE* (m) | $\Delta Error$ (%) | *Skill* |
|---|---|---|---|
| Areão (A) | 0.18 | 14 | 0.920 |
| Barra (BA) | 0.07 | 4 | 0.998 |
| Cacia (CA) | 0.24 | 13 | 0.934 |
| Carregal (C) | 0.26 | 20 | 0.864 |
| Cires (CI) | 0.13 | 7 | 0.993 |
| Costa Nova (CN) | 0.09 | 4 | 0.996 |
| Cais da Pedra (CP) | 0.23 | 15 | 0.934 |
| Laranjo (LA) | 0.27 | 14 | 0.941 |
| Lota (L) | 0.11 | 5 | 0.994 |
| Manchão (M) | 0.32 | 20 | 0.773 |
| Pardilhó (PA) | 0.28 | 19 | 0.870 |
| Ponte Cais 2 (P2) | 0.07 | 6 | 0.998 |
| Puxadouro (PU) | 0.20 | 17 | 0.927 |
| Rio Novo (RN) | 0.19 | 9 | 0.970 |
| São Jacinto (SJ) | 0.09 | 5 | 0.996 |
| Torreira (T) | 0.10 | 7 | 0.991 |
| Vagueira (VG) | 0.22 | 11 | 0.956 |
| Vista Alegre (VA) | 0.23 | 14 | 0.921 |

should be considered excellent. If they range between 5% and 10% of the local amplitude the agreement should be considered very good. Attending this, an excellent agreement was found at BA, CN, L and SJ stations and a very good agreement at CI, P2, RN and T stations. Furthermore, it is highlighted that the percentages do not exceed 20% in any station for the present model configuration.

Concerning *Skill* values, the perfect agreement between model predictions and observations will yield a *Skill* value of one and a complete disagreement yields a *Skill* of zero [Warner et al., 2005]. Furthermore, Dias et al. [2009] state that *Skill* values higher than 0.95 indicate an excellent agreement between model results and observations. For

the present model configuration, should be highlighted that 9 stations (BA, CI, CN, L, P2, RN, SJ, T and VG) evidence *Skill* values higher than 0.95, which denotes an excellent agreement between model and predictions. Furthermore, *Skill* values higher than 0.9 were found for 15 stations (besides the previous, A, CA, CP, LA, PU and VA), which evidences a good agreement between predictions and observations [Dias et al., 2009].

The adjustment between observed and predicted elevations was also quantified through Taylor diagrams (Figure 4.6).

The observed series present a $NSD$ of 1, a $CC$ of 1, and a $RMSD$ of 0, because these parameters are computed in relation to themselves. Consequently, predicted and observed series have similar statistics when $NSD$ and $CC$ are equal to 1 and $RMSD$

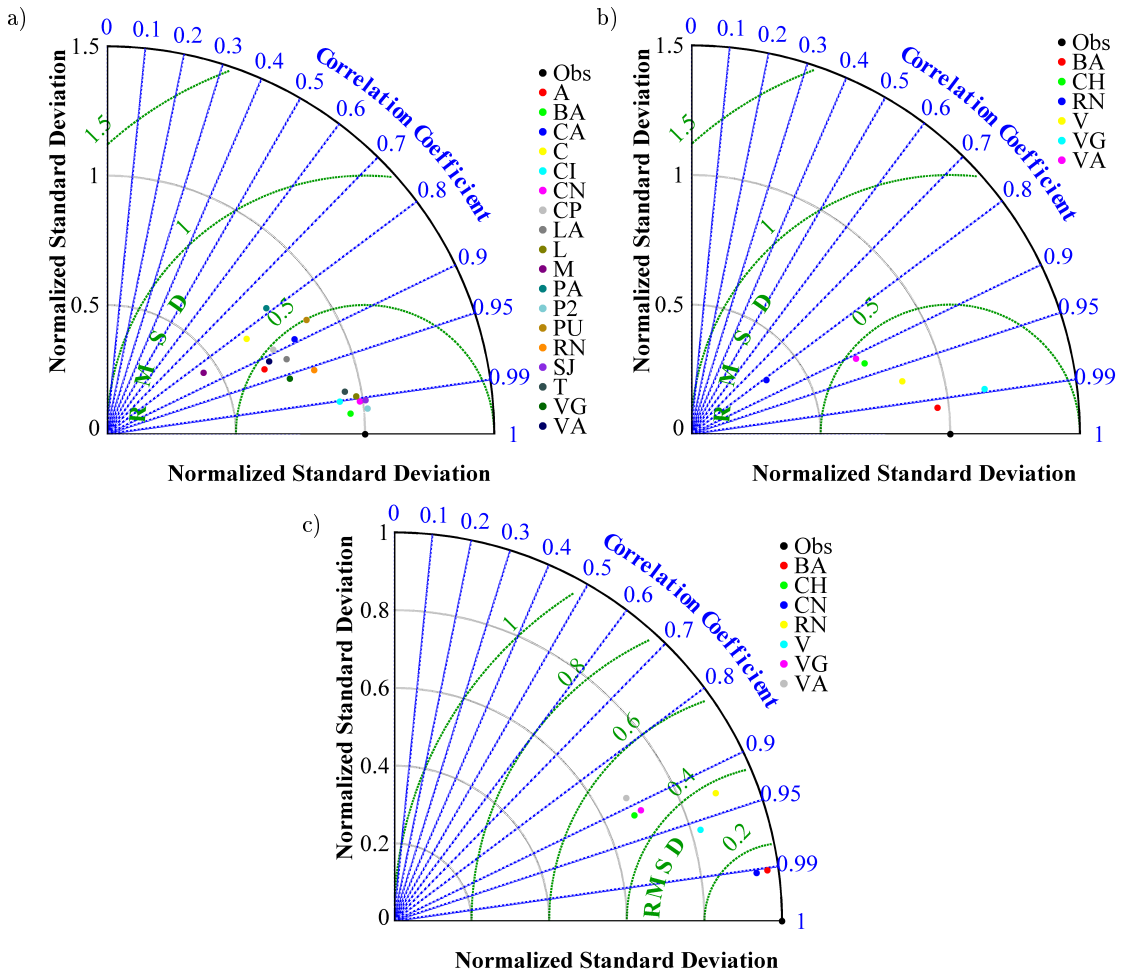


Figure 4.6: Taylor diagrams summarizing statistics of predicted and observed SSE: a) 2002/03; b) 2012 and c) 2013 campaigns. The black point represents the observed series, which have an RMSD of 0, a CC and a NSD of 1.

is equal to 0 (black dot in the diagram). In this way, the agreement between predicted and observed series is higher as lower is the distance between the black dot and each coloured dot represented in the diagram. Consequently, the analysis of Figure 4.6 shows that the model accuracy is lower for the stations at the channels heads than at the central area of the lagoon. Particularly for 2002/03 campaign (Figure 4.6a), the model fit can be considered very good at seven stations (BA, CI, CN, T, L, SJ, and P2) with $RMSD$ lower than 0.18 m, $CC$ higher than 0.98, and $NSD_o$ and $NSD_p$ higher than 0.9. Furthermore, eight stations (A, VA, CP, LA, CA, PU, VG, and RN) present $RMSD$ values between 0.18 and 0.50 m, $CC$ values between 0.85 and 0.98, and $NSD$ values between 0.6 and 0.9, denoting a good agreement between predictions and observations. The worst fit was found for three stations located at the S. Jacinto channel head (M, C, and PA) and may be related with the lack of recent bathymetric data for this region. Concerning the 2012 and 2013 results (Figures 4.6b and 4.6c) and following the same procedure, the model fitting was found very good at BA and CN stations (located close the lagoon inlet) and good in the remaining stations, with the exception of RN station in 2012. The disagreement in this particular case can be partly motivated by higher fluvial discharges during this period given its proximity to the Vouga River mouth. In fact, the fluvial discharges were certainly higher than the mean flow imposed at the model boundary, motivated by the intense precipitation registered at the region over this period.

Although these uncertainties, the overall results showed an excellent agreement between model predictions and observations at the stations located at the lagoon central area, and good agreement at the remaining stations. Furthermore, this model implementation presented better results than all the previous applications to this system [Dias et al., 2000; Vaz et al., 2007; Mendes, 2010; Picado et al., 2010; Tomas et al., 2014]. Particularly, the mesh improvement by the inclusion of intertidal areas and lagoon margins, as well as the update of the lagoon main channels bathymetry proved to improve the model accuracy comparing to the application developed by Picado et al. [2010]. In fact, the $RMSE$ and $Skill$ values found in this study for the lagoon central stations are identical to those obtained by Picado et al. [2010]. However, for the stations located at the channels heads were obtained more accurate predictions,

with $RMSE$ values approximately 8 cm lower than those obtained by Picado et al. [2010].

### 4.2.3 Validation of amplitude and phase of $M_2$ and $M_4$ tidal constituents

Besides the calibration, the hydrodynamic model was also validated by comparing model predictions with observations for other periods and quantities. In this section, two bathymetric configurations were validated, one for 1987 and other one for 2012. This comparison was made to assure that the model reproduces accurately the tidal propagation for both geomorphological configurations, once the model ELCIRC will be used further to investigate the tidal modifications occurred between 1987 and 2012 by assessing tidal asymmetry and tidal ellipses. Therefore, the validation was focused on $M_2$ and $M_4$ harmonic constants, given the dependence of tidal asymmetry on these constituents, and the major importance of the first one on Ria de Aveiro dynamics.

#### 4.2.3.1 Methodology

The 1987 bathymetry was built by interpolating the bathymetric data collected in 1987 to the numerical grid. The 2012 bathymetry corresponds to the configuration used in the calibration section. The topography of the marginal areas is similar for both configurations and corresponds to the topographic data used in the calibration.

The model was forced at the oceanic boundary imposing time series of SSE obtained by harmonic synthesis. The harmonic analysis of the inlet annual tidal records measured at the inlet tidal gauge between 1976 and 2013 highlighted that the $M_{Sf}$, $O_1$, $K_1$, $Q_1$, $N_2$, $M_2$, $S_2$, $M_4$, $MN_4$, $MS_4$, $L_2$, $MU_2$ and $2MS_6$ constituents are the most relevant and therefore are the only considered. Both, harmonic and synthetic analyses were performed using the t_tide package [Pawlowicz et al., 2002]. The synthesized elevation was also slightly corrected in order to account for the tidal distortion between the open boundary and the inlet tidal gauge station. Following this procedure the errors found at the BA station are similar to those obtained in the calibration section. As previously mentioned, the tidal features changed considerably at the lagoon mouth over

the last 30 years. Therefore, to assure the maximum authenticity in model simulations, up-to-date harmonic constants were used for 1987 and 2012 implementations, although the relevance of this change is considered of minor importance comparing with the expected effect of the geomorphological changes that occurred during this period.

As for calibration, the validation simulations considered mean fluvial discharges at the lagoon main tributaries and no wind effects. Also, the model free parameters and the time step are similar to the calibration runs. It is important to highlight that the bottom friction is not exactly the same for 1987 and 2012 configurations, once Manning coefficients depend on each grid node depth, which is not constant for both configurations.

The model was run for 34 days and the amplitude and phase of $M_2$ and $M_4$ constituents was determined by applying harmonic analysis to predicted SSE excluding the first four days of simulation (warming up period). The amplitude and phase of tidal constituents obtained from observed and predicted SSE time series were compared to assess the model performance. SSE data collected in 1987 at 18 lagoon stations was used to validate the 1987 model configuration. The 2012 implementation was validated with data collected in 2002/03 and 2012/13 at 18 and 7 lagoon stations, respectively.

#### 4.2.3.2 Results and discussion

Table 4.4 presents the amplitude and phase of $M_2$ and $M_4$ tidal constituents obtained from observed and predicted SSE time series at the lagoon stations represented in Figure 4.2. The results show that $M_2$ amplitude decreases, while its phase increases toward the channels head's. Contrarily, the amplitude of $M_4$ constituent increases and its phase decreases toward the lagoon extremities. In overall, the harmonic constants obtained from predicted elevation are in agreement with those obtained from observations. The stations located close the lagoon mouth and at the deeper channels present lower deviations than the upstream and shallower ones. Indeed, at BA and CI the model reproduces accurately the amplitude and phase of $M_2$ and $M_4$ constituents, presenting errors lower than 10%. Along the S. Jacinto channel the $M_2$ amplitude errors at the stations SJ and T are lower than 10%, while at V are between 10% and 20%, and between 20% and 40% at the C, PU, PA and M stations. Concerning the

Table 4.4: Amplitude (m) and phase (°) of $M_2$ and $M_4$ tidal constituents, observed (Obs) and predicted (Pred) in 1987/88, 2002/03 and 2012/13.

| | | 1987/88 | | | | 2002/03 | | | | 2012/13 | | | |
|---|---|---|---|---|---|---|---|---|---|---|---|---|---|
| | | $M_2$ | | $M_4$ | | $M_2$ | | $M_4$ | | $M_2$ | | $M_4$ | |
| | | (m) | (°) | (m) | (°) | (m) | (°) | (m) | (°) | (m) | (°) | (m) | (°) |
| A | Obs | - | - | - | - | 0.53 | 131 | 0.12 | 218 | - | - | - | - |
| | Pred | - | - | - | - | 0.35 | 175 | 0.11 | 296 | - | - | - | - |
| BA | Obs | 0.88 | 81 | 0.04 | 280 | 0.98 | 79 | 0.04 | 255 | 0.97 | 78 | 0.04 | 240 |
| | Pred | 0.92 | 81 | 0.04 | 272 | 0.95 | 82 | 0.04 | 255 | 0.94 | 82 | 0.04 | 262 |
| CA | Obs | 0.59 | 127 | 0.04 | 77 | 0.70 | 120 | 0.04 | 50 | - | - | - | - |
| | Pred | 0.44 | 158 | 0.04 | 256 | 0.59 | 142 | 0.06 | 218 | - | - | - | - |
| CH | Obs | - | - | - | - | - | - | - | - | 0.85 | 118 | 0.07 | 39 |
| | Pred | - | - | - | - | - | - | - | - | 0.59 | 113 | 0.08 | 207 |
| CP | Obs | 0.50 | 159 | 0.05 | 169 | 0.63 | 148 | 0.07 | 119 | - | - | - | - |
| | Pred | 0.28 | 205 | 0.07 | 340 | 0.45 | 160 | 0.09 | 258 | - | - | - | - |
| C | Obs | 0.34 | 197 | 0.06 | 304 | 0.55 | 176 | 0.06 | 178 | - | - | - | - |
| | Pred | 0.21 | 233 | 0.04 | 32 | 0.38 | 204 | 0.07 | 349 | - | - | - | - |
| CI | Obs | 0.87 | 91 | 0.05 | 354 | 1.05 | 91 | 0.07 | 325 | - | - | - | - |
| | Pred | 0.91 | 90 | 0.06 | 314 | 0.94 | 90 | 0.06 | 316 | - | - | - | - |
| CN | Obs | 0.89 | 96 | 0.04 | 342 | 0.84 | 89 | 0.05 | 307 | 0.99 | 89 | 0.03 | 292 |
| | Pred | 0.84 | 100 | 0.03 | 23 | 0.93 | 90 | 0.04 | 316 | 0.94 | 90 | 0.03 | 308 |
| LA | Obs | 0.57 | 138 | 0.05 | 166 | 0.87 | 120 | 0.08 | 39 | - | - | - | - |
| | Pred | 0.41 | 153 | 0.06 | 249 | 0.67 | 136 | 0.09 | 198 | - | - | - | - |
| L | Obs | 0.83 | 103 | 0.10 | 7 | 0.93 | 101 | 0.09 | 342 | - | - | - | - |
| | Pred | 0.86 | 103 | 0.05 | 7 | 0.93 | 96 | 0.06 | 340 | - | - | - | - |
| M | Obs | 0.23 | 219 | 0.03 | 300 | 0.62 | 166 | 0.08 | 213 | - | - | - | - |
| | Pred | 0.12 | 256 | 0.02 | 78 | 0.47 | 203 | 0.06 | 350 | - | - | - | - |
| PA | Obs | 0.33 | 190 | 0.03 | 255 | 0.57 | 170 | 0.07 | 156 | - | - | - | - |
| | Pred | 0.22 | 217 | 0.05 | 360 | 0.47 | 174 | 0.08 | 308 | - | - | - | - |
| P2 | Obs | 0.84 | 98 | 0.06 | 8 | 0.95 | 93 | 0.09 | 332 | - | - | - | - |
| | Pred | 0.88 | 97 | 0.06 | 337 | 0.95 | 94 | 0.07 | 331 | - | - | - | - |
| PU | Obs | 0.32 | 194 | 0.05 | 290 | 0.51 | 172 | 0.06 | 257 | - | - | - | - |
| | Pred | 0.21 | 223 | 0.06 | 24 | 0.47 | 187 | 0.07 | 324 | - | - | - | - |
| RN | Obs | 0.63 | 118 | 0.04 | 66 | 0.80 | 96 | 0.07 | 357 | 0.73 | 111 | 0.06 | 10 |
| | Pred | 0.52 | 136 | 0.03 | 231 | 0.70 | 120 | 0.01 | 156 | 0.71 | 122 | 0.01 | 185 |
| SJ | Obs | 0.86 | 90 | 0.05 | 344 | 0.93 | 88 | 0.05 | 311 | - | - | - | - |
| | Pred | 0.90 | 89 | 0.07 | 317 | 0.95 | 89 | 0.04 | 294 | - | - | - | - |
| T | Obs | 0.48 | 140 | 0.06 | 212 | 0.74 | 127 | 0.06 | 146 | - | - | - | - |
| | Pred | 0.41 | 150 | 0.06 | 243 | 0.70 | 133 | 0.06 | 171 | - | - | - | - |
| V | Obs | 0.34 | 169 | 0.04 | 257 | - | - | - | - | 0.75 | 137 | 0.07 | 123 |
| | Pred | 0.29 | 173 | 0.04 | 273 | - | - | - | - | 0.65 | 143 | 0.05 | 186 |
| VG | Obs | 0.49 | 129 | 0.13 | 205 | 0.82 | 105 | 0.06 | 134 | 0.84 | 105 | 0.05 | 143 |
| | Pred | 0.31 | 144 | 0.11 | 239 | 0.60 | 123 | 0.12 | 187 | 0.59 | 125 | 0.12 | 185 |
| VA | Obs | 0.50 | 159 | 0.05 | 169 | 0.63 | 148 | 0.07 | 119 | - | - | - | - |
| | Pred | 0.28 | 205 | 0.07 | 340 | 0.45 | 160 | 0.09 | 258 | - | - | - | - |

Espinheiro channel, the amplitude error for $M_2$ is between 10% and 20% at LA, CH and RN stations and approximately 30% at CA station. Regarding the Ílhavo channel, the lowest $M_2$ amplitude deviations were found at P2 and L stations, with errors lower than 10%. The VA and CP stations present $M_2$ amplitude errors between 20% and 40%. For the Mira channel $M_2$ amplitude errors are lower than 10% for CN station and between 20% and 40% for VG and A stations. The phase errors are lower than 10% for the majority of the stations; the exceptions are A, CA, CP, M, PA and PU stations with errors between 10% and 20%.

Concerning the $M_4$ constituent, the amplitude and phase errors are higher than those obtained for $M_2$ constituent. Indeed, the difficulty in reproducing accurately the harmonic constants of $M_4$ overtide constituent through numerical modelling has been recognized by several authors [Sinha and Pingree, 1997; Picado et al., 2010; Dias et al., 2013b]. According these studies, small errors/variations in local bathymetry/ drag coefficient can generate very different $M_4$ tidal constants. In the application presented here, the $M_4$ amplitude errors are lower than 20% at CA, LA, P2, PU, T and V stations for 1987 bathymetry application and at A, BA, CN, CP, C, LA, M, PA, SJ and T stations for 2012 case. Moreover, errors between 20% and 40% were found at CI, CN, M, and VA for 1987 case and at CI, CN, L, P2 and VA for 2012 case. Regarding the $M_4$ constituent phase, errors lower than 20% were found in A, BA, CI, CN, L, SJ, T, VG and V stations.

By comparing the errors for both configurations, there is no evidence that one is more accurate than the other. It was found that in some stations the 1987 configuration presents lower errors than the 2012 configuration. However, in other stations the 2012 configuration presents lower errors than the 1987 configuration. Accordingly, it is considered that the model accuracy is similar for both configurations.

In summary, the analysis performed demonstrates the model accuracy in reproducing the tidal properties within the lagoon, with higher performance at stations located close the lagoon mouth. As expected, the model accuracy decreases with the distance to the inlet. Furthermore, the errors obtained here for the $M_2$ are quite similar to those presented by Picado et al. [2010] for the previous modelling application to Ria de Aveiro, but the $M_4$ errors obtained in this study are lower, highlighting the

grid enhancement contribution to improve the results, as was already found in the calibration section. In addition, the results obtained showed that the tidal properties changed between 1987 and 2012 and that the model errors are quite similar for both configurations, highlighting the model ability to reproduce the tidal propagation within the lagoon under different morphological conditions.

### 4.2.4 Validation of storm surge events

The model ELCIRC was also validated for storm surge propagation to assure that the model reproduces accurately the storm surge propagation within the lagoon. This verification is extremely important considering that one of the aims of this work is to assess the lagoon flood extent during extreme sea levels, that are generated by both storm surges and tides. Attending this, the SSE data collected during the hydrographic campaigns of 2002/03, 2012 and 2013 was analysed in order to identify storm surge events. Then, the calibrated model configuration was used to simulate the propagation of these events within the lagoon.

#### 4.2.4.1 Methodology

The SSE series recorded in 2002/03, 2012 and 2013 were decomposed in astronomic and residual levels using the t_tide package [Pawlowicz et al., 2002]. The tidal constants, determined through harmonic analysis, were used to construct the astronomic levels through harmonic synthesis. The residual levels were computed as the difference between observed and synthesized astronomic levels. The residual series were then analysed and three storm surge events were identified in:

- December 2002 at the lagoon mouth (BA station) with an amplitude of 0.62 m and then at the stations distributed along Mira Channel (CN, VG and A), which were sampled during the same period;
- April 2012 at the BA station with an amplitude of 0.32 m and then at the V, VA, VG, RN, and CH stations, which were sampled during the same period;
- January 2013 at the BA station with an amplitude of 0.76 m and then at the CN, V, VA, VG, RN and CH stations, which were sampled during the same period.

Model predictions were performed for these periods considering the oceanic boundary forcing by time series of SSE, including astronomical tide and meteorological tide obtained at BA station. Figure 4.7 presents the SSE imposed at the oceanic boundary, and the corresponding astronomical and meteorological tides, for the January 2013 storm surge event, as example. The astronomical tidal condition was generated through harmonic synthesis using the respective year harmonic constants. The synthesized elevation was then corrected as in the section corresponding the validation of tidal constants. The residual levels were used as meteorological tidal condition. These levels were set null before the storm surge event, to prevent the propagation of noise inside the domain.

As for calibration, the validation simulations considered mean fluvial discharges at the lagoon main tributaries and no wind effects. Also, the model free parameters and the time step are similar to the calibration runs. It is important to highlight that the effect of winds on the offshore water levels was included as model boundary condition.

The predicted and observed residual elevations were compared in order to assess the model accuracy in reproducing the propagation of storm surge events along Ria de Aveiro. The residuals for model predictions were determined following the procedure described for the observations. The model accuracy in reproducing the storm surge propagation was quantified by computing the $RMSE$ between predicted and observed

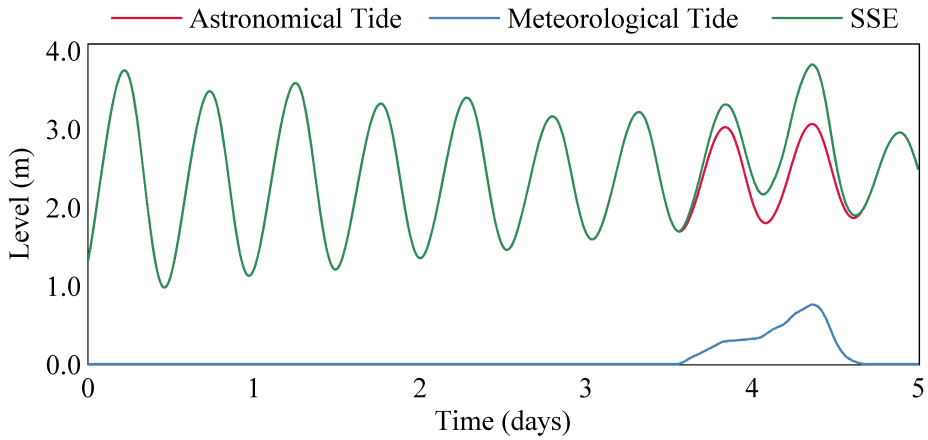


Figure 4.7: SSE (m), as a sum of astronomical and meteorological levels, imposed at the oceanic boundary.

residual series, following equation 4.8. Moreover, the difference between observed and predicted storm surge peak heights was computed.

#### 4.2.4.2 Results and discussion

Figure 4.8 presents the residual levels for the three storm surge events identified. For the December 2002 event (Figure 4.8 n-q), the results evidence that predictions and observations follow similar patterns, although for BA and CN stations the predicted storm surge height is higher than the observed. In contrast, at VG and A stations, the observed surge height is slightly higher than the predicted. The mean deviation between peaks is approximately 10 cm. Furthermore, the $RMSE$ ranges from 4 cm at

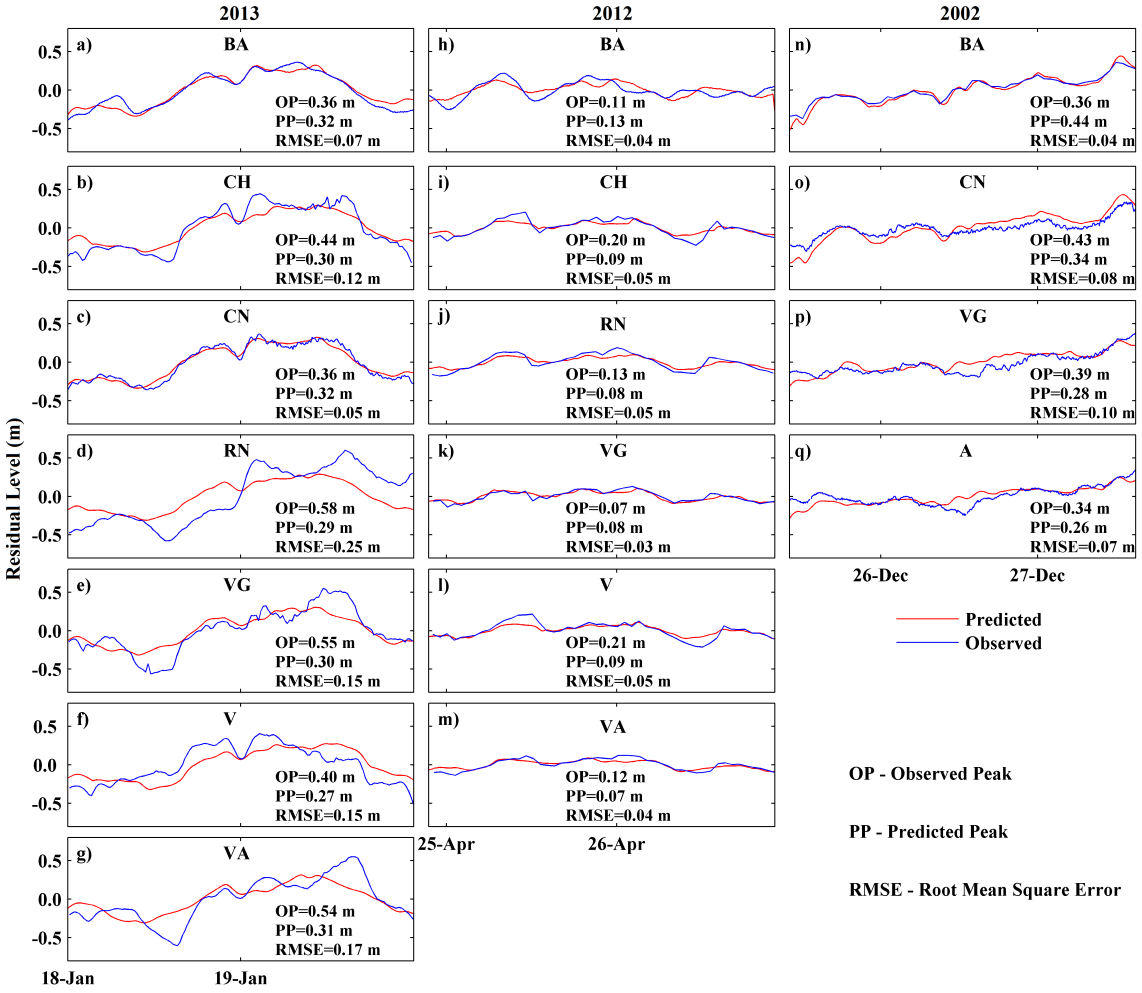


Figure 4.8: Observed and predicted residual levels for the: (a-g) January 2013; (h-m) April 2012; (n-q) December 2002, storm surge events, indicating observed and predicted peaks and $RMSE$.

the inlet to 10 cm at VG, revealing a good agreement between predicted and observed surge height. These results prove the model ability to reproduce the propagation of storm surge events along Mira Channel.

The residual levels for April 2012 (Figure 4.8 h-m) show that predicted and observed residuals follow similar patterns, with the highest differences found at the peaks. The $RMSE$ are lower than 5 cm, and the maximum absolute deviation between peaks ranges from 1 cm at VG to 12 cm at V. The results of the January 2013 event reveal that the deviations between predictions and observations increase with the distance from the lagoon mouth. Globally, the model underestimates the storm surge peaks. The predicted and observed residual levels at BA and CN stations are quite similar, presenting $RMSE$ of 7 and 5 cm, respectively. A maximum $RMSE$ of 25 cm between predicted and observed peaks is found for RN station. This error can be partially explained by the high fluvial discharges in this period as previously referred in the tidal propagation validation discussion.

As predicted residual levels are the difference between model predicted SSE and synthesized astronomical tide, the residual errors found are affected by tidal level errors. Attending this, in general, the model accurately reproduces the observed residuals and therefore is able to predict sea surface levels distribution in Ria de Aveiro under storm surge conditions.

## 4.3 MORSYS2D model

The 2D morphodynamic modelling system MORSYS2D [Fortunato and Oliveira, 2004, 2007; Bertin et al., 2009], schematized in Figure 4.9, was used to simulate the sediment dynamics and the morphological evolution of the Ria de Aveio inlet region. The system integrates the hydrodynamic model ELCIRC and the wave model SWAN, which interact providing the tidal levels and the currents to feed the SAND2D model, that computes sediment transport and updates the bathymetry.

The ELCIRC model in 2D mode was described previously in section 4.1, however as the ELCIRC interacts with the wave model SWAN, specifications related with the effect of short waves on the hydrodynamics are presented in this section. The surface

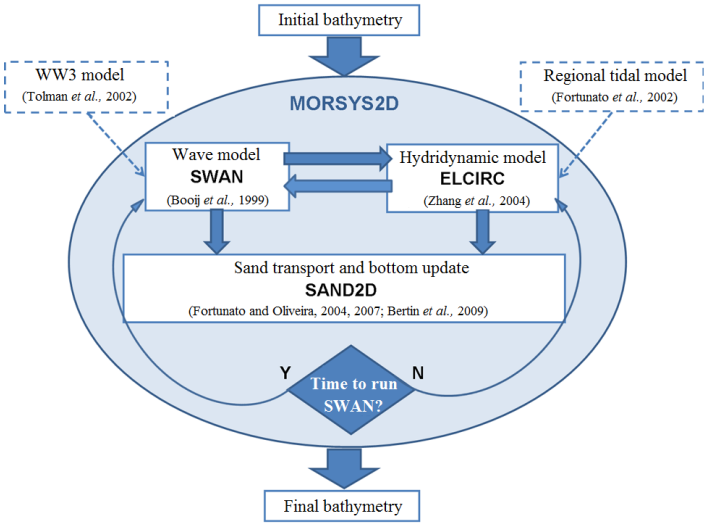


Figure 4.9: Flowchart indicating the MORSYS2D procedure every morphodynamic time step (adapted from Plecha [2011]).

stress, $\tau_{Sx}$ and $\tau_{Sy}$, are computed through equations 4.14 and 4.15 and are included in the friction terms in equations 4.2 and 4.3, respectively.

$$\tau_{Sx} = -\left(\frac{\partial S_{xx}}{\partial x} + \frac{\partial S_{yx}}{\partial y}\right) \tag{4.14}$$

$$\tau_{Sy} = -\left(\frac{\partial S_{yy}}{\partial y} + \frac{\partial S_{xy}}{\partial x}\right) \tag{4.15}$$

The $S_{xx}$, $S_{yy}$, $S_{xy}$ and $S_{yx}$ are the wave radiation stresses, that depend on wave energy ($E$), wave group velocity ($C_g$), wave phase velocity ($C$) and the wave angle to the $x$ axis ($\alpha$) according to the following equations:

$$S_{xx} = \frac{E}{2}\left(2\frac{C_g}{C}\left(\cos^2\alpha + 1\right) - 1\right) \tag{4.16}$$

$$S_{yy} = \frac{E}{2}\left(2\frac{C_g}{C}\left(\sin^2\alpha + 1\right) - 1\right) \tag{4.17}$$

$$S_{xy} = S_{yx} = E\frac{C_g}{C}\sin\alpha\cos\alpha \tag{4.18}$$

Within MORSYS2D model, the ELCIRC is also forced with tidal constants provided by the regional model developed by Fortunato et al. [2002].

The spectral wave model SWAN solves the wave density balance equation (equation

4.19) [Booij et al., 1999], that is used in MORSYS2D to simulate wave propagation in the continental shelf.

$$\frac{\partial}{\partial t}N + \frac{\partial}{\partial x}(c_x N) + \frac{\partial}{\partial y}(c_y N) + \frac{\partial}{\partial \sigma}(c_\sigma N) + \frac{\partial}{\partial \theta}(c_\theta N) = \frac{S}{N} \tag{4.19}$$

$\sigma$ is the wave frequency, $\theta$ the wave angle, $N$ the wave action density, $c_x$ and $c_y$ the wave propagation speeds in $x$ and $y$ directions and $S$ the energy source term that represents the wave transformation processes (e.g. growth by wind; the wave-wave interactions; the influence of bottom friction, etc.)

Within MORSYS2D model, the SWAN is fed by outputs of velocities and elevations from ELCIRC model, which are linearly interpolated to SWAN regular grids. The SWAN is also forced by time series of wave parameters provided from the WW3 model. Significant wave height, period, direction, wavelength, and orbital velocity are outputted from SWAN and used to compute gradients of radiation stresses (equations 4.16, 4.17 and 4.18) used to feed ELCIRC model.

The SAND2D model was developed by Fortunato and Oliveira [2004, 2007] and Bertin et al. [2009], and computes the sediment transport and the resulting bed changes from the Exner equation 4.20:

$$\Delta H^i = \frac{1}{1-\lambda}\nabla Q_*^i \tag{4.20}$$

$\Delta H^i$ is the bottom variation over a time step, $\lambda$ is the sediment porosity and $Q_*^i$ is the sediment flux integrated over a time step, that is computed from equation 4.21:

$$Q_* = Q + \nu(1-\lambda)\left(|Q_x|\frac{\partial H}{\partial x}, |Q_y|\frac{\partial H}{\partial y}\right) \tag{4.21}$$

Where $Q$ is the sediment flux computed at the center of the element and $\nu$ the artificial diffusion. The sediment fluxes due to the effect of tidal currents and waves forcing are simulated by using one of the several formulations available. The numerical simulations presented herein used the Ackers and White [1973] (AW) formulation for tidal currents coupled with waves, following the Plecha [2011] conclusions.

The morphodynamic time step can be constant or variable. In the last case, it is

computed through the Courant Number ($C_u$) (equation 4.22) in order to guarantee the numerical model stability.

$$C_u \approx \frac{bQ^*}{H\Delta x} \tag{4.22}$$

Where $b$ is the velocity power in the transport formulation and $Q^*$ is the instantaneous solid transport.

### 4.3.1 Ria de Aveiro implementation

The MORSYS2D model implementation to the Ria de Aveiro lagoon developed by Plecha [2011] was used here to simulate the lagoon inlet morphodynamics. The grids used in the MORSYS2D model are represented in Figure 4.10. The ELCIRC grid (red) presents 25819 nodes and 43169 elements and covers the lagoon channels. The SWAN model has two nested grids with different dimensions and characteristics (orange and blue). The grid with higher dimension extends from the offshore area, while the finer grid encompasses the inlet area. The SAND2D model computes the sediment fluxes and updates the bathymetry within the inlet region (green grid).

The ELCIRC implementation within the MORSYS2D model presents several differences relative to the implementation described in the previous section, once the implementation should be appropriate to respond adequately the issue under study. For example, the ELCIRC grid within the MORSYS2D discards the inundation of marginal areas, once this feature is irrelevant to describe the sediment dynamics at the inlet. In this case the ELCIRC configuration used was developed by Oliveira et al. [2006] and updated and validated by Plecha [2011]. The bathymetry used as initial condition was created according two surveys performed by the IH in 1987/88 for the entire lagoon and by APA in 2001 for the inlet region. The model was forced at the oceanic boundary by amplitude and phase of ten tidal constituents ($M_{Sf}$, $O_1$, $K_1$, $N_2$, $M_2$, $S_2$, $M_4$, $MN_4$, $MS_4$ and $M_6$) and the mean sea level ($Z_0$) taken from the regional model developed by Fortunato et al. [2002]. The fluvial discharges and the wind stress were neglected, following the Plecha [2011] application. The eddy viscosity ($\epsilon$) was set null and the hydrodynamic time set was set 90 s.

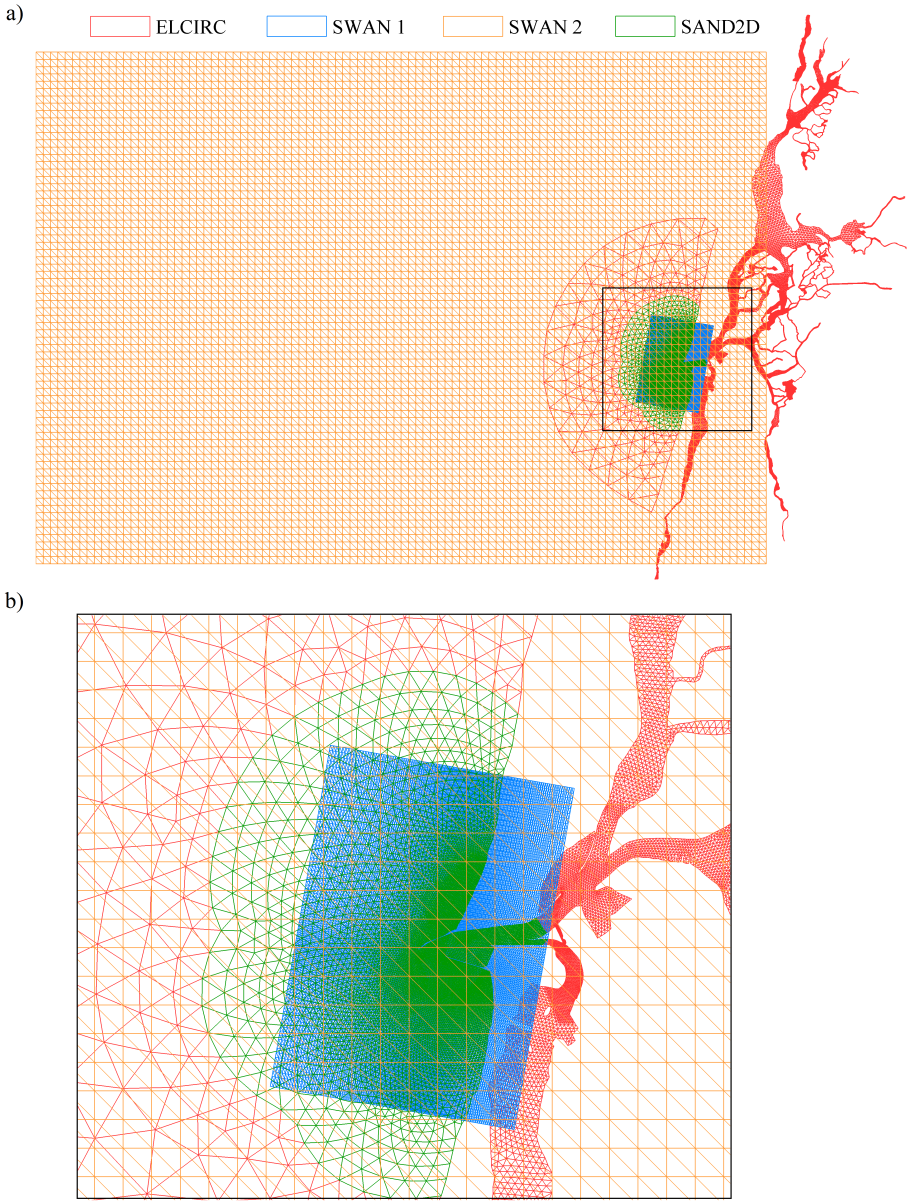


Figure 4.10: MORSYS2D numerical grids for Ria de Aveiro application: a) entire domain; b) Zoom of the inlet region (ELCIRC SWAN 1 SWAN 2 SAND2D).

Concerning SWAN model, the implementation used by Plecha [2011] was used to simulate the waves propagation along the continental shelf. The low resolution grid application is forced with time series of wave data outputted by the WW3 every 6 hours, while the finer grid was fed with the wave data provided by the larger domain. The wave transformation processes considered in this application are the same that are considered by Plecha [2011]. The effect of wave interaction with currents, the energy generation and dissipation by wind, the diffraction, the quadruplet interactions

and the whitecapping were neglected. The waves can be modified by bottom friction, wave breaking, triad wave-wave interaction and wave propagation within a non-uniform water level.

Regarding SAND2D, the implementation developed by Plecha [2011] for the Ria de Aveiro inlet was used. Within this, the sediment fluxes are computed using the AW formulation. Plecha [2011] compared the model accuracy in reproducing the inlet morphodynamics under AW, Soulsby and van Rijn [Soulsby, 1997] and Bijker [1971] formulations. Among these, the AW formulation presents the best results, reproducing accurately the main patterns of erosion and deposition that occurred at the inlet region between June 2001 and September 2005.

The sediment grain size ($d_{50}$) was set variable in space and the porosity ($\lambda$) was set 0.35.

# Chapter 5

# Ria de Aveiro tidal dynamics

## 5.1 Introduction

As previously discussed, the MSLR will impact coastal regions worldwide, affecting among others, the sediment redistribution, the partitioning of habitats, salinity distribution, tidal range and submergence periods [Nicholls, 2011; IPCC, 2014]. However, the landward migration may be restricted due to human occupation and intervention [IPCC, 2014].

The sensitivity of tidal propagation to flooding confinement under MSLR scenarios in coastal areas, and especially in lagoons, was not deeply studied until the present. Pelling et al. [2013a] found that the tidal dynamics in the European Shelf under MSLR conditions is strictly dependent on the coastal geometry, emphasizing the importance to define as precise as possible the position of protection barriers in order to obtain accurate results.

Often, the consequences of MSLR in low-lying coastal systems dynamics are studied admitting vertical walls of unlimited height surrounding the entire domain and consequently no changes in the coastal geometry resulting from higher sea surface levels are allowed [Hong and Shen, 2012; Mendes et al., 2013; Picado et al., 2013; Valentim et al., 2013; Ahmadian et al., 2014; Chua and Xu, 2014]. Moreover, other works consider the inundation of marginal areas but discard the construction of flood protection measures [Fortunato et al., 2013; Yang et al., 2015]. In low-lying coastal lagoons subjected to high human influence, such as Ria de Aveiro, and where flood

protection works are expected, these approaches may not be realistic. It is very likely that in future the inundation problems in Ria de Aveiro will be exacerbated by the MSLR, as the lagoon margins present reduced altitude. Nevertheless, as the lagoon adjacent area is densely populated and presents also important biodiversity resources and several economic activities, flood protection works are expected in order to minimize the negative consequences of predicted marginal inundation.

Once the floods of oceanic origin in Ria de Aveiro are strictly dependent on the tidal conditions, it is absolutely crucial to evaluate the influence of such structures on the lagoon tidal dynamics. Accordingly, this chapter aims to investigate the tidal propagation changes within Ria de Aveiro motivated by geomorphological changes and by the MSLR through hydrodynamic modelling. Particularly, this study is focused initially on tidal modifications that occurred between 1987 and 2012 motivated by the main channels deepening and secondly on tidal modifications expected for the future as consequence of MSLR and consequent construction of flood protection barriers in threatened regions. To achieve this goal the hydrodynamic model ELCIRC, previously calibrated and validated for Ria de Aveiro, was applied to this system. The results of this research will indicate the relevance of including flood protection structures in the future scenarios simulations.

## 5.2 Methodology

Once calibrated and validated the hydrodynamic model was used to assess the tidal propagation within the lagoon, by analysing tidal asymmetry, tidal ellipses and residual currents. Figure 5.1 presents the diagram of configuration runs executed with ELCIRC model. For present mean sea level, model results differences were assessed for 1987 and 2012 configurations. Additional simulations were performed with the 2012 model configuration considering a mean sea level 0.42 m higher than the actual, corresponding to the MSLR estimation for 2100 [Lopes et al., 2011]. These results were used to quantify tidal changes induced by climate changes.

Under MSLR conditions, four lagoon geometric scenarios were defined. These scenarios are not based on local planning, but were built to study the sensitivity of

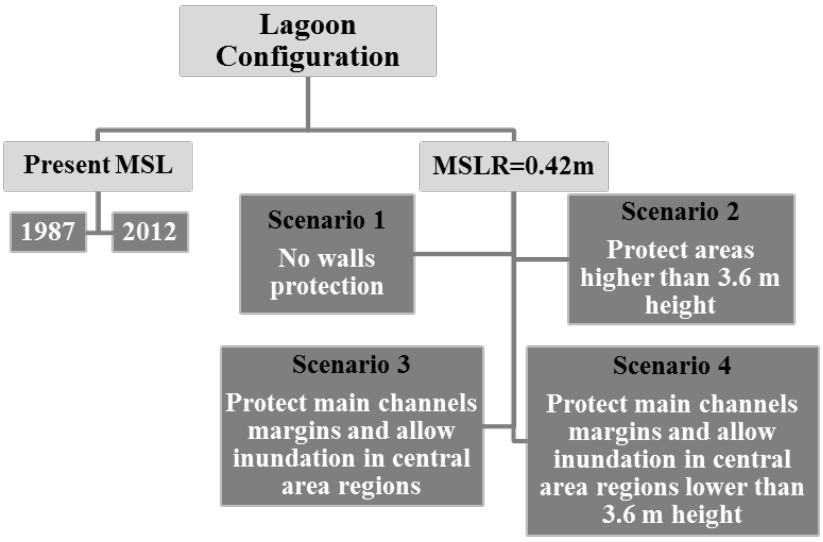


Figure 5.1: Diagram summarizing the simulations performed with ELCIRC model.

tidal propagation to geometric configuration changes considering the flood threatened regions. In scenario 1 the geometric configuration reflects the "do nothing" option, while scenario 2 restricts inundation in areas higher than 3.6 m height (ZH), by implementing barriers with 5 m height in the numerical grid. This contour line was chosen because it restricts the inundation in several regions mainly located in the lagoon central area, providing the sensitivity of tidal dynamics to a possible water flooding restriction in this region. The wall height value although unrealistic was chosen to guarantee that these areas are never flooded during simulation conditions. Scenario 3 considers the construction of barriers with 5 m height along the shoreline to protect the main channels margins where populations and agricultural and industrial activities are present, however allows inundation in the central area region where human occupation is almost inexistent. Finally, scenario 4 is a combination of scenarios 2 and 3, once it considers main channels margins protective barriers and restricts inundation in regions of the central area with topography higher than 3.6 m (ZH). In summary, the scenarios built reflect that under MSLR conditions the lagoon area will increase, although the flood migration may be restricted due to human intervention.

For these scenarios model simulations were performed for 34 days and the analysis excludes the first four days of simulation (warming up period). The tidal asymmetry was assessed for all the grid nodes computing the amplitude ratio ($A_r$) and the relative

phase ($\varphi$), following Aubrey and Speer [1985] (equations 5.1 and 5.2):

$$A_r = \frac{A_{M_4}}{A_{M_2}} \tag{5.1}$$

$$\varphi = 2\theta_{M_2} - \theta_{M_4} \tag{5.2}$$

Where $A_{M_4}$ and $A_{M_2}$ are the amplitudes of $M_4$ and $M_2$ constituents, respectively and $\theta_{M_4}$ and $\theta_{M_2}$ are the phase of $M_4$ and $M_2$ constituents, respectively. $A_r$ indicates the magnitude of tidal asymmetry; as larger is the amplitude ratio the more distorted is the tide. $\varphi$ indicates flood or ebb dominance ($0 < \varphi < 180$ indicates flood dominance and $180 < \varphi < 360$ indicates ebb dominance). Furthermore, tidal ellipses of $M_2$ constituent were computed for all the grid nodes performing harmonic analysis of velocity, using the matlab package developed by Xu [2002]. The semi-major axis ($SEMA$) and the eccentricity ($ECC$) of tidal ellipses were analyzed. The residual currents for all the grid nodes were assessed averaging the currents over 29.56 days (two times the $M_{SF}$ constituent period).

The tidal modifications between 1987 and 2012 were quantified by computing the relative difference of $A_r$, $SEMA$ and residual velocity between 1987 and 2012. Also, the variations in relative phase/ellipses eccentricity between 1987 and 2012 were assessed, by identifying the areas that maintained or modified their dominance/eccentricity.

The tidal modifications changes predicted under MSLR conditions were quantified computing the relative difference of $A_r$, $SEMA$ and residual velocity between 2012 configuration and each scenario configuration. Moreover, the relative difference of $A_r$, $SEMA$ and residual velocity between the scenario 1 configuration and scenarios 2 to 4 were assessed. This analysis compares the "do nothing" option with the scenarios including flood protection structures.

## 5.3 Results and discussion

### 5.3.1 Tidal changes between 1987 and 2012

The amplitude ratio was computed for 1987 and 2012 configurations, in order to characterize the tidal wave distortion. Also, the tidal distortion changes over this period were evaluated by computing the relative difference of amplitude ratios between 1987 and 2012. The results highlight that the tidal distortion increases toward the channels head's for both cases (Figures 5.2a and 5.2b). Nevertheless, the tidal wave is less distorted nowadays than in the past for most of the domain (Figure 5.2c). Indeed, at the lagoon main channels the amplitude ratio decreased around 40% from 1987 to 2012, although maximum declines can achieve 60% in some restricted areas. Contrarily, the tidal distortion increased at shallow areas located at the channels head's.

The lagoon tidal dominance was characterized for both configurations by computing the relative phase. Moreover, the regions that changed its tidal dominance from 1987 to 2012 were identified . The results evidence that the lagoon is ebb-dominated from the entrance until approximately the middle of its main channels and flood-dominated upstream for both configurations (Figures 5.2d and 5.2e). Despite the similarities, the ebb dominance is actually extending further upstream at the S.Jacinto channel comparing to 1987 (Figure 5.2f).

The tidal currents were evaluated by computing the $M_2$ constituent tidal ellipses. The $M_2$ constituent represents most of the total tidal energy, and therefore, $M_2$ tidal ellipses can be considered representative of tidal currents in Ria de Aveiro [Dias, 2001]. The $SEMA$ results (Figures 5.3a and 5.3b) for both configurations show highest currents at the inlet and main channels entrance (can achieve 1.4 m/s), which are the lagoon deeper areas. Contrarily, at the narrowest and shallowest channels the currents are weaker (lower than 0.4 m/s). The results also evidence that the magnitude of tidal currents generally increased between 1987 and 2012 (Figure 5.3c). The highest rates of magnitudes increase from 1987 to 2012 were found in S. Jacinto and Mira channels head's. Here the current intensity for 2012 is nearly twice that obtained in 1987. Concerning the $M_2$ ellipses eccentricity (Figures 5.3d and 5.3e), the results evidence areas of clockwise (CW) ($ECC < 1$) and anti-clockwise (ACW) ($ECC > 1$) rotation

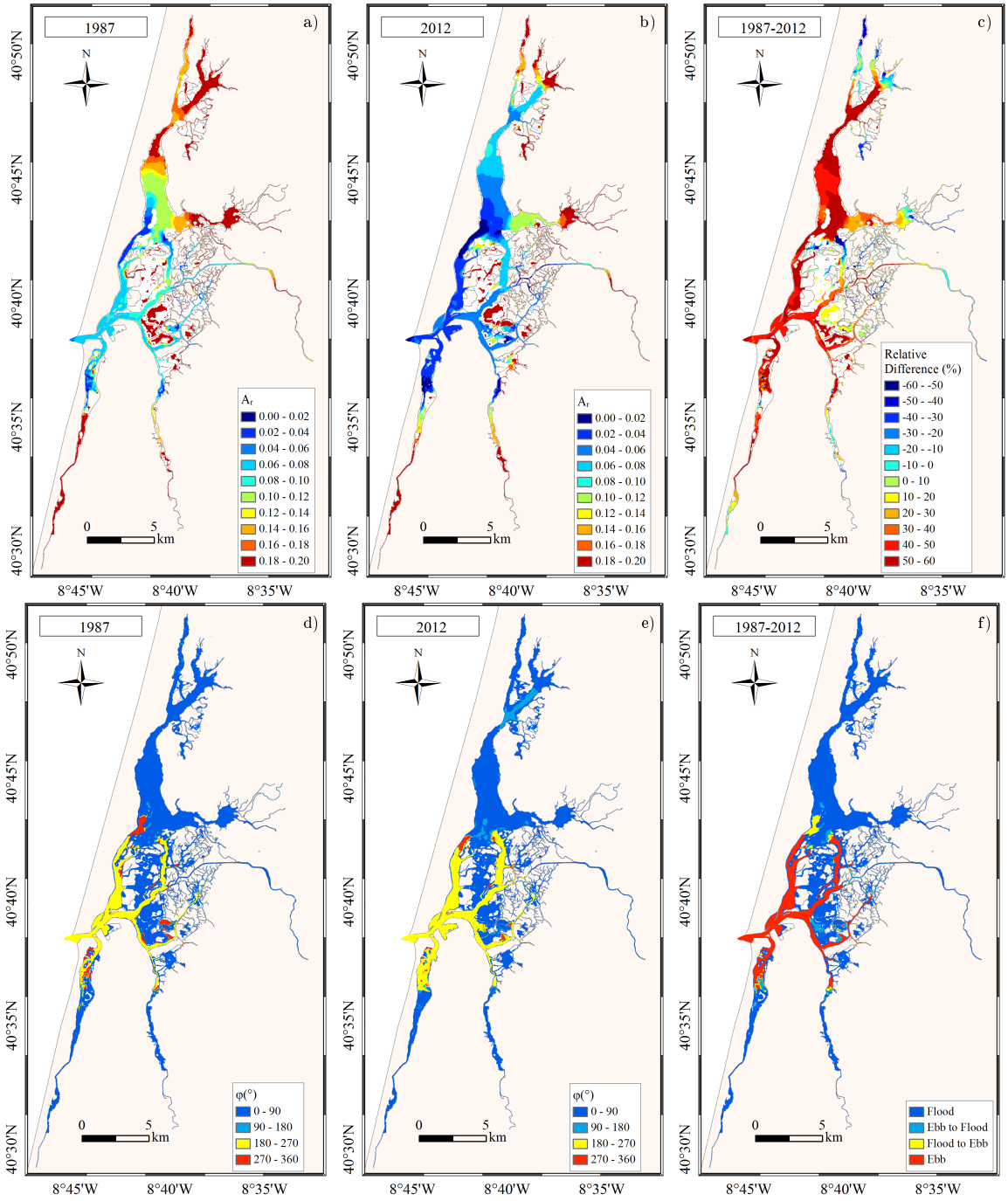


Figure 5.2: Amplitude ratio ($A_r$) for: a) 1987; and b) 2012 configurations. c) $A_r$ relative difference (%) between 1987 and 2012. Relative phase ($\varphi$) for: d) 1987; and e) 2012 configurations. f) Relative phase variations between 1987 and 2012 configurations.

for both configurations. The $M_2$ currents rotation is similar for both configurations (Figure 5.3f), except in some areas of S. Jacinto channel that changed from clockwise to anti-clockwise rotation.

The residual currents were computed for each configuration, as well as their relative

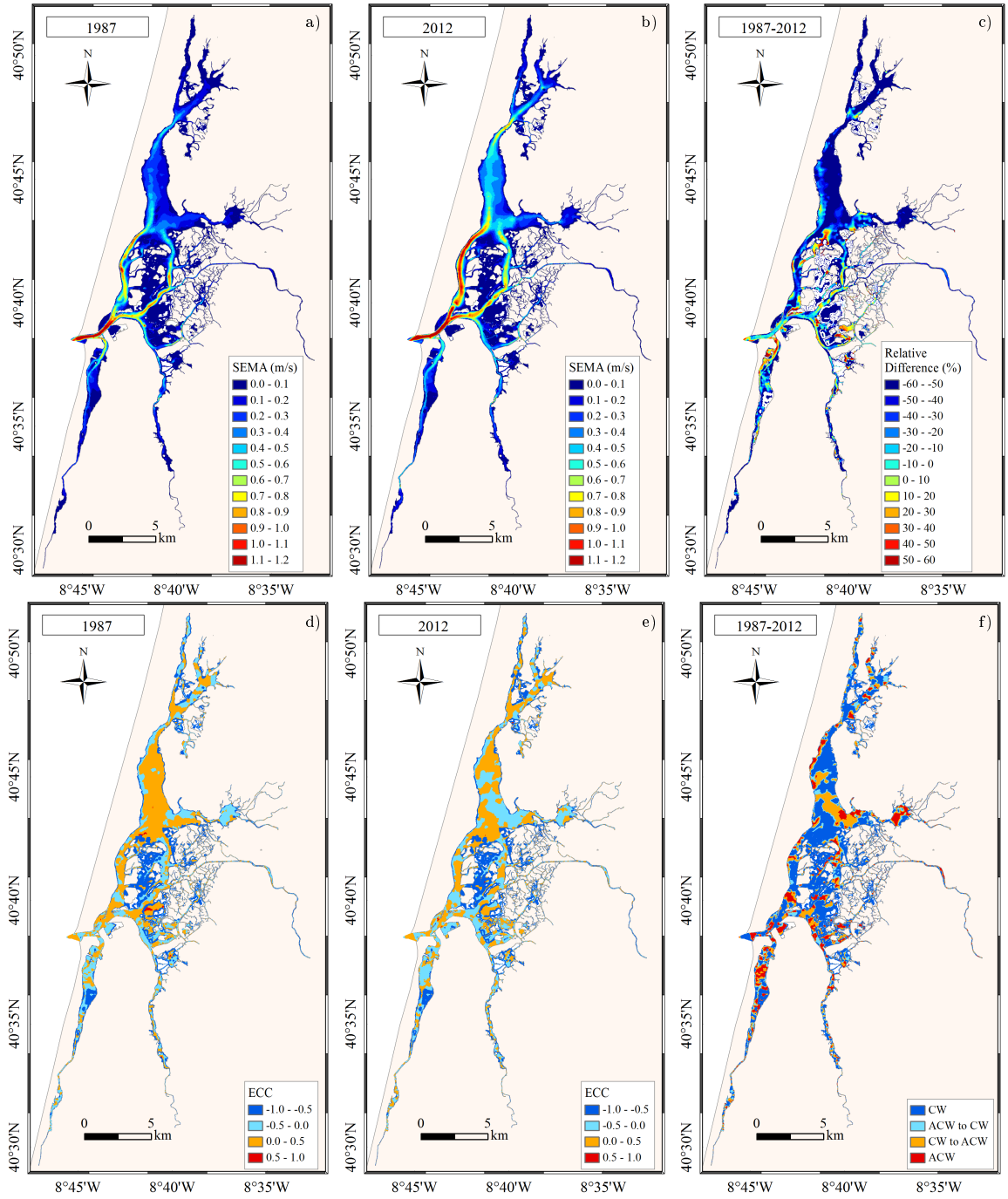


Figure 5.3: Semi-major axis ($SEMA$) of $M_2$ tidal ellipses for: a) 1987; and b) 2012 configurations. c) $SEMA$ relative difference (%) between 1987 and 2012 configurations. Tidal ellipses eccentricity ($ECC$) for; d) 1987; and e) 2012 configurations. f) $ECC$ changes between 1987 and 2012 configurations.

difference between 1987 and 2012. Figures 5.4a and 5.4b show that residual currents present similar patterns for both configurations. The highest residual currents were found at the lagoon entrance (can achieve 0.2 m/s), decreasing their magnitude toward

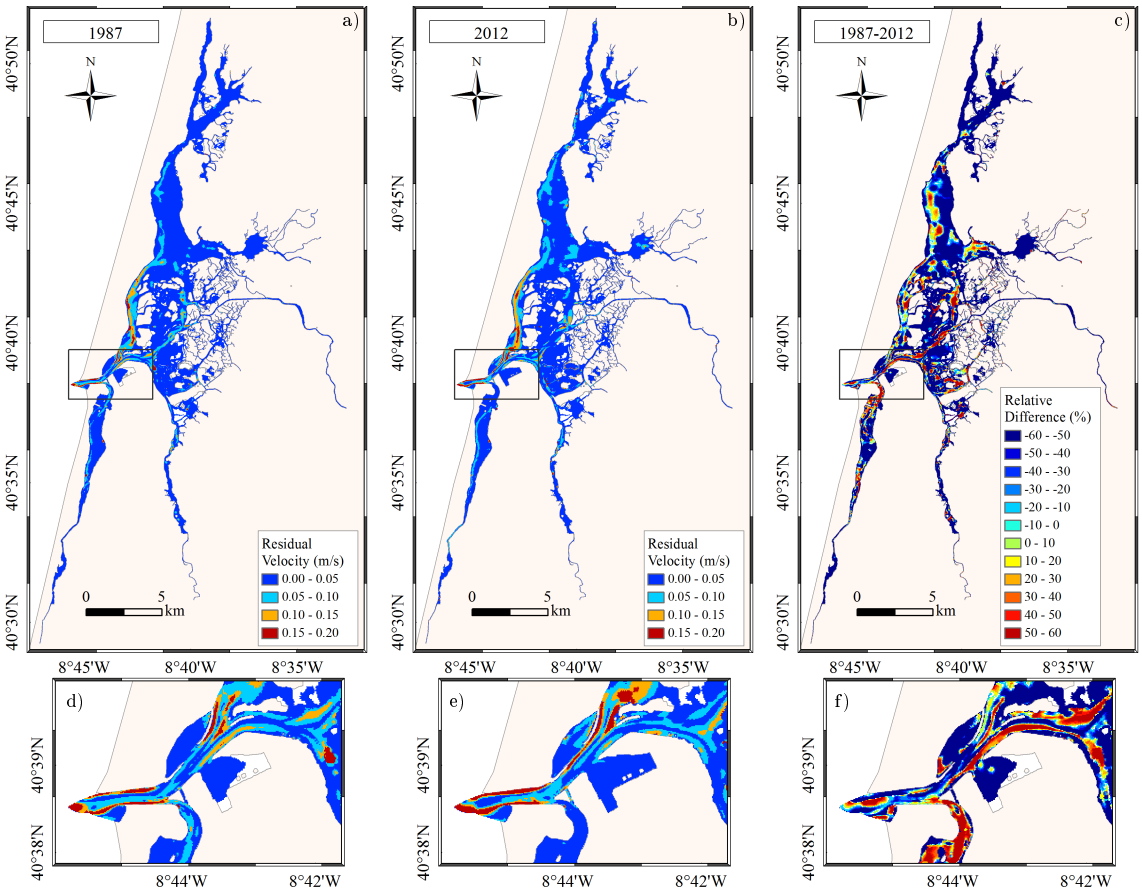


Figure 5.4: Magnitude of residual velocity (m/s) for: a, d) 1987; and b, e) 2012. c, f) Residual velocity relative difference (%) between 1987 and 2012 configurations.

the channels head's (lower than 0.05 m/s). Despite the analogous patterns, from 1987 to 2012 the residual currents magnitude increased in the shallow areas and narrow channels and decreased in the deeper channels (Figure 5.4c).

The residual currents were analysed in detail for the lagoon entrance (Figures 5.4d, 5.4e and 5.4f) revealing a general decrease of its magnitude between 1987 and 2012 in agreement with tidal asymmetry results. Nevertheless, this is not a regular pattern, considering the influence of local geometry on the generation of residual currents. Taking into account that the residual circulation in this area is generally seaward (following the ebb dominance previously described), these results evidence a reduction in the lagoon natural trend to export properties.

The residual currents and lagoon dominance results found in this study are in agreement with Dias [2001], Oliveira et al. [2006] and Lopes et al. [2011] results, evidencing that the lagoon upper areas act as sediment traps, while the entrance area

tends to export sediments to the ocean. Furthermore, the tidal currents increase suggests higher sedimentation exchanges from 1987 to 2012, which increased the margins erosion and the water turbidity, corroborating the Azevedo et al. [2013] and Cunha et al. [2013] studies that found a decline in the area covered by *Zostera noltii* from 1984 to 2010 in Ria de Aveiro. Despite its general decline, seagrasses play an important role on coastal ecosystems due to its high primary production, promoting biological diversity [Borum et al., 2004]. Hence their long-term maintenance should be a crucial target on coastal management [Borum et al., 2004]. In summary, between 1987 and 2012 tidal influence and tidal currents increased within the lagoon, while residual currents decreased/increased in the deepest/shallow areas, inducing changes on the biological conditions of the system, namely constraining the seagrasses areas.

### 5.3.2 Tidal changes under MSLR

The relative difference of amplitude ratio between 2012 configuration and each MSLR simulation was computed to evaluate changes in the tidal distortion forecasted under MSLR conditions (Figure 5.5). For all geometric configurations the results show that tidal distortion will increase at the lagoon mouth and central area and decrease at the lagoon upper reaches under MSLR conditions comparing to present mean sea level. The highest tidal distortion deviations were found for scenarios 3 and 4, which consider the protection of the main channels margins. Indeed, the tidal distortion decreases/increases 60% at the lagoon central area/middle of S. Jacinto and Mira channels.

Also, the difference between non-flood protection ("do nothing") and flood protection configurations were examined computing the relative difference between non-protection (scenario 1) and protection configurations (scenarios 2, 3 and 4) (Figure 5.6). The results evidence that the tidal distortion tends to be exacerbated at the lagoon entrance and central area and attenuated at the inner regions under flood protection configurations comparing to the non-protection configuration. The deviations can exceed 60% in some areas, highlighting that the tidal distortion is highly sensitive to the geometric configuration of the lagoon.

The current ellipses $SEMA$ relative difference between 2012 configuration and each

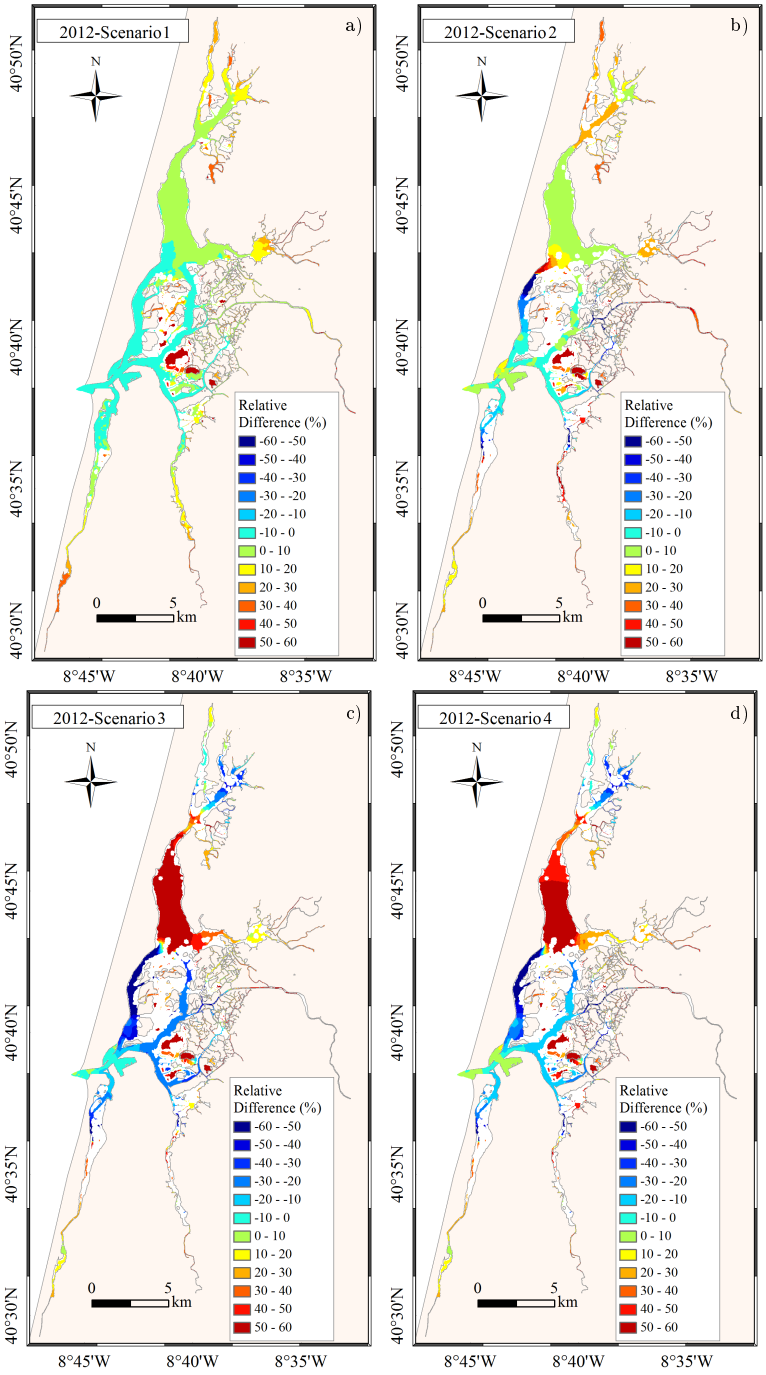


Figure 5.5: $A_r$ relative difference (%) between 2012 and a) Scenario 1, b) Scenario 2, c) Scenario 3 and d) Scenario 4.

MSLR scenario was also assessed. The results (Figure 5.7) show that tidal currents will increase for most of the lagoon under MSLR conditions, independently of the geometric configuration. The highest current amplification was found for scenarios 1 and 2.

The relative difference between non-protection and protection geometric configurations (Figure 5.8) evidences that tidal currents tend to be attenuated under

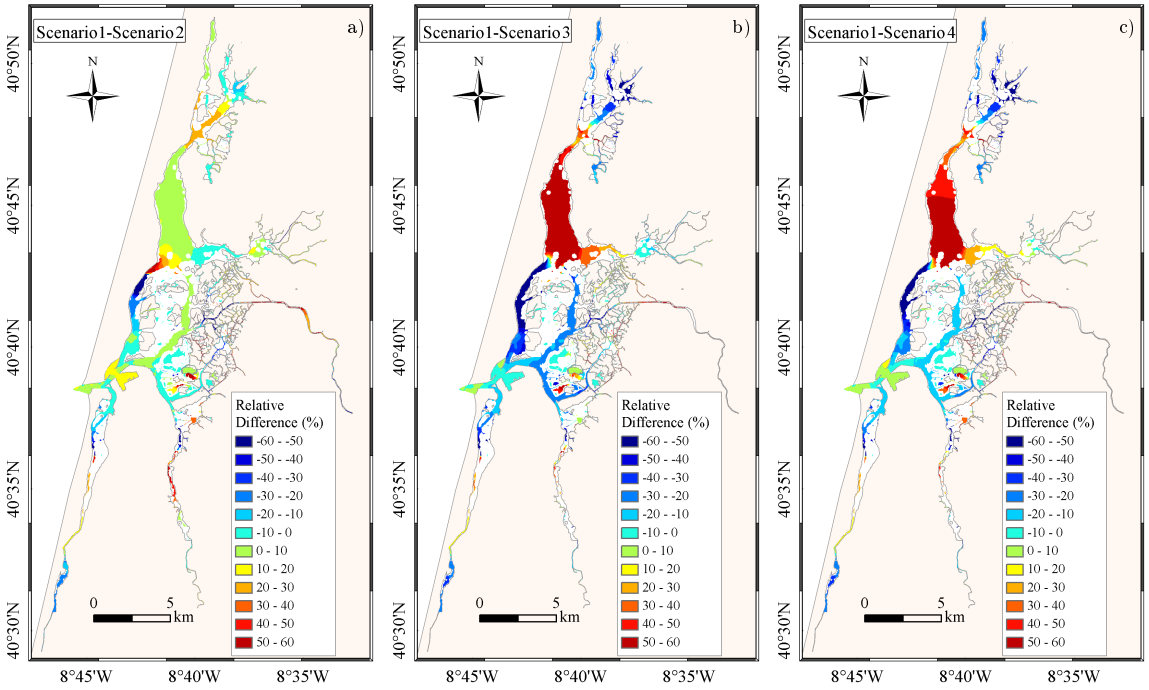


Figure 5.6: $A_r$ relative difference (%) between Scenario 1 and a) Scenario 2, b) Scenario 3, c) Scenario 4.

flood protection configurations. Moreover, the deviations between scenarios are considerable and can achieve 20% in some regions.

Concerning residual currents, the relative difference between 2012 and MSLR simulations (Figure 5.9) highlights its general magnitude increase when marginal flooding is allowed (scenario 1). When flood protection barriers are considered (scenarios 2, 3 and 4) residual currents increase at the lagoon central area and decrease at the lagoon main channels.

The deviations between scenarios were quantified by computing the relative difference between non-protection (scenario 1) and protection (scenarios 2, 3 and 4) configurations (Figure 5.10). Results highlight that residual currents tend to increase in S. Jacinto, Espinheiro and Ílhavo channels and to decrease in Mira channel from scenario 2 to scenario 1. Concerning scenarios 3 and 4, residual currents are generally lower than for scenario 1 for the overall domain. Particularly at the inlet region, the deviations between protection and non-protection configurations are similar and can exceed 60%, emphasizing that residual currents are strictly dependent on the lagoon geometric configuration.

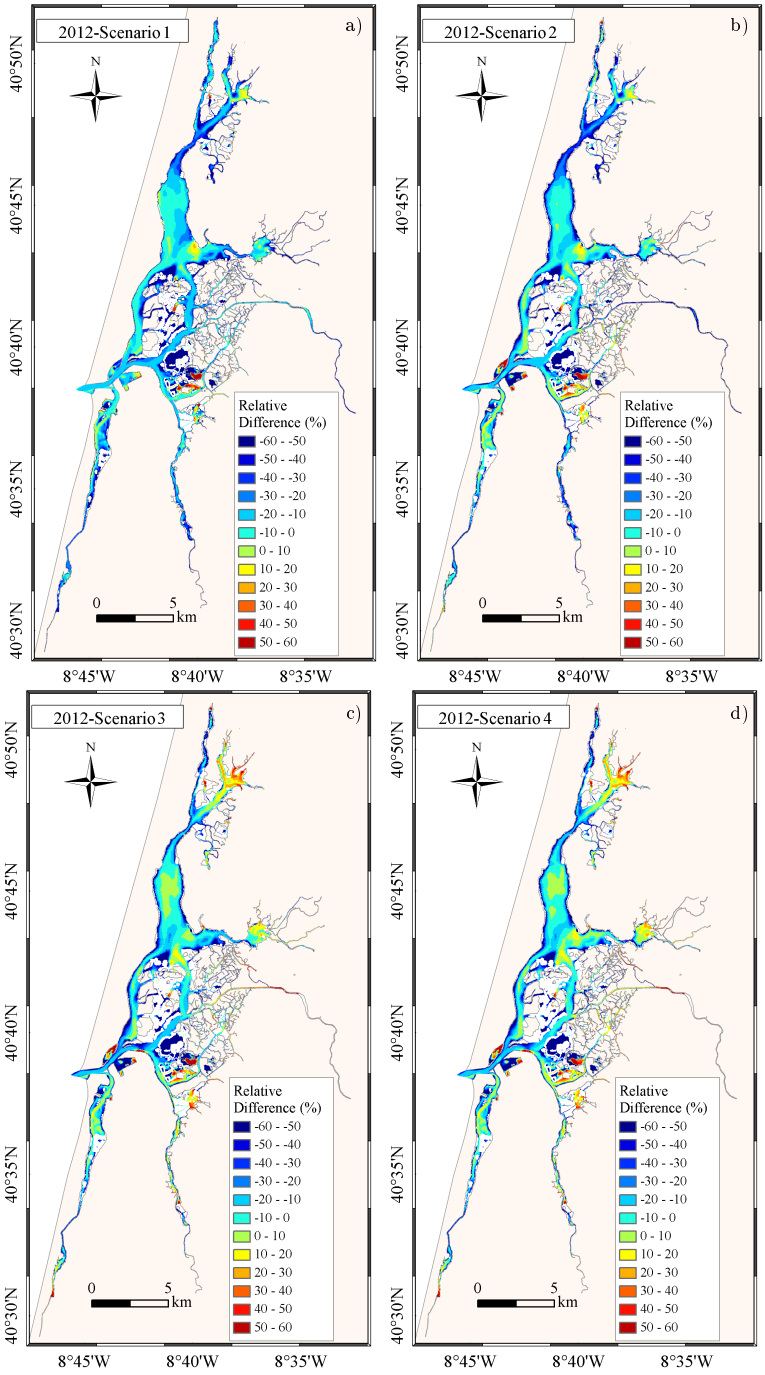


Figure 5.7: *SEMA* relative difference (%) between 2012 and a) Scenario 1, b) Scenario 2, c) Scenario 3 and d) Scenario 4.

There are studies reporting the influence of MSLR on coastal tidal dynamics in the presence or absence of protective coastal barriers; however studies addressing this issue in coastal lagoon systems were not found, highlighting the relevance of the present research. Indeed, Pelling et al. [2013a] and Pelling and Green [2014] found that the magnitude of the changes induced by MSLR at the European Shelf tidal dynamics is

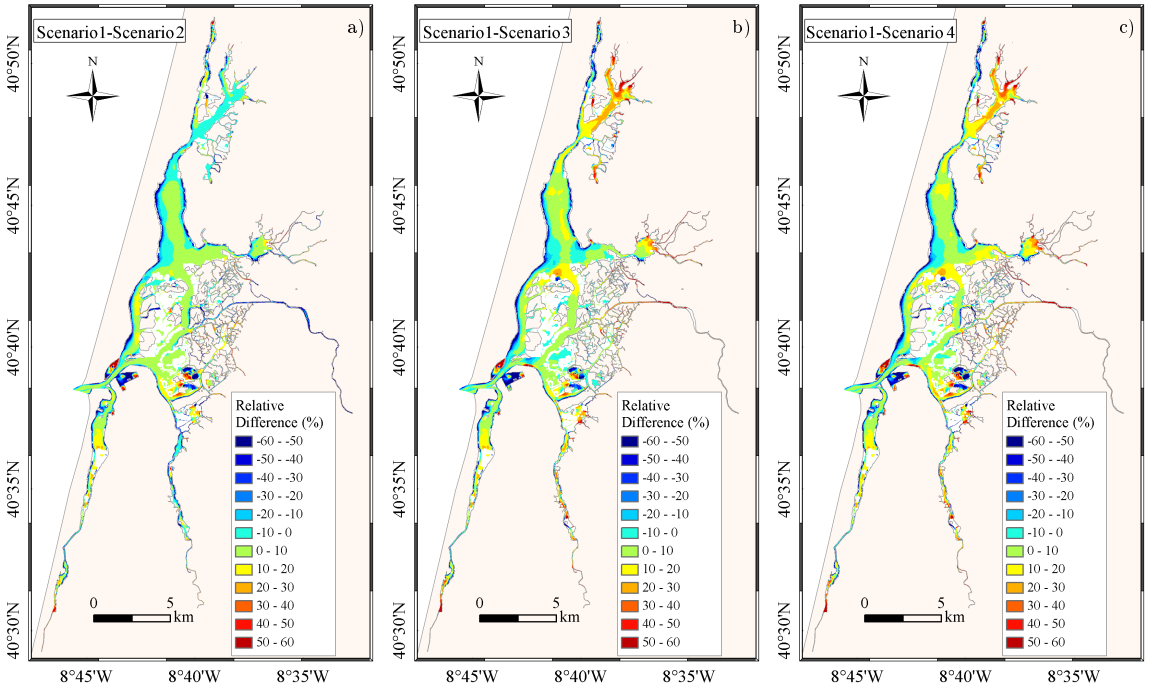


Figure 5.8: *SEMA* relative difference (%) between Scenario 1 and a) Scenario 2, b) Scenario 3, c) Scenario 4.

strongly dependent on the level of coastal defence. At a finer spatial scale, Pelling and Green [2013] and Pelling et al. [2013b] found that the inclusion of flood defences in numerical models for the Gulf of Maine and for the Bohai Sea, respectively, is crucial for accurate MSLR studies, emphasizing the significant deviations detected between predictions considering or not flood defences. Consequently, the results presented here are in agreement with those studies and accentuate the need to include flood defences when studying the effect of MSLR on tidal dynamics of coastal lagoons subjected to human influence, like for example Ria Formosa, Venice, Vistula and Marano-Grado coastal lagoons. Recently, Ferrarin et al. [2014] corroborate this hypothesis, once they found that tidal changes observed between 1930 and 2012 within the Venice lagoon are essentially induced by geomorphological modifications, highlighting the need to account for coastal defences in long-term MSLR studies.

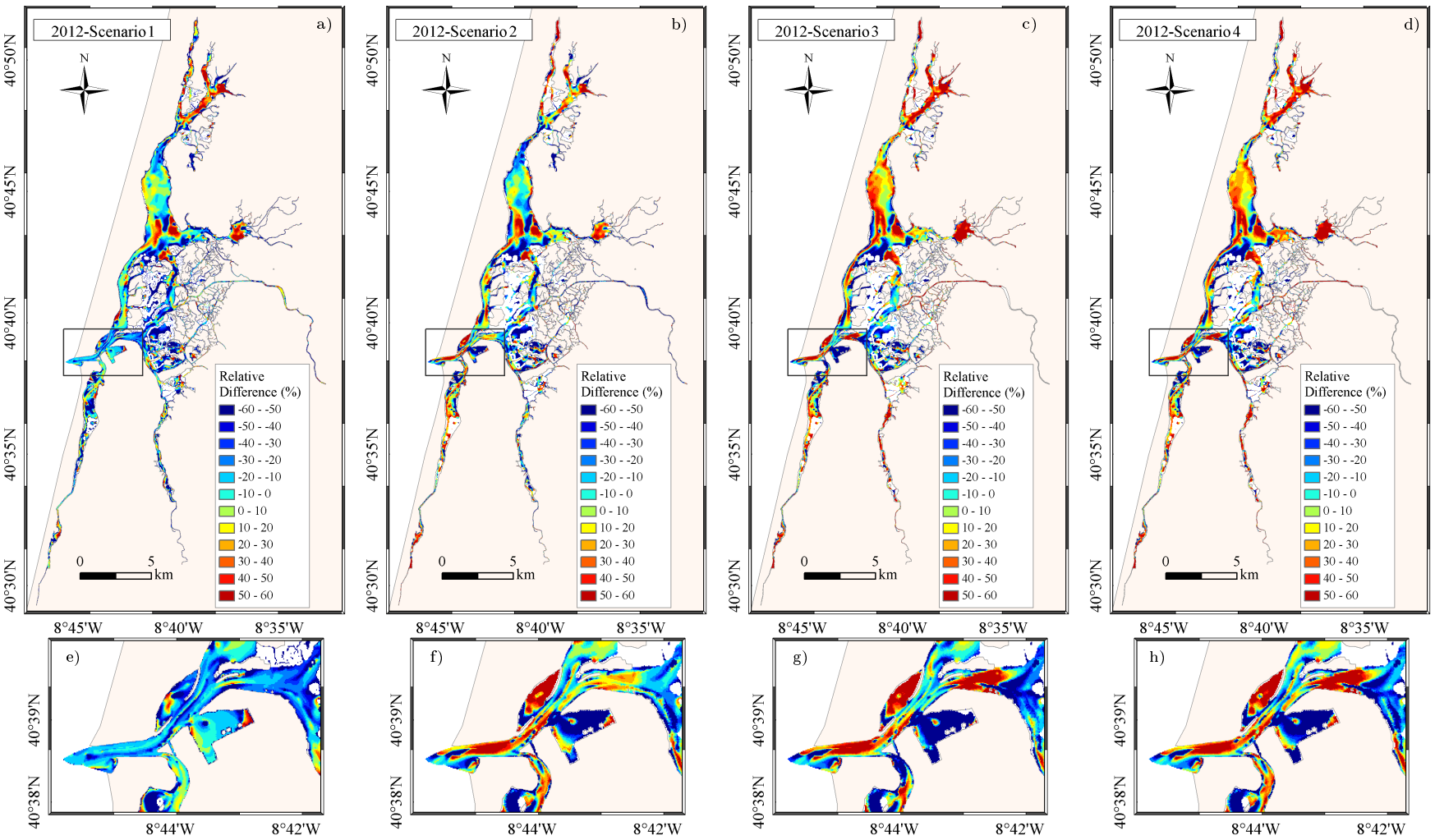


Figure 5.9: Residual velocity relative difference (%) between 2012 and: a, e) Scenario 1, b, f) Scenario 2, c, g) Scenario 3 and d, h) Scenario 4.

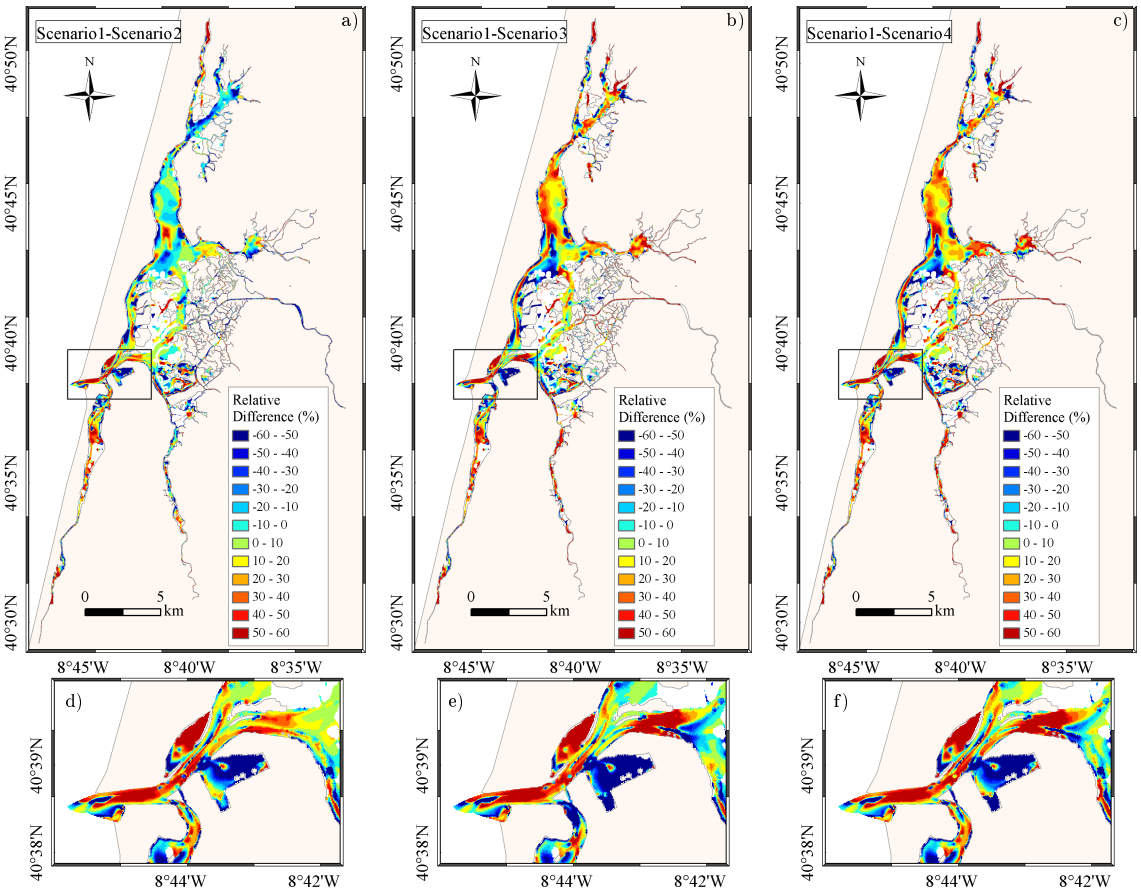


Figure 5.10: Residual velocity relative difference (%) between Scenario 1 and a) Scenario 2, b) Scenario 3 and c) Scenario 4.

## 5.4 Conclusions

Considering that the floods of oceanic origin are strictly dependent on the tidal conditions, this study researches the influence of geomorphological changes and MSLR on Ria de Aveiro tidal dynamics through hydrodynamic modelling.

The model was first applied to evaluate changes in tidal propagation between 1987 and 2012, period characterized by a deepening of the lagoon main channels, that increased its accommodation space and modified the bottom friction. As consequence, a/an decrease/increase of tidal distortion in the deeper/shallower channels was observed. The lagoon dominance is quite similar for both dates showing ebb dominance at entrance and central area and flood dominance at upper areas. Moreover, a general increase of tidal currents was found, as well as a decrease of residual currents in the lagoon central area, highlighting the reduction in properties exchange between

the lagoon and the ocean and shifting the sediments distribution and the biological signatures of the lagoon.

The second model application investigated future changes in tidal dynamics motivated by the MSLR, considering hypothetical geometric lagoon configurations including or not flood protection barriers in critical areas. Independently of the geometric configuration a decrease/increase of tidal distortion at the lagoon central area/upper areas is forecasted following the trend observed from 1987 to 2012. Moreover, an intensification of tidal currents is predicted under MSLR conditions, which is stronger when no flood protection barriers are considered. In addition, an intensification of residual currents is expected at the lagoon central area, amplifying the properties export to the ocean under MSLR conditions. Given that biological distribution and productivity are highly dependent on the lagoon hydrodynamics, future changes on biological patterns are expected under MSLR conditions. Particularly, the higher sediment transport expected under MSLR conditions could be a trigger factor intensifying the pressures over seagrasses.

In general the tidal properties trends are similar for all geometric configurations under MSLR conditions, however the changes magnitude is highly dependent on the lagoon geometric configuration. Indeed, the deviations between the "do nothing" option and the flood protection scenarios can achieve 60% for tidal distortion and residual currents and 20% for tidal currents. Therefore, this investigation demonstrates that long term studies aiming to forecast future lagoons physical and biogeochemical properties should consider not only the MSLR, but should also take into account the lagoon future geomorphology. Therefore, both natural and anthropogenic factors determining the geomorphological behaviour of the system should be assessed to predict the future lagoon configuration. Accordingly, in low-lying systems under strong human pressure (such as Ria de Aveiro), the influence of MSLR on tidal properties should be studied integrating numerical modelling with flood defence structural measures in order to account for the future human induced geomorphological changes of the coastal system.

In summary, this research proved that the mean sea level and the geomorphological conditions determine the tidal propagation within the lagoon. Attending this,

and considering that floods of oceanic origin are strictly dependent on the tidal conditions, the hydrodynamic simulations should integrate the expected flood protection infrastructures when assessing inundation under future scenarios.

# Chapter 6

# Lagoon flood extent - dependence on the morphology

## 6.1 Introduction

The water flow dynamics within coastal lagoons is strongly dependent on the bathymetric and geometric configuration of each system [Araújo et al., 2008; Picado et al., 2010; Zhang et al., 2010; Jewell et al., 2012; Ferrarin et al., 2014]. In this way, modifications in flow dynamics can change the water levels and consequently modify the flooding patterns in low-lying coastal areas, such as Ria de Aveiro. Moreover, as found in Chapter 5, an accurate definition of future morphological patterns is crucial towards a precise evaluation of the effects of climate changes on coastal systems.

The global objective of this chapter is to investigate the dependence of the lagoon flooding patterns on the morphology. Firstly, the hydrodynamic model ELCIRC will be applied to assess changes in the lagoon flooding patterns motivated by the geomorphological changes between 1987 and 2012. Secondly, the morphodynamics of the inlet region will be investigated by applying the morphodynamic model MORSYS2D. This analysis was included in order to understand if climate changes will impact the inlet morphodynamics, modifying consequently the lagoon water dynamics. Lopes et al. [2011] studied already the influence of MSLR on the inlet morphodynamics and found that MSLR will not change the erosion/deposition patterns of the inlet area, but will intensify the sedimentary fluxes. Despite the occurrence of both deposition

and erosion, they found that the inlet channel tends to be filled with sediments. As consequence, higher volume of deposited sediments is predicted under MSLR conditions [Lopes et al., 2011]. As the influence of wave regime modifications induced by climate changes on the inlet region morphodynamics was not studied yet, the present application intends to investigate if the clockwise rotation of waves found for the future climate (Chapter 3) will change the inlet morphodynamics.

## 6.2 Methodology

### 6.2.1 Flood extent and tidal prism changes between 1987 and 2012

Four numerical bathymetries are used in this study, constructed based on topo-hydrographic data from surveys of the lagoon main channels carried out in 1987 and 2011 and of the inlet region carried out in 2001 and 2012 (see Chapter 2 for more details). Simulations with ELCIRC model were made using the four numerical bathymetries (Table 6.1). The model was forced in each case imposing at the ocean open boundary time series of SSE determined by harmonic synthesis of the thirteen most important local constituents (following section 4.2.3.1). Three tidal conditions were analyzed, corresponding to neap tide, mean tide and spring tide, which amplitudes were determined in Chapter 3 (Table 3.1. The ELCIRC model was run for 5 days, considering mean values of fluvial discharges [Génio et al., 2008] and assuming that

Table 6.1: Details of the constructed numerical bathymetries.

| Bathymetry | Details |
|---|---|
| 1987 | 1987 General bathymetric survey |
| 2001 | Bathymetry of 1987 updated at the inlet region with data collected in 2001 |
| 2011 | Bathymetry of 2001 updated at the lagoon main channels with data collected in 2011 |
| 2012 | Bathymetry of 2011 updated at the inlet region with data collected in 2012 |

wind stress is negligible. The numerical results will be used to assess the lagoon flooded area and the tidal prism at the cross-sections represented in Figure 6.1. To assess the tidal prism modifications between 1987 and 2012, the tidal prism increase ratio ($IR$) was computed following to equation 6.1:

$$IR_{i+1} = \frac{(TP_{i+1} - TP_i)}{TP_i} \times 100 \tag{6.1}$$

Where $i$ is the index defining the year of a numerical bathymetry and $i+1$ represents the year of the following numerical bathymetry. This analysis will identify potential changes on the redistribution of water among the lagoon channels, over 1987 and 2012.

### 6.2.2 Inlet morphodynamics

The morphodynamic model MORSYS2D was used to simulate the sediment dynamics at the inlet region. The implementation used was previously validated by [Plecha, 2011]. The representative wave regimes characteristic of present and future climates previously determined in Chapter 3 were used to feed the model. In this work the model was run for 60 days using a constant time step of 3600 s and for 365 days using an adaptative time step ranging from 900 s to 3600 s. The 60 days runs (starting on January 1$^{st}$) were used to study the residual sediment fluxes that were obtained by averaging the sediment fluxes over two $M_{Sf}$ periods, while the 365 days simulations were used to investigate potential morphological variation trends. Besides the computational costs, the uncertainty of morphodynamic results increases linearly

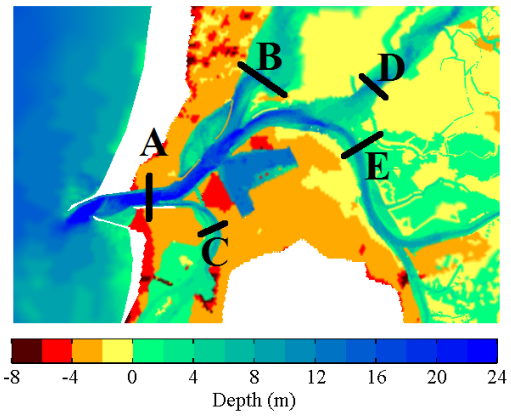


Figure 6.1: Location of cross-sections where the tidal prism was computed.

with time [Fortunato et al., 2009]. Attending this, a year simulation is commonly adopted to investigate morphological variation trends. The sedimentation rates were evaluated at the regions represented in Figure 6.2.

## 6.3 Results and discussion

### 6.3.1 Flood extent and tidal prism changes between 1987 and 2012

The hydrodynamic model ELCIRC was run for each configuration previously described, and the flooded area was determined for each case (Table 6.2). Between 1987 and 2012 the lagoon flooded area increases approximately 3%, 7% and 16% for neap, mean and spring tide conditions, respectively. Moreover, the bathymetric differences that occurred in the inlet region (between 1987 and 2012 and between 2011 and 2012) did not influence the extension of the flooded area. The highest increase in the flood extension area was found between 2001 and 2011 configurations, with an increase of 3%, 6% and 12% under neap, mean and spring tide conditions, respectively. These results show that the deepening of the lagoon main channels (not just of the inlet) is the major factor determining the increase of the lagoon flooded area. It is is important to highlight that the dredging operations carried out in the main channels in the nineties are recorded in the 2011 bathymetry. In this way, it is concluded that the increase in flooded area can be partially motivated by these dredging operations.

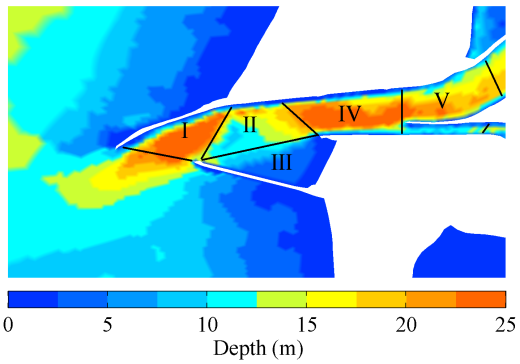


Figure 6.2: Numerical bathymetry of the inlet region representing the regions where sedimentation rates were computed.

Table 6.2: Lagoon flooded area ($km^2$), considering the 1987, 2001, 2011 and 2012 configurations.

| Configuration | Neap Tide | Mean Tide | Spring Tide |
|---|---|---|---|
| 1987 | 65 | 68 | 77 |
| 2001 | 65 | 69 | 80 |
| 2011 | 67 | 73 | 89 |
| 2012 | 67 | 73 | 89 |

Figure 6.3 represents the flood extent maps for each bathymetric configuration and for each tidal condition considered. The bathymetric changes influence is higher in spring tide and at the upper reaches of S. Jacinto channel, which show the highest increase in flood extent. Although with a minor significance, some central lagoon regions were also flooded in response to depth variations. The flood extent in Mira and Ílhavo channels is similar for each model configuration, demonstrating that bathymetric changes did not influence significantly the inundation extent in these channels. The opposite trend observed between S. Jacinto and Mira and Ílhavo channels is explained

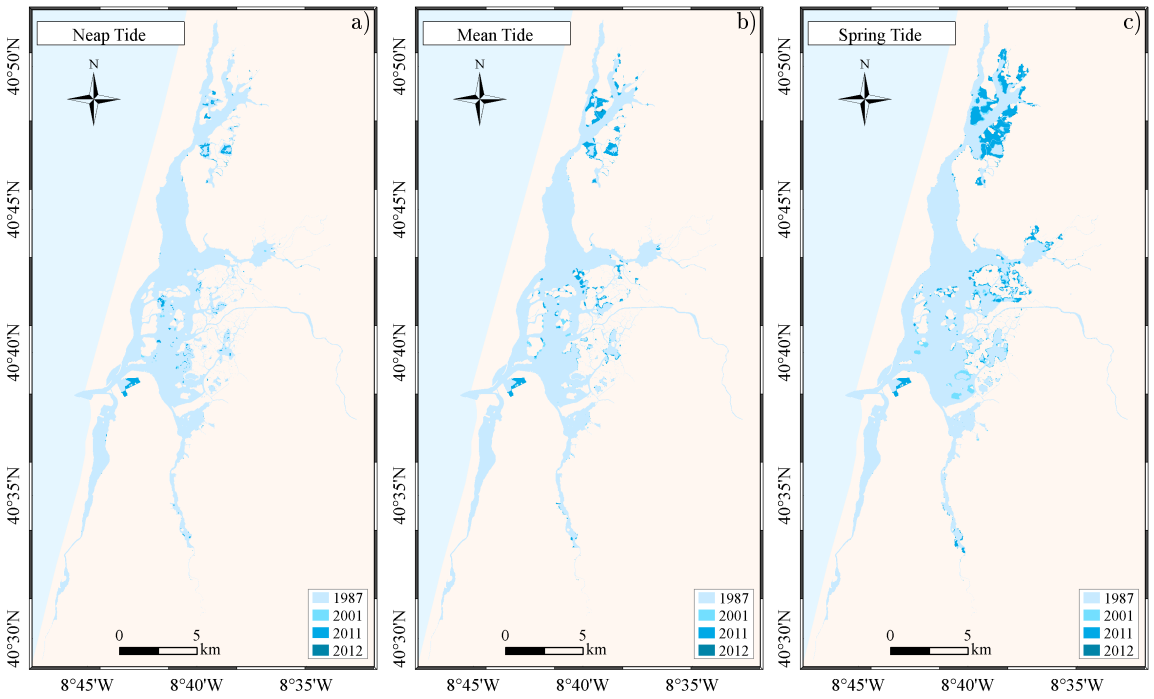


Figure 6.3: Flood extent maps for a) neap, b) mean and c) spring tide conditions, considering the 1987, 2001, 2011 and 2012 configurations.

by the distinct geomorphological changes occurred in these channels, as well as by the topography of their margins. Indeed, among the lagoon main channels, the S. Jacinto channel experienced the highest bathymetric changes (see Figure 2.2), while the bathymetric changes occurred in Mira and Ílhavo channels were almost negligible (see Figure 2.2). Additionally, the marginal areas adjacent the S. Jacinto channel present lower and flat topography than those adjacent the Mira and Ílhavo channels (see Figure 4.3).

The tidal prism results (Figure 6.4) are in agreement with the flooded area extension, once the highest modifications were observed from 2001 to 2011 configurations (where the main channels deepening is included). Also, results evidence that the generalized deepening of the lagoon channels between 1987 and 2012 induced a global increase on tidal prism at the cross-sections analyzed. This outcome was expected by several reasons: the cross-sectional area increases with the channels deepening, enabling a large volume of water to cross the lagoon sections; the total water volume flowing through the inlet has to fill a higher lagoon volume resulting from the channels deepening; as friction decreases with the rising depth, the velocities inside the lagoon become higher producing higher tidal prisms.

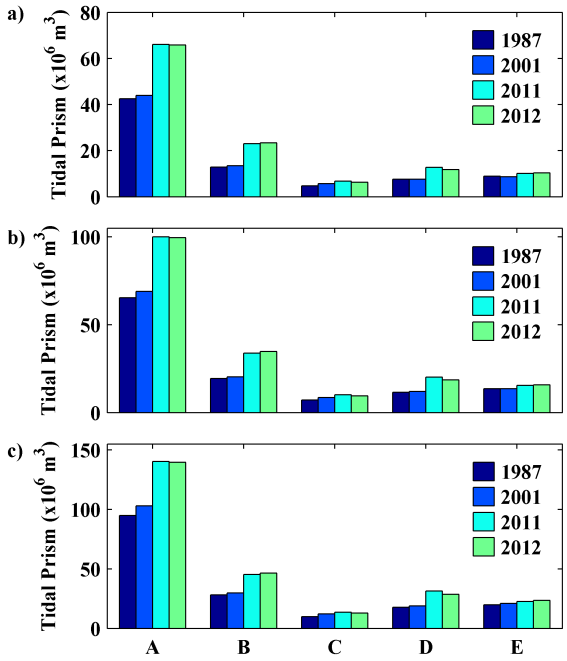


Figure 6.4: Tidal prism in each cross-section for: a) neap tide; b) mean tide; and c) spring tide.

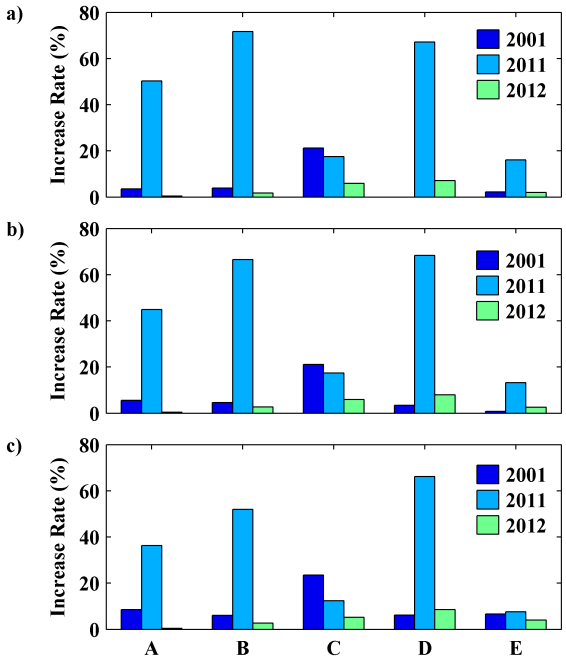


Figure 6.5: Tidal prism increase ratio (%) in each cross-section relative to precedent bathymetry for: a) neap tide; b) mean tide; and c) spring tide.

Figure 6.5 presents the tidal prism increase rate between bathymetric configurations for neap, mean and spring tide conditions. Its analysis show that the tidal prism is increasing along the time in all the cross-sections analysed and independently of the tidal conditions. Despite this, the tidal prism amplification highly depends on the bathymetric changes between bathymetric surveys. Indeed, tidal prism increase rates of 9%, 43% and 1% were found at the inlet cross-section for 2001, 2011 and 2012 bathymetries. This pattern highlights that the highest tidal prism amplification occurred between 2001 and 2011, in response to the main channels deepening (partially motivated by dredging operations).

The results also evidence that the tidal prism rise is not uniform for all the cross-sections. Indeed, between 2001 and 2011, at the inlet (cross-section A) the tidal prism increased on average approximately 43%, while at cross-sections B, C, D and E the amplification was on average 63%, 16%, 67% and 12%, respectively. The lowest rates found in Mira (C) and Ílhavo (E) channels are in agreement with the flood extent results, that evidence minor changes in these channels over 2001 and 2011. Furthermore, between 1987 and 2001 the increase rate at the inlet is approximately 9%, while at the cross-sections B, C, D and E the tidal prism increase rate was on

average 6%, 23%, 6% and 7%, respectively. Here, the highest increase rate was found in Mira (C) channel. This distinct pattern of Mira channel highlights that the inlet region deepening induced higher tidal prism changes than the main channels deepening. It is also evident that between 2011 and 2012 the changes in the tidal prism are negligible.

In summary, the tidal prism increase is emphasized in cross-sections A (inlet), B (S. Jacinto) and D (Espinheiro), presenting the highest values at cross-sections B and D. This non-uniformity of tidal prism increase at the cross-sections evidences that the bathymetric changes modified the water flow within the lagoon. Particularly, the deepening of inlet region observed between 1987 and 2001 induced a higher increase in the tidal prism at the Mira channel than in the other channels. Otherwise, the deepening of the lagoon main channels found between 2001 and 2011 leaded to a higher increase of tidal prism at S. Jacinto and Espinheiro channels than in the other channels.

The flood extent and tidal prism results may be discussed now considering the geomorphology of the lagoon channels (see Figure 4.3) and the bathymetric changes between 1987 and 2012 (see Figure 2.2). This analysis evidenced that the highest changes in the tidal prism occurred in the regions that experienced the highest bathymetric changes. Indeed, the tidal prism increases found at the S. Jacinto channel between 2001 and 2011 are related with the major deepening of this channel, motivated in part by dredging operations. As the S. Jacinto channel margins present low and flat topography, this tidal prism increase resulted in an increase of the flood extent. Conversely, the tidal prism increase of approximately 23% at Mira channel between 1987 and 2001 (motivated by the inlet deepening) did not induce significant changes in the Mira channel flood extent, once their margins present higher height than the other lagoon main channels.

It should be highlighted that the deepening of the lagoon main channels, rather than the inlet deepening, was the major factor determining the lagoon flood extent changes between 1987 and 2012. Attending this, it is concluded that the dredging of main channels increased the floods threat of oceanic origin in marginal areas of low and flat topography, located mainly in the S. Jacinto channel.

### 6.3.2 Inlet morphodynamics

The residual sediment fluxes were computed for present and future wave regimes (Figure 6.6), and the results evidence patterns similar for both conditions. The sediment fluxes observed nearshore are approximately two orders of magnitude higher than those observed at the inner lagoon. However, given the importance of the inner morphological changes on the establishment of the lagoon inundation patterns, the inner fluxes were analysed in detail here. The sediment fluxes at the inlet channel highlight the existence of two recirculation patterns, one located between the breakwaters and the other located upstream and extending for most of the entrance channel. The first vortex presents an anticlockwise rotation and evidences the entrance/exit of sediments close to the southern/northern breakwater. The second vortex rotates clockwise inducing sediment fluxes directed landward/seaward at the upper/lower part of the channel.

The relative difference between the residual fluxes magnitude for future and present climates is represented in Figure 6.7. Results evidence areas where sediment fluxes decrease and other areas where they increase. However, both positive and negative differences are very small (approximately 2%) in most of the inner channel, highlighting insignificant changes on the sedimentary fluxes under future wave regime. Offshore the differences are higher, reaching 10% in some areas close the coastline.

The bathymetric changes after one year of simulation are illustrated in Figure 6.8.

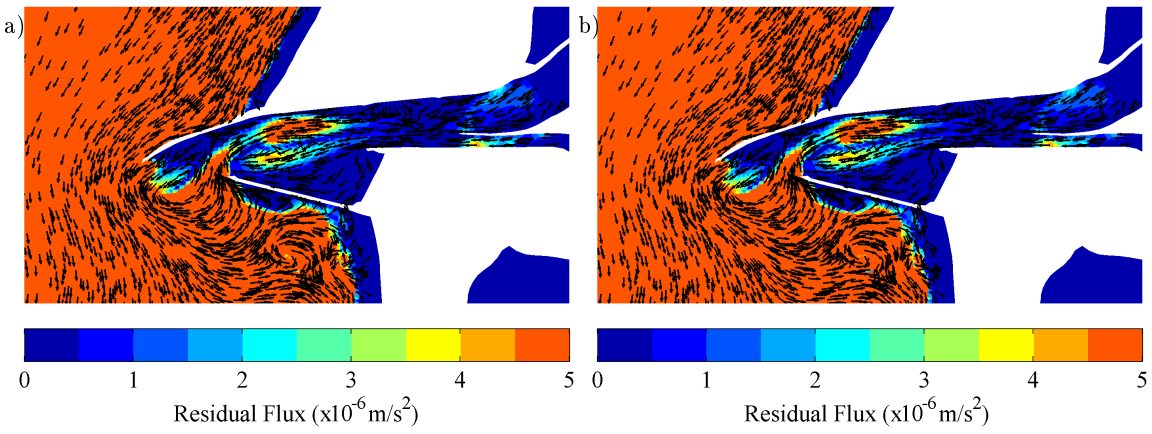


Figure 6.6: Residual sediment transport ($\times 10^{-6}$m/s$^2$) under: a) Present wave regime; b) Future wave regime.

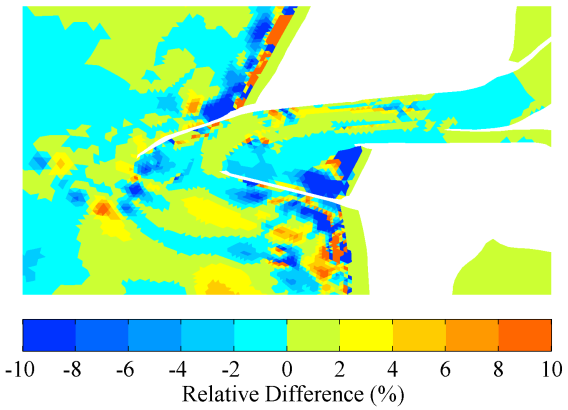


Figure 6.7: Relative difference (%) between future and present residual fluxes.

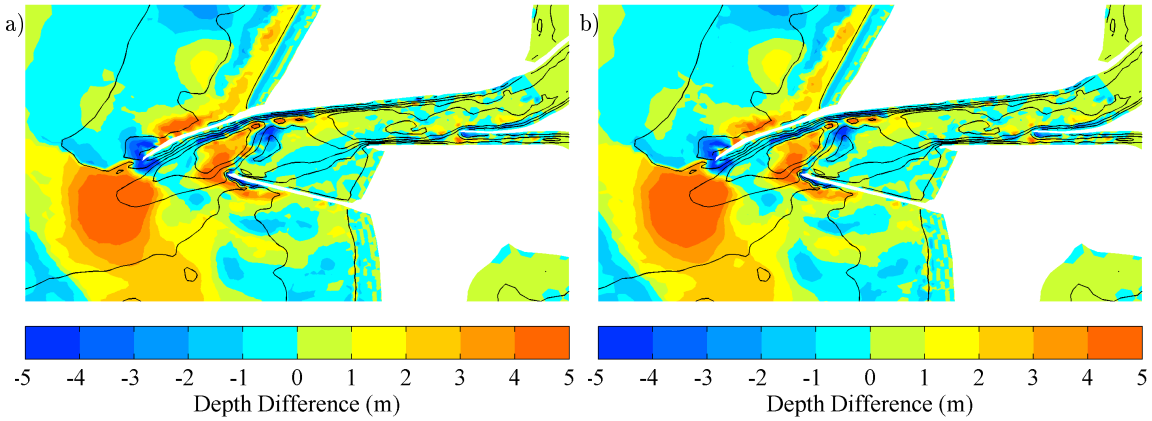


Figure 6.8: Depth difference (m) between initial and predicted bathymetries under: a) Present wave regime; b)Future wave regime. Black lines are the contours of the initial bathymetry.

As found for the sedimentary fluxes, the bathynetric variations patterns are similar for both climates. The predicted depth variations at the inner channel, of approximately 1 m, are small when compared with changes obtained at the entrance and nearshore, that can achieve 5 m. Nevertheless, the changes found at the inner channel reveal a prevalence for sedimentation. The results highlight that the deeper area located between the breakwaters (see Figure 6.2) tends to be filled by sediments eroded seaward and landward of its vicinity.

The relative difference between predicted bathymetries for future and present climates is presented in Figure 6.9. The percentages found are low, approximately 2% at the inner channel, highlighting that the wave regime changes imposed will not change significantly the morphodynamics of the inlet. It is also evident that the

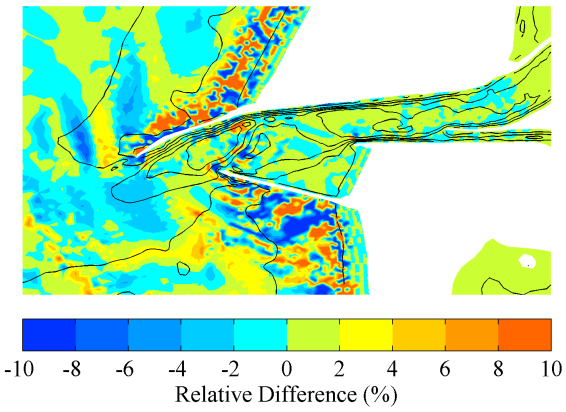


Figure 6.9: Relative difference (%) between predicted bathymetries for future and present wave regimes. Black lines are the contours of the initial bathymetry.

sedimentation observed close to the breakwater immediately downstream the inlet tends to be accentuated (approximately 5%) under future wave climate. Higher differences between both climates can be found close to the coastline, however these trends are not discussed once are out of the scope of this work.

In general, the patterns found for bathymetric variations and for residual fluxes are in agreement with those obtained by Plecha [2011] and by Lopes et al. [2011] in previous applications of MORSYS2D to the Ria de Aveiro inlet region. Despite the similarities the re-circulation pattern between the breakwaters was not predicted in Lopes et al. [2011] study. However this mismatch can be explained considering that wave forcing was not considered in the Lopes et al. [2011] application. Thus, it can be concluded that this re-circulation pattern is result of the interaction between tidal currents and waves. Comparing with the Plecha [2011] study, the differences are restricted to the lagoon entrance and nearshore area. Given the importance of waves forcing in these regions, the dissimilarities found on the sedimentary exchanges can be partially explained by the differences in the wave regimes used to feed the model in both studies.

The sedimentation rates (Table 6.3) were computed at the regions represented in Figure 6.2, for both climates. The results confirm the deposition trend at the inlet region and highlight insignificant changes on sedimentation rates for future wave regime. Attending these results and those obtained by Lopes et al. [2011], it is expected that climate changes will intensify the deposition in the inlet region.

Despite the natural trend for deposition, it is expected that the future morphological

Table 6.3: Sedimentation rates ($m^3$/day) in the regions represented in the Figure 6.2.

| | | I | II | III | IV | V |
|---|---|---|---|---|---|---|
| Wave Climate | Present | +122 | +49 | -3 | +33 | +39 |
| | Future | +117 | +50 | -3 | +33 | +39 |
| MSLR [Lopes et al., 2011] | Present | -25 | +18 | +5 | +8 | +37 |
| | Future | -37 | +30 | +8 | +17 | +63 |

changes in this lagoon region will be largely controlled by human actions, as in the past. Particularly, the dredging operations at the inlet channel should continue in the future, when necessary to maintain, or even increase, the maritime traffic to Aveiro harbour. In addition, geometric changes may also occur in the APA jurisdiction area in order to improve the maritime traffic conditions or even to enlarge the harbour area. Attending this, and considering the large uncertainty about the future human influence on the inlet region, as well as the minor changes predicted and the reduced effect that changes have on the flood extent (see previous section), it will be assumed in the future sections of this study that the future inlet bathymetry will be identical to the actual. Therefore, the future scenarios simulations performed hereafter, consider the actual bathymetric configuration.

## 6.4 Conclusions

This chapter reported the sensitivity of the lagoon flooded area to morphological changes. First, the flood extent changes between 1987 and 2012 were investigated. The results show that the Ria de Aveiro flood extent is highly sensitive to bathymetric changes. Indeed, the deepening of the inlet region and lagoon main channels observed between 1987 and 2012 induced an increase of the lagoon flooded area of 3%, 7% and 16% for neap, mean and spring tide conditions, respectively. It was found that the main channels dredging operations performed in the nineties increased the threat of floods of oceanic origin in low-lying marginal regions, located mainly in the S. Jacinto channel head and in the lagoon central area. Furthermore, the results of tidal prism at the lagoon main channels revealed important modifications between 1987 and 2012,

namely changes in the redistribution of the water volume flowing into the lagoon main channels. Between 1987 and 2012 a generalized increase of lagoon tidal prism was found, however the highest increases were found at S. Jacinto and Espinheiro channels between 2001 and 2011 configurations.

Secondly, it was investigated the influence of climate changes on the inlet morphodynamics, considering the dependence of the flooded area on the lagoon geomorphology. In this context, the Ria de Aveiro inlet morphodynamics can be modified in response to MSLR or to the clockwise rotation of the wave regime forecasted for the Aveiro region. Lopes et al. [2011] previously studied the influence of MSLR on the inlet morphodynamics and found that the deposition trend observed currently tends to be exacerbated in the future. The MORSYS2D model application presented here complements the Lopes et al. [2011] investigation, generating data that allows to research the influence of the clockwise rotation of future wave regime on the inlet morphodynamics. Results evidence that the inlet region presents a natural trend for deposition, corroborating the Lopes et al. [2011] work. The results also confirm that wave regime plays a minor role on the inlet morphodynamics and therefore no significant changes were found under climate change conditions, comparing to the present. Indeed, the MORSYS2D results highlight for both wave regimes that the inlet region has a natural trend for deposition. This trend is unfavourable to the maritime traffic need associated to the Aveiro harbour activities. In this way, it is expected that dredging operations at the inlet channel will continue in the future to provide safe navigability conditions. Attending these findings, and considering the uncertainty of future geomorphological changes due to the anticipated anthropogenic interventions in the inlet region, it is concluded that the present bathymetry should be used hereafter when assessing the flood extent under future scenarios.

# Chapter 7

# Lagoon flood extent - dependence on the driving forces

## 7.1 Introduction

As previously described the flood extent depends on the magnitude of flood drivers. Attending that each coastal system presents unique flood drivers, the flood extent should be evaluated locally. Furthermore, the precise evaluation of flood extent is fundamental towards a precise flood risk assessment [Asselman et al., 2009]. As previously discussed, given the lack of monitoring this assessment is often surpassed through the application of numerical models. Indeed, once calibrated and validated for a given coastal region they provide high resolution flood data. Moreover, they are powerful tools on exploring the physical processes behind the flood patterns.

Attending these concerns this chapter aims to investigate the sensitivity of the lagoon flood extent to the magnitude of oceanic and fluvial drivers, forecasted for present and future climates. To achieve this goal the hydrodynamic model ELCIRC previously calibrated and validated was used to assess inundation in Ria de Aveiro under different sea levels and river discharges conditions, designed according the characterization of the Ria de Aveiro driving forces presented in Chapter 3. The 2012 geomorphological configuration was used to simulate both the present and future climates following the conclusions of the previous Chapter.

## 7.2 Methodology

### 7.2.1 Dependence on oceanic forcing

Considering the characterization of oceanic flood drivers performed in Chapter 3, were defined the scenarios presented in Table 7.1. The neap tide, mean tide and spring tide scenarios were defined to investigate the variability of the lagoon flooded area to tidal oscillations. The remain scenarios correspond to sea levels generated by combinations of tide, storm surge and mean sea level. The MSLR_MT is representative of mean tide under MSLR conditions. The extreme sea level (ESL) scenarios represent the storm surge conditions. The MHWS is the tidal reference of ESL scenarios. To reproduce the storm surge propagation, the model was forced at the oceanic boundary by time series of SSE including astronomic tide and meteorological tide (storm surge) as described in Chapter 4. Accordingly, the tidal condition was generated using the 2012 harmonic constants for the Barra tidal gauge, while the storm surge height was generated synthetically using a sine function, assuming that storm surge persists

Table 7.1: Description of scenarios simulated by ELCIRC (Levels are referred to ZH).

| Scenario | Tidal Level (m) | Storm Surge (m) | MSL (m) | Total Level (m) |
|---|---|---|---|---|
| Neap Tide | 2.80 | 0.00 | 0.00 | 2.80 |
| Mean Tide | 3.00 | 0.00 | 0.00 | 3.00 |
| Spring Tide | 3.60 | 0.00 | 0.00 | 3.60 |
| MSLR_MT | 3.00 | 0.00 | 0.42 | 3.42 |
| MHWS | 3.30 | 0.00 | 0.00 | 3.30 |
| ESL_1 | 3.30 | 0.55 | 0.00 | 3.85 |
| ESL_2 | 3.30 | 0.93 | 0.00 | 4.23 |
| ESL_3 | 3.30 | 1.07 | 0.00 | 4.37 |
| ESL_4 | 3.30 | 1.17 | 0.00 | 4.47 |
| ESL_5 | 3.30 | 1.26 | 0.00 | 4.56 |
| ESL_6 | 3.30 | 0.55 | 0.42 | 4.27 |
| ESL_7 | 3.30 | 1.26 | 0.42 | 4.98 |

generally during 3 days. Figure 7.1 presents the oceanic boundary forcing of ESL_4 as example. As it can be seen, the astronomical and meteorological tides were combined in such a way that the peak of storm surge coincides with the tidal level defined in Table 7.1. The maximum storm surge heights imposed were 0.55, 0.93, 1.07, 1.17, and 1.26 m, for return periods of 2, 10, 25, 50, and 100 years, respectively, which correspond to the difference between ESL scenarios determined in Chapter 3 and the tidal level of 3.30 m (MHWS). The 0.42 m MSLR scenario corresponds to the Lopes et al. [2011] projection for the end of the 21$^{st}$ century.

The ELCIRC model was run for 5 days, considering mean values of fluvial discharges [Génio et al., 2008] and assuming that wind stress is negligible. The model results were used to map the flood extent, and to determine the lagoon flooded area for each scenario. Moreover, the tidal prism at the lagoon mouth and at the mouth of the main channels was determined (Figure 6.1).

### 7.2.2 Dependence on fluvial forcing

The sensitivity of the lagoon flooded area to the fluvial forcing was evaluated by simulating the lagoon flow for peak discharges of 2, 10, 25, 50 and 100 years return periods, for both present and future climates, under mean tide conditions. The time series of flow were generated synthetically using the peak discharges of SWAT model determined in Chapter 3 (Tables 3.3 and 3.4) and attending the following rules:

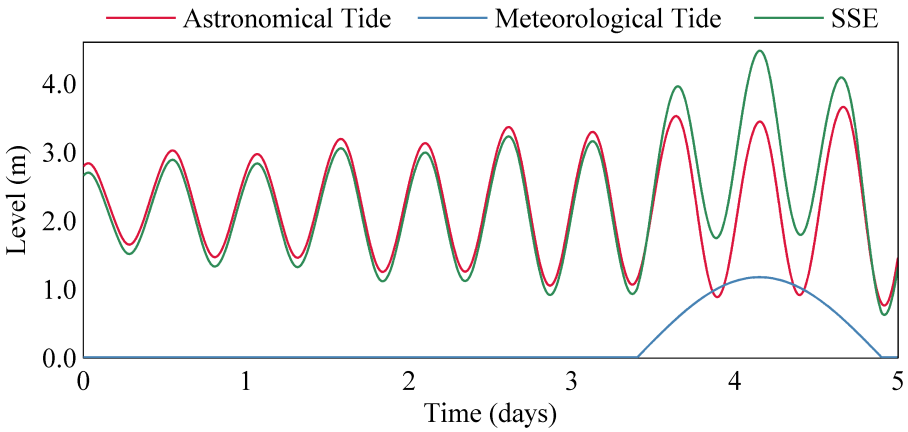


Figure 7.1: SSE (m) imposed at the oceanic boundary, resulting from the sum of astronomical and meteorological levels.

- The river flow before the flood is constant and corresponds to the average baseflow;
- The rising limb progresses linearly from the baseflow to the peak flow in 1.5 days;
- The falling limb evolves linearly from the peak flow to the baseflow in 1.5 days.

The baseflow was determined for each tributary using the single parameter digital filter developed by Nathan and McMahon [1990].

At the oceanic boundary, the model was forced by time series of SSE generated using the 2012 harmonic constants for the inlet tidal gauge, as described for oceanic forcing. Figure 7.2 presents the time series of SSE and fluvial discharges of 2 years return periods imposed at the open boundaries, as example. The tidal and fluvial conditions were imposed in such a way that the peak discharge was coincident with the high level of mean tide at the rivers mouth. In this way, it is necessary to account for the tide delay between the lagoon mouth and these regions, that was estimated in 1.5 hours, attending the $M_2$ phase results presented in Table 4.4. The phase difference for $M_2$ constituent between BA (inlet) and RN (close the Vouga river mouth) stations is approximately 40° (≈1.5 hours). The model was run for 5 days, and the results were used to map flood extent and to determine the lagoon flooded area.

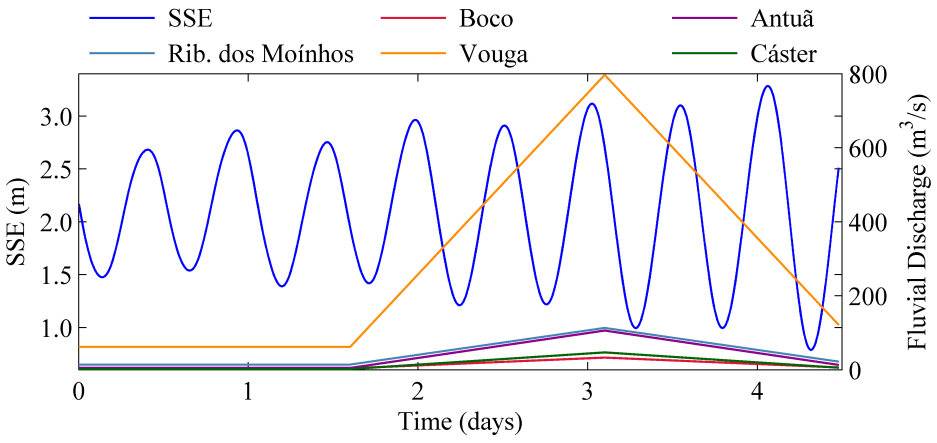


Figure 7.2: SSE (m), and fluvial discharges ($m^3/s$), imposed as boundary condition.

## 7.3 Results and discussion

### 7.3.1 Dependence on oceanic forcing

#### 7.3.1.1 Flood extent

The flood extent was obtained by identifying in the model grid the wet nodes along the tidal cycle considered in Table 7.1. It is considered that an element is wet when the three nodes that compose this element are wet. In this way, the flooded area was obtained by adding the area of each one of the wet elements. The results show that the lagoon flooded area (Table 7.2) in high tide of mean tide is 73 km$^2$ and this value can increase/decrease 22%/8% in high tide of spring and neap tide conditions, respectively. Also, for mean tide conditions, it is predicted that the flooded area will increase by 16% due to MSLR.

Concerning the scenarios ESL_1 to ESL_7 (which consider storm surge events) the flooded area is 99, 111, 117, 121, 124, 118, and 145 km$^2$ from scenarios ESL_1

Table 7.2: Lagoon flooded area (km$^2$) and marginal area flooded (km$^2$), relative to the mean tide, for each scenario presented in Table 7.1.

| Scenario | Total Area (km$^2$) | Marginal Area (km$^2$) |
|---|---|---|
| Neap Tide | 67 | - |
| Mean Tide | 73 | - |
| Spring Tide | 89 | 16 |
| MSLR_MT | 85 | 12 |
| MHWS | 81 | 8 |
| ESL_1 | 99 | 26 |
| ESL_2 | 111 | 38 |
| ESL_3 | 117 | 44 |
| ESL_4 | 121 | 48 |
| ESL_5 | 124 | 51 |
| ESL_6 | 118 | 45 |
| ESL_7 | 145 | 72 |

to ESL_7, respectively. These results evidence that the lagoon flooded area increase approximately 36%, 52%, 60%, 66%, 70%, during storm surge events of 2, 10, 25, 50 and 100 years, respectively, comparing to the mean tide case. The scenarios ESL_6 and ESL_7 reflect the worst cases, once storm surge and MSLR were considered simultaneously. In these situations the lagoon flooded area is 62% and 99% higher than for the MHWS case, respectively. These results turn evident that the lagoon flooded area is highly dependent on sea surface oscillations. The flooded area ranges between 67 and 145 $km^2$, when the maximum level ranges between 2.80 and 4.98 m at the lagoon mouth, respectively.

Flood extent maps were constructed for each case in order to identify the most endangered regions to sea level oscillations (Figure 7.3). Figure 7.3a presents the flood extent variability during high water of neap, mean and spring tide conditions. The flood extent maps show that for the Mira channel the area flooded is similar for the overall tidal conditions analysed. Contrarily, the inundated area at the heads of S. Jacinto channel and at the lagoon central region increases for higher tidal levels. Regarding the flood extent changes forecasted under MSLR conditions, the most endangered regions are once again the ones located at the lagoon central region and at the heads of S. Jacinto channel (Figure 7.3b). Under storm surge conditions (Figure 7.3c), the flood extent increases with the height of the storm surge. The lagoon central area and the marginal areas of S. Jacinto, Espinheiro and Ílhavo channels are flooded under storm surge events. Figure 7.3d highlights that the inundation caused by storm surge events tends to increase considerably under MSLR conditions.

In summary, the maps show that the lagoon flood extent is not uniform, revealing regions more prone to inundation motivated by sea surface level variations than others. In this way, the more threatened regions are located at S. Jacinto and Espinheiro channels heads. Also, some regions located at the lagoon central area and at Ílhavo channel are flooded; however, the flood extent in these regions is lower than that detected at Espinheiro and S. Jacinto channels.

The Ria de Aveiro flooding under extreme water levels was previously studied by Fortunato et al. [2013]. Those authors estimated that the lagoon flooded area ranges between 165 and 174 $km^2$ for maximum levels of 4.20 and 4.48 m. The major differences

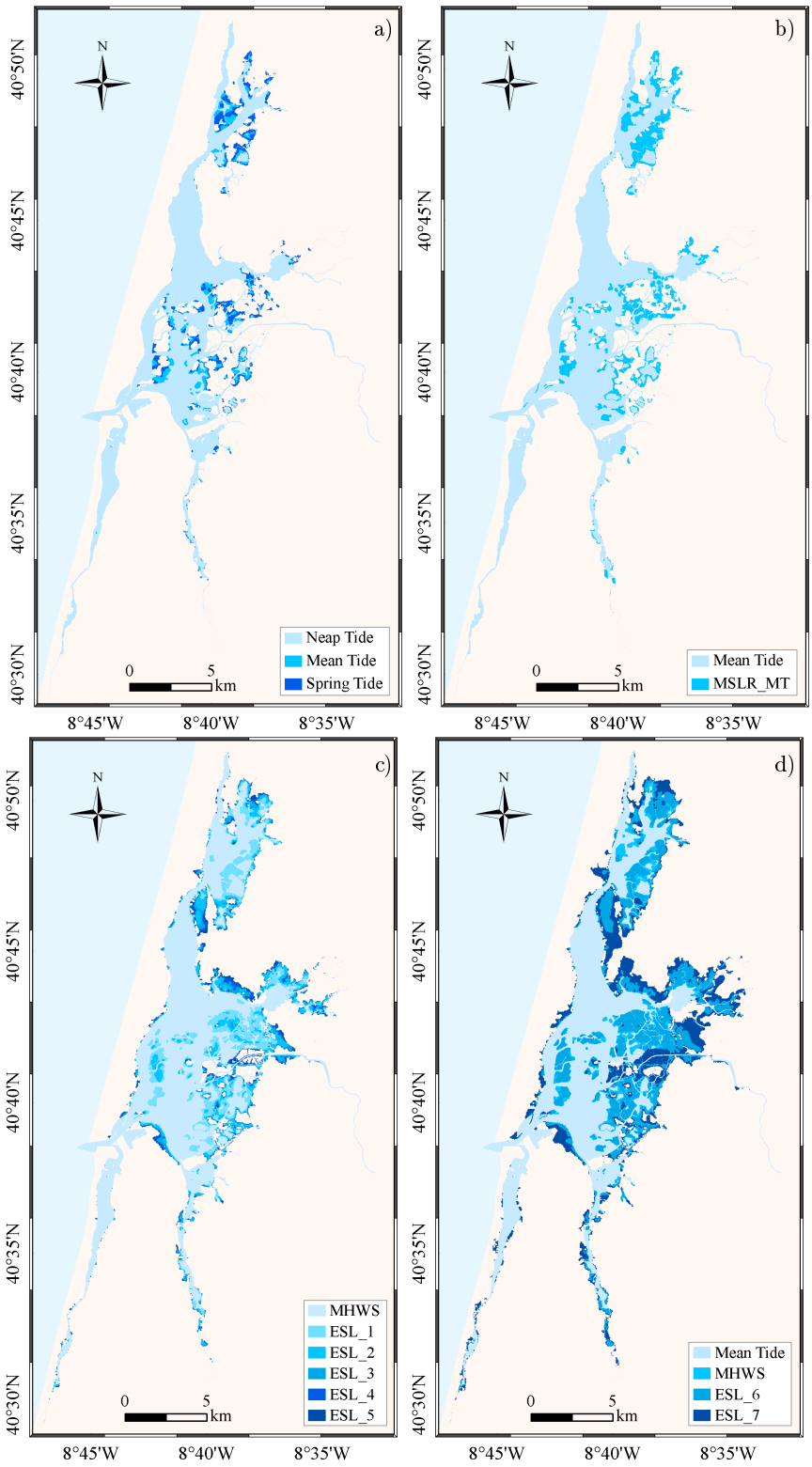


Figure 7.3: Flood extent maps under different: a) tidal levels; b) mean sea levels; c) storm surge levels; d) combinations of tide, storm surge and mean sea level.

between maps presented here and those by Fortunato et al. [2013] are found at the BVL region, which has 46 $km^2$ of area. Indeed, the results presented here highlight that BVL region is only significantly flooded under scenario ESL_7. Contrarily, the Fortunato et al. [2013] results evidence the BVL flooding for all scenarios, even under present mean sea level conditions. This result can be questionable given that there are no evidences of dike breach and overtopping since its conclusion in the eighties. Moreover, some differences on the application of the numerical models can also explain differences between results:

- The numerical grid used in this study is finer and more detailed, mainly at the lagoon central area, than that used by Fortunato et al. [2013].
- The accuracy of this model implementation was evaluated in the overall lagoon extension (since the lagoon mouth to the channels upper reaches), while the Fortunato et al. [2013] implementation only evaluates the model accuracy at the lagoon central area.
- The present model application was validated for three storm surge events, while the Fortunato et al. [2013] implementation compares the predicted flood extent for 100 years return period of oceanic origin, with the maximum flood extent derived by the SECUR-Ria project, caused by multiple flood drivers (fluvial discharges, precipitation).

Inundation studies performed in other low-lying coastal systems worldwide concluded also that the extent of flood is strictly dependent on sea surface oscillations [Peng et al., 2004; Purvis et al., 2008; Sheng et al., 2010; Kuhn et al., 2011]. Nevertheless, comparing the results obtained by those authors, it can be concluded that the propensity of coastal regions to inundation is not uniform around the world. Furthermore, the magnitude of short- and long-term oscillations varies worldwide, highlighting the relevance of local coastal inundation studies in low-lying coastal systems, such Ria de Aveiro lagoon.

#### 7.3.1.2 Tidal prism

The tidal prism was computed at the cross-sections represented in Figure 6.1 for each scenario presented in Table 7.1 to understand how the sea water is distributed among the lagoon main channels. The results are presented in Table 7.3. As expected the tidal prism is highly dependent on tidal conditions. The volume of water crossing the inlet in neap tide conditions is approximately 55% of the volume in spring tide conditions. The total water volume crossing the inlet is distributed among the lagoon channels. In mean tide conditions the tidal prism at S. Jacinto (B), Mira (D), Espinheiro (E) and Ílhavo (F) channels is approximately 35%, 10%, 19% and 16% respectively, of the tidal prism at the lagoon mouth (A). The tidal prism changes induced by tidal modifications range between $65.8\times10^6$ $m^3$ and $120.0\times10^6$ $m^3$ at the inlet for neap and spring tide conditions, respectively. These estimations are higher than previous results by Picado et al. [2010] and Lopes et al. [2011]. Using the 2001 bathymetry, these authors estimated tidal prisms at the inlet ranging between $30\times10^6$ $m^3$ and $70\times10^6$ $m^3$ for neap and spring tide conditions, respectively. The differences

Table 7.3: Tidal prism ($\times10^6$ $m^3$) computed at the cross-sections represented in the Figure 6.1 for each scenario defined in Table 7.1.

| Scenario | A | B | C | D | E |
|---|---|---|---|---|---|
| Neap Tide | 65.8 | 23.4 | 6.3 | 11.8 | 10.3 |
| Mean Tide | 99.6 | 34.7 | 9.5 | 18.6 | 15.8 |
| Spring Tide | 139.7 | 46.5 | 12.9 | 28.7 | 23.5 |
| MSLR_MT | 126.5 | 40.5 | 11.3 | 24.9 | 20.5 |
| MHWS | 120.0 | 39.3 | 11.1 | 23.9 | 20.2 |
| ESL_1 | 158.2 | 50.7 | 13.8 | 36.2 | 27.6 |
| ESL_2 | 189.3 | 60.5 | 15.4 | 46.5 | 33.6 |
| ESL_3 | 201.4 | 64.6 | 15.9 | 50.6 | 36.4 |
| ESL_4 | 210.6 | 67.9 | 16.3 | 53.5 | 38.4 |
| ESL_5 | 219.5 | 70.5 | 16.7 | 56.2 | 40.0 |
| ESL_6 | 184.2 | 58.0 | 15.2 | 45.9 | 32.8 |
| ESL_7 | 252.6 | 84.3 | 19.1 | 68.0 | 45.2 |

found can be explained by the different morphology of numerical implementations used in each study. The Picado et al. [2010] and Lopes et al. [2011] implementations used the bathymetry of 1987 and 2001, while this implementation use up to date bathymetric data. Furthermore, the previous implementations do not consider water circulation in some intertidal regions, neither allow flooding of marginal areas.

Results reveal that the tidal prism will increase approximately 20% during mean tides under MSLR conditions. Also, it is predicted that the volume of water crossing the inlet during a mean tide under MSLR conditions ($126.5\times10^6$ m$^3$) is slightly lower than that actually observed during spring tide conditions ($139.7\times10^6$ m$^3$). Results evidence that tidal prism presents high variability in response to sea level changes. Indeed, during neap tide the tidal prism is $65.8\times10^6$ m$^3$, however this value can increase to $252.6\times10^6$ m$^3$ for the scenario with the highest sea surface level imposed as boundary condition.

The distribution of water among the lagoon channels was studied in detail in order to understand the factors that drive the water flow propagation along the lagoon. In this way, the tidal prism increase rate for scenarios ESL_1 to ESL_7 relative to the MHWS was computed (Figure 7.4). These scenarios were chosen once they have the same reference tidal condition (MHWS). Results evidence that the increase rates are not similar between sections. Indeed, the tidal prism increase rates tend to be exacerbated at S. Jacinto, Espinheiro, and Ílhavo channels and attenuated at Mira channel. These results can be related with the physical features of the lagoon channels

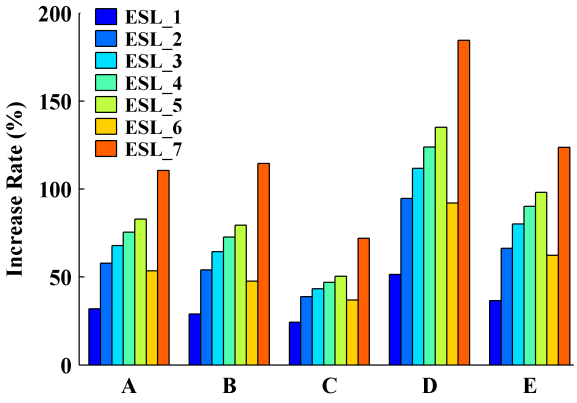


Figure 7.4: Tidal prism increase rate for scenarios ESL_1 to ESL_7 relative to the tidal prism of MHWS.

(namely the area and depth), which determine the water flow propagation. As the water column increases with the sea surface level rises, the bottom friction decreases for all channels generating higher velocities. Accordingly, with the increase in the sea surface heights the bottom friction tends to have a higher decrease in Mira channel than in other channels. This fact appears to be contradictory with tidal prism results; however, when the flood extent of the overall channels is compared, it is evident that for Mira channel it is practically identical for all scenarios, in contrast to the other channels, which extension is highly dependent on sea surface level imposed as boundary condition. Thus, the differences found on the available water volume accommodation of each channel explain the tidal prism differences found between channels. In this way, it is concluded that the morphological features, which control the tidal prism, are determinant on the establishment of the flood extent. Indeed, the Mira channel presents lower propensity to marginal inundation than the other channels, because its marginal areas present higher topography and, consequently, the tidal prism rise is not so exacerbated. Contrarily, the marginal areas of the Espinheiro, S. Jacinto, and Ílhavo channels are threatened to inundation given that they present reduced topography and, as a consequence, the tidal prism amplification motivated by sea surface level rise tends to be exacerbated in these channels.

### 7.3.2 Dependence on fluvial forcing

The lagoon flooded area under high discharge conditions was determined, by identifying the wet nodes along three hours of simulation, after the peak discharge. This period corresponds to the maximum flood extent, once after the peak discharge, fluvial discharges and tidal levels decrease.

As expected, the lagoon flooded area (Table 7.4) increases for higher fluvial discharges. Indeed, considering the present climate estimates, the lagoon flooded area increase 49%, 71%, 90%, 96% and 100% relative to the flooded area in mean tide conditions (73 $km^2$).

It is predicted a reduction of the marginal flooded area under climate change conditions. Decrease rates of 55%, 31%, 30%, 26% and 21% were found for discharges of 2, 10, 25, 50 and 100 years, respectively. For present climate, the area flooded during an

Table 7.4: Lagoon flooded area ($km^2$) and marginal area flooded ($km^2$), relative to the mean tide, for each return period.

| | Present Climate | | | | | Future Climate | | | | |
|---|---|---|---|---|---|---|---|---|---|---|
| Return Period | 2 | 10 | 25 | 50 | 100 | 2 | 10 | 25 | 50 | 100 |
| Total Area ($km^2$) | 109 | 125 | 139 | 143 | 145 | 89 | 109 | 119 | 125 | 130 |
| Marginal Area ($km^2$) | 36 | 52 | 66 | 70 | 73 | 16 | 36 | 46 | 52 | 57 |

event of 2 years return period is similar to that expected for an event of 10 years return period under future climate. Additionally, the flooded area that currently presents a recurrence period of 10 years, in the future climate will be equalled or exceeded only every 50 years.

The flood extent maps (Figure 7.5) evidence that the regions prone to inundation of fluvial origin are located in the margins of the lagoon close to the mouth of the tributaries.

Analysing the flood extent around the overall tributaries, it is found that the adjacent regions of the Vouga and Antuã rivers are highly flooded. This occurs not only because the Vouga and Antuã rivers present the highest discharges, but also due the low and flat topography of the region. As consequence, when the water overflows the river channels it easily inundates an extensive area. It is interesting to note that the flood extent in the vicinity of the Vouga river is almost similar for all return periods, revealing that this region is flooded almost every year. Also, it is verified that the flood extent tends to increase towards the lagoon central area as the river discharges increase.

## 7.4 Conclusions

The sensitivity of Ria de Aveiro marginal flooding under different scenarios of sea level and river discharges was explored in this chapter.

Regarding the sensitivity of flooded area to oceanic forcing, results showed that the lagoon flooded area is extremely sensitive to sea level oscillations (both short and long term). Indeed, the lagoon flooded area is approximately 33% higher for spring tide than

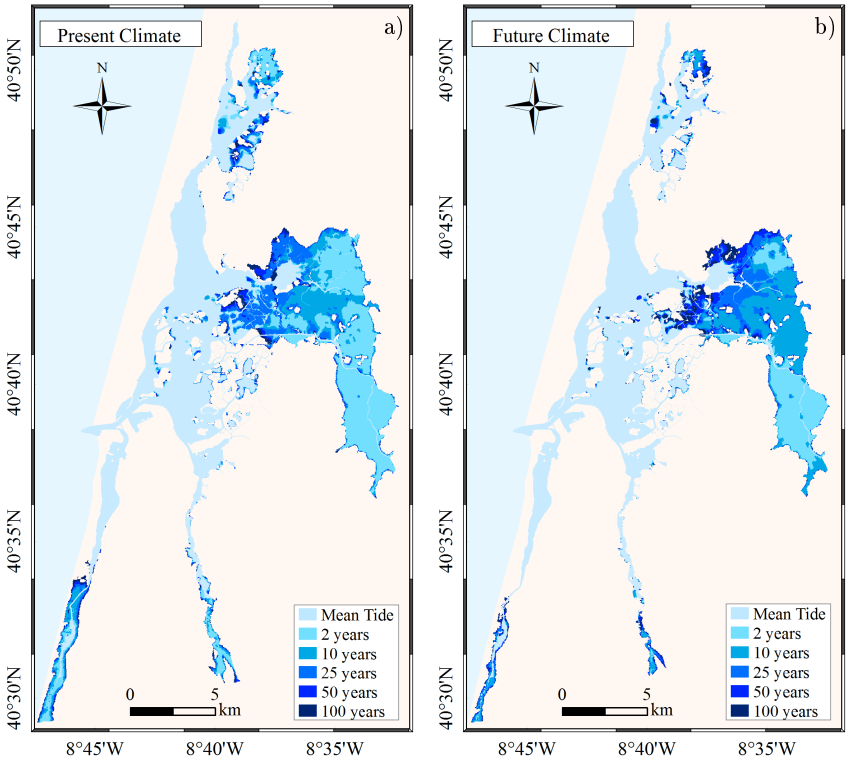


Figure 7.5: Flood extent maps under different discharge conditions, for present and future climates.

for neap tide. Also, during storm surge events the flooded area increases considerably, approximately 36%, 52%, 60%, 66% and 70%, for events of 2, 10, 25, 50 and 100 years return periods, respectively. Moreover, for mean tide conditions, it is predicted that the lagoon flooded area will increase by 16% for 0.42 m MSLR scenario, comparing to the present. However, the flood extent rise is not uniform along the lagoon. Indeed, the more threatened regions are located at the heads of S. Jacinto channel and at the lagoon central area, corresponding to regions of lower marginal topography.

Concerning the tidal prism results, as expected were found maximum values for the higher water levels; nevertheless the increase rate is not uniform along the lagoon main channels. The tidal prism rise tends to be higher in the channels adjoining areas of low topography where accommodation space for water is greater. In summary, the depth of the lagoon channels and the topography of its marginal regions are determinant on the establishment of flood extent patterns, once both factors determine the volume of water crossing each channel during the flood.

The results evidence that the lagoon flooded area is also highly dependent on

the river discharge. Results highlight that the lagoon flooded area can duplicate for discharges of 100 years return period, relative to the mean discharge conditions. The regions affected by fluvial floods are mainly located in the margins of channels heads, where rivers inflow. The flood extent of Vouga and Antuã marginal lowlands is considerably higher than the area flooded by the remain tributaries. It is also predicted a flooded area reduction under climate change conditions, in response to the forecasted river discharges reduction, which is accentuated for the lowest return periods (2, 10 and 25 years).

# Chapter 8

# Flood hazard and risk assessment

## 8.1 Introduction

The European Floods Directive (2007/60/EC), that was transposed to the Portuguese national law through the Decree-Law No. 115/2010 of 22 October, requires the elaboration of flood hazard and flood risk maps at the most appropriate scale, by Member States. Flood hazard maps shall cover the geographical areas that may be flooded according to different scenarios, and for each scenario should be assessed:

- the flood extent;
- water depths or water level, as appropriate;
- where appropriate, the flow velocity or the relevant water flow.

Flood risk maps should include the potential adverse consequences associated with flood scenarios and expressed in terms of the following:

- indicative number of inhabitants potentially affected;
- type of economic activity of the area potentially affected;
- installations which might cause accidental pollution in case of flooding and potentially affected protected areas;

- other information which the Member State considers useful, such as the indication of areas where floods with a high content of transported sediments and debris floods can occur and information on other significant sources of pollution.

The European Exchange Circle on Flood Mapping (EXCIMAP) was created to gather the existing experiences and know-how in Europe and to improve flood mapping practices. With this purpose, EXCIMAP developed the *Handbook on good practices for flood mapping in Europe* [EXCIMAP, 2007]. By compiling examples and experiences of all Europe, this technical guide provides guidance on flood mapping, supporting Member States to understand the requirements for flood mapping elaboration presented in the Floods Directive. Also, the FLOODsite project(`http://www.floodsite.net/default.htm`) was developed to attend and answer the Floods Directive requirements. A wide team comprising 37 organisations partners from 13 different countries developed guidance and applications reports of flood risk analysis that were made available through the Communication and Dissemination Plan.

Following the requirements of Floods Directive, this work aims to assess and map flood hazard and risk in Ria de Aveiro region for the present and future climate conditions. This goal was achieved following the best practices and guidelines present in the EXCIMAP handbook and FLOODsite project reports.

## 8.2 Methodology

As previously discussed, the floods in Ria de Aveiro occur when sea levels or fluvial discharges are high or even when both conditions occur simultaneously. Attending this, several simulations that combine different sea levels and river discharges were designed (Figure 8.1). The simulations were performed with ELCIRC model, which results were used to assess flood hazard and flood risk in Ria de Aveiro. Basically, these scenarios combine sea levels and river discharges under mean conditions and under adverse conditions of 2, 10, 25, 50 and 100 years return periods, for present and future climates. The "O" and "F" are indicative of oceanic and fluvial forcing, respectively, while after the "O" and "F" is indicated the magnitude of oceanic and fluvial forcing. Accordingly, and as example, the scenario O2FM combines sea levels

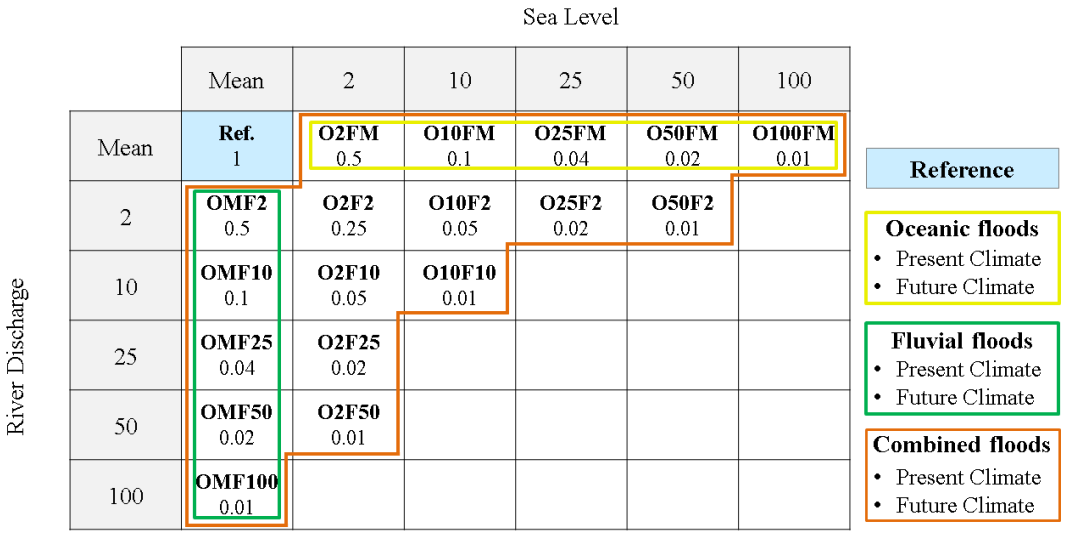


Figure 8.1: Description of simulations combining sea levels and river discharges, indicating the respective probability of occurrence ("O" and "F" are indicative of oceanic and fluvial forcing, respectively; after "O" and "F" is indicated the magnitude of oceanic and fluvial forcing, that can be mean conditions (M) or events with 2 to 100 years return periods).

for 2 years return periods with mean fluvial discharges, while scenario OMF2 combines mean tide conditions with river discharges for 2 years return periods. The reference simulation considers mean tide and mean discharge conditions.

This set of simulations was used to assess flood hazard and risk under six distinct cases:

**Oceanic Present** - Floods of oceanic origin under present climate conditions;

**Oceanic Future** - Floods of oceanic origin under future climate conditions;

**Fluvial Present** - Floods of fluvial origin under present climate conditions;

**Fluvial Future** - Floods of fluvial origin under future climate conditions;

**Combined Present** - Floods of combined origin under present climate conditions;

**Combined Future** - Floods of combined origin under future climate conditions.

Initially the simulations O2FM to O100FM (yellow rectangle in Figure 8.1) were used to characterize floods of oceanic origin, while simulations OMF2 to OMF100 (green rectangle in Figure 8.1) were used to characterize floods of fluvial origin. The

floods of combined origin were characterized using simultaneously the results of the overall simulations (orange polygon in Figure 8.1). Floods of oceanic, fluvial and combined origin were studied under present and future climate conditions, using sea levels and river discharges projections derived in Chapter 3. Regarding sea levels, the extreme projections (Table 3.2) were used for the present and future climates. However, for the future climate it is also considered a MSLR of 0.42 m. For river discharges, the projections of SWAT model for present and future climates presented in the Tables 3.3 and 3.4, respectively, were used.

The probability of occurrence of each event, needed to compute flood hazard and risk, was calculated as the inverse of the return period. The probability of combined events was determined by the product of the probabilities of individual events, admitting that high sea levels and high river discharges events are independent. This approach is acceptable once the correlation coefficient between discharges of Vouga river (simulated by SWAT model between 1976 and 2011) and sea levels at the inlet (recorded between 1976 and 2011) is -0.045. The combinations represented by white squares were not simulated once the probability of occurrence is lower than 0.01 (less than one time in a hundred years).

### 8.2.1 Flood hazard

The intensity and frequency of floods in Ria de Aveiro was evaluated by constructing maps of flood depth, flood probability and annual average hazard. The flood depth maps were constructed for each simulation scenario and represent the maximum depth achieved in each grid element. The flood probability maps were constructed for events of oceanic, fluvial and combined origin and represent the predicted flood extent for each scenario (Figure 8.1). The annual average hazard ($\overline{H}$) for floods of oceanic, fluvial and combined origin was computed as the integral of water depth ($D$) by the probability ($P$) through equation 8.1:

$$\overline{H} = \sum_{i=1}^{k} D_i \times \Delta P_i \tag{8.1}$$

where $i$ represents each simulation scenario and $D_i$ and $\Delta P_i$ were determined through equations 8.2 and 8.3, respectively:

$$D_i = \frac{D(P_{i-1}) + D(P_i)}{2} \tag{8.2}$$

$$\Delta P_i = \mid P_i - P_{i-1} \mid \tag{8.3}$$

The integral is schematically represented in Figure 8.2, where the annual hazard is interpreted as the area under the water depth-probability function. Basically, the water depth-probability curve was obtained by identifying pairs of water depth ($D_i$) and probability ($P_i$) of each simulation that composes the flood events of oceanic, fluvial and combined origin.

### 8.2.2 Identifying assets exposed to flood hazard

Once delimited the flood extent for all simulations, the social, economic and ecological assets located between the mean tide flood extent and the upper limit of numerical domain were identified according the Floods Directive (Table 8.1). With this propose, the hydrodynamic model numerical grid was transposed to the GIS environment and intersected with geographic information of the area. The spatial distribution of assets on the numerical grid extent is represented in Figure 8.3.

The resident population data collected in the 2011 general population census, that was made available by the INE, was used to quantify the number of inhabitants exposed

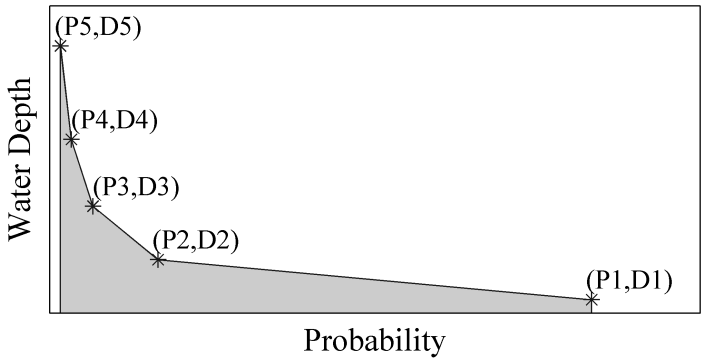


Figure 8.2: Water depth as function of probability.

Table 8.1: Assets exposed to flood hazard.

| Indicator | Exposed Assets | Data Source |
|---|---|---|
| Social | Inhabitants | Statistics Portugal (INE)<br>www.ine.pt |
| Economic | Land Use | Directorate-General for the Territory (DGT)<br>http://www.dgterritorio.pt/a_dgt/ |
| | Roads | OpenStreetMap<br>http://www.openstreetmap.org |
| | Buildings | SPRES project<br>http://ariel.lnec.pt/spres/ |
| Ecological | Classified Areas | Institute for the Conservation of Nature and Forest (ICNF)<br>http://www.icnf.pt/portal |
| | Habitats | Polis Litoral Ria de Aveiro<br>http://www.polisriadeaveiro.pt/index.php<br>PLRA [2011a] |

to flood hazard (Figure 8.3a). The BGRI of 2011 census was used to disaggregate the data to the local scale.

The land use data at level II, given by the DGT was modified in order to detail the economic activities located within artificial surfaces class. The categorization of the areas with economic activities was supported by the Portuguese Classification of Economic Activities (CAE-Rev.3) (Decree-Law No. 381/2007 of 14 November). Accordingly, the land use was categorized as residential, commercial accommodation and restaurants, industry, transport and storage, aquaculture, saliniculture, agriculture, forest and semi natural areas and no economic use (Figure 8.3b).

The buildings located inside the numerical domain were inventoried and classified according their functional behaviour as residential, commercial, industrial, services, agricultural, saliniculture and aquaculture and no use (Figure 8.3c).

The roads network extracted from the OpenStreetMap was classified according the

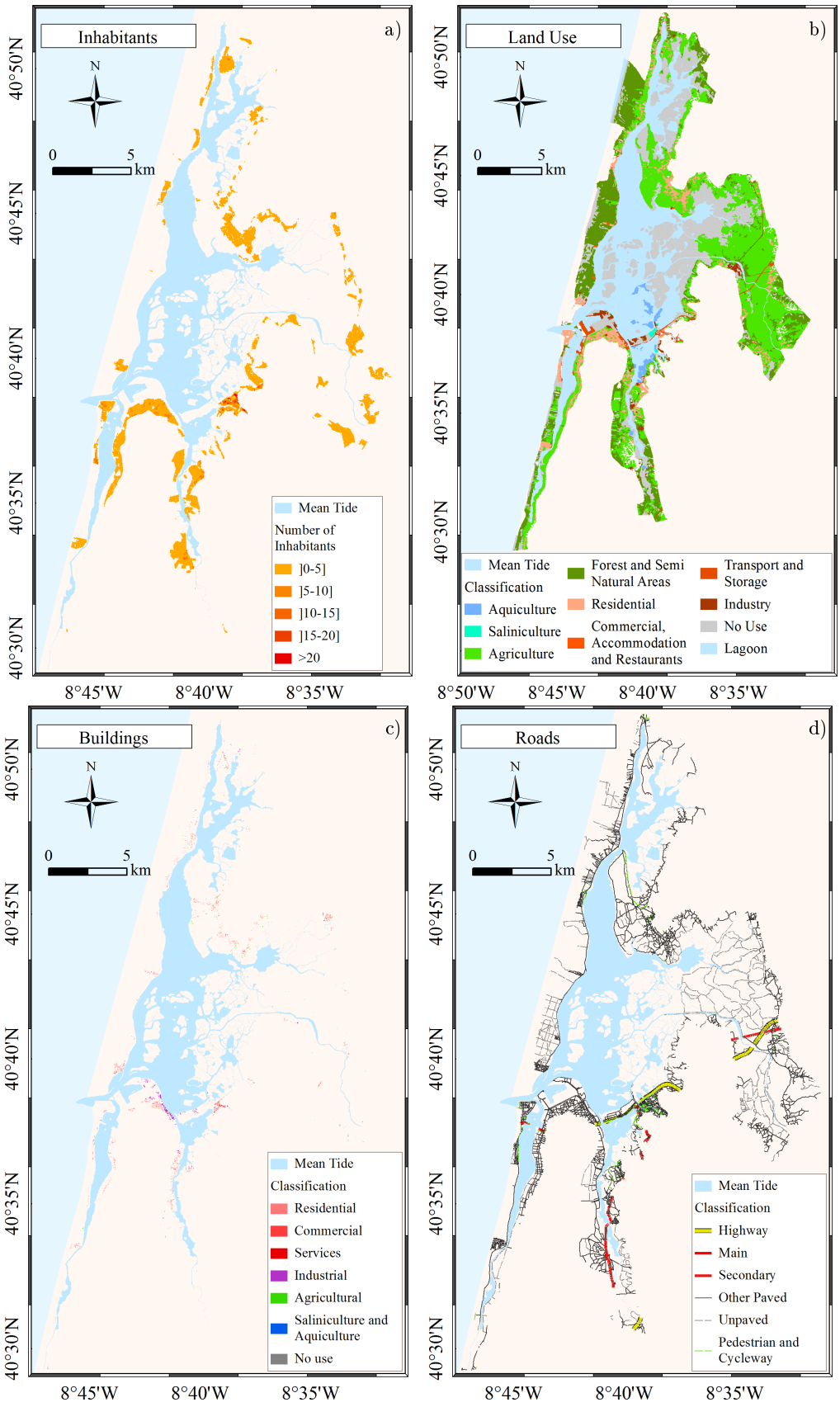


Figure 8.3: Spatial distribution of exposed assets: a) Inhabitants; b) Land use; c) Buildings; d) Roads; e) Classified areas; f) Habitats.

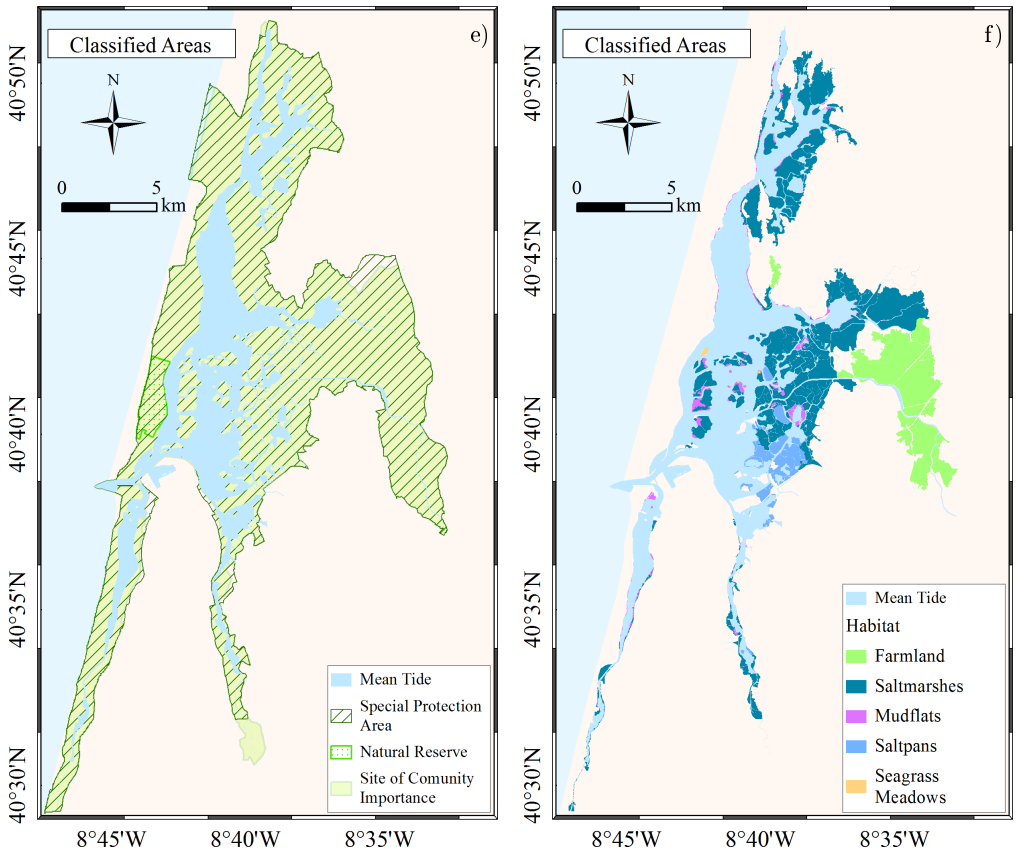


Figure 8.3: (Continued) Spatial distribution of exposed assets: a) Inhabitants; b) Land use; c) Buildings; d) Roads; e) Classified areas; f) Habitats.

National Road Plan (Decree-Law No. 222/98, of 17 of July) as highway, main roads, secondary roads and other roads. However, as most of the itineraries located in the study area are inserted in the other roads class, the other roads were decomposed in other paved roads, unpaved roads and pedestrian and cycleway roads (Figure 8.3d).

The classified areas include SCI, SPA and NR areas (Figure 8.3e). Finally, the habitats were classified as farmland, saltmarshes, mudflats, saltpans and seagrass meadows attending the LAGOONS [2011] and PLRA [2011a] studies (Figure 8.3f).

The flood extent of each simulation presented in the Figure 8.1 was intersected with each asset chart. The number of inhabitants, the land use area, the buildings area, the roads length, the classified regions area and the habitats area flooded in each scenario were quantified.

### 8.2.3 Flood risk

As defined in the Flood Directive, the flood risk $R$ can be quantified through equation 8.4:

$$R = C_f \times P \tag{8.4}$$

where $C_f$ is the potential adverse consequence of the flood event. According to EXCIMAP [2007], the consequences of the flood event $C_f$ are function of the value of assets ($V_f$), of susceptibility to be damaged ($S_f$) and of the exposure to floods ($E_f$) through equation 8.5:

$$C_f = V_f \times S_f \times E_f \tag{8.5}$$

In practice the negative consequences induced on the exposed assets were determined in each grid element for each scenario presented in Figure 8.1. This requires to determine the value, the susceptibility and exposure of assets in each grid element. According to EXCIMAP [2007], the exposure represents the probability of the element at risk to be present when the event occurs and therefore should be set between 0 to 1. In this study it is considered that the exposure of each asset is 1, which is equivalent to consider that the assets are static.

Concerning the value of the exposed elements, a throughout investigation about the social, economic and ecological behaviour of the territory was carried out, in order to estimate the value of each exposed element in each grid element. The number of inhabitants present in each grid element represent the value of inhabitants indicator. Although it can be estimated in monetary terms, the value of economic assets were attributed as relative weight, ranging between 0 and 1 (Table 8.2). This approach was followed by two reasons. First, it were not found monetary values for the study area for all indicators. Secondly, some uncertainties and significant incongruities between data sources were found on the existent values (INE, housing companies, insurance companies, PLRA [2011a]). Concerning the land use categories, the value attributed corresponds to the weight of economic activities on the GVA of Ria de Aveiro region

Table 8.2: Relative value of assets exposed to flood events.

| Land Use | Relative Value | Building Use | Relative Value | Road type | Relative Value |
|---|---|---|---|---|---|
| Residential | 0.00 | Residential | 0.50 | Highway | 1.00 |
| Commercial Accommodation, and Restaurants | 0.60 | Commercial | 0.90 | Other Paved | 0.20 |
| Industry | 0.40 | Services | 0.80 | Unpaved | 0.01 |
| Transport and Storage | 0.40 | Industrial | 1.00 | Pedestrian and Cycleway | 0.01 |
| Agriculture | 0.02 | Agricultural | 0.02 | | |
| Forest | 0.02 | Saliniculture and Aquiculture | 0.02 | | |
| Aquiculture | 0.02 | | | | |
| Saliniculture | 0.01 | | | | |

[PLRA, 2011a]. Regarding the buildings, its value was estimated as the sum of building structure and content. It is considered that the most valuable buildings have industrial use, that are followed by commercial, services and residential buildings. These values are in accordance with de Moel et al. [2014] estimates for the Rotterdam area. The value of buildings used on agriculture, aquiculture and saliniculture was set 2% of the industrial buildings. Regarding the roads, highway presents the highest value, followed by other paved, unpaved and pedestrian and cycleway roads, as suggested by de Moel et al. [2014]. Although the existence of main and secondary roads in the numerical domain (see Figure 8.3), they are not affected in any of the scenarios presented in Figure 8.1 and for this reason are not presented in Table 8.2. Finally, it is considered that the sensible habitat areas are ecologically more valuable than the classified areas. In this way, the ecological value of sensible habitats was set 0.7, while the value of classified areas was set 0.3.

The susceptibility was defined in the EXCIMAP [2007] as the damaging effect on the element at risk, and therefore depends on the magnitude of floods and on the

preparedness of exposed assets, as well as on their capability to cope with floods. For example, the damaging effect of a given flood event on an individual depends on the magnitude of the event but also on their mobility, which is commonly associated to gender, age and disabilities. Despite this, the EXCIMAP [2007] highlights that susceptibility is commonly defined as function of flood depth only. Accordingly, it is considered that the susceptibility of the social and economic elements is a function of flood depth, as suggested by Merz et al. [2004], Penning-Rowsell et al. [2005], EXCIMAP [2007], Messener et al. [2007] and Merz et al. [2010]. Contrarily, the susceptibility of the ecological elements was set equal to 1, once there is no clear evidences that the negative effects of floods on the ecology depends on the flood depth. Following this, the depth damage functions (Figure 8.4) were designed considering that the damage is higher as higher is the flood depth, and adjusting the depth damage functions presented in the literature to the case of Ria de Aveiro flood events characteristics.

The flood hazard matrix developed by Wallingford [2006] for risk to people were analysed in the context of Ria de Aveiro flood depths. It was found that most of the events are within the "danger for some" class. Thus, in order to differentiate the damage to inhabitants within the Ria de Aveiro region a depth damage function divided in three stages was constructed (Figure 8.4a). It is considered that depths lower than 1 m represent a maximum damage of 30% to inhabitants. Moreover, the damage slope is exacerbated between 1.0 and 2.0 m depths, once as the depth increases the danger

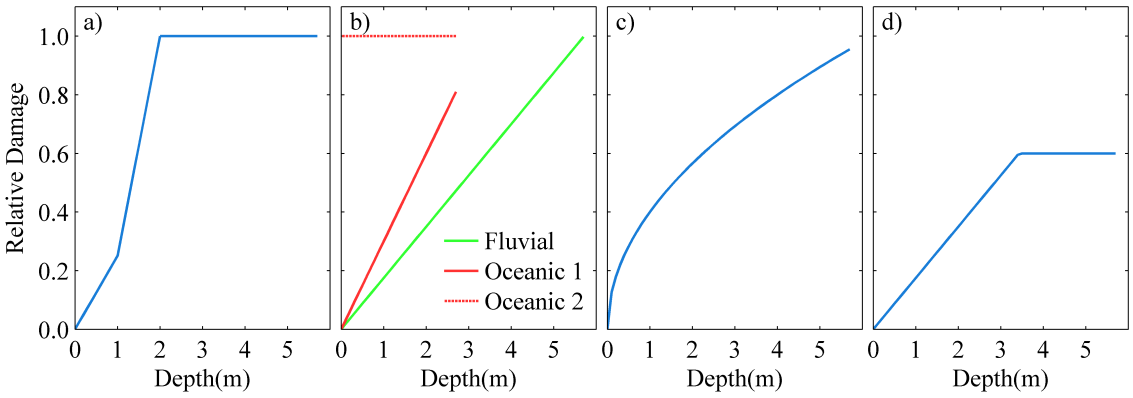


Figure 8.4: Depth damage functions for a) Inhabitants; b) Land use; c) Buildings; d) Roads.

to people also increases. Finally, flood depths higher than 2.0 m represent a potential loss of life.

Concerning the depth damage relation for economic activities (Figure 8.4b), it was considered that the damage effect of saltwater inundation in agricultural fields will lead to a total loss of production (curve "Oceanic 2" in Figure 8.4b). This approach reflects the facts documented in the local newspapers and the tendency of agricultural fields abandonment observed in the region. For the remaining activities, a distinction between flood events of oceanic (curve "Oceanic 1" in Figure 8.4b) and fluvial (curve "Fluvial" in Figure 8.4b) origin was made, once saltwater induces more damage on machines and electrical components than freshwater. Therefore, floods of oceanic origin induce longer activity disruptions than those of fluvial origin, once the first require more time for damage repair.

Regarding the buildings, it is considered that the relative flood damage ($D_r$) is a function of the flood depth ($D$), following equation 8.6:

$$D_r = 0.4\sqrt{D} \tag{8.6}$$

This relation indicates that when the flood depth is 1 m, the relative flood damage of a building is 40% [Messener et al., 2007]. Regarding the roads, it was considered that the relative damage does not exceed 60%. The analysis of the consequences of past events in the region indicates that the damage on roads is partial.

At this stage, the negative consequences of floods on inhabitants, land use, buildings, roads and ecology were determined. The next step consisted in the aggregation of negative consequences ($C_{f_i}$) and probability ($P_i$) of simulations scenarios that compose the flood events of oceanic, fluvial and combined origin, in order to compute the respective annual average risk ($\overline{R}$) following equation 8.7:

$$\overline{R} = \sum_{i=1}^{k} C_{f_i} \times \Delta P_i \tag{8.7}$$

Where $i$ represents each simulation scenario and $C_{f_i}$ and $\Delta P_i$ were determined through

equations 8.8 and 8.3, respectively:

$$C_{f_i} = \frac{C_f(P_{i-1}) + C_f(P_i)}{2} \tag{8.8}$$

This means that the annual average risk of each exposed asset is the integral of the consequences over the probability of respective flood events [Meyer et al., 2007]. The integral is schematically represented in Figure 8.5.

The next step was the aggregation of flood risk of each asset into a global flood risk. For that, it is necessary to standardize the risk of each asset and then to define criteria weights in order to express the relative importance of each criterion [Meyer et al., 2007]. Here the criterion weights were estimated following the pairwise comparison method [Saaty, 1977]. In summary, each criterion is compared to all the others and a value between 1 and 9 is allocated according their relative importance (Table 8.3). In this study the pairwise comparison matrix was built (Table 8.4) taking into account the following:

- The inhabitants criteria is more important than any other criterion;
- The three economic indicators have the same relative importance;
- The ecological criterion is considered the least important.

These rules were established regarding not only the socio-economic and ecological behaviour of Ria de Aveiro region, but also considering the results of similar multi-criteria applications worldwide [Kubal et al., 2009; Meyer et al., 2009; Dassanayake et al., 2013]. The sensitivity of flood risk to criterion weights was investigated in

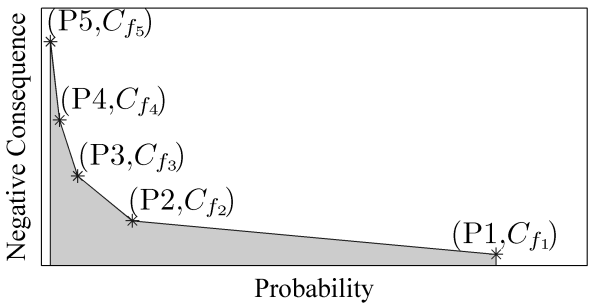


Figure 8.5: Negative consequence as function of probability.

Table 8.3: Importance scale of pairwise comparison

| Importance Scale | Definition |
|---|---|
| 1 | Equal importance |
| 2 | Equal to moderate importance |
| 3 | Moderate importance |
| 4 | Moderate to strong importance |
| 5 | Strong importance |
| 6 | Strong to very strong importance |
| 7 | Very strong importance |
| 8 | Very strong to extremely strong importance |
| 9 | Extreme importance |

Table 8.4: Pairwise comparison matrix for flood risk criteria

| Criterion | Inhabitants | Land Use | Buildings | Roads | Ecology |
|---|---|---|---|---|---|
| Inhabitants | 1 | 5 | 5 | 5 | 7 |
| Land Use | 1/5 | 1 | 1 | 1 | 4 |
| Buildings | 1/5 | 1 | 1 | 1 | 4 |
| Roads | 1/5 | 1 | 1 | 1 | 4 |
| Ecology | 1/7 | 1/4 | 1/4 | 1/4 | 1 |

Meyer et al. [2009] and Kubal et al. [2009] works. They found that flood risk is highly dependent on the estimation of criterion weights. However, the likely scenarios attribute greater importance on socio-economic indicators. Table 8.5 presents the criterion weights, that were computed from the pairwise matrix. Finally, the flood risk was scored in Low, Medium, High and Very High according the intervals presented in Table 8.6. These values were attributed after carefully analysis of the flood risk patterns in the Ria de Aveiro region.

Table 8.5: Criterion weights obtained from the pairwise comparison matrix.

| Criterion | Weight |
|---|---|
| Inhabitants | 0.50 |
| Land Use | 0.15 |
| Buildings | 0.15 |
| Roads | 0.15 |
| Ecology | 0.05 |

Table 8.6: Score for the flood risk values.

| Risk Value | Score |
|---|---|
| $]0.00 - 0.01]$ | Low |
| $]0.01 - 0.02]$ | Medium |
| $]0.02 - 0.05]$ | High |
| $]0.05 - 1.00]$ | Very High |

## 8.3 Results and discussion

### 8.3.1 Flood hazard

The intensity of floods was evaluated by constructing flood depth maps (Figures 8.6 to 8.11) for each scenario presented in Figure 8.1, under present and future climates. As expected, for all cases analysed the flood depth increases for higher return periods.

Regarding the flood events of oceanic origin (Figures 8.6 and 8.9), the areas flooded are located primary on the lagoon central area and in the upper reaches of S. Jacinto channel. Then, as the return period increases, the flooded area tends to expand through the main channels margins. The marginal flooding of Mira channel is considerably lower than the observed for the remaining channels. Under climate change conditions higher flood depths are predicted, due to MSLR. It is also evident that Murtosa, Estarreja, Ovar and Aveiro are the municipalities most endangered by flood events of oceanic origin.

For floods of fluvial origin (Figures 8.7 and 8.10), the water depths found are

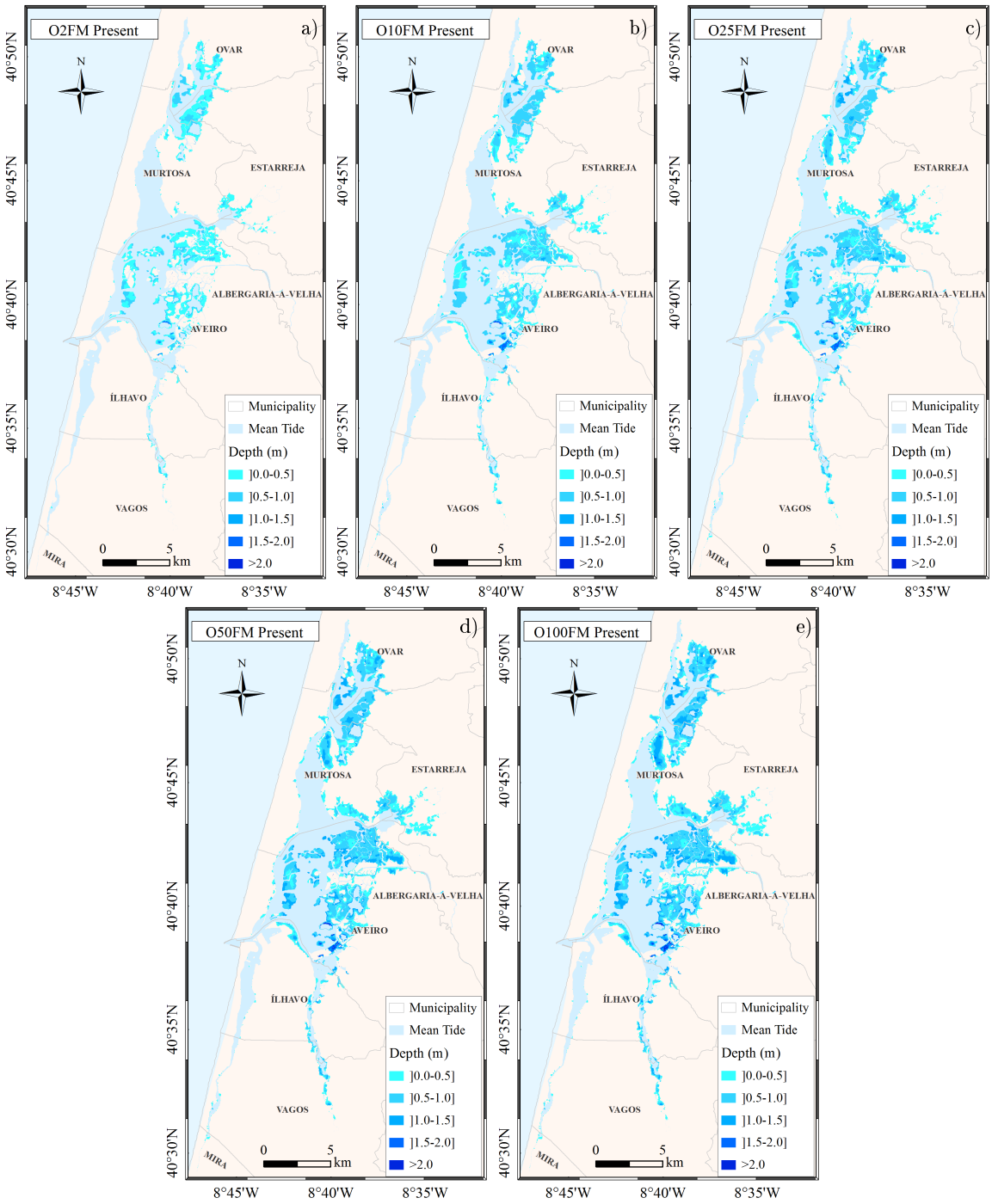


Figure 8.6: Flood depth maps for events of oceanic origin under present climate for scenarios: a) O2FM; b) O10FM; c) O25FM; d) O50FM; e) O100FM.

generally higher than those obtained for oceanic induced floods. The inundated regions are located in the vicinity of the lagoon tributaries. The inundation caused by the Vouga discharge is highlighted in all flood maps given its extent and magnitude. Also, the Antuã discharge plays a determinant role on the establishment of flood patterns in

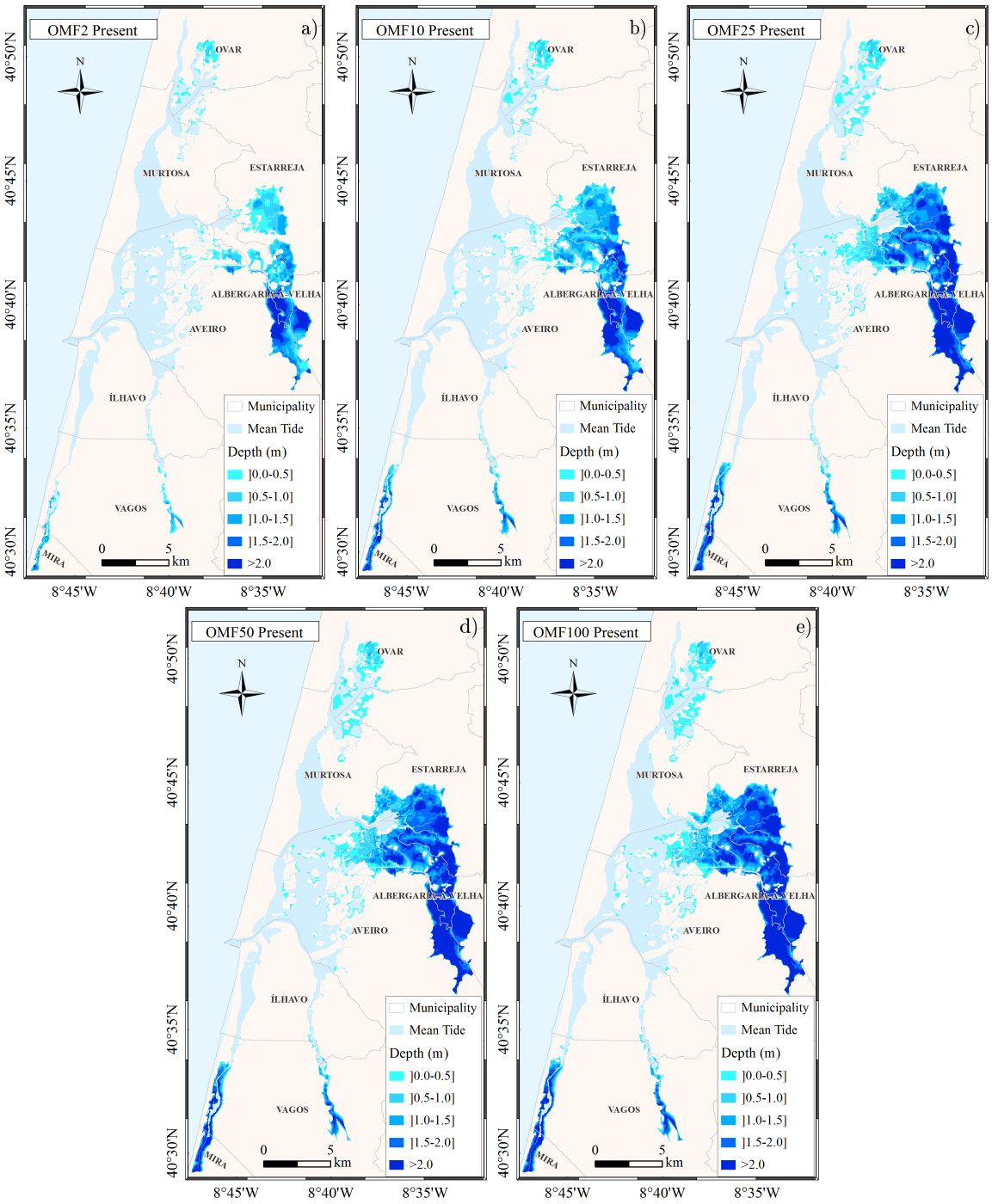


Figure 8.7: Flood depth maps for events of fluvial origin under present climate for scenarios: a) OMF2; b) OMF10; c) OMF25; d) OMF50; e) OMF100.

the BVL region. The magnitude and extent of inundation caused by Cáster, Boco and Ribeira dos Moinhos is considerably lower than that caused by those rivers. Within the study area, the municipalities of Albergaria-a-Velha, Aveiro and Estarreja are the most endangered by floods of fluvial origin. During mean tide conditions the municipalities

of Murtosa and Ílhavo are not affected by those events. It is also evident that the flood depths decrease under climate change conditions comparing to the present climate, as consequence of the predicted decrease of river discharges.

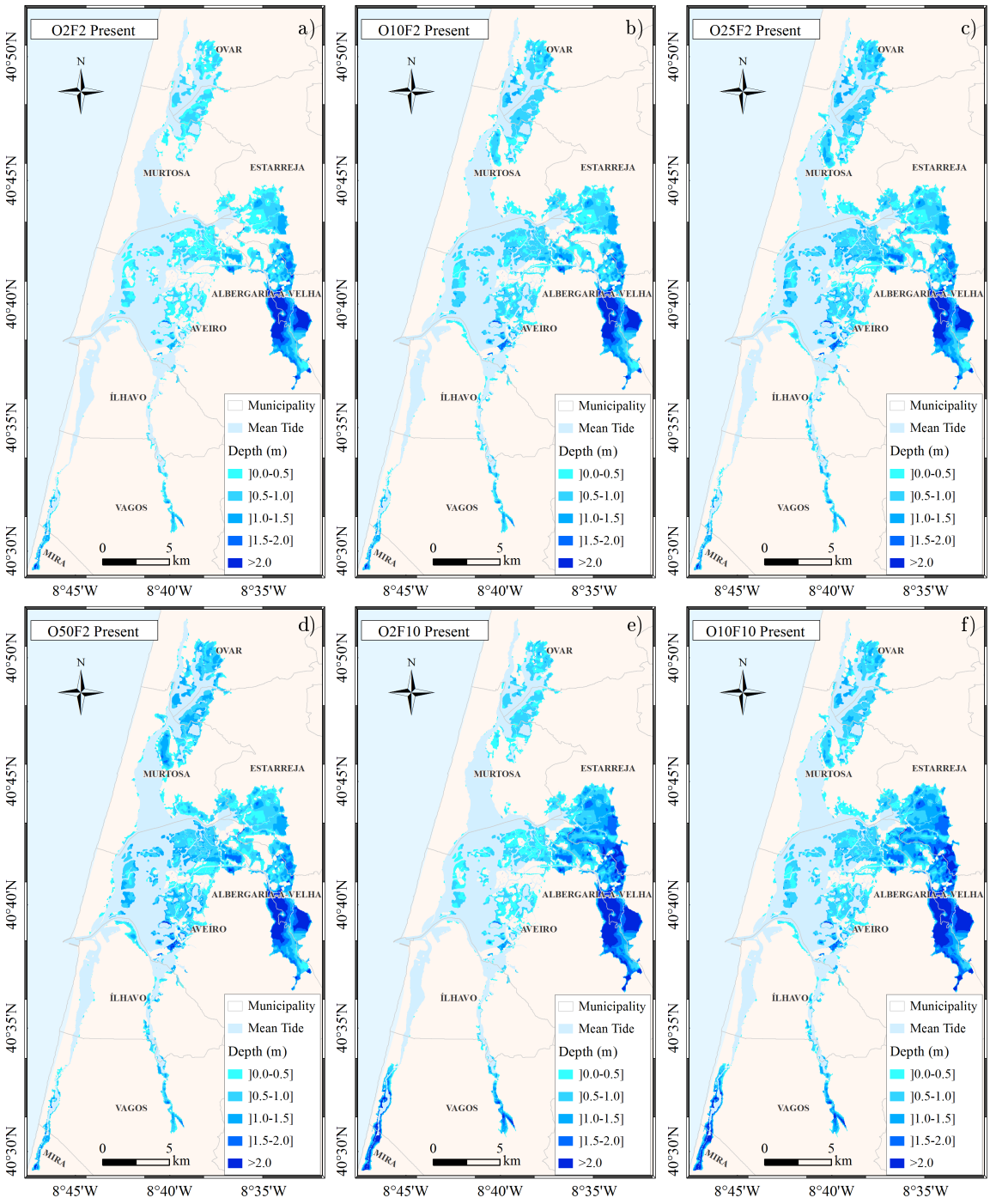


Figure 8.8: Flood depth maps for events of combined origin under present climate for scenarios: a) O2F2; b) O10F2; c) O25F2; d) O50F2; e) O2F10; f) O10F10; g) O2F25; h) O2F50.

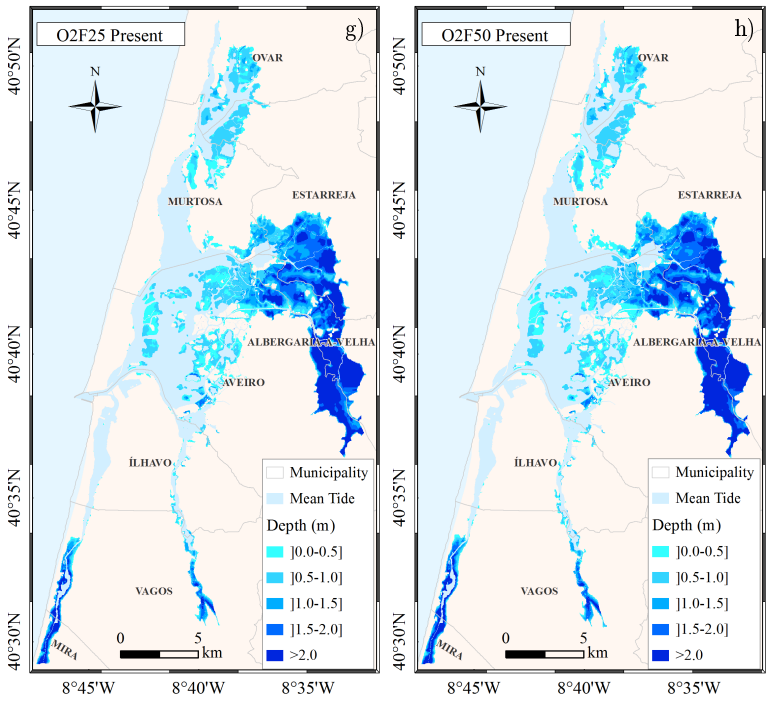


Figure 8.8: (Continued) Flood depth maps for events of combined origin under present climate for scenarios: a) O2F2; b) O10F2; c) O25F2; d) O50F2; e) O2F10; f) O10F10; g) O2F25; h) O2F50.

Concerning the events combining high sea levels and high river discharges (Figures 8.8 and 8.11), it was found that the flood extent is considerable higher than that obtained when high sea levels or high discharges occur individually. Furthermore, the results evidence the existence of some restricted areas that are flooded only when high sea levels and high discharges occur simultaneously.

Moreover, in general, it is evident for all the scenarios that the inundation depths found in the vicinity of the lagoon tributaries are higher than those obtained for the remaining lagoon. As example, for scenario O2F2, the majority of the lagoon adjacent area presents inundation depths lower than 1 m, however some regions located in the vicinity of Vouga river present water depths higher than 2 m. Results evidence also that inundation depths change in some areas dominated by oceanic flood events, when river discharges change. This is evident when comparing the inundation patterns in Murtosa municipality under scenarios O2FM, O2F2, O2F10, O2F25 and O2F50 that present similar oceanic boundary conditions but different river discharges. This fact highlights that the landward propagation of oceanic waters is affected by the river discharges and the seaward river discharges propagation is affected by the sea surface

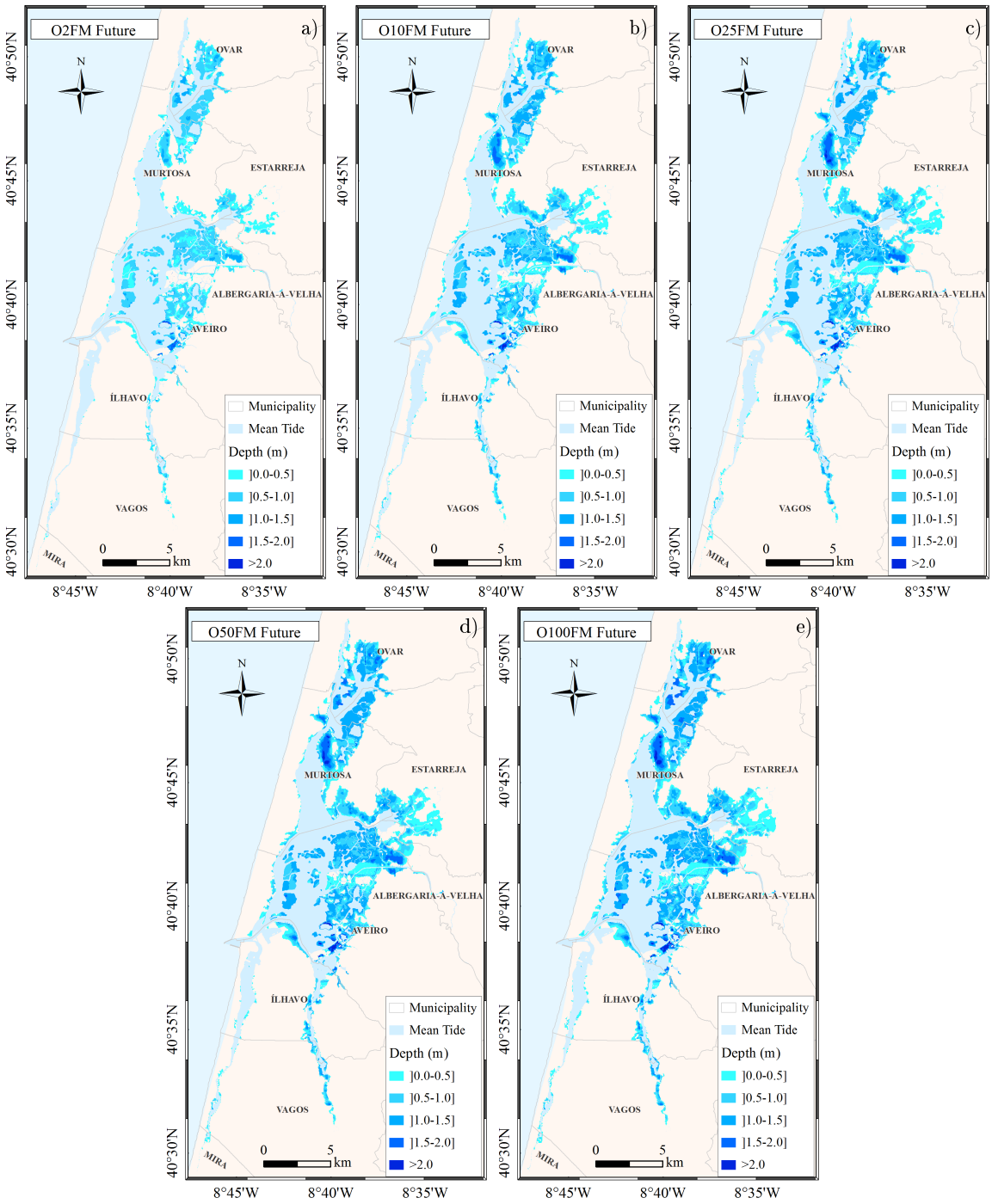


Figure 8.9: Flood depth maps for events of oceanic origin under future climate for scenarios: a) O2FM; b) O10FM; c) O25FM; d) O50FM; e) O100FM.

level. Indeed, in the transition zones where saltwater and freshwater interact, there is an accumulation of water induced by opposite forcing. By one hand, the oceanic water is unable to penetrate the lagoon upper reaches. On the other hand, the water coming from the rivers cannot move seaward because the tide is moving landward. In this way,

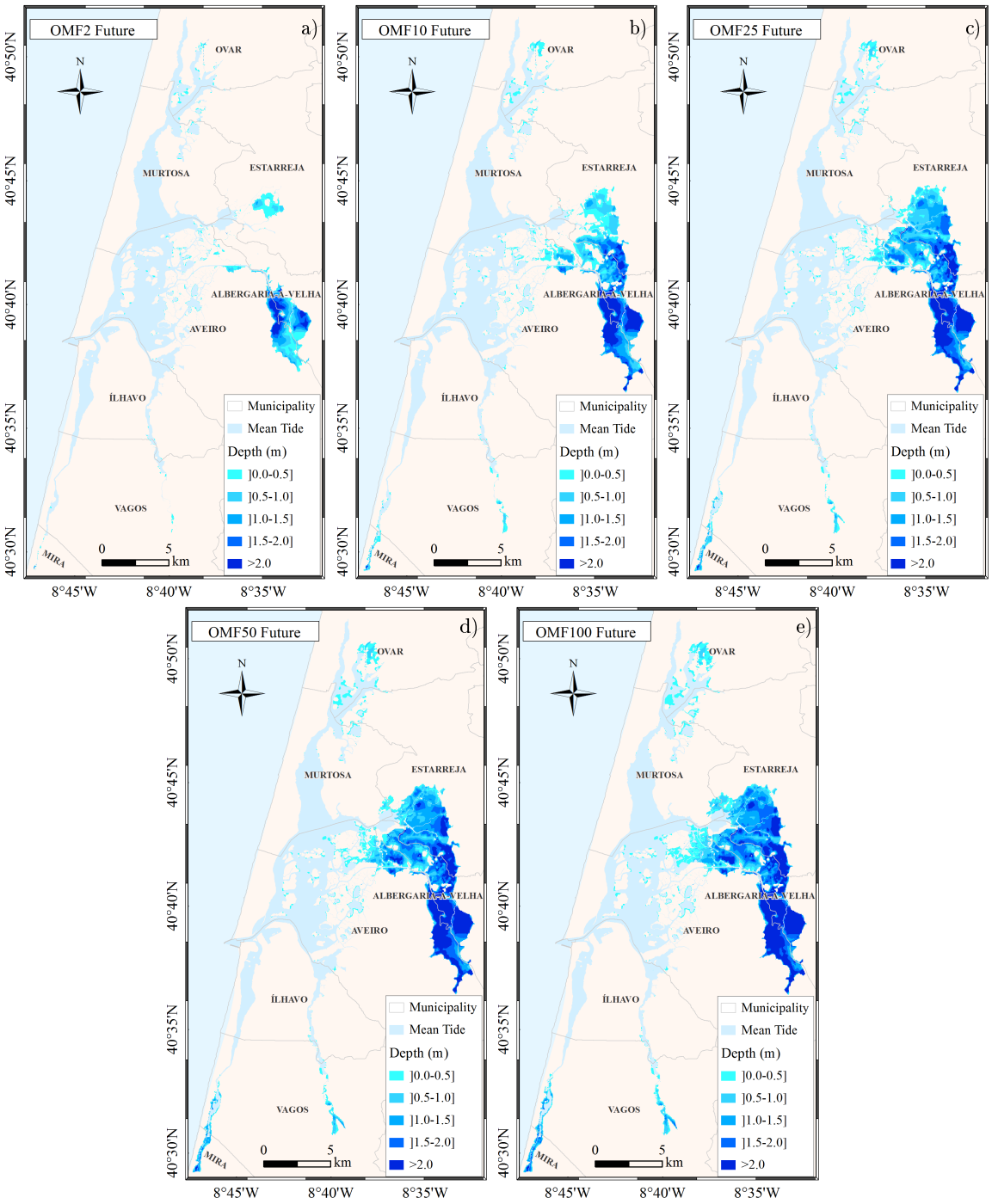


Figure 8.10: Flood depth maps for events of fluvial origin under future climate for scenarios: a) OMF2; b) OMF10; c) OMF25; d) OMF50; e) OMF100.

the trapped water is forced to fill the adjacent marginal regions. This effect is present in all the combined scenarios, however is more evident in the vicinity of Vouga and Antuã mouths, considering the higher flood extent observed in this region.

Under climate change conditions, the landward movement induced by oceanic water

tends to increase once sea levels will be higher. In contrast, the seaward movement induced by river discharges tends to decrease following the predicted river discharges reduction. In this way, the oceanic waters tend to penetrate further landward. This fact

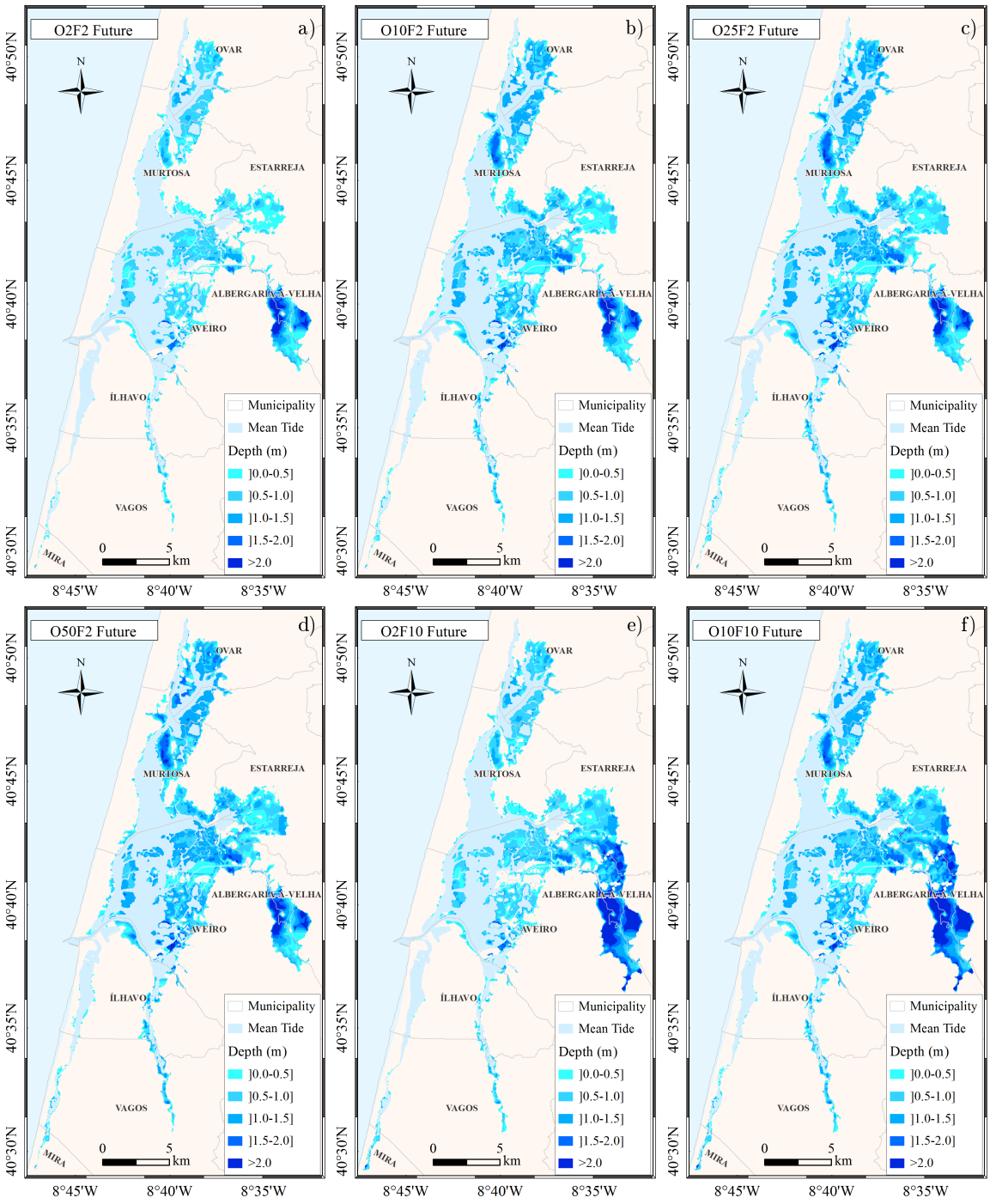


Figure 8.11: Flood depth maps for events of combined origin under future climate for scenarios: a) O2F2; b) O10F2; c) O25F2; d) O50F2; e) O2F10; f) O10F10; g) O2F25; h) O2F50.

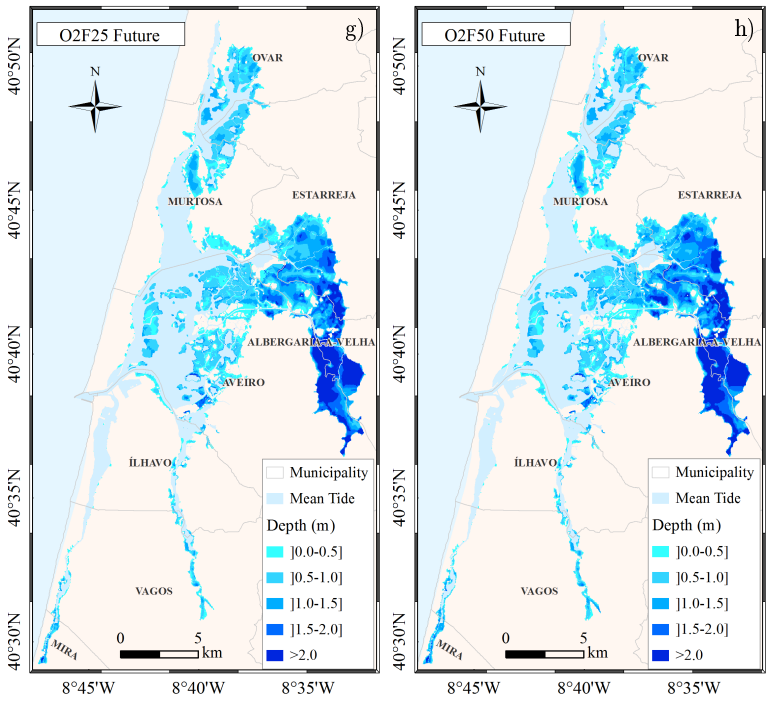


Figure 8.11: (Continued) Flood depth maps for events of combined origin under future climate for scenarios: a) O2F2; b) O10F2; c) O25F2; d) O50F2; e) O2F10; f) O10F10; g) O2F25; h) O2F50.

suggests that the saltwater intrusion observed and reported nowadays will be intensified under climate change conditions.

The frequency of flood events was evaluated by constructing probability maps for flood events of oceanic, fluvial and combined origin under both present and future climates (Figure 8.12). The maps evidence that the floods of oceanic origin tend to occur more frequently under climate change conditions comparing to the present climate. This fact is more evident in the lagoon central area and at the margins of S. Jacinto channel, which floods are dominated by oceanic forcing. Contrarily, the probability of flood events of fluvial origin tends to decrease for the future climate in some areas dominated by fluvial forcing, responding to the river discharges reduction. The flood probability of events of combined origin reflects the tendency found for those induced by oceanic and fluvial forcing. Thus, the flood probability tends to increase in the areas dominated by oceanic forcing and to decrease in the areas adjacent to the rivers mouths.

Flood hazard maps were created combining flood depth and flood probability maps (Figure 8.13). The flood hazard was normalized and categorized in 4 classes: low,

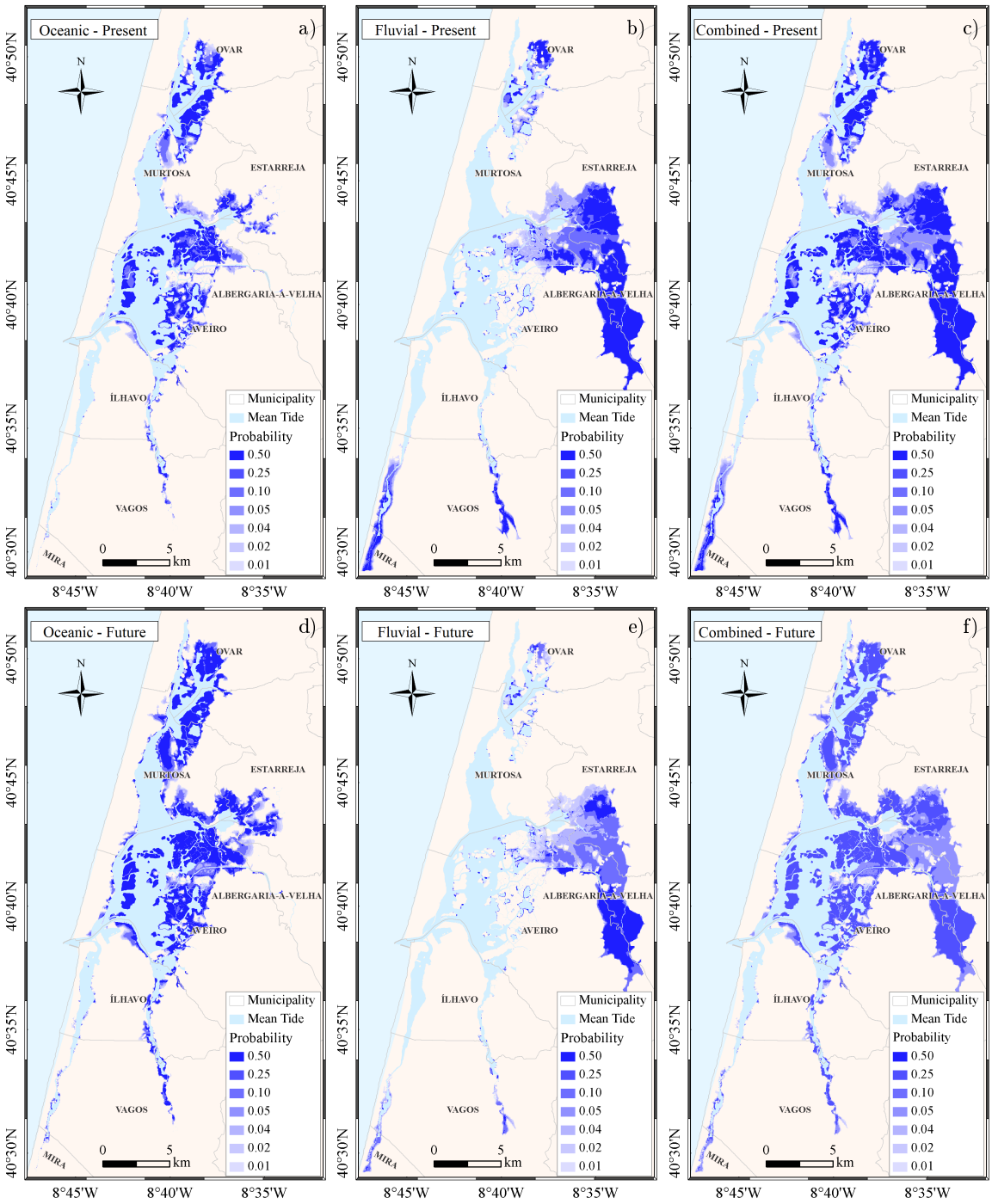


Figure 8.12: Flood probability maps for events of: a), d) oceanic origin; b), e) fluvial origin; c), f) combined origin; under present and future climates, respectively.

moderate, high, and very high by applying the Jenks natural breaks classification method [Jenks, 1967]. In summary, this method reduces the variance within classes and maximizes the variance between classes. The analysis of the maps presented in Figure 8.13 highlights that flood events of fluvial origin have higher hazard than those

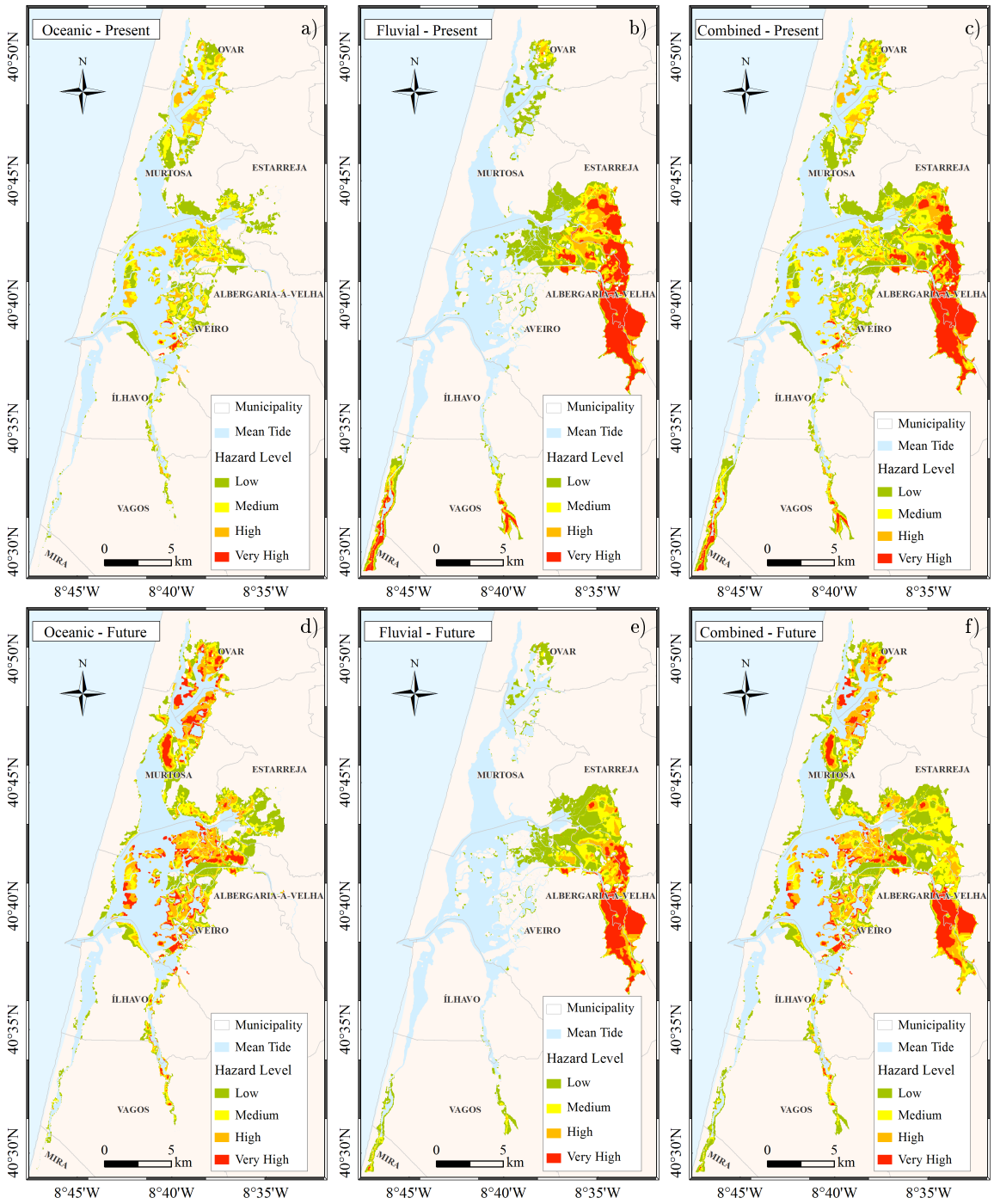


Figure 8.13: Flood hazard maps for events of: a), d) oceanic origin; b), e) fluvial origin; c), f) combined origin; under present and future climates, respectively.

of oceanic origin. It is also clear that the flood hazard for events of oceanic/fluvial origin tends to increase/decrease under climate change conditions. Consequently, the hazard of floods of combined origin tends to increase/decrease in the areas dominated by oceanic/fluvial forcing under climate change conditions.

### 8.3.2 Identifying assets exposed to flood hazard

The flood extent predicted by the hydrodynamic model was intersected with the population density of the region, and the number of inhabitants exposed to flood events was determined (Table 8.7). The exposure of inhabitants to flood events of oceanic origin is higher than that of fluvial origin, for each one of the return periods. Indeed, for the present climate, the number of inhabitants exposed to floods of oceanic origin ranges between 189 and 1567 for return periods of 2 and 100 years, respectively, while the number of inhabitants exposed to floods of fluvial origin ranges between 157 and 958 for return periods of 2 and 100 years, respectively. The exposure of inhabitants to

Table 8.7: Number of inhabitants potentially affected by flood events ("P" and "F" represent present and future climates, respectively).

| | | Present | Future |
|---|---|---|---|
| Oceanic | O2FM | 189 | 829 |
| | O10FM | 667 | 1980 |
| | O25FM | 909 | 2327 |
| | O50FM | 1266 | 2608 |
| | O100FM | 1567 | 2949 |
| Fluvial | OMF2 | 157 | 44 |
| | OMF10 | 289 | 185 |
| | OMF25 | 500 | 227 |
| | OMF50 | 679 | 256 |
| | OMF100 | 958 | 269 |
| Combined | O2F2 | 378 | 952 |
| | O10F2 | 992 | 2156 |
| | O25F2 | 1402 | 2539 |
| | O50F2 | 1720 | 2848 |
| | O2F10 | 562 | 1197 |
| | O10F10 | 1299 | 2383 |
| | O2F25 | 1008 | 1320 |
| | O2F50 | 1340 | 1469 |

oceanic/fluvial induced floods will increase/decrease under climate change conditions. Concerning floods of oceanic origin, it is estimated that the number of inhabitants exposed will increase between 338% and 90% for return periods of 2 and 100 years, respectively. The inhabitants decrease rate expected for events of fluvial origin is lower and ranges between 55% and 70%.

The results also show that the number of inhabitants exposed to floods of combined origin accomplishes the tendency observed for events of oceanic and fluvial origin. In this way, for the same return period, the number of inhabitants exposed to inundation increases with higher sea level conditions (for example, the number of inhabitants exposed to inundation for scenarios O10F2 and O2F10 is 992 and 562, respectively). It is found that the number of inhabitants exposed to inundation will increase under climate change conditions, for all events of combined origin. This fact highlights that the increase in the number of inhabitants exposed to floods of oceanic origin overlaps the decrease found for events of fluvial origin. Furthermore, it was found that the inhabitants increase rate of events of combined origin is higher as intense is the oceanic forcing.

The land exposure to floods was investigated by computing the area of land use affected by each simulation event (Table 8.8). The results evidence that for events of oceanic origin, most of the inundated area has no economic use. Indeed, the "no use" class represents between 60% to 80% of the total inundated area, depending on the considered scenario. This is followed in lesser extent by forest and semi natural areas, residential areas, agricultural fields, industrial areas and areas used on transport and storage activities. The remaining classes present null or very low flooded area. Also, it is important to highlight that the areas predominantly residential, agricultural, industrial and used for transport and storage activities are highly sensitive to sea level oscillations, once the flooded area for that classes presents high change rates between scenarios. For example, for the present climate it is predicted that the agricultural area flooded will increase approximately 1200% for the 100 years return period ($684.6\times10^4$ $m^2$) comparing with the 2 years return period ($52.1\times10^4$ $m^2$). The results further evidence that the exposure of land to flood events of oceanic origin will increase under climate change conditions. The highest change was found for 2 years return period

Table 8.8: Land use area ($\times 10^4$ m$^2$) affected by flood events ("P" and "F" represent present and future climates, respectively).

| | | | Residential | Commercial, Accommodation and Restaurants | Industry | Transport and Storage | Agriculture | Forest and Semi Natural | No Use | Total |
|---|---|---|---|---|---|---|---|---|---|---|
| Oceanic | O2FM | P | 1.6 | 1.7 | 3.0 | 5.2 | 52.1 | 5.8 | 2108.9 | 2636.9 |
| | | F | 18.1 | 6.6 | 27.5 | 26.6 | 438.6 | 32.7 | 3368.8 | 4582.1 |
| | O10FM | P | 9.7 | 5.6 | 21.6 | 20.6 | 248.7 | 22.2 | 3012.5 | 3957.4 |
| | | F | 68.4 | 15.6 | 48.3 | 35.4 | 968.8 | 92.5 | 4068.1 | 6094.2 |
| | O25FM | P | 21.8 | 6.8 | 30.8 | 28.3 | 405.3 | 33.6 | 3330.0 | 4537.5 |
| | | F | 85.0 | 18.6 | 59.2 | 37.3 | 1163.2 | 129.0 | 4308.4 | 6646.3 |
| | O50FM | P | 35.1 | 9.2 | 36.8 | 30.5 | 542.8 | 45.6 | 3515.3 | 4935.4 |
| | | F | 100.8 | 19.5 | 64.3 | 38.7 | 1330.5 | 163.1 | 4483.8 | 7087.5 |
| | O100FM | P | 45.2 | 12.2 | 41.0 | 32.0 | 684.1 | 58.5 | 3690.4 | 5316.7 |
| | | F | 117.2 | 20.7 | 70.9 | 42.8 | 1495.6 | 203.4 | 4611.4 | 7486.1 |
| Fluvial | OMF2 | P | 4.6 | 0.0 | 8.5 | 16.9 | 2300.0 | 233.3 | 969.6 | 3607.9 |
| | | F | 0.4 | 0.0 | 1.3 | 9.4 | 1165.0 | 89.9 | 304.1 | 1597.6 |
| | OMF10 | P | 12.7 | 0.0 | 12.1 | 19.7 | 2976.1 | 352.5 | 1683.6 | 6094.2 |
| | | F | 3.2 | 0.0 | 8.8 | 15.8 | 2484.7 | 203.1 | 805.0 | 3578.1 |
| | OMF25 | P | 29.7 | 0.0 | 15.4 | 20.8 | 3317.2 | 406.9 | 2572.8 | 6582.7 |
| | | F | 6.4 | 0.0 | 12.4 | 18.4 | 3009.6 | 279.8 | 1741.2 | 4568.4 |
| | OMF50 | P | 50.2 | 0.0 | 16.4 | 21.4 | 3423.9 | 433.6 | 2773.2 | 6962.6 |
| | | F | 8.9 | 0.0 | 13.5 | 19.5 | 3096.8 | 307.5 | 2108.3 | 5178.3 |
| | OMF100 | P | 68.0 | 0.0 | 17.6 | 21.4 | 3533.4 | 470.1 | 2960.8 | 7335.3 |
| | | F | 9.9 | 0.0 | 13.5 | 19.5 | 3096.8 | 307.5 | 2108.3 | 5702.0 |
| Combined | O2F2 | P | 6.4 | 1.9 | 13.0 | 22.2 | 2401.3 | 244.5 | 3146.2 | 6373.8 |
| | | F | 23.3 | 6.8 | 30.8 | 35.8 | 1757.6 | 136.6 | 3722.8 | 6405.5 |
| | O10F2 | P | 22.6 | 6.3 | 34.4 | 42.3 | 2657.9 | 274.4 | 3971.8 | 7709.0 |
| | | F | 74.6 | 16.6 | 53.3 | 43.8 | 2330.0 | 212.9 | 4438.0 | 7993.0 |
| | O25F2 | P | 39.1 | 8.9 | 43.4 | 46.0 | 2849.4 | 288.4 | 4234.6 | 8264.9 |
| | | F | 96.8 | 19.3 | 60.9 | 46.0 | 2575.1 | 261.9 | 4633.4 | 8571.6 |
| | O50F2 | P | 53.0 | 11.1 | 48.1 | 48.2 | 3001.7 | 303.9 | 4395.5 | 8649.5 |
| | | F | 112.9 | 19.7 | 68.7 | 47.8 | 2741.2 | 300.6 | 4766.2 | 8976.4 |
| | O2F10 | P | 16.3 | 2.2 | 16.6 | 26.4 | 3044.9 | 359.7 | 3642.4 | 7693.5 |
| | | F | 30.1 | 7.6 | 38.2 | 43.2 | 2995.7 | 252.0 | 4146.0 | 8231.8 |
| | O10F10 | P | 40.2 | 6.6 | 41.2 | 45.8 | 3322.3 | 387.2 | 4323.6 | 8909.9 |
| | | F | 81.8 | 17.7 | 63.5 | 50.3 | 3492.0 | 325.0 | 4699.5 | 9576.7 |
| | O2F25 | P | 42.1 | 3.6 | 21.6 | 29.3 | 3443.1 | 417.8 | 4104.1 | 8689.7 |
| | | F | 36.1 | 8.0 | 40.4 | 44.7 | 3320.2 | 297.6 | 4358.9 | 8841.8 |
| | O2F50 | P | 63.5 | 4.5 | 24.5 | 35.9 | 3596.4 | 450.1 | 4255.6 | 9078.2 |
| | | F | 43.5 | 8.2 | 43.8 | 46.4 | 3492.4 | 328.5 | 4460.0 | 9177.7 |

events, with an increase of 816% of the industrial area flooded (from $3.0\times10^4$ m$^2$ in the present climate to $27.5\times10^4$ m$^2$ in the future climate).

Regarding the floods of fluvial origin, it was found that most of flooded area has agricultural use. Indeed, it is predicted that the agricultural flooded area represents between 50% and 75% of the total marginal area, depending on the scenario considered. This is followed by areas with no economic activity use, that represent between 25% and 40% of the total marginal area. The results also evidence that the exposure of commercial, accommodation and restaurants areas is insignificant comparing with other classes. It is predicted that the exposure of land to floods of fluvial origin will decrease under climate change conditions, comparing to the present climate, in response to the forecasted river discharges decrease. The residential areas present the highest decrease rates, that range between 75% and 90%. An interesting fact was found comparing the residential area flooded by events of oceanic and fluvial origin. Indeed, for the present climate the residential areas are more exposed to events of fluvial origin than that of oceanic origin. However, this behaviour tends to be inverted under climate change conditions.

Concerning the events of combined origin, the results evidence that most of the flooded area presents no economic use, representing approximately between 50% and 60% of the total marginal area flooded. The agricultural area flooded represents between 25% and 40% of the total marginal area flooded. The results further evidence that the land exposure increases under climate change conditions for events of combined origin. Although the residential, commercial, accommodation and restaurants flooded areas constitute a small percentage of the total marginal flooded area, these areas present high change rates between scenarios, highlighting its high sensitivity to flood events.

The exposure of buildings to flood events was evaluated by computing the area of the buildings inundated during flood events (Table 8.9). Regarding the events of oceanic origin, most of the flooded buildings are residential, commercial and industrial. Indeed, these typologies represent more than 90% of the total area of buildings flooded. Within these three typologies, the industrial buildings represent more than 70% of the total area of buildings flooded, except for scenario O2FM. The results also highlight that

Table 8.9: Building area ($\times 10^4$ m$^2$) affected by flood events ("P" and "F" represent present and future climates, respectively).

| | | | Residential | Commercial | Industrial | Agricultural | Total |
|---|---|---|---|---|---|---|---|
| Oceanic | O2FM | P | 0.4 | 0.3 | 0.4 | 0.0 | 1.2 |
| | | F | 1.1 | 0.6 | 8.3 | 0.0 | 10.3 |
| | O10FM | P | 1.2 | 0.6 | 6.3 | 0.0 | 8.2 |
| | | F | 2.3 | 1.9 | 11.2 | 0.2 | 15.9 |
| | O25FM | P | 1.2 | 0.8 | 8.8 | 0.0 | 11.0 |
| | | F | 2.4 | 2.1 | 12.6 | 0.2 | 17.7 |
| | O50FM | P | 1.6 | 1.3 | 9.7 | 0.0 | 12.7 |
| | | F | 2.9 | 2.3 | 13.4 | 0.2 | 19.1 |
| | O100FM | P | 1.8 | 1.5 | 10.4 | 0.1 | 14.1 |
| | | F | 3.1 | 2.3 | 14.0 | 0.2 | 20.0 |
| Fluvial | OMF2 | P | 0.0 | 0.0 | 0.0 | 0.0 | 0.0 |
| | | F | 0.0 | 0.0 | 0.0 | 0.0 | 0.0 |
| | OMF10 | P | 0.0 | 0.0 | 0.0 | 0.3 | 0.3 |
| | | F | 0.0 | 0.0 | 0.0 | 0.0 | 0.0 |
| | OMF25 | P | 0.5 | 0.0 | 0.1 | 0.4 | 1.0 |
| | | F | 0.1 | 0.0 | 0.0 | 0.2 | 0.4 |
| | OMF50 | P | 0.5 | 0.0 | 0.5 | 0.4 | 1.0 |
| | | F | 0.1 | 0.0 | 0.0 | 0.2 | 0.4 |
| | OMF100 | P | 0.5 | 0.0 | 0.1 | 0.4 | 1.0 |
| | | F | 0.1 | 0.0 | 0.0 | 0.2 | 0.4 |
| Combined | O2F2 | P | 0.5 | 0.3 | 0.6 | 0.0 | 1.6 |
| | | F | 1.2 | 0.8 | 8.2 | 0.0 | 10.4 |
| | O10F2 | P | 1.2 | 0.6 | 7.6 | 0.1 | 9.7 |
| | | F | 2.3 | 2.0 | 11.7 | 0.3 | 16.5 |
| | O25F2 | P | 1.6 | 1.2 | 9.2 | 0.1 | 12.3 |
| | | F | 2.5 | 2.3 | 12.7 | 0.3 | 18.1 |
| | O50F2 | P | 1.8 | 1.4 | 9.9 | 0.3 | 16.5 |
| | | F | 2.9 | 2.3 | 13.6 | 0.3 | 19.4 |
| | O2F10 | P | 0.6 | 0.4 | 0.7 | 0.3 | 2.1 |
| | | F | 1.3 | 1.0 | 7.5 | 0.1 | 10.0 |
| | O10F10 | P | 1.5 | 0.7 | 8.4 | 0.3 | 10.8 |
| | | F | 2.3 | 2.0 | 12.0 | 0.3 | 16.9 |
| | O2F25 | P | 1.3 | 0.5 | 0.9 | 0.4 | 3.0 |
| | | F | 1.5 | 1.0 | 7.5 | 0.4 | 10.5 |
| | O2F50 | P | 1.5 | 0.5 | 1.0 | 0.4 | 3.4 |
| | | F | 1.5 | 1.0 | 8.3 | 0.4 | 11.4 |

the exposure of buildings to these events will increase under climate change conditions. Particularly, for the 2 years return period, the area flooded increases approximately 758%, from $1.2\times10^4$ m$^2$ in the present climate to $10.3\times10^4$ m$^2$ in the future climate. For the 100 years return period the increase rate is considerably lower (approximately 42%).

The exposure of buildings to flood events of fluvial origin is considerably lower than that for events of oceanic origin. Indeed, for the overall scenarios the total area flooded does not exceed $1.0\times10^4$ m$^2$.

As expected, the building area affected by events of combined origin increases with the sea level and river discharges imposed as model boundary condition. Nevertheless, it is important to highlight that the building inundated area for combined events is higher than the area of single events with the same return period. For example, for the scenario O50F2 that combines sea levels with 50 years return period and river discharges with 2 years return period, the total building flooded area is $16.5\times10^4$ m$^2$. However, the flooded area for scenario O50FM and OMF2 is 12.7 and $0.0\times10^4$ m$^2$, respectively. This situation shows that the effect of high sea level events in the building area flooded is highly dependent on the river discharge. Also, the building flooded area for scenario O2F50 is $3.4\times10^4$ m$^2$, while for scenarios O2FM and OMF50 is 1.2 and $1.0\times10^4$ m$^2$, respectively. This reflects that the influence of high discharge events on the buildings flooded is highly dependent on the sea level. It is also important to address that the building area flooded by events of combined origin increases under climate change conditions.

The exposure of roads was quantified by computing the length affected by inundation events (Table 8.10). Analysing all the simulations, were not found main and secondary roads affected by flood events. The results evidence that the other paved and unpaved roads classes are the most affected by floods of oceanic origin. Indeed, for these events the affected length of other paved roads represents more than 50% of the total length of inundated roads, except for scenario O2FM (43%). The unpaved roads represent more than 30% of the total length, except for scenario O2FM (52%). Also, it is evident that the exposure of roads to floods of oceanic origin tends to increase significantly under climate change conditions, mainly for sea levels of 2 years return

Table 8.10: Length ($\times 10^3$ m) of roads potentially affected by flood events ("P" and "F" represent present and future climates, respectively).

| | | | Highway | Other Paved | Unpaved | Pedestrian and Cycleway | Total |
|---|---|---|---|---|---|---|---|
| Oceanic | O2FM | P | 0.4 | 4.9 | 6.0 | 0.3 | 11.5 |
| | | F | 0.7 | 27.8 | 21.2 | 2.7 | 52.5 |
| | O10FM | P | 0.7 | 19.3 | 14.3 | 2.0 | 36.4 |
| | | F | 1.1 | 64.9 | 35.3 | 5.2 | 107.1 |
| | O25FM | P | 0.7 | 32.8 | 20.1 | 2.9 | 56.4 |
| | | F | 1.2 | 76.2 | 41.7 | 6.4 | 126.0 |
| | O50FM | P | 0.7 | 41.2 | 23.5 | 3.3 | 68.9 |
| | | F | 1.3 | 86.2 | 48.1 | 7.9 | 144.2 |
| | O100FM | P | 1.1 | 50.8 | 28.1 | 4.0 | 84.2 |
| | | F | 1.7 | 96.9 | 54.0 | 9.5 | 162.9 |
| Fluvial | OMF2 | P | 4.2 | 6.1 | 89.4 | 0.0 | 100.3 |
| | | F | 2.3 | 1.2 | 43.7 | 0.0 | 47.3 |
| | OMF10 | P | 4.5 | 13.2 | 114.9 | 0.0 | 133.5 |
| | | F | 4.1 | 4.7 | 93.0 | 0.0 | 102.5 |
| | OMF25 | P | 4.6 | 21.9 | 130.1 | 0.0 | 157.6 |
| | | F | 4.2 | 7.5 | 110.9 | 0.0 | 123.5 |
| | OMF50 | P | 4.7 | 29.2 | 133.0 | 0.0 | 168.1 |
| | | F | 4.3 | 9.4 | 117.1 | 0.0 | 131.7 |
| | OMF100 | P | 4.7 | 35.6 | 137.8 | 0.0 | 179.4 |
| | | F | 4.4 | 11.2 | 121.9 | 0.0 | 138.5 |
| Combined | O2F2 | P | 4.5 | 12.8 | 94.9 | 0.5 | 113.2 |
| | | F | 2.8 | 34.4 | 69.4 | 2.8 | 109.0 |
| | O10F2 | P | 4.7 | 33.3 | 104.6 | 2.6 | 145.8 |
| | | F | 3.2 | 69.7 | 86.8 | 5.5 | 165.8 |
| | O25F2 | P | 4.7 | 47.8 | 109.9 | 3.2 | 166.4 |
| | | F | 3.3 | 83.7 | 93.6 | 7.9 | 189.2 |
| | O50F2 | P | 5.2 | 57.6 | 113.2 | 3.9 | 180.7 |
| | | F | 3.6 | 93.8 | 99.6 | 9.1 | 207.0 |
| | O2F10 | P | 4.7 | 22.1 | 119.3 | 0.8 | 147.9 |
| | | F | 4.6 | 41.6 | 114.0 | 3.0 | 163.7 |
| | O10F10 | P | 4.9 | 46.4 | 127.4 | 2.8 | 182.6 |
| | | F | 5.0 | 76.6 | 126.9 | 6.4 | 216.0 |
| | O2F25 | P | 4.8 | 37.4 | 133.2 | 1.2 | 177.7 |
| | | F | 4.6 | 47.0 | 125.4 | 3.1 | 181.1 |
| | O2F50 | P | 5.1 | 49.5 | 137.9 | 1.6 | 195.4 |
| | | F | 4.7 | 52.7 | 130.5 | 3.1 | 192.1 |

period. Effectively, it is expected that the length of roads inundated will increase by 356%, from 11.5 km in the present climate to 52.5 km in the future climate. For events of 100 years return periods the increase rate expected is 93%.

Regarding the floods of fluvial origin, the results show that the unpaved roads represent more than 85% of the total inundated length. They are followed by other paved roads that represent approximately 10% of the total inundated length. The extension of the inundated highway roads is lower, however it can not be neglected given its importance on the daily movements of persons and goods, but also given its importance to rescue plans. It is also predicted that the roads exposed to floods of fluvial origin tends to decrease under climate change conditions. Indeed, the length of inundated roads will decrease approximately 21% under climate change conditions comparing to the present climate, except for scenario OMF2 where the decrease rate found is 50%.

As for events of oceanic and fluvial origin, the other paved and unpaved roads are the most exposed to floods of combined origin. Under climate change conditions the roads exposed to these floods reflect the tendency observed for single events of oceanic and fluvial origin. On one hand the exposure of other paved roads tends to increase with the sea level rise. On the other hand the exposure of unpaved roads tends to decrease as the river discharges decrease. Despite this, in general the total length of inundated roads tends to increase under climate change conditions, comparing to present, except for scenario O2F2.

Table 8.11 presents the area of classified regions affected by inundation events. The results show that the flooded area with SPA and SCI classification is quite similar for the same scenario. The area classified as NR is only affected with return periods higher than 2 years. For the worst cases, the inundated area can achieve approximately $0.5\times10^4$ m$^2$. The exposure o classified areas to events of oceanic origin tends to increase under climate change conditions, as consequence of MSLR. An opposite trend is found for events of fluvial origin, as a decrease of fluvial discharges is predicted under climate change conditions. The events of combined origin highlight that globally the classified areas flooded tend to increase under climate change conditions.

Finally, the area of habitats exposed was assessed for each flood event scenario

Table 8.11: Area ($\times 10^4$ m$^2$) of classified regions affected by flood events ("P" and "F" represent present and future climates, respectively).

| | | | SPA | SCI | NR |
|---|---|---|---|---|---|
| Oceanic | O2FM | P | 2627.0 | 2619.2 | 0.0 |
| | | F | 4498.1 | 4467.4 | 10.4 |
| | O10FM | P | 3898.2 | 3873.4 | 7.3 |
| | | F | 5891.5 | 5831.3 | 30.1 |
| | O25FM | P | 4440.1 | 4407.5 | 12.1 |
| | | F | 6396.9 | 6329.0 | 38.2 |
| | O50FM | P | 4803.8 | 4766.1 | 15.3 |
| | | F | 6800.6 | 6728.6 | 42.7 |
| | O100FM | P | 5155.0 | 5113.1 | 22.9 |
| | | F | 7159.7 | 7084.2 | 51.9 |
| Fluvial | OMF2 | P | 3377.6 | 3438.7 | 0.0 |
| | | F | 1536.4 | 1545.5 | 0.0 |
| | OMF10 | P | 4878.7 | 4884.8 | 0.0 |
| | | F | 3370.4 | 3409.6 | 0.0 |
| | OMF25 | P | 6214.6 | 6205.4 | 0.0 |
| | | F | 4319.6 | 4319.0 | 0.0 |
| | OMF50 | P | 16564.3 | 6554.9 | 0.0 |
| | | F | 4898.1 | 4856.2 | 0.0 |
| | OMF100 | P | 6892.4 | 6887.3 | 0.0 |
| | | F | 5400.0 | 5360.3 | 0.0 |
| Combined | O2F2 | P | 6128.9 | 6172.2 | 0.1 |
| | | F | 6244.6 | 6221.7 | 11.2 |
| | O10F2 | P | 7399.4 | 7406.3 | 9.9 |
| | | F | 7710.2 | 7657.0 | 31.9 |
| | O25F2 | P | 7907.1 | 7904.2 | 13.4 |
| | | F | 8244.4 | 8183.5 | 39.6 |
| | O50F2 | P | 8257.9 | 8249.1 | 21.0 |
| | | F | 8607.1 | 8541.4 | 45.8 |
| | O2F10 | P | 7370.3 | 7373.8 | 0.0 |
| | | F | 7920.8 | 7906.9 | 11.8 |
| | O10F10 | P | 8505.5 | 8494.6 | 11.5 |
| | | F | 9140.8 | 9092.9 | 34.0 |
| | O2F25 | P | 8294.9 | 8283.4 | 0.0 |
| | | F | 8483.6 | 8422.8 | 12.1 |
| | O2F50 | P | 8641.5 | 8629.0 | 3.4 |
| | | F | 8776.8 | 8716.5 | 12.3 |

(Table 8.12). The results show that the area flooded covered by seagrass meadows is quite similar between scenarios. This fact is easily explained as most of the seagrass meadows are located in intertidal zones, and therefore are flooded each tidal cycle. Saltmarshes, mudflats and saltpans present the highest area flooded during events of oceanic origin. For these habitats, the area flooded increases with the sea level rise. Although the farmland area affected in lower extent, it has high variability to sea level oscillations. For example, the flooded area ranges from 1.6 to $72.4\times10^4$ $m^2$ for sea levels with 2 and 100 years return periods, respectively. Moreover, the farmland area flooded increases significantly under climate change conditions, mainly for sea level events with 2 years return period (3369%).

Regarding the events of fluvial origin, saltmarshes and farmlands are the most affected habitats. Farmland and saltmarshes flooded area is highly sensitive to river discharge variations. Effectively, the flooded area increases 41% and 188% for the farmland and saltmarshes, respectively, for river discharge events with 2 and 100 years return periods. Under climate change conditions, the habitats flooded area tends to decrease once river discharges are predicted to decrease. The highest decrease rates of 55% and 67% were found for farmland and saltmarshes habitats, respectively, for events with 2 years return period.

The events of combined origin evidence that the area flooded of mudflats and saltpans presents low variation rates between scenarios. Contrarily, farmland and saltmarshes inundated area is sensitive to these flood events. Particularly, it is predicted that the area flooded of farmland/saltmarshes will decrease/increase 48%/16% under future climate, comparing to the present, for scenario O2F2.

### 8.3.3 Flood risk

Once identified the assets exposed to flood events, their negative impacts on social, economic and ecological indicators were determined in each grid element according to the procedure previously described. Figures 8.14 to 8.19 present the flood risk maps for events of oceanic, fluvial and combined origin for both present and future climates.

For all cases, the flood risk for inhabitants and buildings indicators is limited to restricted areas throughout the lagoon margins, reflecting the location of population

Table 8.12: Area ($\times 10^4$ m$^2$) of habitats affected by flood events ("P" and "F" represent present and future climates, respectively).

| | | | Farmland | Saltmarshes | Mudflats | Saltpans | Seagrass Meadows |
|---|---|---|---|---|---|---|---|
| Oceanic | O2FM | P | 1.6 | 1689.6 | 404.3 | 222.9 | 5.3 |
| | | F | 55.5 | 2632.1 | 507.9 | 351.7 | 5.3 |
| | O10FM | P | 32.2 | 2378.6 | 498.3 | 330.9 | 5.3 |
| | | F | 118.9 | 3089.3 | 549.2 | 393.8 | 5.3 |
| | O25FM | P | 45.1 | 2593.9 | 512.1 | 358.6 | 5.3 |
| | | F | 136.0 | 3254.2 | 556.5 | 408.3 | 5.3 |
| | O50FM | P | 56.9 | 2721.5 | 527.1 | 369.6 | 5.3 |
| | | F | 161.5 | 3361.1 | 566.0 | 420.6 | 5.6 |
| | O100FM | P | 72.4 | 2827.8 | 534.6 | 378.5 | 5.3 |
| | | F | 189.3 | 3452.7 | 573.2 | 432.3 | 5.6 |
| Fluvial | OMF2 | P | 1154.2 | 815.6 | 66.9 | 19.1 | 0.0 |
| | | F | 512.5 | 268.8 | 39.1 | 10.3 | 0.0 |
| | OMF10 | P | 1490.0 | 1286.3 | 114.0 | 28.3 | 0.0 |
| | | F | 1380.8 | 637.7 | 60.0 | 17.7 | 0.0 |
| | OMF25 | P | 1605.9 | 2030.9 | 174.3 | 41.4 | 0.0 |
| | | F | 1540.0 | 1036.8 | 71.0 | 20.4 | 0.0 |
| | OMF50 | P | 1614.8 | 2030.9 | 202.9 | 47.2 | 3.1 |
| | | F | 1572.8 | 1360.2 | 106.9 | 23.9 | 0.0 |
| | OMF100 | P | 1625.5 | 2347.8 | 221.5 | 51.4 | 3.1 |
| | | F | 1592.8 | 1674.4 | 130.3 | 28.0 | 1.9 |
| Combined | O2F2 | P | 1186.1 | 2541.3 | 442.5 | 257.6 | 5.3 |
| | | F | 612.9 | 2961.3 | 513.3 | 358.4 | 5.3 |
| | O10F2 | P | 1229.1 | 3109.6 | 511.2 | 349.9 | 5.3 |
| | | F | 733.0 | 3407.6 | 552.0 | 398.1 | 5.3 |
| | O25F2 | P | 1246.8 | 3270.0 | 529.0 | 367.7 | 5.3 |
| | | F | 782.2 | 3524.6 | 563.1 | 414.2 | 5.6 |
| | O50F2 | P | 1263.4 | 3373.0 | 538.3 | 377.9 | 5.3 |
| | | F | 824.4 | 3597.8 | 569.2 | 427.5 | 5.6 |
| | O2F10 | P | 1514.1 | 2854.3 | 464.5 | 268.0 | 5.3 |
| | | F | 1453.4 | 3195.4 | 518.1 | 363.0 | 5.3 |
| | O10F10 | P | 1524.9 | 3316.7 | 526.0 | 353.9 | 5.3 |
| | | F | 1518.2 | 3554.8 | 554.0 | 402.5 | 5.3 |
| | O2F25 | P | 1607.0 | 3180.2 | 491.3 | 293.4 | 5.3 |
| | | F | 1563.4 | 3352.8 | 523.5 | 364.2 | 5.3 |
| | O2F50 | P | 1617.5 | 3278.0 | 510.3 | 301.6 | 5.3 |
| | | F | 1592.6 | 3418.5 | 525.6 | 365.8 | 5.3 |

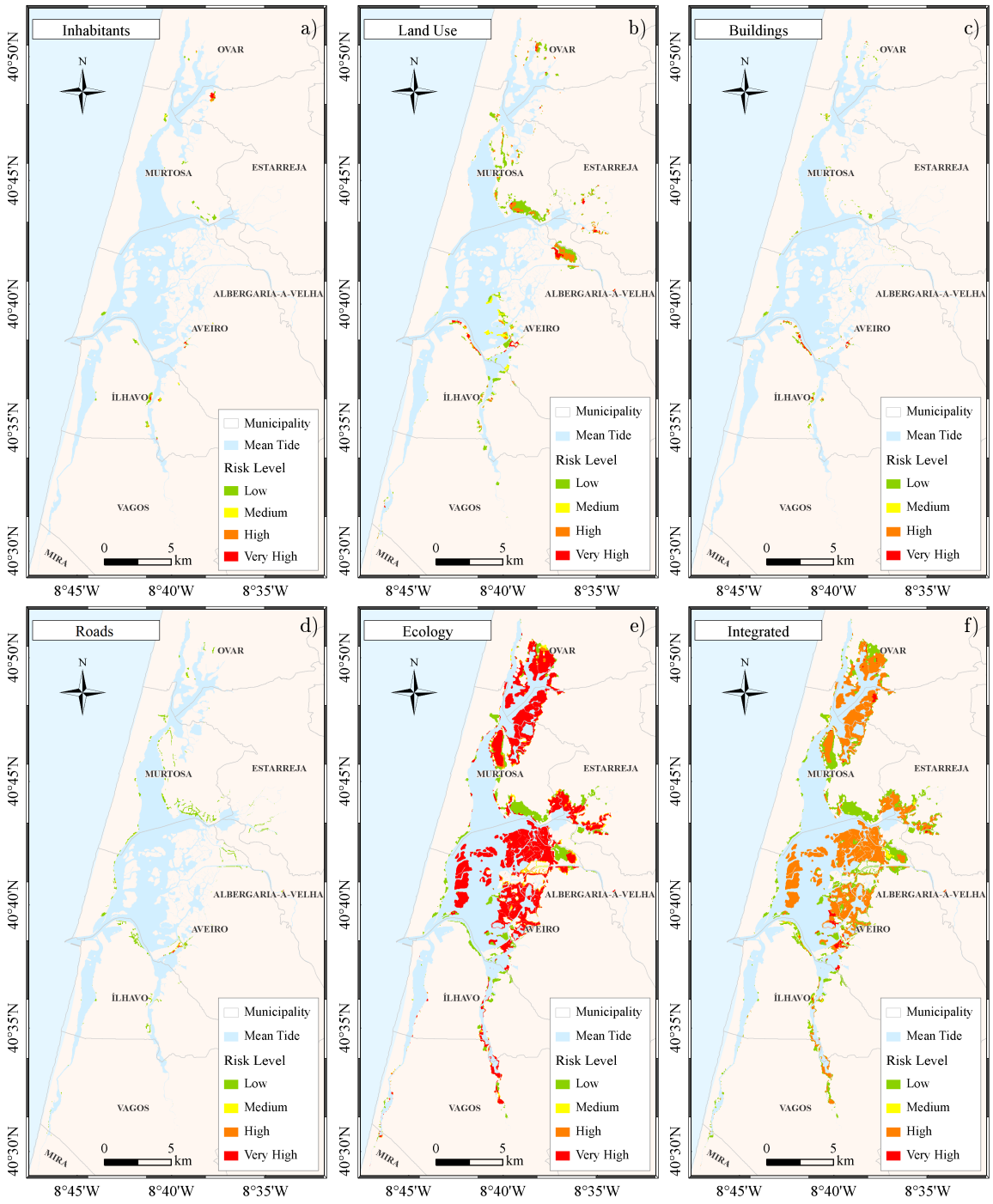


Figure 8.14: Flood risk maps for events of oceanic origin under present climate: a) inhabitants, b) land use, c) buildings d) roads, e) ecology, f) integrated.

clusters. Although small and sparse, these clusters present often high to very high flood risk. The area at risk for land use and roads indicators is wider, highlighting the presence of economic activities at the lagoon margins. Regarding the ecological risk, most of the inundated area presents a very high classification related with the

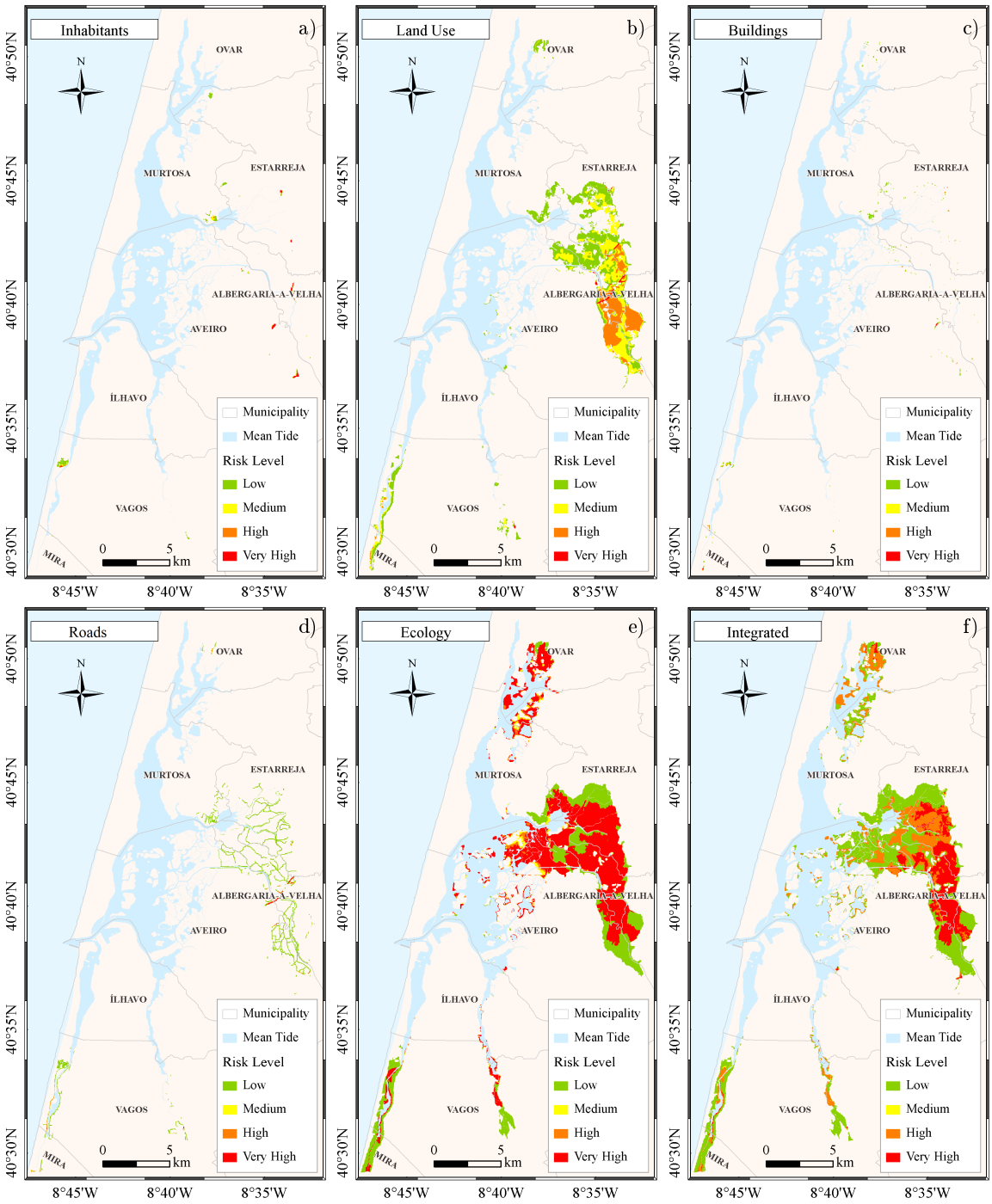


Figure 8.15: Flood risk maps for events of fluvial origin under present climate: a) inhabitants, b) land use, c) buildings d) roads, e) ecology, f) integrated.

presence of extensive valuable habitats. For each case the integrated risk reflects the contribution of each asset. However, the ecological contribution is highlighted in all maps once the ecological risk covers most of the marginal area.

Analysing the flood risk maps for events of oceanic origin in detail (Figures 8.14 and

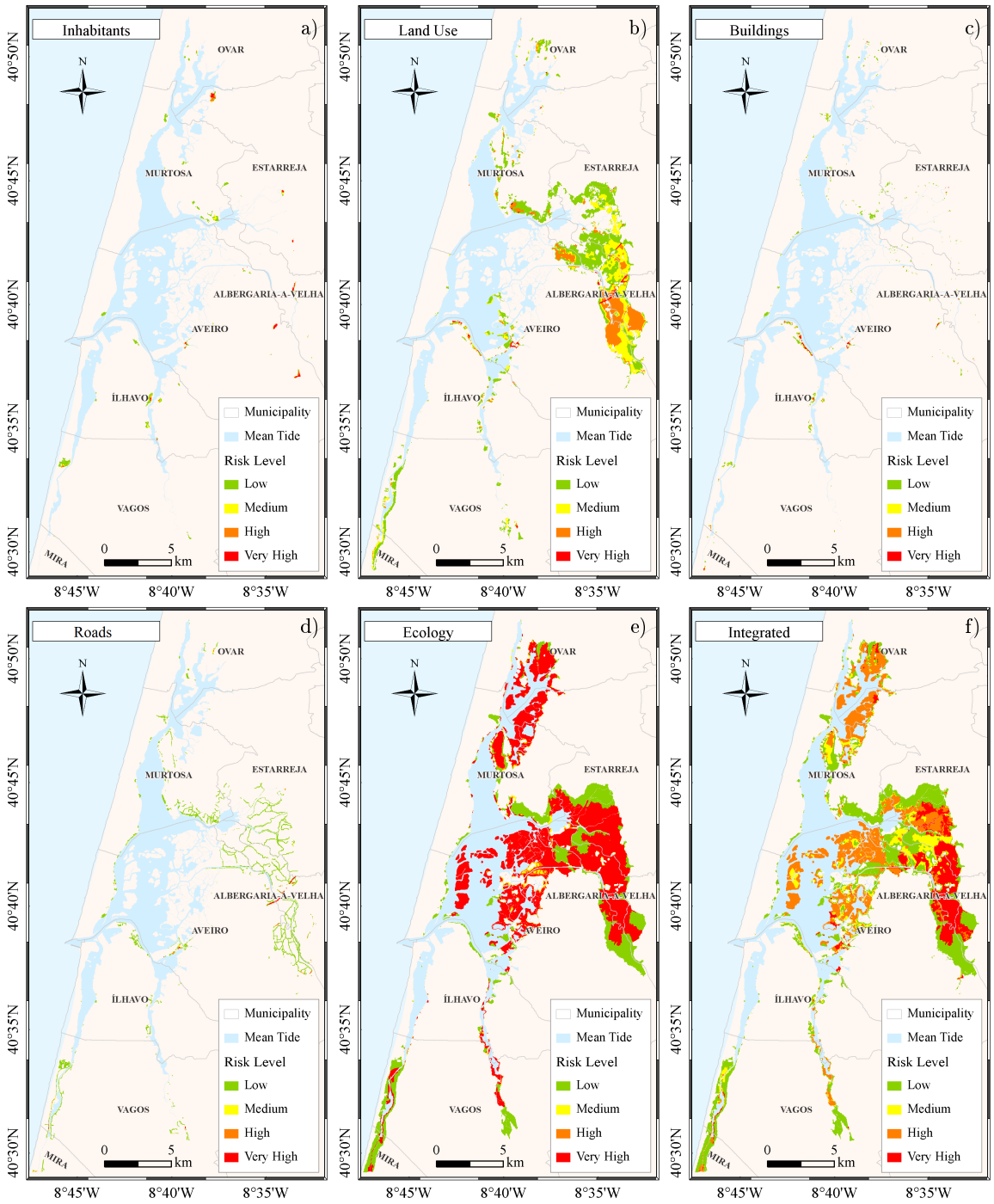


Figure 8.16: Flood risk maps for events of combined origin under present climate: a) inhabitants, b) land use, c) buildings d) roads, e) ecology, f) integrated.

8.17), were identified population clusters at risk in Ílhavo, Aveiro, Estarreja, Ovar and Murtosa municipalities (Figures 8.14a and 8.17a). These floods induce also negative consequences on economic activities that were evaluated through land use (Figures 8.14b and 8.17b). The industrial area located close the Aveiro harbour in the Ílhavo

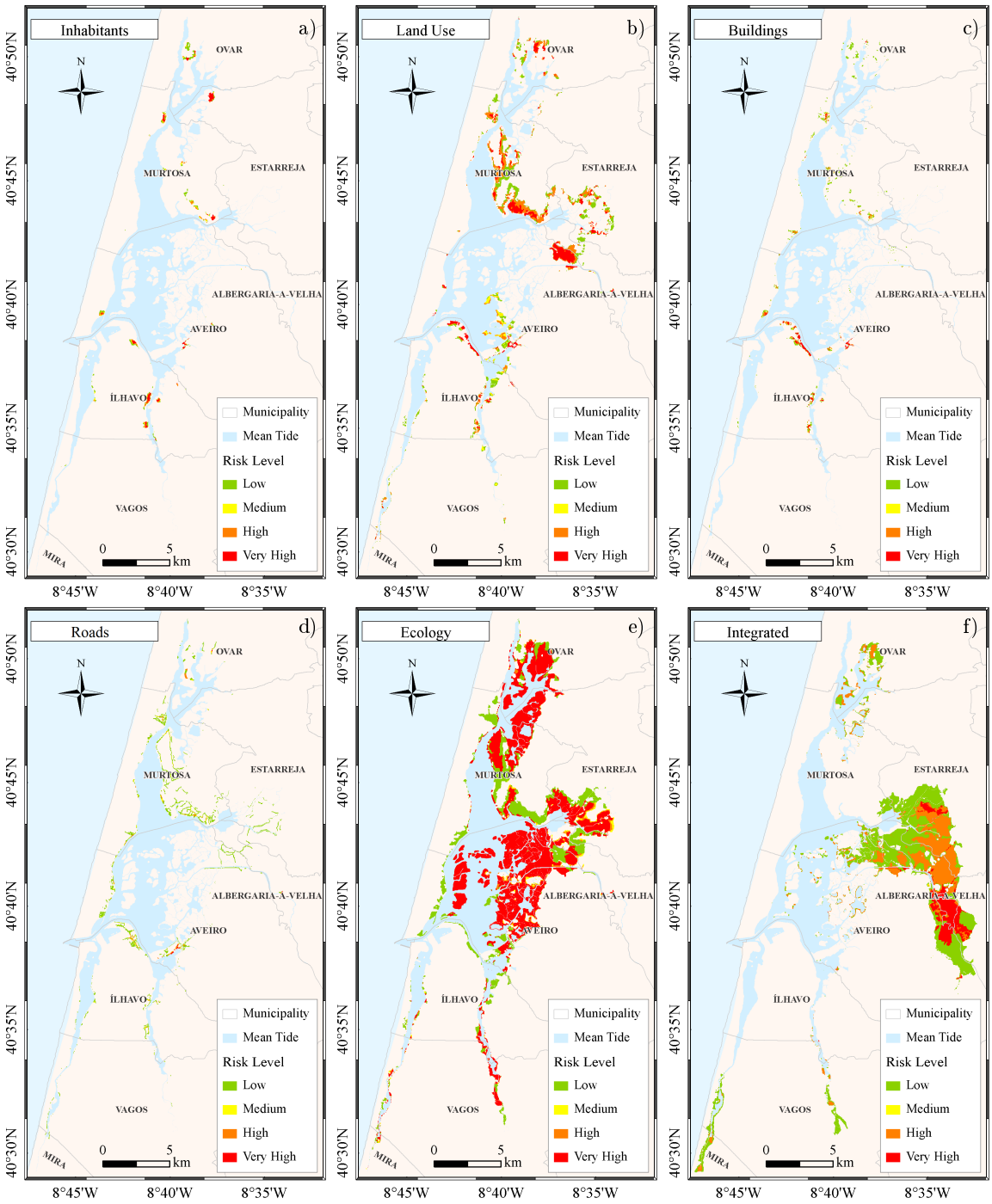


Figure 8.17: Flood risk maps for events of oceanic origin under future climate: a) inhabitants, b) land use, c) buildings d) roads, e) ecology, f) integrated.

municipality (see Figure 8.3b), presents very high risk of flooding. In the Aveiro municipality, a small area of the Aveiro town presents very high risk of flooding due to potential damage caused on commercial, accommodation and restaurants activities. Still in the Aveiro municipality, an agricultural area close the Vouga river mouth

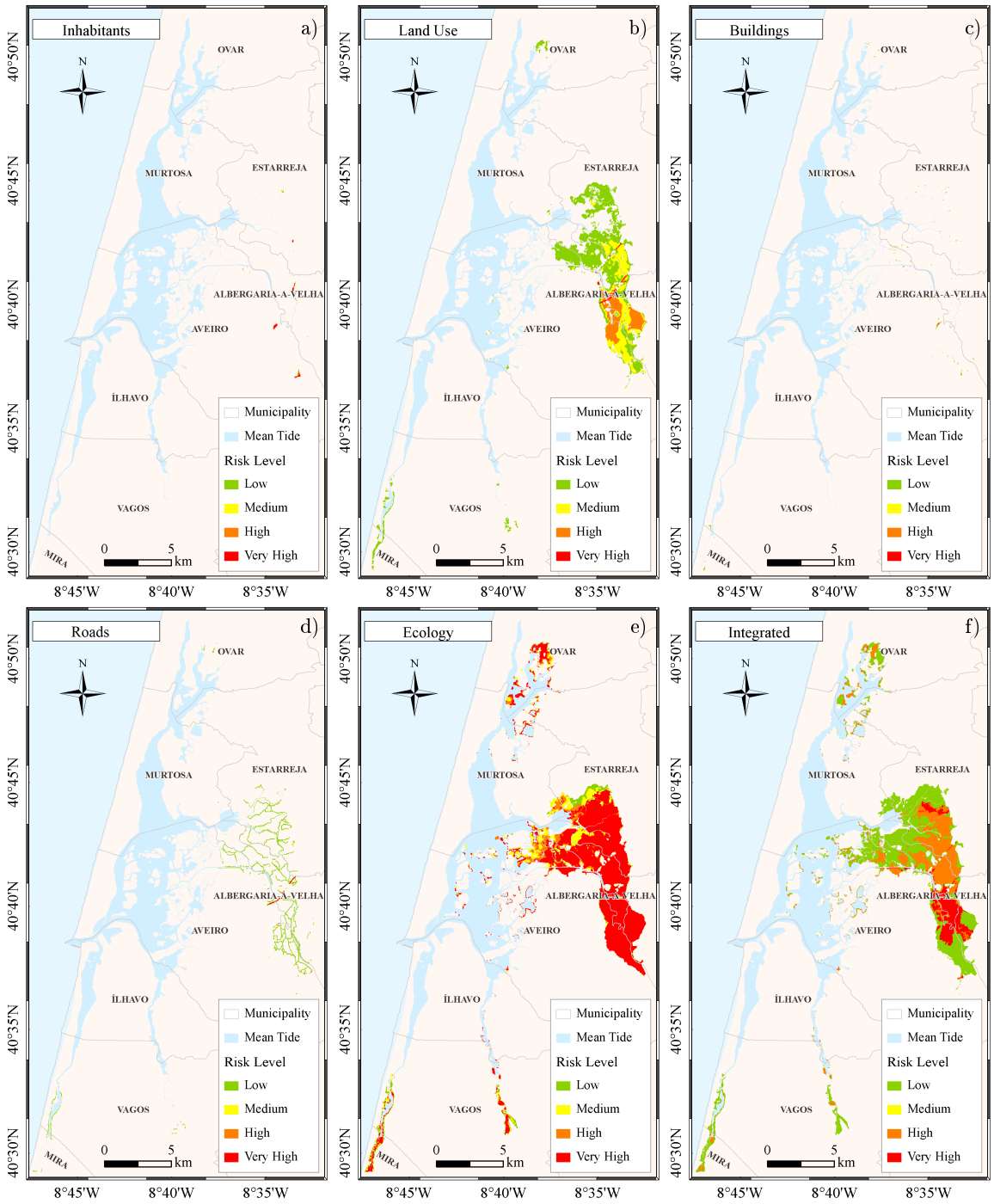


Figure 8.18: Flood risk maps for events of fluvial origin under future climate: a) inhabitants, b) land use, c) buildings d) roads, e) ecology, f) integrated.

presents very high risk of flooding of oceanic origin. The areas at risk located in Estarreja, Murtosa and Ovar municipalities are mainly agricultural fields exposed to saltwater intrusion. Regarding the flood risk for buildings (Figures 8.14c and 8.17c), the areas adjacent to the Aveiro harbour and located in Aveiro down town present the

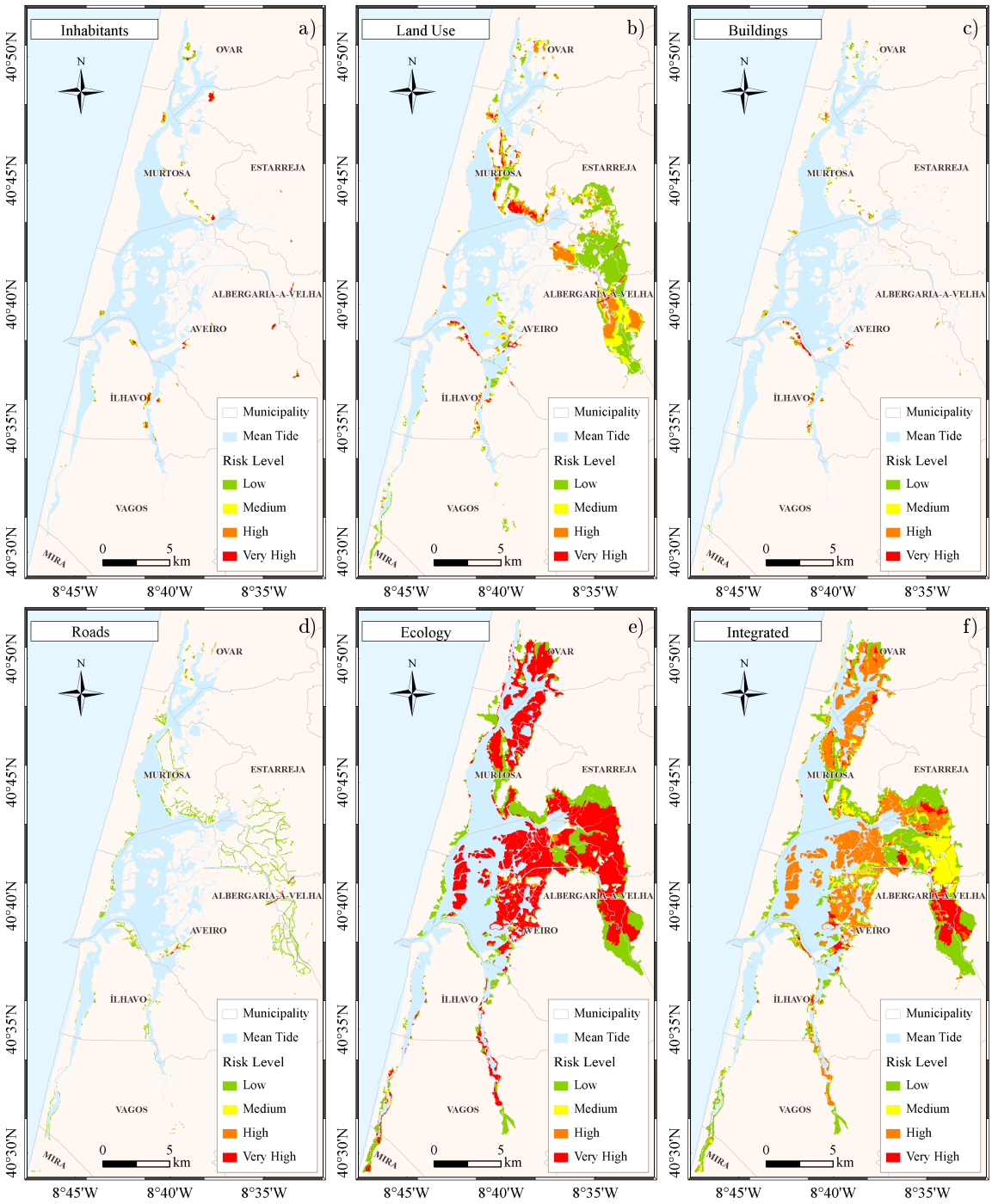


Figure 8.19: Flood risk maps for events of combined origin under future climate: a) inhabitants, b) land use, c) buildings d) roads, e) ecology, f) integrated.

highest risk. Close to the Aveiro harbour, these events induce damage on industrial buildings, while at the Aveiro down town they affect buildings used for commerce, accommodation, restaurants and services (see Figure 8.3c). It is also evident that residential buildings are in risk throughout the lagoon margins. In general the roads

present low to moderate risk (Figures 8.14d and 8.17d). The low flood depths generated by these floods explain, in part, the low risk values obtained. Moreover, most of the affected roads are within the other paved and unpaved classes, contributing also to the low values obtained. Additionally, it was found that the highway section located close the Aveiro town can potentially be affected by events of oceanic origin, presenting consequently very high risk of flooding. The results also evidence that these events can affect negatively the Ria de Aveiro ecology by inducing damage on the existent habitats (Figures 8.14e and 8.17e). Indeed, these events endanger the lagoon central area and the heads of S. Jacinto channel, where are located large areas of saltmarshes and saltpans (see Figure 8.3f). Analysing the integrated flood risk for both climates (Figures 8.14f and 8.17f), it was found that the lagoon central, the heads of S. Jacinto channel and the margins of Ílhavo channel present the highest risk of flooding for events of oceanic origin. Some restricted areas located in the harbour adjacent region, in the margins of Ílhavo channel, around the Aveiro town, adjacent to the BVL watercourses and at the upper reaches of S. Jacinto channel present very high risk of flooding for present climate. The maps show that these areas will be larger under climate change conditions. Moreover, it is evident the emergence of new areas presenting very high risk of flooding along the margins of S. Jacinto channel and at the Murtosa municipality.

For floods of fluvial origin were identified restricted settlements (inhabitants and residential buildings) at very high risk of flooding in the Aveiro, Albergaria-a-Velha and Estarreja municipalities (Figures 8.15a, 8.15c, 8.18a and 8.18c). Regarding the damage on land use (Figures 8.15b and 8.18b), it was found that most of the areas at risk are used for agriculture (see Figure 8.3b). The areas presenting high and very high risk of flooding are mainly located in the margins of Vouga river, where flood hazard is very high (see Figure 8.13). As for events of oceanic origin, most of the roads affected by events of fluvial origin present low risk (Figures 8.15d and 8.18d). In this case, despite the high and very high hazard of events, most of the affected itineraries are in the unpaved roads class (see Figure 8.3d), explaining therefore the low risk. Also, most of the inundated areas present very high risk for the ecology (Figures 8.15e and 8.18e), affecting mainly farmland areas (see Figure 8.3f). Regarding the integrated risk (Figures 8.15f and 8.18f), most of the areas adjacent to Vouga and Antuã rivers present

high and very high risk of flooding. Moreover, in lesser extent, the areas adjacent to the remain tributaries present high to very high risk of flooding. The extension of high risk areas tends to decrease under climate change conditions, considering the predictions for fluvial discharges decrease.

The flood risk maps for events of combined origin (Figures 8.16 and 8.19), highlight the tendencies of single events described before. Indeed, most of the area adjacent to the Vouga and Antuã rivers presents very high risk of flooding due to the severity of fluvial flood events that cause damage on socio-economic and ecological assets. Moreover, the lagoon central area and the areas adjacent the S. Jacinto channel head present high risk of flooding due to the predicted damage on habitats. When sea levels are high, some settlements located in the margins of S. Jacinto and Ílhavo channels are flooded, however as these settlements are restricted, its presence may not always be evident in the maps. Comparing the maps for present and future climates it is evident that the areas at risk tend to increase throughout the regions dominated by oceanic forcing. Otherwise, the areas at risk tend to decrease in regions dominated by fluvial forcing.

The difference between integrated flood risk for present and future climates was also computed for floods of oceanic, fluvial and combined origin. The positive and negative differences were grouped in order to identify the regions where flood risk decrease or increase (Figure 8.20). The results evidence that flood risk induced by events of oceanic origin tends to increase in the entire region as result of MSLR. Oppositely, a reduction of flood risk is expected for events of fluvial origin, as consequence of low river discharges predicted for the future climate. Following these tendencies, the flood risk for events of combined origin tends to increase over the lagoon central area and margins of the main channels and to decrease over the regions adjacent the rivers mouth.

## 8.4 Conclusions

In this chapter, it was successfully assessed the flood hazard and flood risk in the Ria de Aveiro region. Flood events of oceanic, fluvial and combined origin were characterized under present and future climate conditions.

Regarding flood hazard the main findings achieved were:

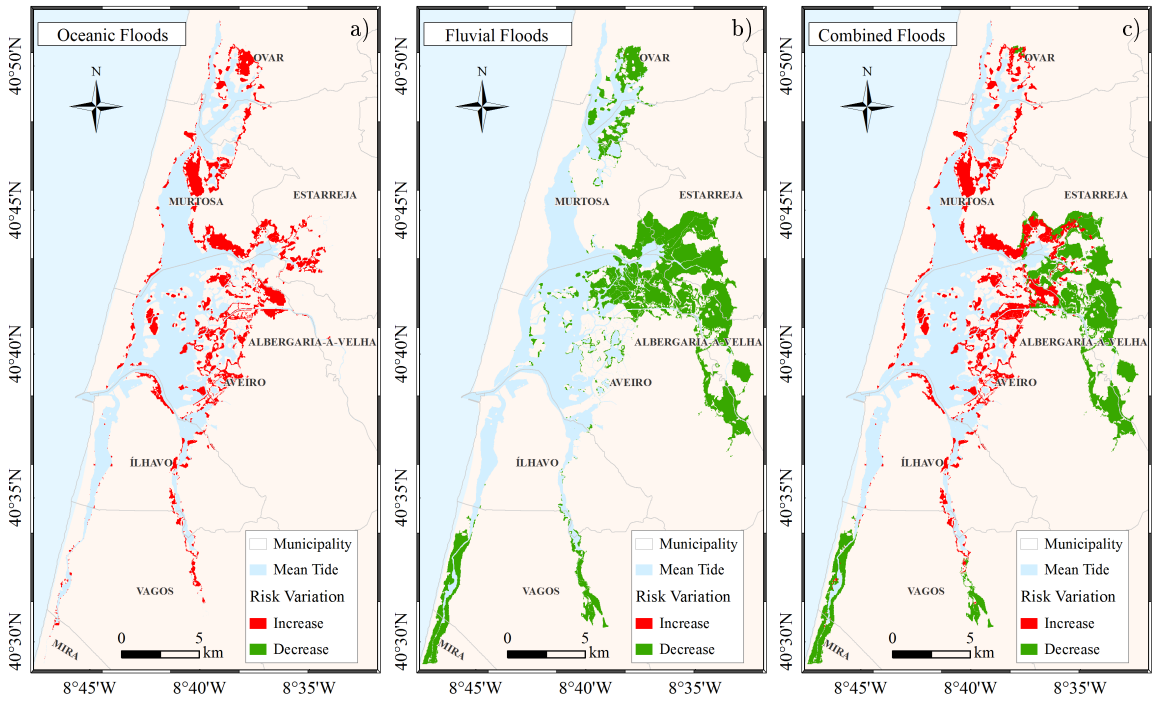


Figure 8.20: Variation of flood risk between future and present climate.

- Floods of oceanic origin primarily affect the margins of the main channels and central area while events of fluvial origin affect the heads of lagoon main channels. Besides these areas, the events of combined origin also affect the areas adjacent to the transition zones;

- The flood depths for events of fluvial origin are considerably higher than those generated by events of oceanic origin. For this reason, the areas adjacent to the mouth of Vouga and Antuã rivers are the most hazardous;

- The flood probability maps evidence that the main channels marginal regions/heads of lagoon main channels tend to be flooded more/less frequently under future climate, relative to the present.

- It is predicted a reduction/increase of flood hazard in regions dominated by fluvial/oceanic forcing for the end of the 21$^{st}$ century, given the decrease/increase of river discharges/sea levels foreacasted.

This study demonstrated that flood events affect socio-economic activities and the ecology of Ria de Aveiro region. It was found that:

- The settlements (inhabitants and residential areas) are more exposed to events of oceanic origin than that of fluvial origin;
- The agriculture is the activity most affected by flood events. Indeed, agricultural areas are flooded during events of oceanic, fluvial and combined origin;
- Although in lesser extent, floods affect also commercial, accommodation and restaurants, industry and transport and storage activities. These activities are more threatened by events of oceanic and combined origin than by events of fluvial origin.
- As most of the Ria de Aveiro region is classified as SPA and SCI, most of the flooded area is classified as SPA and SCI;
- Saltmarshes and mudflats are the habitats most affected by events of oceanic origin, while events of fluvial origin affect in higher extent farmlands and saltmarshes;
- The exposure of social, economic and ecological indicators to events of combined origin is significantly higher than that for events of oceanic and fluvial origin.

The flood risk maps were obtained by combining probability and the adverse impacts of floods on the exposed assets. The main findings achieved were:

- The areas adjacent to the Vouga and Antuã rivers are nowadays the most endangered by flood events. In these regions, flood events induced by high river discharges are frequent and cause damage mainly on agriculture, unpaved roads and farmland habitats;
- Regarding events of oceanic origin, the highest risk areas are located in the BVL region and in the margins of S. Jacinto and Ílhavo channels. In the BVL region floods affect essentially agriculture and farmland habitats, while in the channels margins affect human settlements and economic activities (agriculture, industry, commerce, accommodation and restaurants and transport and storage activities);

- The lagoon central area is also affected by events of oceanic and combined origin. This area presents high risk of flooding given the potential negative impacts of floods on habitats;

- Under climate change conditions, the flood risk tends to decrease in the regions adjacent the rivers and to increase in the lagoon central area and main channels margins. This tendency reflects the decrease/increase of river discharges/sea levels predicted for the end of the 21$^{st}$ century.

In summary, this work identified and delimited the areas most exposed and endangered by flood events in the entire Ria de Aveiro region, generating the results and conditions for future investigations at finer scales. Although out of the scope of this research, it is considered extremely valuable that these results may be used in the future to analyse in detail flood risk patterns for critical areas. Such analysis is extremely worthwhile to support municipal plans of spatial planning as well as rescue plans.

# Chapter 9

# Structural measures for flood risk reduction

## 9.1 Introduction

The flood risk assessment required in the Floods Directive aims to contribute for the reduction of the adverse consequences of floods. In this way the directive establishes that flood risk management plans should integrate prevention, protection and preparedness. Flood prevention can be established by avoiding construction in flood-prone areas, by adapting future developments to the risk of flooding, and by promoting appropriate land use practices. Flood protection implies the implementation of measures to reduce the likelihood and/or the impact of floods. Flood preparedness should focus on the development of flood forecasts and early warning systems to inform the communities as well as the management and intervention agencies.

Flood protection structures are designed to protect coastal and river areas, including urban, agricultural and other economically valuable areas. Dikes, dams, levees, floodways, retention basins, embankments and seawalls are common examples of defence structures against floods.

The heightening of river or coastal margins by building dikes, leeves, embankments, etc., is the most widely used tool for flood protection. The Netherlands flood protection system is one of the most known, and includes approximately 3500 km of primary flood defences [Kind, 2014]. Such structures are designed to protect a given area to a certain

flood level and therefore do not provide absolute safety against floods. Additionally, these structures can suffer ruptures during flood events reducing or even losing their protective function. A well known example of this, is the levee and floodwall failures occurred in August 2005 during the passage of hurricane Katrina, causing inundation in 80% of New Orleans [Pardue et al., 2005]. Moreover, the vulnerability of areas protected by flood defences often increases, once they present a false sense of security encouraging socio-economic development. Attending this, the implementation of such structures should always be complemented with non structural measures (regulations, emergency plans, etc.) [Merz et al., 2010].

In coastal systems, subject to both oceanic and fluvial forcing, barriers to control the exchanges with the sea have been installed. The Maeslant barrier on the Rhine River and the Thames Barrier are just two examples. Among floods in coastal lagoons, the case of the Venice lagoon is the most known worldwide, considering the inundation caused in the city of Venice. Venice Lagoon presents a very complex geometry, and connects with the Adriatic Sea through three inlets. The MoSE (Experimental Electromechanic Module) project, actually in final stage, has been designed in order to mitigate the effects of flooding in the city of Venice and the surrounding lagoon by controlling the flow between the Adriatic sea and the lagoon (`https://www.mosevenezia.eu/?lang=en`). With an investment of 5493 millions of Euro, 78 mobile gates have been installed in the inlet channels (`https://www.mosevenezia.eu/?lang=en`). Basically, during normal tidal conditions, the gates rest on the bottom, without affecting exchanges between the sea and the lagoon. When sea level exceeds a defined safeguarding level, the barriers emerge preventing the input of sea water (`https://www.mosevenezia.eu/?lang=en`). When the system is in complete functioning, barriers could protect a large area with high social-economic, ecological and historical value.

Attending these concerns, this chapter will explore the effectiveness of possible structural measures on Ria de Aveiro flood risk mitigation. To achieve this goal several structural measures were designed to protect some endangered areas, and the hydrodynamic model previously developed in this study was then used to simulate the flood pathway for the scenarios presented in Figure 8.1. Finally, flood risk was

assessed through the methodology described in previous Chapter. The effectiveness of designed measures was evaluated by computing the difference between flood risk with and without the flood protection measure.

## 9.2 Methodology

The first step consisted on the design of structural measures that were after implemented on the model numerical grid. The structural measures were designed taking in consideration the mechanisms that drive the Ria de Aveiro floods and the socio-economic and ecological patterns of the region, that were investigated in previous Chapter. In summary, the measures purposed should:

- control the seawater intrusion that affect settlements and economic activities on the lagoon main channels margins;
- improve the drainage of freshwater to the ocean, to minimize the damage on agricultural activities, settlements and roads.

It is right that a system like MoSE, able to control the water exchanges between the lagoon and the ocean will mitigate damage caused by high sea levels in the Ria de Aveiro region. However, given the investment necessary it is very unlikely the implementation of a similar system in the Ria de Aveiro inlet. Moreover, such a structure will cause traffic disruptions in Aveiro harbour and can not serve the APA interests. In this way, alternatively to changes in the inlet configuration, five structural changes in the inner lagoon are researched (Figure 9.1):

**Embankments** - located along some stretches of the lagoon margins;

**Dike A** - extension of BVL dike discarding hydraulic structures;

**Dike B** - extension of BVL dike considering hydraulic structures;

**Saltpans A** - enlarge the lagoon capacity by using saltpans as reservoirs during storms;

**Saltpans B** - reduce the lagoon capacity by restricting inundation in saltpans area.

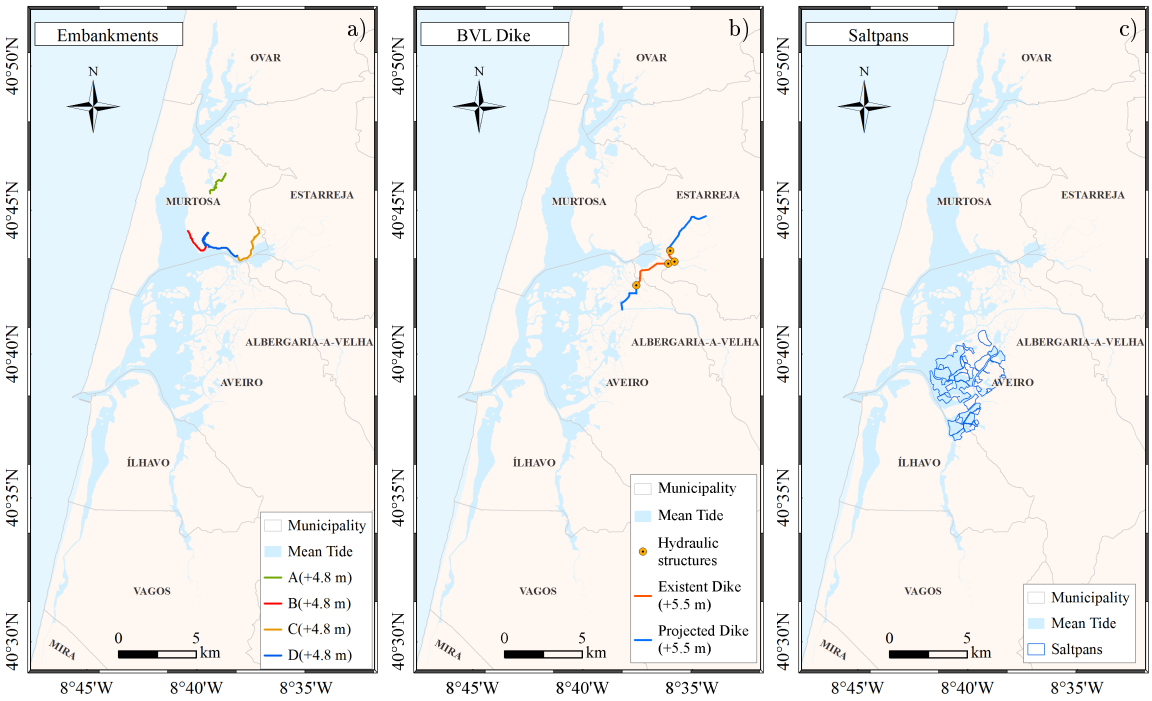


Figure 9.1: Location of the designed flood structures: a) Embankments; b) BVL dike; c) Saltpans.

The first case refers to flood embankments located along some stretches of the lagoon margins (Figure 9.1a). These structures were already built during the period of this research (between December 2012 and September 2014). The works were performed by Sociedade Polis Ria de Aveiro and Murtosa municipality and aim to reduce the adverse impacts of flooding events in the embankment adjacent areas. Despite its implementation, no investigations were made in order to understand the influence of these structures on the flood risk of the Ria de Aveiro region.

Two scenarios were developed regarding the extension of BVL dike (Figure 9.1b). As previously referred, the BVL dike was built in the eighties in order to prevent the salinization of agricultural fields. However, it is known that the existent structure do not protect the entire region and therefore a significant part is still threatened by saltwater intrusion. The dike extension was implemented in the numerical grid according to the original design work plan [IHERA, 1996/97]. Besides the dike extension, the works include the implementation of hydraulic structures to control the exchanges of water between the lagoon and the BVL area. According this two scenarios were tested:

**Dike A** - the dike is continuous, discarding the implementation of hydraulic structures. In this way, there is no water exchanges between the lagoon and the BVL area.

**Dike B** - the dike is disrupted by hydraulic structures that control the exchanges between the lagoon and BVL region. These structures are opened during high discharges to improve the drainage of freshwater, and closed during low discharges to prevent saltwater intrusion.

The inexistence of hydraulic structures is out of the scope of the extension dike original design work plan. However, this case intends to simulate the consequences of malfunctioning of these structures. Indeed, the present dike has an hydraulic structure permanently closed since several years for lack of maintenance.

The last case aims to reduce the lagoon marginal flooding by changing the abandoned saltpans geometry:

**Saltpans A** - excavate the saltpans inner region to 2 m (ZH) and repair/construct saltpans walls allowing the input of water when the water level exceeds 3.5 m (ZH). With an area of $15\times10^6$ $m^2$, these tanks can store $82.5\times10^6$ $m^3$ of water;

**Saltpans B** - repair/construct saltpans walls at a sufficient height to restrict saltpans inundation in the whole range of sea levels and river discharge conditions predicted.

For each structural modification the ELCIRC model was used to simulate the flood pathway for all the scenarios presented in Figure 8.1, for present and future climates. The model results were then used to assess flood risk attending the procedure described in previous Chapter. The effectiveness of each structure was evaluated elaborating flood risk variation maps.

## 9.3 Results and discussion

### 9.3.1 Implementation of flood barriers

#### 9.3.1.1 Embankments

Figure 9.2 presents flood risk variation maps induced by the heightening of some stretches of the lagoon margins (Figure 9.1a). The regions marked by green/red indicate that flood risk decreased/increased with the structural change. It is clear that the embankments contribute to a flood risk reduction in the marginal areas adjacent to the structure. These structures are particularly efficient in the Murtosa municipality mitigating the adverse effects of flood events of oceanic, fluvial and combined origin. Although the benefits in the areas adjacent to the embankments, these structures also induce an increase of flood risk in several marginal areas, particularly when sea levels are high (events of oceanic and combined origin). The regions most affected are the lagoon central area and the marginal areas of S. Jacinto and Espinheiro channels. Moreover, this behaviour tends to be exacerbated under climate change conditions due to the MSLR, worsening flood damage in the unprotected regions. It is therefore a short-term solution that mitigates flood damage in the structure adjacent areas, but increases the risk in the unprotected regions, enhancing the need for other marginal protection structures in future.

#### 9.3.1.2 Extension of BVL dike

Figure 9.3 presents flood risk variation maps induced by the extension of BVL dike discarding the existence of hydraulic structures. The extension of BVL dike mitigates the risk of events of oceanic origin (Figure 9.3a and 9.3d). Its implementation is particularly important under MSLR conditions, protecting an extensive area from saltwater intrusion. Concerning events of fluvial origin (Figure 9.3b and 9.3e), its implementation will increase the flood damage, once the dike hinders the Vouga and Antuã drainage into the lagoon. This effect tends to decrease under climate change conditions once the predicted reduction on river discharges. Moreover, the northern part of the dike (inserted in Estarreja municipality) is overtopped when Antuã

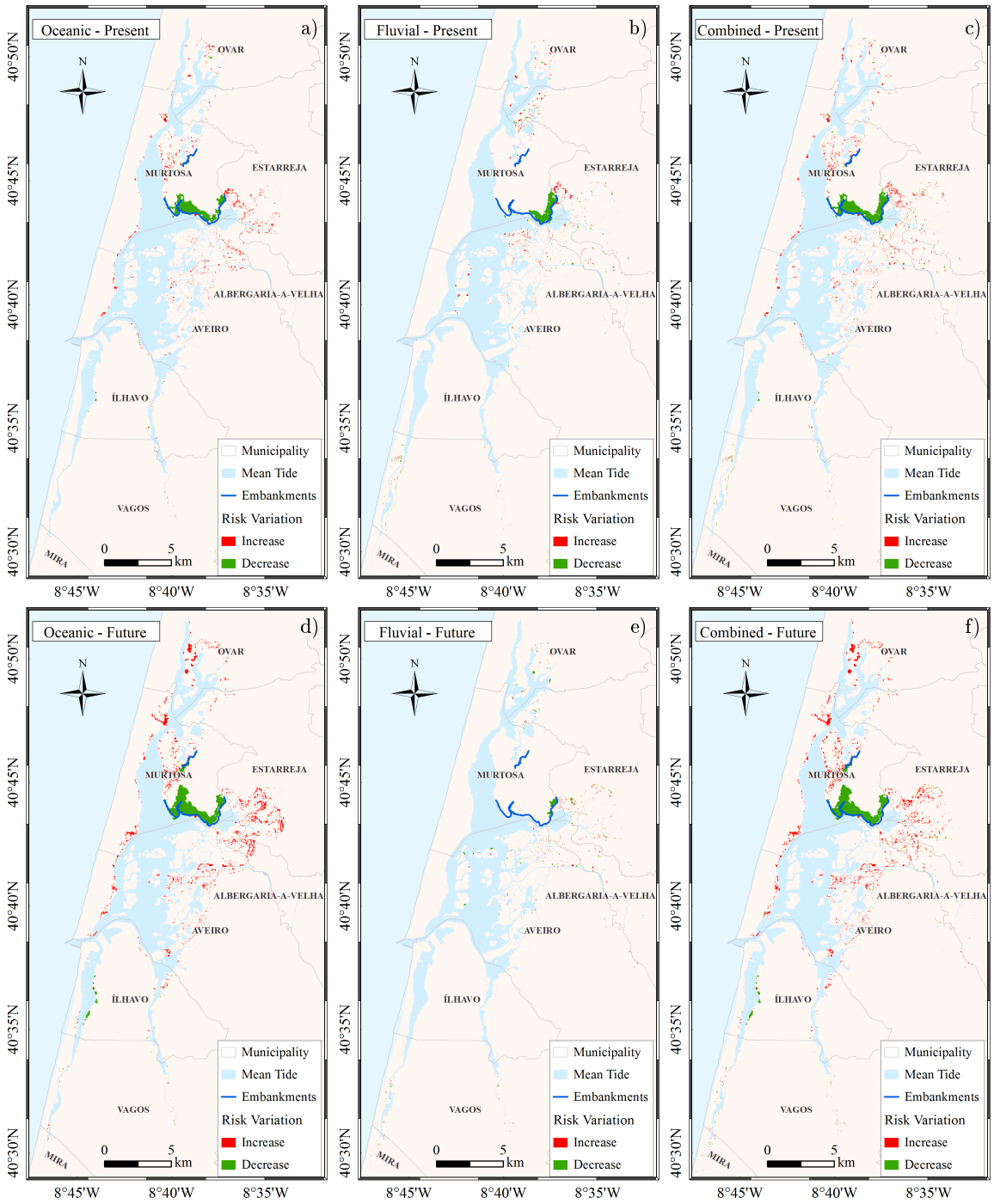


Figure 9.2: Flood risk variation maps induced by the construction of embankments.

discharges are high, increasing the risk of flooding in the adjacent regions. Regarding events of combined origin, the variation in risk is dependent on the period under analysis. Indeed, for present climate the extension of BVL dike discarding hydraulic structures contributes to increase the flood risk. Contrarily, the dike tends to be more efficient under climate change conditions, considering the predicted reduction of river

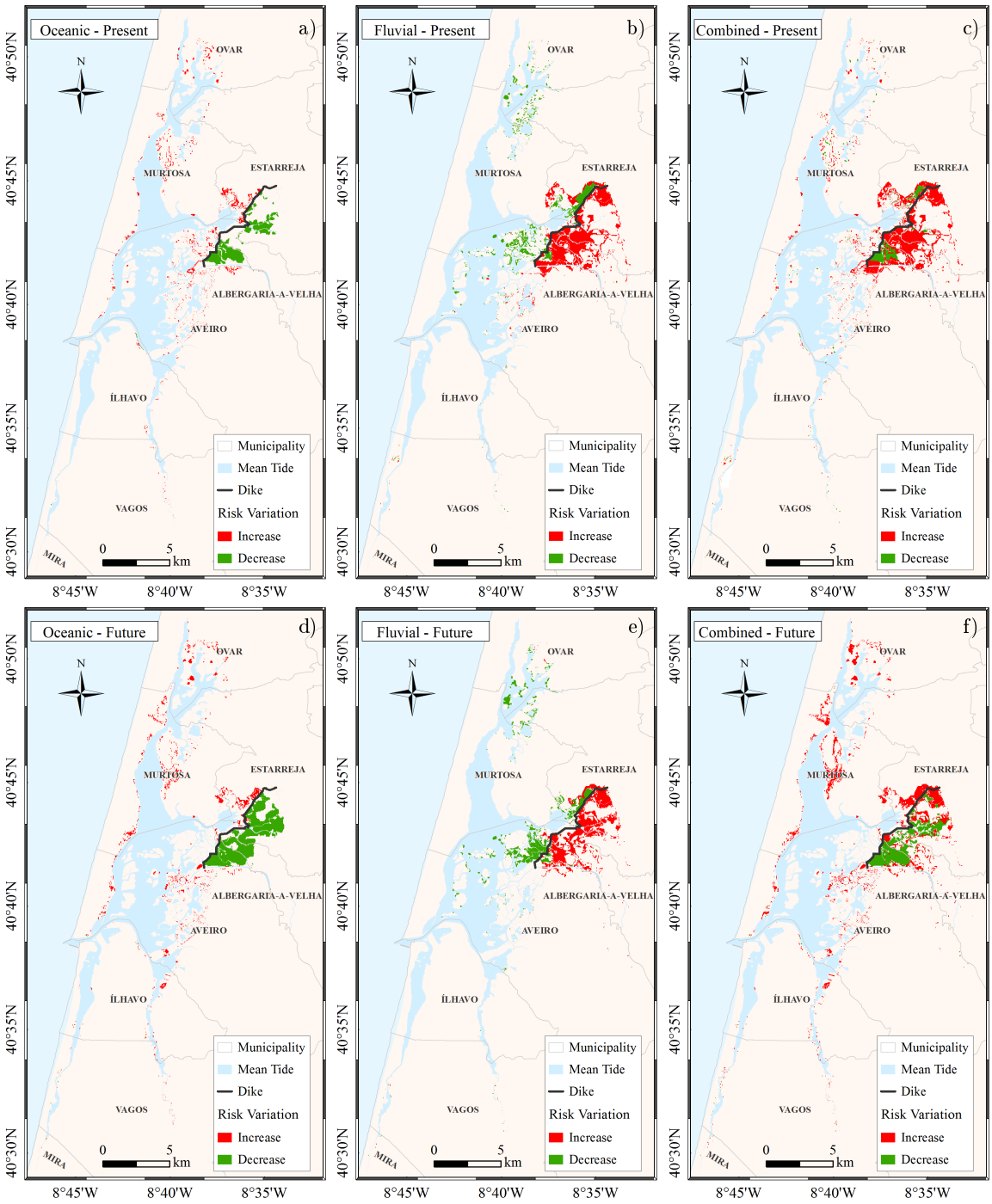


Figure 9.3: Flood risk variation maps induced by the extension of BVL dike discarding hydraulic structures.

discharges and MSLR. Despite its efficiency in protecting the BVL region, this structure aggravates flood risk in the S. Jacinto channel margins and in the lagoon central areas.

Figure 9.4 presents the flood risk variation maps for the extension of BVL dike considering the implementation of 4 hydraulic structures. The maps for events of

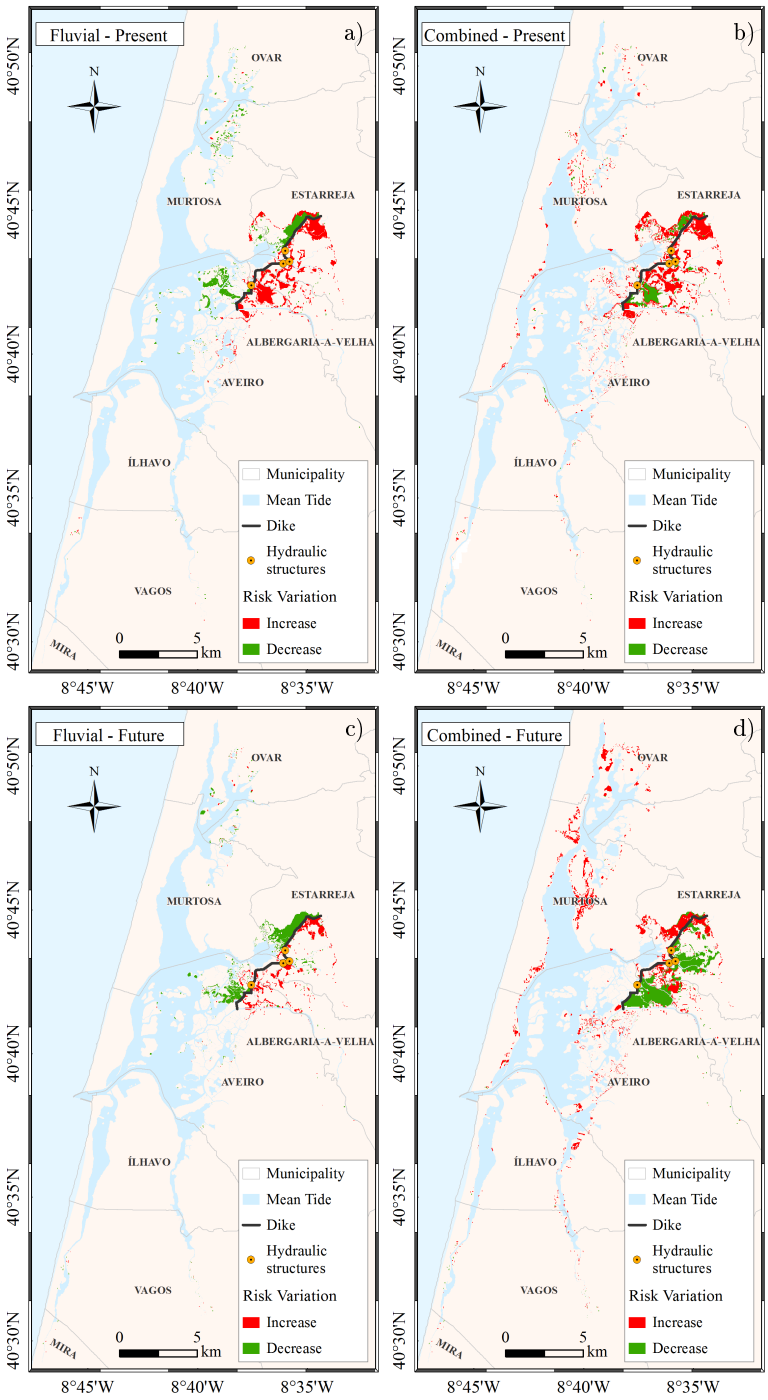


Figure 9.4: Flood risk variation maps induced by the implementation of BVL dike considering hydraulic structures.

oceanic origin are similar to the previous case (and by this reason are not presented in Figure 9.4), once the hydraulic structures are closed during high sea levels, avoiding saltwater intrusion in the BVL region. As without hydraulic structures, the risk for events of fluvial origin increases in BVL region, once the dike hinders the freshwater

drainage. Once again it is evident that the extension of the BVL dike tends to be more efficient in mitigating flood risk in BVL region under future climate. Despite the benefits for the BVL region, this structure tends to aggravate flood risk in the margins of S. Jacinto channel and lagoon central regions, as referred before.

The flood risk for scenarios Dike A and Dike B was compared in order to understand the effect of hydraulic structures. The flood risk variation maps (Figure 9.5) show that flood risk decreases when hydraulic structures are considered, indicating that these structures are essential to minimize flooding induced by freshwater drainage into the lagoon.

The influence of flood barriers (embankments or dikes) on local drainage was already studied. The FEMA [2007] and Merz et al. [2010] recognized that flood embankments may affect local drainage and may not bring substantial improvements. Also, the effectiveness of flood defences can increase considerably if they were accomplished by regulations that control the vulnerability of protected areas. Indeed, regulatory measures controlling the land use are essential, once flood barriers give a false sense of security encouraging, the development in protected areas.

### 9.3.2 Changes in the geometry of abandoned saltpans

Initially was investigated the possibility to use saltpans as reservoirs storing water during high water levels. Figure 9.6 presents the flood risk variation maps induced by the implementation of retention basins in saltpans. For events of oceanic origin (Figure 9.6a and 9.6d) the maps reveal that flood risk tends to increase in the saltpans surroundings, once the water depth increases. For the present climate, the risk for events of oceanic origin in main channels marginal areas tends to decrease with the implementation of reservoirs. However, such improvement are sparse and restricted to small areas. Contrarily, for future climate, the reservoirs induce a slight increase of risk for these events along the channels margins. This fact reveals that the designed saltpans capacity is insufficient to store the excess of water. Indeed, for present climate, events with return periods of 2 and 100 years induce an increase in the tidal prism of $38.2\times10^6$ m$^3$ and $99.5\times10^6$ m$^3$, relative to the MHWS conditions (see Table 7.3). These volumes are higher for the future climate, $64.2\times10^6$ m$^3$ and $132.6\times10^6$ m$^3$ for 2 and

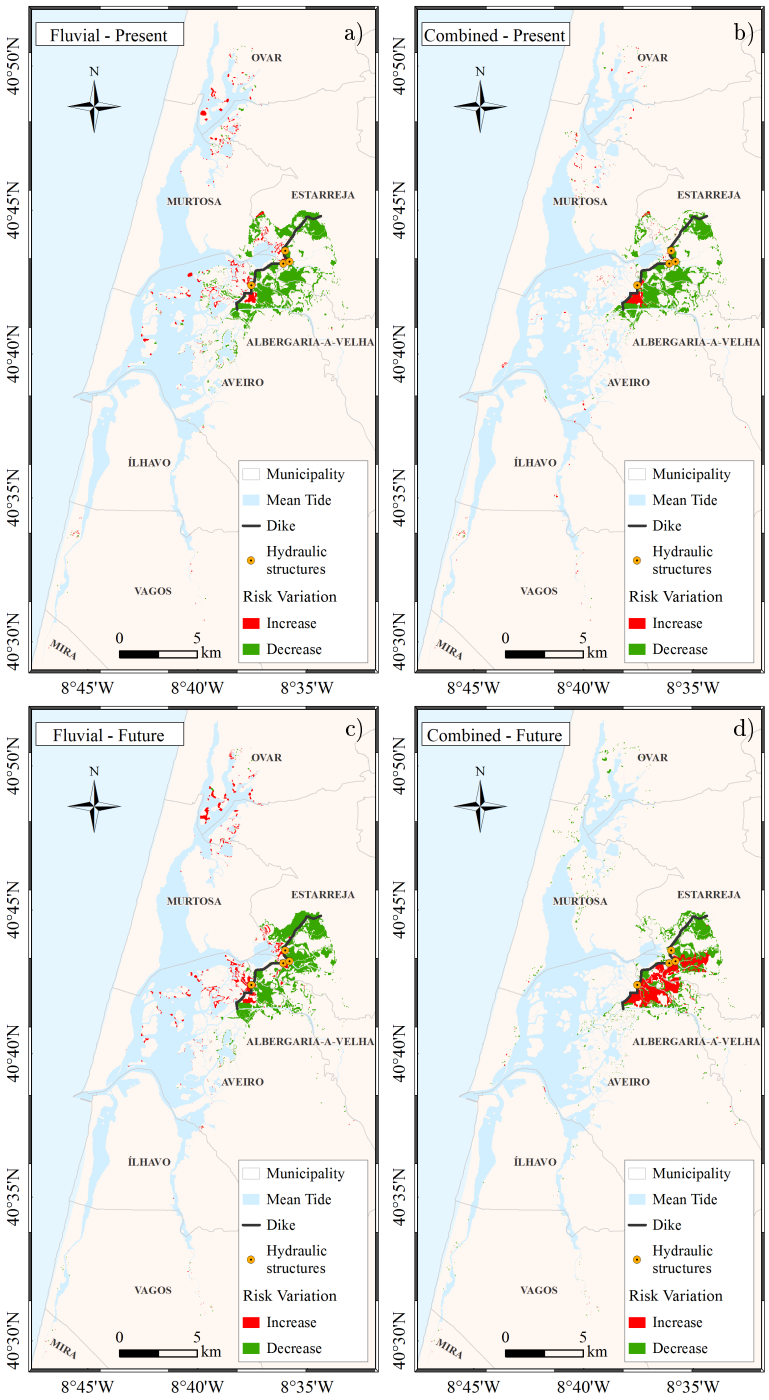


Figure 9.5: Flood risk variation maps induced by the implementation of hydraulic structures in the BVL dike.

100 years return periods, respectively, explaining the ineffectiveness of reservoirs under MSLR conditions. Indeed, the capacity of these reservoirs ($82.5\times10^6$ $m^3$) is insufficient to store the exceeding water.

Regarding events of fluvial origin (Figure 9.6b and 9.6e), the maps evidence that

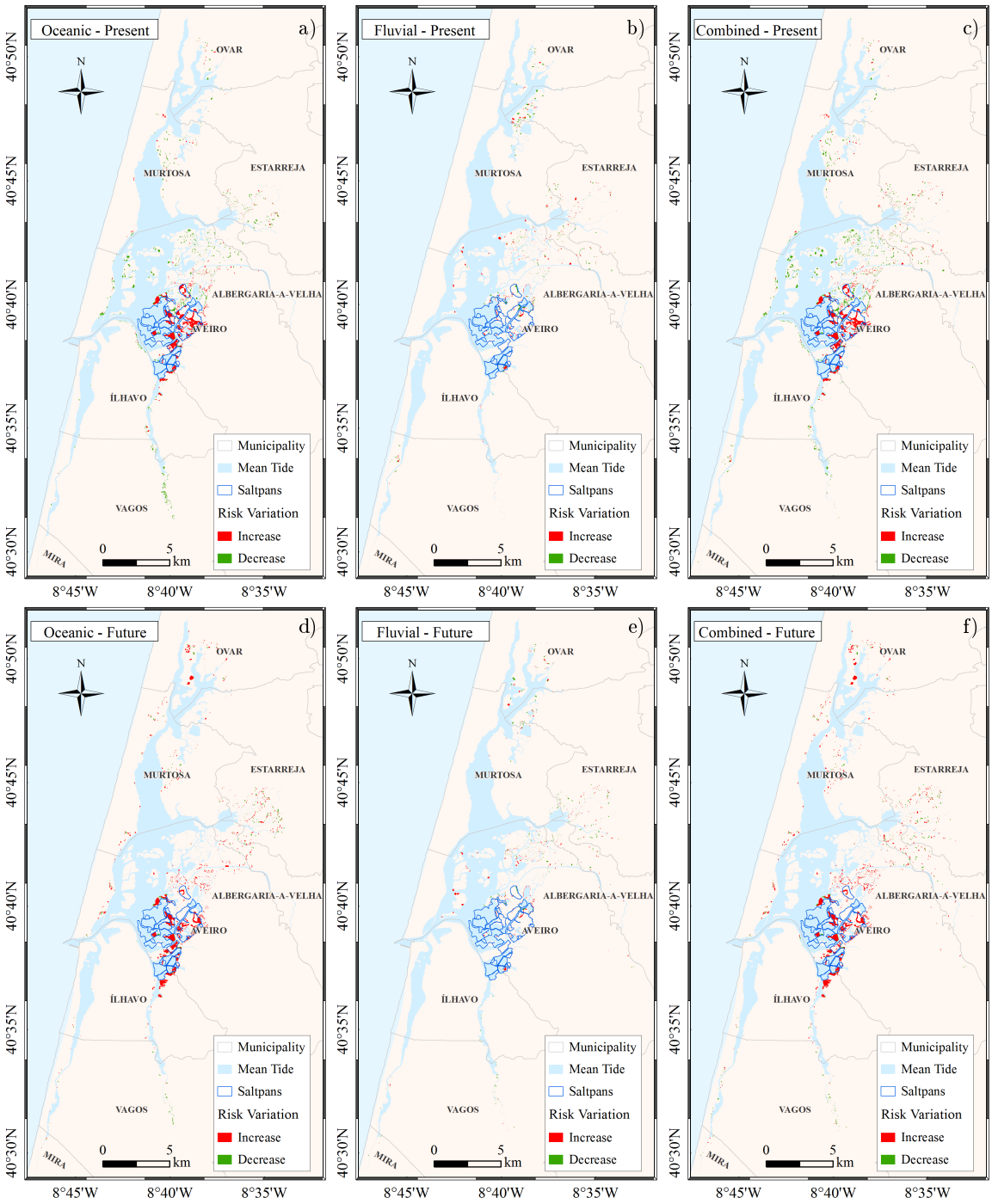


Figure 9.6: Flood risk variation maps induced by the implementation of saltpans as reservoirs.

the implementation of reservoirs do not influence the Ria de Aveiro flood risk. As the reservoirs are located out of the rivers influence, the risk is maintained. Attending this, the events of combined origin (Figure 9.6c and 9.6f) reflect the tendency of events of oceanic origin. The use of reservoirs to store the flood water are among the most

frequently implemented storm water management systems in fluvial floods. This have been successfully applied along the Rhine and Meuse rivers in Netherlands [Silva et al., 2004]. The storage of water results in flood peak attenuation and consequently lowers the water levels downstream of the detention areas [Silva et al., 2004]. Attending this, future works should investigate the use of reservoirs to mitigate flood risk in regions dominated by fluvial forcing.

The use of reservoirs to store water during high sea levels is not so common. The influence of polders on flood hazard reduction has gaining interest, after episodes of dike breaching during storms. It was verified that the inundation of polder areas reduces inundation in other regions, highlighting that they can serve as reservoirs mitigating flood risk around. Consulting the Online Managed Realignment Guide (OMReG) (`http://www.omreg.net/`), the restoration of wetlands through managed realignment (breaching, or removing seawalls to allow tidal waters from adjacent coasts or estuaries onto the land) or regulated tidal exchange (to develop intertidal habitats behind permanent sea defences) were successfully implemented for example in Exe, Meuse, Elbe, Rhine and Scheldt estuaries. In these cases, besides flood protection, these man-made wetlands brought considerable ecological benefits [Pethick, 2002]. Attending this, it is considered that further investigations should be made regarding the creation of reservoirs in Ria de Aveiro as these systems may mitigate flood risk of events of oceanic origin.

Besides the inundation of saltpans, the effect of restricting saltpans inundation on Ria de Aveiro flood risk was also investigated. Figure 9.7 presents the flood risk variation maps induced by restricting saltpans inundation. It is evident a flood risk reduction in the saltpans areas, once the flooding restriction imposed in these areas. The maps also show that this restriction aggravates flood risk in the entire area, with exception of Ílhavo channel margins (Figures 9.7a and 9.7d). Regarding events of fluvial origin (Figures 9.7b and 9.7e), no significant differences were observed. The banks are located out of the rivers influence area and therefore do not influence the drainage of freshwater during high discharges. In this way, the variation risk maps for events of combined origin (Figures 9.7c and 9.7f) are similar to those for events of oceanic origin. Attending these results, to restrict the inundation in the saltpans areas can only be

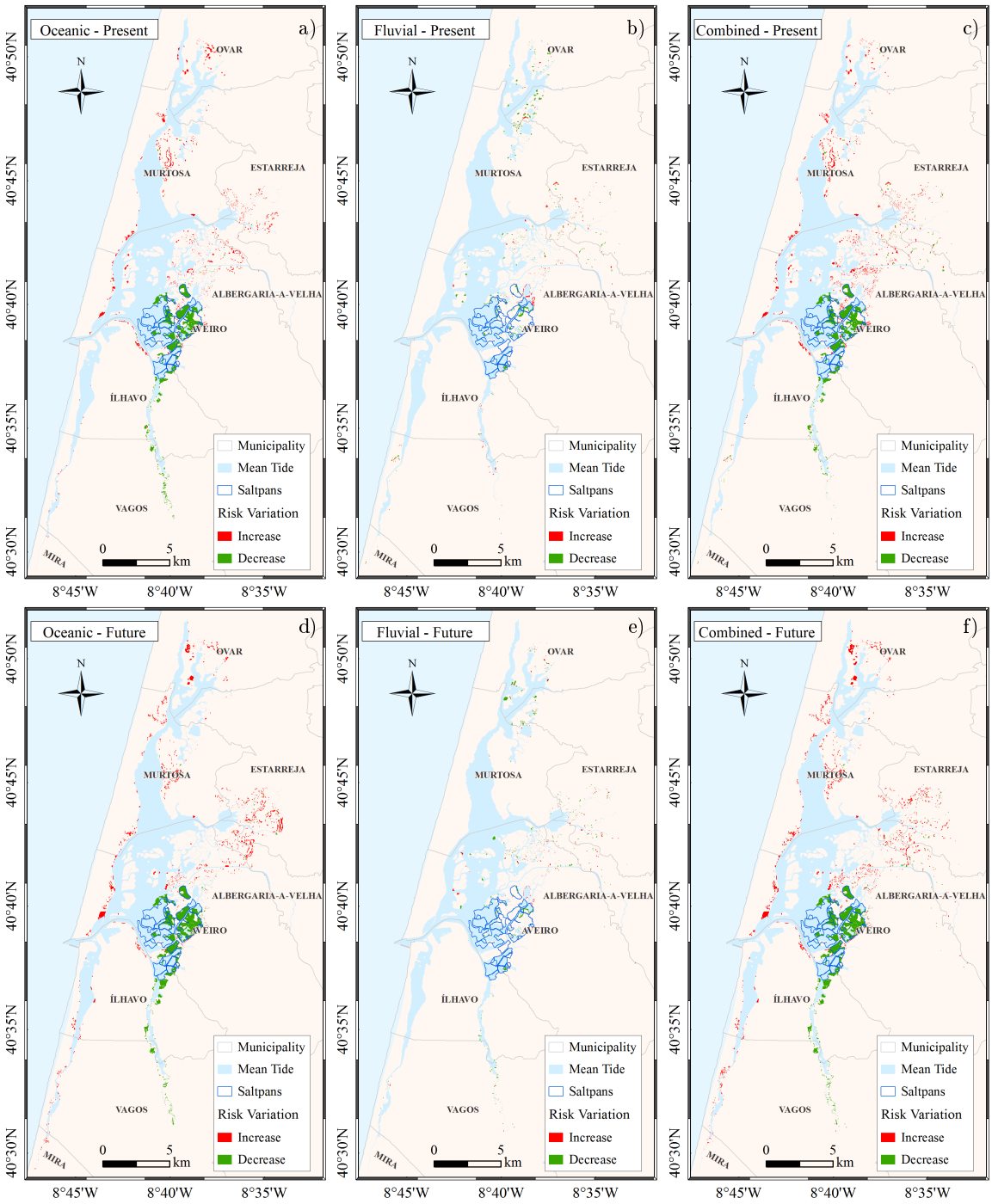


Figure 9.7: Flood risk variation maps induced by the implementation of saltpans as constraint areas.

effective in reducing flood risk along the margins of Ílhavo channel. However, given the negative consequences induced in the remaining regions, it is concluded that this measure is ineffective on mitigation Ria de Aveiro flood risk.

## 9.4 Conclusions

In this work the effectiveness of structural measures on mitigating the Ria de Aveiro flood risk was successfully investigated. Initially, the implementation of flood barriers along some stretches of the lagoon channels was studied. The results highlighted that this is a short term solution that mitigates flood risk in the embankments adjacent regions, aggravating the flood risk in the unprotected regions. Therefore this type of structure increases the need for more marginal protection structures in future. Also, its implementation should be accomplished by regulation measures that control the land use, in order to prevent the increase of their vulnerability.

Regarding the extension of BVL dike, this structure affects flood risk for both events of oceanic and fluvial origin. If, on one hand, it is efficient on mitigating risk of events of oceanic origin in the BVL region, on the other hand hampers the rivers drainage, increasing flood risk induced by fluvial events in the BVL region. Attending this, the extension of the dike should be accomplished by the installation of hydraulic structures, which correct functioning is determinant on mitigating river drainage problems in the BVL region. The river drainage problems are exacerbated in the dike northern part, where the hydraulic structures are insufficient to drain the Antuã discharge. Hydrodynamic results evidence dike overtopping during highest discharges, increasing flood risk downstream the dike. Attending this, short alterations to the present work plan should be studied in order to mitigate river drainage problems. In summary, the extension of the dike will mitigate the saltwater intrusion in the BVL region, which is fundamental to maintain the equilibrium between agriculture and nature discussed in Chapter 2. Moreover, the floods induced by high river discharges are not so dangerous for agriculture as those induced by high sea levels, and may even increase the fertility of soils, once the deposition of organic matter during flooding. This fact should be taken into account when analysing the balance between positive and negative impacts of this structure.

The last intervention studied was the change of saltpans geometry. This change do not influence the effects of events of fluvial origin, once saltpans are located out of the river influence. To restrict the inundation of saltpans increases the marginal flood

risk, demonstrating that it is not a good solution to mitigate flood risk. Contrarily, the use of saltpans as reservoirs brought small improvements on flood risk for marginal areas. Therefore, it is considered that the use of saltpans as reservoirs should be further studied in detail. Moreover, managed realignment was already applied successfully in other estuarine systems, providing besides protection against floods, ecological benefits.

Finally, this research demonstrated that the flood protection structural works, although implemented in restricted areas, affect the flood risk for the entire Ria de Aveiro region, mitigating flood risk in some areas but increasing flood risk in others. Consequently, the cooperation between the different municipalities is fundamental for the effective management of the Ria de Aveiro area at the inter-municipal level, corroborating the Alves et al. [2011] and Dolbeth et al. [2016] works.

# Chapter 10

# Final conclusions and future work

The main objective of this dissertation was to assess flood risk for events of oceanic, fluvial and combined origin in Ria de Aveiro region under present and future scenarios. Additionally, this study intended to propose and evaluate the effectiveness of structural measures on flood risk mitigation. Under this scope was applied a multidisciplinary approach that integrates: 1) statistical analysis of driving forces data; 2) numerical modelling applications; and 3) coupling of flood data predictions with socio-economic and ecological information in geographic information systems to assess flood risk.

The characterization of the Ria de Aveiro driving forces revealed that the tide is the forcing that causes greater variations in sea level ($>$ 3 m). The mean height of storm surge events is 0.43 m, although the maximum height can exceed 1 m for the most adverse events. Moreover, the most intense storm surge events do not always induce extreme sea levels, once they depend also on the tidal level. Also, between 1976 and 2013, the mean sea level increased at the lagoon mouth at a rate of 2.2 mm/year. The wave regime offshore the Aveiro inlet is characterized predominantly by waves propagating from NW and NNW directions with significant heights between 0.5 m and 2.5 m. The Vouga river presents the highest peak discharge inflowing into the lagoon, ranging between 797 $m^3/s$ and 1943 $m^3/s$, for 2 and 100 years return periods, respectively.

It is expected that climate changes will change the lagoon driving forces specially considering that some of driving forces are affected by atmospheric factors. Under climate change scenarios it is predicted an increase of sea levels (as consequence

of MSLR), a clockwise rotation of wave regime and a decrease of river discharges, comparing to the present climate.

The hydrodynamic model ELCIRC was used to characterise the flood pathway in Ria de Aveiro in response to different driving forces. Calibration and validation results evidence that the model accurately reproduces both tidal and storm surge levels within the lagoon, highlighting its adequate application to characterize the flow dynamics in Ria de Aveiro.

The ELCIRC model was firstly applied to study the influence of geomorphological changes and MSLR on Ria de Aveiro tidal dynamics. The main finding of this application was that tidal dynamics is highly dependent on both lagoon geomorphology and mean sea level. Particularly, the deepening of the lagoon main channels between 1987 and 2012 induced a/an decrease/increase of tidal distortion in the deeper/shallower channels, a general increase of tidal currents and a decrease of residual currents in the lagoon central area. Moreover, it was found that long term studies aiming to forecast future lagoons physical and biogeochemical properties should consider not only the MSLR, but should also take into account the lagoon future geomorphology.

The sensitivity of the lagoon flooded area to morphological changes was investigated. It was found that the deepening of the inlet region, and specially of the lagoon main channels between 1987 and 2012 induced an increase of the lagoon flooded area of 3%, 7% and 16% for neap, mean and spring tide conditions, respectively. The regions located in the margins of S. Jacinto channel head and lagoon central area were the most affected. Regarding the future lagoon morphological configuration there is great uncertainty associated, once the natural morphological changes are under constant anthropogenic influence. Moreover it is predicted that the clockwise rotation found for future wave regime will not change the inlet morphodynamics. In this way, the deposition trend tends to be intensified as consequence of MSLR. However, as this tendency is contrary to the needs for maritime traffic associated to the Aveiro harbour, it is expected that dredging activities at the inlet channel will continue in the future in order to provide navigability conditions and therefore keeping the actual depths for the future climate.

The hydrodynamic model was also used to study the sensitivity of Ria de Aveiro marginal flooding under different scenarios of sea level and river discharges. The lagoon flooded area is extremely sensitive to sea level oscillations (both short and long term). Indeed, the lagoon flooded area is approximately 33% higher for spring tide than for neap tide. Also, it is expected that the lagoon flooded area will increase by 16% for 0.42 m MSLR scenario, relative to the present. The flooded area is also highly dependent on the river discharge. Results highlight that the lagoon flooded area can duplicate for discharges of 100 years return period, relative to the mean tide and mean discharge conditions. It is also predicted a flooded area reduction under climate change conditions, following the discharge reduction for the lagoon main tributaries.

Flood hazard and risk maps for events of oceanic, fluvial and combined origin under present and future climates were also designed. Maps evidence that the central area regions and the marginal areas of S. Jacinto and Ílhavo channels are the most endangered by events of oceanic origin. These events predominantly affect settlements and economic activities located in the channels margins. Regarding events of fluvial origin, the maps evidence that the flooding is restricted to the marginal areas of river channels, with particular emphasis for Antuã and Vouga rivers. These events predominantly affect economic activities (mainly agriculture), small settlements and roads. Floods of combined origin affect regions dominated by both oceanic and fluvial forcing, highly endangering the regions adjacent to the transition zones, once the drainage of freshwater discharges is hindered by high sea levels. Besides socio-economic activities, all events endanger habitats present in most of the region. Under future climate it is predicted an intensification/a reduction of flood risk for events of oceanic/fluvial origin.

Finally, the effectiveness of structural measures on mitigating the Ria de Aveiro flood risk was investigated by changing the lagoon geomorphology. Results revealed that the heightening of margins, already implemented, is a short term solution that mitigates flood risk in the embankments adjacent areas, aggravating the flood risk in the unprotected areas, demanding therefore the need for more marginal protection structures in future. The extension of BVL dike is effective on preventing the salt water intrusion in the BVL area, however should be accomplished by the installation

of hydraulic structures to mitigate river drainage problems, that will be intensified in the BVL region. The changes in the saltpans geometry only affects flooding of oceanic origin, once these structures are located in the lagoon central area, out of the river influence. This preliminary analysis highlighted that the restriction of saltpans inundation is ineffective on flood risk mitigation. However the use of saltpans as reservoirs mitigates flood risk in main channels marginal areas.

Attending this, flood risk in Ria de Aveiro region was successfully assessed by applying the Source-Pathway-Receptor conceptual model but, it is important to highlight that the results obtained here have an uncertainty associated. Indeed, it is recognized among the scientific community that there is an underlying uncertainty associated to each element that propagates towards flood risk assessment [Apel et al., 2004, 2008; Merz et al., 2008]. Concerning, the estimation of the magnitude and frequency of flood drivers, potential uncertainties derive from errors primary on measurements/predictions and secondly on statistical analysis [Apel et al., 2004]. Also, the hydrodynamic model accuracy depends on the precision of bathymetric and topographic measurements, on model parametrizations and on the grid resolution. Finally, uncertainties related with the consequences of floods on receptors derive from the risk calculation method, the value and susceptibility and weighting of exposed elements. Despite the agreement between flood risk results and the historical background of Ria de Aveiro flooding, the estimations obtained here can be improved in the future. Given the high dependence of flood extent projections on flood drivers predictions, it is considered indispensable to revise these projections as new datasets become available. Accordingly, the sea level return periods should be updated later as longer records become available. Also, the lack of river discharges monitoring originated a great uncertainty on river discharges predictions. This limitation can only be overcame through a long term monitoring program. Moreover, the oceanic and fluvial drivers should be analysed in the future given the projections of the $5^{\text{th}}$ IPCC report. This was not included in this research once there was only downscaling data available supported on the $4^{\text{th}}$ IPCC report. The numerical results can be improved by incorporating the numerical grid in the SELFE hydrodynamic model [Zhang and Baptista, 2008]. Despite the previous SELFE applications to the Ria de

Aveiro [Rodrigues, 2012; Tomas et al., 2014] does not show more accurate results, this change will clearly improve the computational efficiency. Furthermore, this update will open the application of SELFE in 3D mode, which can potentially improve the results, particularly during high discharges where the stratification may be important [Vaz et al., 2009]. Another aspect to improve as soon as there is available data, is the update of the digital terrain model. Given the dependence of water levels on the lagoon geomorphology, an high resolution topo-bathymetric survey of the entire region will improve certainly the accuracy of numerical results, specially in the narrow channels heads and close the Vouga and Antuã rivers mouth, where the data are from 1987. Finally, a better knowledge of the Ria de Aveiro socio-economic and ecological systems can also improve the flood risk results, supporting a precise parametrization of value, susceptibility and weighting of exposed assets.

Although the uncertainties, the approach followed here produced reliable results, in accordance with the past flood events occurred in Ria de Aveiro. Thus, it is considered that the methodology applied here can be applied to other estuarine systems to assess flood risk. Particularly, a similar methodology can be applied to assess flood risk in the other national estuarine areas, such as, Cávado, Douro, Mondego and Tagus estuaries and Ria Formosa, that were identified in the flood risk management plan as critical zones APA [2015]. In the case of Tagus estuary, such analysis is simplified once the social vulnerability of estuarine margins was already studied in detail by Tavares et al. [2015]. Thus, in this case the flood risk can be obtained simply by combining flood hazard, obtained from hydrodynamic modelling, with flood vulnerability obtained by those authors.

Finally, this work demonstrated the potential of numerical modelling on supporting flood risk management. Indeed, numerical models have the potential to support the three main pillars of flood risk management, highlighted in the Floods Directive: prevention, protection and preparedness. Firstly, the damage caused by flood events can be prevented through appropriate land use planning, that should adapt the future territorial developments to the high resolution flood risk mapping obtained through hydrodynamic simulations. Secondly, flood risk can be mitigated by implementing flood protection structural measures, which design, impact and efficiency should be

supported on numerical modelling. Thirdly, the predictive potential of numerical models can be used to increase preparedness for floods by performing operational flood forecast. Accordingly, future work to be performed in the context of flood risk assessment may focus, by one hand on the dissemination of the thesis results by local authorities and territorial managers, and by the other hand on the development of an operational flood forecasting system for the Ria de Aveiro area for use in the preparation of flood warnings. It is important to have in consideration that the results of present research emphasize the general flood risk patterns for Ria de Aveiro, while for local authorities it is considered relevant to analyse flood risk results at finer scales. Often, more than knowing what happens in general terms, those entities are interested to know in detail the flood characteristics in critical areas located in their regions. In this context, it is important to have in mind that the results of this thesis were obtained with a high resolution corresponding to the grid element of the numerical model. Thus, besides the general patterns of Ria de Aveiro flooding, future tasks may comprises the analysis of thesis results on a finer scale highlighting flood risk assessment in critical areas. Moreover, the dissemination of flood forecasting results through a web platform, similar to the existent actually for oil spill forecast [Oliveira et al., 2014], will improve flood warning in case of emergency. Although important, this task can only be fully successful implemented when complemented with continuous monitoring of river discharges.

# References


Ackers P. and White W.R. (1973). Sediment transport: a new approach and analysis. *Journal of the Hydraulics Division*, 99:2041–2060.

Ahmadian R., Olbert A.I., Hartnett M. and Falconer R.A. (2014). Sea level rise in the Severn Estuary and Bristol Channel and impacts of a Severn Barrage. *Computers & Geosciences*, 66:94–105.

Alongi D.M. (1998). *Coastal Ecosystem Processes.* Marine sciences series, Boca Raton: CRC press, 419 pp.

Alves F.L., Coelho C., Coelho C.D. and Pinto P. (2011). Modelling coastal vulnerabilities - tool for decision support system at inter-municipality level. *Journal of Coastal Research*, SI64:966–970.

AMBIECO (2011). *Estudo da Caracterização da Qualidade Ecológica da Ria de Aveiro.* Tech. Rep., Sociedade Polis Litoral Ria de Aveiro, 226 pp.

Andrade C., Pires H.O., Taborda R. and Freitas M.C. (2006). Zonas costeiras. In *Alterações Climáticas em Portugal. Cenários, Impactos e Medidas de Adaptação - Projecto SIAM II* (Santos F. and Miranda P., eds.). Gradiva, Lisboa, 169–208.

Andrade C., Pires H.O., Taborda R. and Freitas M.C. (2007). Projecting future changes in wave climate and coastal response in Portugal by the end of the 21st century. *Journal of Coastal Research*, 50:263–257.

Andresen T., Curado M.J., Almeida P., Arroja L., Arsénio P., Bóia C., Coelho C., Crespi A., Eça P., Ferreira I., Gomes F.G., Gonçalves J.M., Imperial F., Jordão A., Jorge J., Leão F., Lopes L., Luís A., Magalhães I., Martins F., Miguens F., Nunes

M., Páscoa F., Pinho P., Pinho R., Repas A., Ribeiro L.P., Santos H.P., Santos D., Silva M.M. and Silva C. (2001). *Estudo de Impacte Ambiental do Projecto de Desenvolvimento Agrícola do Vouga - Bloco do Baixo Vouga Lagunar - Relatório Final*. Tech. Rep., University of Aveiro.

Anthony A., Atwood J., August P., Byron C., Cobb S., Foster C., Fry C., Gold A., Hagos K., Heffner L., Kellogg D.Q., Lellis-Dibble K., Opaluch J.J., Oviatt C., Pfeiffer-Herbert A., Rohr N., Smith L., Smythe T., Swift J. and Vinhateiro N. (2009). Coastal lagoons and climate change: ecological and social ramifications in U.S. Atlantic and Gulf coast ecosystems. *Ecology and Society*, 14(1):8.

Antunes C. and Taborda R. (2009). Sea level at Cascais tide gauge: Data, analysis and results. *Journal of Coastal Research*, SI 56:218–222.

APA (2014). *Agenda Navegar 2014: Navios Maiores, Mais Carga*. Tech. Rep., APA, S.A., 96 pp.

APA (2015). *Plano de Gestão dos Riscos de Inundações - Rede Hidrográfica 4 - Vouga, Mondego e Lis*. Tech. Rep., Agência Portuguesa do Ambiente, 112 pp.

Apel H., Merz B. and Thieken A.H. (2008). Quantification of uncertainties in flood risk assessments. *International Journal of River Basin Management*, 6(2):149–162.

Apel H., Thieken A.H., Merz B. and Blöschl G. (2004). Flood risk assessment and associated uncertainty. *Natural Hazards and Earth System Science*, 4(2):295–308.

Araújo I.B., Bos M.S., Bastos L.C. and Cardoso M.M. (2013). Analysing the 100 year sea level record of Leixões, Portugal. *Journal of Hydrology*, 481:76–84.

Araújo I.B., Dias J.M. and Pugh D.T. (2008). Model simulations of tidal changes in a coastal lagoon, the Ria de Aveiro (Portugal). *Continental Shelf Research*, 28(8):1010–1025.

Araújo I.G.B. (2005). *Sea Level Variability: Examples from the Atlantic Coast of Europe*. PhD Thesis, University of Southampton, 216 pp.

Arnold J.G., Allen P.M. and Bernhardt G. (1993). A comprehensive surface-groundwater flow model. *Journal of Hydrology*, 142(1-4):47–69.

Asselman N., Bates P., Woodhead S., Fewtrell T., Soares-Frazão S., Zech Y., Velickovic M., de Wit A., ter Maat J., Verhoeven G. and Lhomme J. (2009). *Flood Inundation Modelling - Model Choice and Proper Application.* Tech. Rep., Hr Wallingford, 142 pp.

Aubrey D.G. and Speer P.E. (1985). A study of non-linear tidal propagation in shallow inlet estuarine systems.Part I. observations. *Estuarine Coastal and Shelf Science*, 21(2):185–205.

Azevedo A., Sousa A.I., Silva J.D.L.E., Dias J.M. and Lillebø A.I. (2013). Application of the generic DPSIR framework to seagrass communities of Ria de Aveiro: a better understanding of this coastal lagoon. *Journal of Coastal Research*, SI 65:19–24.

Azevedo A.C.O.A. (2010). *Sistema Integrado de Modelação para Apoio à Prevenção e Mitigação de Acidentes de Hidrocarbonetos em Estuários e Orla Costeira.* PhD Thesis, University of Lisbon, 224 pp.

Balica S.F., Popescu I., Beevers L. and Wright N.G. (2013). Parametric and physically based modelling techniques for flood risk and vulnerability assessment: A comparison. *Environmental Modelling & Software*, 41:84–92.

Bertin X., Bruneau N., Breilh J.F., Fortunato A.B. and Karpytchev M. (2012). Importance of wave age and resonance in storm surges: The case Xynthia, Bay of Biscay. *Ocean Modelling*, 42:16–30.

Bertin X., Li K., Roland A., Zhang Y., Breilh J.F. and Chaumillon E. (2014). A modeling-based analysis of the flooding associated with Xynthia, central Bay of Biscay. *Coastal Engineering*, 94:80–89.

Bertin X., Oliveira A. and Fortunato A.B. (2009). Simulating morphodynamics with unstructured grids: Description and validation of a modeling system for coastal applications. *Ocean Modelling*, 28(1-3):75–87.

Bhaskaran P.K., Gayathri R., Murty P.L.N., Bonthu S. and Sen D. (2014). A numerical study of coastal inundation and its validation for Thane cyclone in the Bay of Bengal. *Coastal Engineering*, 83:108–118.

Booij N., Ris R.C. and Holthuijsen L.H. (1999). A third-generation wave model for coastal regions - 1. Model description and validation. *Journal of Geophysical Research-Oceans*, 104(C4):7649–7666.

Borum J., Duarte C.M., Krause-Jensen D. and Greve T.M. (2004). *European Seagrasses: an Introduction to Monitoring and Management*. The M&MS project, 88 pp.

Büchele B., Kreibich H., Kron A., Thieken A., Ihringer J., Oberle P., Merz B. and Nestmann F. (2006). Flood-risk mapping: contributions towards an enhanced assessment of extreme events and associated risks. *Natural Hazards and Earth System Science*, 6(4):485–503.

Bunya S., Dietrich J.C., Westerink J.J., Ebersole B.A., Smith J.M., Atkinson J.H., Jensen R., Resio D.T., Luettich R.A., Dawson C., Cardone V.J., Cox A.T., Powell M.D., Westerink H.J. and Roberts H.J. (2010). A high-resolution coupled riverine flow, tide, wind, wind wave, and storm surge model for southern Louisiana and Mississippi. Part I: Model development and validation. *Monthly Weather Review*, 138(2):345–377.

Burzel A., Dassanayake D.R. and Oumeraci H. (2015). Spatial modeling of tangible and intangible losses in integrated coastal flood risk analysis. *Coastal Engineering Journal*, 57(01):1540008.

Casas-Prat M. and Sierra J.P. (2013). Projected future wave climate in the NW Mediterranean Sea. *Journal of Geophysical Research - Oceans*, 118(7):3548–3568.

Castro C.L., Pielke R.A. and Leoncini G. (2005). Dynamical downscaling: Assessment of value retained and added using the regional atmospheric modeling system (RAMS). *Journal of Geophysical Research - Atmospheres*, 110(D5):D05108.

Chan Y.K. (1983). *Statistics of Extreme Sea-levels in Hong Kong.* Royal Observatory. Tech. Note No.35, 24 pp.

Chen W.B., Liu W.C., Fu H.S. and Jang J.H. (2015). Assessing the influences of a flood diversion project on mitigating river stage, inundation extent and economic loss. *Water*, 7(4):1731–1750.

Chua V.P. and Xu M. (2014). Impacts of sea-level rise on estuarine circulation: An idealized estuary and San Francisco Bay. *Journal of Marine Systems*, 139:58–67.

Church J.A. and White N.J. (2006). A 20th century acceleration in global sea-level rise. *Geophysical Research Letters*, 33(1).

Church J.A. and White N.J. (2011). Sea-level rise from the late 19th to the early 21st century. *Surveys in Geophysics*, 32(4-5):585–602.

Coelho C. (2005). *Riscos de Exposição de Frentes Urbanas para Diferentes Intervenções de Defesa Costeira.* PhD Thesis, University of Aveiro, 404 pp.

Coelho C.A., Alves F.L., Ferreira R.V., Valente S., Teixeira T., Ribeiro C., Ferreira A., Castanheira E., Esteves T., Coelho C., Pinto P. and Silva F. (2007). *Definição das Condições de Risco de Cheia, Incêndios Florestais, Erosão Costeira e Industriais na Área de Intervenção da AMRIA. Estudo Realizado no Âmbito do Protocolo de Colaboração com a AMRIA - Associação de Municípios da Ria.* Tech. Rep., Departamento de Ambiente e Ordenamento, Universidade de Aveiro, 44 pp.

Collet I. and Engelbert A. (2013). *Coastal Regions: People Living Along the Coastline, Integration of NUTS 2010 and Latest Population Grid.* Tech. Rep. KS-SF-13-030-EN-N, Eurostat, 12 pp.

Condon A.J. and Sheng Y.P. (2012). Optimal storm generation for evaluation of the storm surge inundation threat. *Ocean Engineering*, 43:13–22.

Cunha A.H., Assis J.F. and Serrao E.A. (2013). Seagrasses in Portugal: A most endangered marine habitat. *Aquatic Botany*, 104:193–203.

Cunha L.V., Ribeiro L., Oliveira R.P. and Nascimento J. (2006). Recursos hídricos. In *Alterações Climáticas em Portugal. Cenários, Impactos e Medidas de Adaptação - Projecto SIAM II* (Santos F.D. and Miranda P., eds.). Gradiva, Lisboa, 116–168.

da Silva J.F. and Duck R.W. (2001). Historical changes of bathymetry and tidal amplitude in the Ria de Aveiro, Portugal - trends for future evolution. *Climate Research*, 18:17–24.

da Silva J.F., Duck R.W. and Catarino J.B. (2004). Seagrasses and sediment response to changing physical forcing in a coastal lagoon. *Hydrology and Earth System Sciences*, 8(2):151–159.

Dassanayake D.R., Burzel A. and Oumeraci H. (2013). Coastal flood risk: Integration of intangible losses in flood risk analysis. In *Proceedings of 7th International Conference on Asian and Pacific Coasts*, 640–647.

de Moel H. and Aerts J.C.J.H. (2011). Effect of uncertainty in land use, damage models and inundation depth on flood damage estimates. *Natural Hazards*, 58(1):407–425.

de Moel H., van Vliet M. and Aerts J.C.J.H. (2014). Evaluating the effect of flood damage-reducing measures: a case study of the unembanked area of Rotterdam, the Netherlands. *Regional Environmental Change*, 14(3):895–908.

Dias J.A. and Taborda R. (1988). Evolução recente do nível médio do mar em Portugal. *Anais do Instituto Hidrográfico*, 9:83–97.

Dias J.M. (2001). *Contribution to the Study of the Ria de Aveiro Hydrodynamics*. PhD Thesis, University of Aveiro, 288 pp.

Dias J.M. and Alves F.L. (2013). *Risco de Cheias e Estratégias de Adaptação para a Zona Costeira e Lagunar da Ria de Aveiro*. University of Aveiro, CESAM - Centro de Estudos do Ambiente e do Mar, 52 pp.

Dias J.M., Alves F.L., Coelho C., Rocha A., Fortunato A.B., Lopes C.L., Sousa L., Pereira C., Rodrigues N. T. Ribeiro, Silva P.A., Azevedo A., Roebeling P., Plecha S., Picado A., Marques C., Rodrigues M., Silva J., Fernandes M., Silva E. and da Silva

M.M. (2013a). *ADAPTARia: Modelação das Alterações Climáticas no Litoral da Ria de Aveiro - Estratégias de Adaptação para Cheias Costeiras e Fluviais.* Tech. Rep., University of Aveiro, 267 pp.

Dias J.M., Lopes C.L., Coelho C., Pereira C., Alves F.L., Sousa L.P., Antunes I.C., Fernandes M.L. and Phillips M. (2014). Influence of mean sea level rise on Ria de Aveiro littoral: adaptation strategies for flooding events and shoreline retreat. *Journal of Coastal Research*, SI70:320–325.

Dias J.M. and Lopes J.F. (2006). Calibration and validation of hydrodynamic, salt and heat transport models for Ria de Aveiro lagoon (Portugal). *Journal of Coastal Research*, SI39:1680–1684.

Dias J.M., Lopes J.F. and Dekeyser I. (2000). Tidal propagation in Ria de Aveiro lagoon, Portugal. *Physics and Chemistry of the Earth Part B-Hydrology Oceans and Atmosphere*, 25(4):369–374.

Dias J.M., Lopes J.F. and Dekeyser I. (2003). A numerical system to study the transport properties in the Ria de Aveiro lagoon. *Ocean Dynamics*, 53(3):220–231.

Dias J.M., Sousa M.C., Bertin X., Fortunato A.B. and Oliveira A. (2009). Numerical modeling of the impact of the Ancão Inlet relocation (Ria Formosa, Portugal). *Environmental Modelling & Software*, 24(6):711–725.

Dias J.M., Valentim J.M. and Sousa M.C. (2013b). A numerical study of local variations in tidal regime of Tagus Estuary, Portugal. *PLoS ONE*, e80450(12):8.

Dodet G., Bertin X. and Taborda R. (2010). Wave climate variability in the North-East Atlantic Ocean over the last six decades. *Ocean Modelling*, 31(3-4):120–131.

Dolbeth M., Stålnacke P., Alves F.L., Sousa L.P., Gooch G.D., Khokhlov V., Tuchkovenko Y., Lloret J., Bielecka M., Różyński G., Soares J.A., Baggett S., Margonski P., Chubarenko B.V. and Lillebø A.I. (2016). An integrated pan-european perspective on coastal lagoons management through a mosaic-DPSIR approach. *Scientific Reports*, 6:19400.

Domeneghetti A., Vorogushyn S., Castellarin A., Merz B. and Brath A. (2013). Probabilistic flood hazard mapping: effects of uncertain boundary conditions. *Hydrology and Earth System Sciences*, 17(8):3127–3140.

Duck R.W. and da Silva J.F. (2012). Coastal lagoons and their evolution: A hydromorphological perspective. *Estuarine Coastal and Shelf Science*, 110:2–14.

EEA (2007). *CLC2006 technical guidelines.* Tech. Rep., European Environment Agency, 66 pp.

EXCIMAP (2007). *Handbook on Good Practices for Flood Mapping in Europe.* Tech. Rep., European Environment Agency, 57 pp.

Fasbender D. and Ouarda T.B.M.J. (2010). Spatial bayesian model for statistical downscaling of AOGCM to minimum and maximum daily temperatures. *Journal of Climate*, 23(19):5222–5242.

FEMA (2007). *Selecting Appropriate Mitigation Measures for Floodprone Structures.* Tech. Rep., Federal Emergency Management Agency, 198 pp.

Ferrarin C., Bajo M., Bellafiore D., Cucco A., De Pascalis F., Ghezzo M. and Umgiesser G. (2014). Toward homogenization of Mediterranean lagoons and their loss of hydrodiversity. *Geophysical Research Letters*, 41(16):5935–5941.

FitzGerald D.M., Fenster M.S., Argow B.A. and Buynevich I.V. (2008). Coastal impacts due to sea-level rise. *Annual Review of Earth and Planetary Sciences*, 36:601–647.

Fortunato A.B., Bertin X. and Oliveira A. (2009). Space and time variability of uncertainty in morphodynamic simulations. *Coastal Engineering*, 56(8):886–894.

Fortunato A.B. and Oliveira A. (2004). A modeling system for tidally driven long-term morphodynamics. *Journal of Hydraulic Research*, 42(4):426–434.

Fortunato A.B. and Oliveira A. (2007). Improving the stability of a morphodynamic modeling system. *Journal of Coastal Research*, SI50:486–490.

Fortunato A.B., Pinto L., Oliveira A. and Ferreira J.S. (2002). Tidally generated shelf waves off the western Iberian coast. *Continental Shelf Research*, 22(14):1935–1950.

Fortunato A.B., Rodrigues M., Dias J.M., Lopes C. and Oliveira A. (2013). Generating inundation maps for a coastal lagoon: A case study in the Ria de Aveiro (Portugal). *Ocean Engineering*, 64:60–71.

Fowler H.J. and Kilsby C.G. (2007). Using regional climate model data to simulate historical and future river flows in northwest England. *Climatic Change*, 80(3-4):337–367.

Gallien T.W., Schubert J.E. and Sanders B.F. (2011). Predicting tidal flooding of urbanized embayments: A modeling framework and data requirements. *Coastal Engineering*, 58(6):567–577.

Gao G.D., Wang X.H. and Bao X.W. (2014). Land reclamation and its impact on tidal dynamics in Jiaozhou Bay, Qingdao, China. *Estuarine Coastal and Shelf Science*, 151:285–294.

García A.M., Ónega F.J., Crecente R., van Holst F., Abts E., Timmermans W. and Stolk M. (2012). *FACTS: Forms for Adapting to Climate change through Territorial Strategies*. Alva Gráfica, Spain, 117 pp.

Génio L., Sousa A., Vaz N., Dias J.M. and Barroso C. (2008). Effect of low salinity on the survival of recently hatched veliger of nassarius reticulatus (l.) in estuarine habitats: A case study of Ria de Aveiro. *Journal of Sea Research*, 59(3):133–143.

Giorgi F., Jones C. and Asrar G.R. (2009). Addressing climate information needs at the regional level: the CORDEX framework. *World Meteorological Organization (WMO) Bulletin*, 58(3):175–183.

Gong W.P., Shen J., Cho K.H. and Wang H.V. (2009). A numerical model study of barotropic subtidal water exchange between estuary and subestuaries (tributaries) in the Chesapeake Bay during northeaster events. *Ocean Modelling*, 26(3-4):170–189.

Gouldby B. and Samuels P. (2005). *Language of Risk - Project Definitions*. Tech. Rep., Hr Wallingford, 39 pp.

Guerreiro M., Fortunato A.B., Freire P., Rilo A., Taborda R., Freitas M.C., Andrade C., Silva T., Rodrigues M., Bertin X. and Azevedo A. (2015). Evolution of the hydrodynamics of the Tagus Estuary (Portugal) in the 21st century. *Journal of Integrated Coastal Zone Manegement*, 15(1):65–80.

Hawkes P.J. (2008). Joint probability analysis for estimation of extremes. *Journal of Hydraulic Research*, 46(2):246–256.

Hayter E.J. and Gailani J.Z. (2014). Fundamentals of sediment transport. In *Processes, Assessment and Remediation of Contaminated Sediments* (Reible D.D., ed.), Vol. 6. 25–79.

Hertig E. and Jacobeit J. (2008). Assessments of Mediterranean precipitation changes for the 21st century using statistical downscaling techniques. *International Journal of Climatology*, 28(8):1025–1045.

Hesse C., Bielecka M., Stefanova A., Robakiewicz M., Staroszczyk R., Zalewski M., Khokhlov V., Tuchkovenko Y., Lloret J., Silva J.D.L.E., Dias J.M., Lilebø A.I., Chubarenko B. and Krysanova V. (2015). Impacts of potential climate change on lagoons and their catchments. In *Coastal Lagoons in Europe: Integrated Water Resource Strategies (Chapter 13)* (Lilebø A.I., Stalnacke P. and Gooch G.D., eds.). International Water Association (IWA), 115–131.

Holdgate M.W. (1979). *A Perspective of Environmental Pollution*. Cambridge University Press, Chichester, 290 pp.

Hong B. and Shen J. (2012). Responses of estuarine salinity and transport processes to potential future sea-level rise in the Chesapeake Bay. *Estuarine Coastal and Shelf Science*, 104:33–45.

Hosseinipour E., Vargas S., O'Brien K. and Kasraie H. (2012). 2-D fine grid hydrodynamic modeling for more accurate floodplain mapping in Southern California. In *Proceedings of World Environmental and Water Resources Congress*, 1096–1107.

IHERA (1996/97). *Princípios e Orientações das Intervenções do MADRP nos Campos do Baixo Vouga Lagunar.* Tech. Rep., Instituto de Hidráulica, Engenharia Rural e Ambiente, 123 pp.

IPCC (2007). *Climate Change 2007: The Physical Science Basis. Contribution of Working Group I to the Fourth Assessment Report of the Intergovernmental Panel on Climate Change.* Cambridge University Press, Cambridge, United Kingdom and New York, NY, USA, 996 pp.

IPCC (2013). *Climate Change 2013: The Physical Science Basis. Contribution of Working Group I to the Fifth Assessment Report of the Intergovernmental Panel on Climate Change.* Cambridge University Press, Cambridge, United Kingdom and New York, NY, USA, 1535 pp.

IPCC (2014). *Climate Change 2014: Impacts, Adaptation, and Vulnerability. Part A: Global and Sectoral Aspects. Contribution of Working Group II to the Fifth Assessment Report of the Intergovernmental Panel on Climate Change.* Cambridge University Press, Cambridge, United Kingdom and New York, NY, USA, 1132 pp.

Jenks G. (1967). The data model concept in statistical mapping. *International Yearbook of Cartography*, 7:186–190.

Jewell S.A., Walker D.J. and Fortunato A.B. (2012). Tidal asymmetry in a coastal lagoon subject to a mixed tidal regime. *Geomorphology*, 138(1):171–180.

Jonkman S.N., Bočkarjova M., Kok M. and Bernardini P. (2008). Integrated hydrodynamic and economic modelling of flood damage in the Netherlands. *Ecological Economics*, 66(1):77–90.

Jonkman S.N. and Vrijling J.K. (2008). Loss of life due to floods. *Journal of Flood Risk Management*, 1(1):43–56.

Jung Y., Kim D., Kim D., Kim M. and Lee S.O. (2014). Simplified flood inundation mapping based on flood elevation-discharge rating curves using satellite images in gauged watersheds. *Water*, 6(5):1280–1290.

Kaplan E.L. and Meier P. (1958). Nonparametric estimation from incomplete observations. *Journal of the American Statistical Association*, 53:457–481.

Kew S.F., Selten F.M., Lenderink G. and Hazeleger W. (2013). The simultaneous occurrence of surge and discharge extremes for the Rhine delta. *Natural Hazards and Earth System Science*, 13(8):2017–2029.

Kind J.M. (2014). Economically efficient flood protection standards for the Netherlands. *Journal of Flood Risk Management*, 7(2):103–117.

Kjerfve B. (1994). *Coastal Lagoon Processes*. Elsevier, Amsterdam, 577 pp.

Klerk W.J., Winsemius H.C., van Verseveld W.J., Bakker A.M.R. and Diermanse F.L.M. (2015). The co-incidence of storm surges and extreme discharges within the Rhine-Meuse Delta. *Environmental Research Letters*, 10(3):035005.

Krysanova V., Meiner A., Roosaare J. and Vasilyev A. (1989). Simulation modelling of the coastal waters pollution from agricultural watershed. *Ecological Modelling*, 49(1-2):7–29.

Kubal C., Haase D., Meyer V. and Scheuer S. (2009). Integrated urban flood risk assessment - adapting a multicriteria approach to a city. *Natural Hazards and Earth System Science*, 9(6):1881–1895.

Kuhn M., Tuladhar D. and Corner R. (2011). Visualising the spatial extent of predicted coastal zone inundation due to sea level rise in south-west Western Australia. *Ocean & Coastal Management*, 54(11):796–806.

Kuiry S.N., Sen D. and Bates P.D. (2010). Coupled 1D-Quasi-2D flood inundation model with unstructured grids. *Journal of Hydraulic Engineering*, 136(8):493–506.

LAGOONS (2011). *Results of the Problem Based Science Analysis: The Ria de Aveiro Lagoon*. Tech. Rep., LAGOONS Report D3.2.1, 50 pp.

Lemos C.M.R.S. (2008). *Base de Dados Geoambiental SIG para apoio à Gestão do Risco em Aveiro*. MSc Thesis, University of Aveiro, 189 pp.

Li P., Li G.X., Qiao L.L., Chen X., Shi J.H., Gao F., Wang N. and Yue S.H. (2014). Modeling the tidal dynamic changes induced by the bridge in Jiaozhou Bay, Qingdao, China. *Continental Shelf Research*, 84:43–53.

Liu J.C., Lence B.J. and Isaacson M. (2010). Direct joint probability method for estimating extreme sea levels. *Journal of Waterway Port Coastal and Ocean Engineering-Asce*, 136(1):66–76.

Lopes C.L., Azevedo A. and Dias J.M. (2013a). Flooding assessment under sea level rise scenarios: Ria de Aveiro case study. *Journal of Coastal Research*, SI65:766–771.

Lopes C.L., Plecha S., Silva P.A. and Dias J.M. (2013b). Influence of morphological changes in a lagoon flooding extension: case study of Ria de Aveiro (Portugal). *Journal of Coastal Research*, SI65:1158–1163.

Lopes C.L., Silva P.A., Dias J.M., Rocha A., Picado A., Plecha S. and Fortunato A.B. (2011). Local sea level change scenarios for the end of the 21st century and potential physical impacts in the lower Ria de Aveiro (Portugal). *Continental Shelf Research*, 31(14):1515–1526.

Lopes J., Dias J. and Dekeyser I. (2001). Influence of tides and river inputs on suspended sediment transport in the Ria de Aveiro lagoon, Portugal. *Physics and Chemistry of the Earth, Part B: Hydrology, Oceans and Atmosphere*, 26(9):729–7340.

Loukas A. and Vasiliades L. (2014). Streamflow simulation methods for ungauged and poorly gauged watersheds. *Natural Hazards and Earth System Science*, 14(7):1641–1661.

Marcos M., G. J., D. G. and Pérez B. (2011). Changes in storm surges in southern europe from a regional model under climate change scenarios. *Global and Planetary Change*, 77(3-4):116–128.

Marinheiro J.M.S. (2008). *Assoreamento da Ria de Aveiro : Causas e Soluções*. MSc Thesis, University of Aveiro, 136 pp.

Marsland S.J., Haak H., Jungclaus J.H., Latif M. and Roske F. (2003). The max-planck-institute global ocean/sea ice model with orthogonal curvilinear coordinates. *Ocean Modelling*, 5(2):91–127.

Maskell J., Horsburgh K., Lewis M. and Bates P. (2014). Investigating river-surge interaction in idealised estuaries. *Journal of Coastal Research*, 30(2):248–259.

McGranahan G., Balk D. and Anderson B. (2007). The rising tide: assessing the risks of climate change and human settlements in low elevation coastal zones. *Environment and Urbanization*, 19(1):17–37.

Mendes R. (2010). *Numerical modeling of the Ria de Aveiro plume: a preliminary study.* MSc Thesis, University of Aveiro, 50 pp.

Mendes R., Vaz N. and Dias J.M. (2013). Potential impacts of the mean sea level rise on the hydrodynamics of the Douro river estuary. *Journal of Coastal Research*, SI65:1951–1956.

Mendicino G. and Senatore A. (2013). Evaluation of parametric and statistical approaches for the regionalization of flow duration curves in intermittent regimes. *Journal of Hydrology*, 480:19–32.

Merz B., Kreibich H. and Apel H. (2008). Flood risk analysis: uncertainties and validation. *Österreichische Wasser- und Abfallwirtschaft*, 60(5-6):89–94.

Merz B., Kreibich H., Schwarze R. and Thieken A. (2010). Review article "assessment of economic flood damage". *Natural Hazards and Earth System Science*, 10(8):1697–1724.

Merz B., Kreibich H., Thieken A. and Schmidtke R. (2004). Estimation uncertainty of direct monetary flood damage to buildings. *Natural Hazards and Earth System Science*, 4(1):153–163.

Messener F., Penning-Rowsell E., Green C., Meyer V., Tunstall S. and van der Veen A. (2007). *Evaluating Flood Damages: Guidance and Recommendations on Principles and Methods.* Tech. Rep., Hr Wallingford, 178 pp.

Messner F. and Meyer V. (2006). Flood damage, vulnerability and risk perception - challenges for flood damage research. In *Flood Risk Management: Hazards, Vulnerability and Mitigation Measures* (Schanze J., Zeman E. and Marsalek J., eds.), Vol. 67. 149–167.

Meyer V., Haase D. and Scheuer S. (2007). *GIS-based multicriteria analysis as decision support in flood risk management.* Tech. Rep., Hr Wallingford, 55 pp.

Meyer V. and Messner F. (2005). *National Flood Damage Evaluation Methods - A Review of Applied Methods in England, the Netherlands, the Czech Republic and Germany.* Tech. Rep., Hr Wallingford, 44 pp.

Meyer V., Scheuer S. and Haase D. (2009). A multicriteria approach for flood risk mapping exemplified at the Mulde river, Germany. *Natural Hazards*, (48):17–39.

Moreira M.H., Queiroga H., Machado M.M. and Cunha M.R. (1993). Environmental gradients in a southern Europe estuarine system: Ria de Aveiro, Portugal implications for soft bottom macrofauna colonization. *Netherland Journal of Aquatic Ecology*, 27(2):465–482.

Nathan R.J. and McMahon T.A. (1990). Evaluation of automated techniques for base flow and recession analyses. *Water Resources Research*, 26(7):1465–1473.

Neves R. (2007). Numerical models as decision support tools in coastal areas. In *Assessment of the Fate and Effects of Toxic Agents on Water Resources* (Gonenc I.E., Koutitonsky V.G., Rashleigh B., Ambrose R.B. and Wolflin J.P., eds.). Springer Netherlands, 171–195.

Nicholls R.J. (2011). Planning for the impacts of sea level rise. *Oceanography*, 24(2):144–157.

Nicholls R.J., Hoozemans F.M.J. and Marchand M. (1999). Increasing flood risk and wetland losses due to global sea-level rise: regional and global analyses. *Global Environmental Change-Human and Policy Dimensions*, 9:S69–S87.

Nicholls R.J., Marinova N., Lowe J.A., Brown S., Vellinga P., De Gusmao D., Hinkel J. and Tol R.S.J. (2011). Sea-level rise and its possible impacts given a 'beyond 4 degrees c world' in the twenty-first century. *Philosophical Transactions of the Royal Society a-Mathematical Physical and Engineering Sciences*, 369(1934):161–181.

Oliveira A., Fortunato A.B. and Dias J.M. (2006). Numerical modeling of Ria de Aveiro inlet dynamics. In *Proceedings of 30th International Conference on Coastal Engeneering* (Smith J.M., ed.), Vol. 4, 3282–3294.

Oliveira A., Jesus G., Gomes J.L., Rogeiro J., Azevedo A., Rodrigues M., Fortunato A.B., Dias J.M., Tomas L.M., Oliveira E.R., Alves F.L. and den Boer S. (2014). An interactive WebGIS observatory platform for enhanced support of coastal management. *Journal of Coastal Research*, SI70:507–512.

Oumeraci H., Kortenhaus A., Burzel A., Naulin M., Dassanayake D.R., Jensen J., Wahl T., Mudersbach C., Gönnert G., Gerkensmeier B., Fröhle P. and Ujeyl G. (2015). Xtremrisk - integrated flood risk analysis for extreme storm surges at open coasts and in estuaries: Methodology, key results and lessons learned. *Coastal Engineering Journal*, 57(01):1540001.

Pardue J.H., Moe W.M., McInnis D., Thibodeaux L.J., Valsaraj K.T., Maciasz E., van Heerden I., Korevec N. and Yuan Q.Z. (2005). Chemical and microbiological parameters in New Orleans floodwater following Hurricane Katrina. *Environmental Science & Technology*, 39(22):8591–8599.

Pawlowicz R., Beardsley B. and Lentz S. (2002). Classical tidal harmonic analysis including error estimates in matlab using t-tide. *Computers & Geosciences*, 28(8):929–937.

Pedrozo-Acuña A., Rodríguez-Rincón J.P., Arganis-Juárez M., Domínguez-Mora R. and González Villareal F.J. (2015). Estimation of probabilistic flood inundation maps for an extreme event: Pánuco River, México. *Journal of Flood Risk Management*, 8(2):177–192.

Pelling H.E. and Green J.A.M. (2013). Sea level rise and tidal power plants in the Gulf of Maine. *Journal of Geophysical Research-Oceans*, 118(6):2863–2873.

Pelling H.E. and Green J.A.M. (2014). Impact of flood defences and sea-level rise on the european shelf tidal regime. *Continental Shelf Research*, 85:96–105.

Pelling H.E., Green J.A.M. and Ward S.L. (2013a). Modelling tides and sea-level rise: To flood or not to flood. *Ocean Modelling*, 63:21–29.

Pelling H.E., Uehara K. and Green J.A.M. (2013b). The impact of rapid coastline changes and sea level rise on the tides in the Bohai Sea, China. *Journal of Geophysical Research-Oceans*, 118(7):3462–3472.

Peng M.C., Xie L. and Pietrafesa L.J. (2004). A numerical study of storm surge and inundation in the Croatan-Albemarle-Pamlico Estuary System. *Estuarine Coastal and Shelf Science*, 59(1):121–137.

Penning-Rowsell E., Johnson C., Tunstall S., Tapsell S., Morris J., Chatterton J. and Green C. (2005). *The Benefits of Flood and Coastal Risk Management: A Manual of Assessment Techniques*. Middlesex University.

Perez-Ruzafa A., Marcos C., Perez-Ruzafa I.M. and Perez-Marcos M. (2013). Are coastal lagoons physically or biologically controlled ecosystems- revisiting r vs. K strategies in coastal lagoons and estuaries. *Estuarine Coastal and Shelf Science*, 132:17–33.

Pethick J. (2002). Estuarine and tidal wetland restoration in the United Kingdom: Policy versus practice. *Restoration Ecology*, 10(3):431–437.

Picado A., Dias J.M. and Fortunato A.B. (2010). Tidal changes in estuarine systems induced by local geomorphologic modifications. *Continental Shelf Research*, 30(17):1854–1864.

Picado A., Lopes C.L., Mendes R., Vaz N. and Dias J.M. (2013). Storm surge impact in the hydrodynamics of a tidal lagoon: the case of Ria de Aveiro. *Journal of Coastal Research*, SI65:796–801.

Pickering M.D., Wells N.C., Horsburgh K.J. and Green J.A.M. (2012). The impact of future sea-level rise on the european shelf tides. *Continental Shelf Research*, 35:1–15.

Plate E.J. (2002). Flood risk and flood management. *Journal of Hydrology*, 267(1-2):2–11.

Plecha S. (2011). *Contribution to the Study of the Ria de Aveiro Inlet Morphodynamics*. PhD Thesis, University of Aveiro, 163 pp.

PLRA (2011a). *Estudo de Actividades Económicas e suas Dinâmicas*. Tech. Rep., Sociedade Polis Litoral Ria de Aveiro, 348 pp.

PLRA (2011b). *Estudos da Evolução e da Dinâmica Costeira e Estuarina TOMO II - Ria de Aveiro, Relatório 3*. Tech. Rep., Sociedade Polis Litoral Ria de Aveiro, 265 pp.

Pugh D.T. (1987). *Tides, Surges and Mean Sea-Level*. Wiley and Sons, Chichester, 472 pp.

Pugh D.T. (2004). *Changing Sea levels. Effects of Tides, Weather and Climate*. Cambridge University Press, Cambridge, 280 pp.

Purvis M.J., Bates P.D. and Hayes C.M. (2008). A probabilistic methodology to estimate future coastal flood risk due to sea level rise. *Coastal Engineering*, 55(12):1062–1073.

Ramsey III E., Werle D., Suzuoki Y., Rangoonwala A. and Lu Z. (2011). Limitations and potential of satellite imagery to monitor environmental response to coastal flooding. *Journal of Coastal Research*, 28(2):457–476.

Reeve D.E., Li Y., Larson M., Hanson H., Donnelly C., Jiménez J.A., Mendoza E.T., Zech Y., Soares Frazão S., Bettess R., Stripling S. and Brampton A. (2007). *Predicting morphological changes in rivers, estuaries and coasts*. Tech. Rep., Hr Wallingford, 207 pp.

Rego J.L. and Li C.Y. (2010). Storm surge propagation in Galveston Bay during Hurricane Ike. *Journal of Marine Systems*, 82(4):265–279.

Ribeiro N.A., Fortunato A.B. and Rocha A.C. (2012). Efeito das alterações climáticas no regime de agitação marítima no Atlântico Norte e costa portuguesa. In *Proceedings of 2as Jornadas de Engenharia Hidrográfica*, 163–166.

Rodrigues A.M., Quintino V., Sampaio L., Freitas R. and Neves R. (2011). Benthic biodiversity patterns in Ria de Aveiro, Western Portugal: Environmental-biological relationships. *Estuarine Coastal and Shelf Science*, 95(2-3):338–348.

Rodrigues M.F.G. (2012). *Análise dos Efeitos de Factores Climáticos e Antropogénicos na Ria de Aveiro.* PhD Thesis, University of Aveiro, 270 pp.

Rodrigues T.F.C. (2011). *Ciclones no Oceano Atlântico Norte - Clima Actual e Cenário Futuro.* MSc Thesis, University of Aveiro, 55 pp.

Roeckner E., Bäuml G., Bonaventura L., Brokopf R., Esch M., Giorgetta M., Hagemann S., Kirchner I., Kornblueh L., Manzini E., Rhodin A., Schlese U., Schulzweida U. and Tompkins A. (2003). *The Atmospheric General Circulation Model ECHAM5. Part I: Model Description.* Tech. Rep. No.349, Max Planck Institute for Meteorology, 127 pp.

Saaty T. (1977). A scaling method for priorities in hierarchical structures. *Journal of Mathematical Psychology*, 15(3):234–281.

Schanze J. (2006). Flood risk management - a basic framework. In *Flood Risk Management - Hazards, Vulnerability and Mitigation Measures* (Schanze J., Zeman E. and Marsalek J., eds.). Springer, The Netherlands, 1–20.

Scheuer S., Haase D. and Meyer V. (2011). Exploring multicriteria flood vulnerability by integrating economic, social and ecological dimensions of flood risk and coping capacity: from a starting point view towards an end point view of vulnerability. *Natural Hazards*, 58(2):731–751.

Schoof J.T., Pryor S.C. and Surprenant J. (2010). Development of daily precipitation projections for the United States based on probabilistic downscaling. *Journal of Geophysical Research*, 115(D13).

Shen J., Wang H., Sisson M. and Gong W. (2006a). Storm tide simulation in the Chesapeake Bay using an unstructured grid model. *Estuarine Coastal and Shelf Science*, 68(1-2):1–16.

Shen J., Zhang K.Q., Xiao C.Y. and Gong W.P. (2006b). Improved prediction of storm surge inundation with a high-resolution unstructured grid model. *Journal of Coastal Research*, 22(6):1309–1319.

Sheng Y.P., Zhang Y.F. and Paramygin V.A. (2010). Simulation of storm surge, wave, and coastal inundation in the Northeastern Gulf of Mexico region during Hurricane Ivan in 2004. *Ocean Modelling*, 35(4):314–331.

Shimura T., Mori N. and Mase H. (2015). Future projection of ocean wave climate: Analysis of SST impacts on wave climate changes in the Western North Pacific. *Journal of Climate*, 28(8):3171–3190.

Silva J.D.L.E., Azevedo A., Lillebø A.I. and Dias J.M. (2013). Turbidity under changing physical forcing over two contrasting locations of seagrass meadows. *Journal of Coastal Research*, SI65:2023–2028.

Silva W., Dijkman J.P.M. and Loucks D.P. (2004). Flood management options for the Netherlands. *International Journal of River Basin Management*, 2(2):101–112.

Sinha B. and Pingree R.D. (1997). The principal lunar semidiurnal tide and its harmonics: baseline solutions for $M_2$ and $M_4$ constituents on the North-West European Continental Shelf. *Continental Shelf Research*, 17(11):1321–1365.

Song D.H., Wang X.H., Zhu X.M. and Bao X.W. (2013). Modeling studies of the far-field effects of tidal flat reclamation on tidal dynamics in the East China Seas. *Estuarine Coastal and Shelf Science*, 133:147–160.

Sousa L.P., Lilebø A.I., Soares J.A. and Alves F.L. (2015). The management story of Ria de Aveiro. In *Coastal Lagoons in Europe: Integrated Water Resource Strategies (Chapter 4)* (Lilebø A.I., Stalnacke P. and Gooch G.D., eds.). International Water Association (IWA), 33–38.

Sousa L.P., Lillebø A.I., Gooch G.D., Soares J.A. and Alves F.L. (2013). Incorporation of local knowledge in the identification of Ria de Aveiro lagoon ecosystem services (Portugal). *Journal of Coastal Research*, SI65:1051–1056.

Stefanova A., Krysanova V., Hesse C. and Lillebø A.I. (2015). Climate change impact assessment on water inflow to a coastal lagoon: the Ria de Aveiro watershed, Portugal. *Hydrological Sciences Journal*, 60(5):929–948.

Tabor K. and Williams J.W. (2010). Globally downscaled climate projections for assessing the conservation impacts of climate change. *Ecological Applications*, 20(2):554–565.

Tavares A.O., dos Santos P.P., Freire P., Fortunato A.B., Rilo A. and Sá L. (2015). Flooding hazard in the Tagus estuarine area: The challenge of scale in vulnerability assessments. *Environmental Science & Policy*, 51:238–255.

Taylor K.E. (2001). Summarizing multiple aspects of model performance in a single diagram. *Journal of Geophysical Research-Atmospheres*, 106(D7):7183–7192.

Thieken A.H., Apel H. and Merz B. (2015). Assessing the probability of large-scale flood loss events: a case study for the river Rhine, Germany. *Journal of Flood Risk Management*, 8(3):247–262.

Ticehurst C., Guerschman J.P. and Chen Y. (2014). The strengths and limitations in using the daily MODIS open water likelihood algorithm for identifying flood events. *Remote Sensing*, 6(12):11791.

Tolman H.L. (2009). *User Manual and System Documentation of WAVEWATCH III Version 3.14*. Tech. Rep., NOAA/NWS/NCEP/MMAB, 194 pp.

Tomas L.M., Rodrigues M., Fortunato A.B., Azevedo A., Leitão P.C., Oliveira A., Rocha A., Lopes J.F. and Dias J.M. (2014). Salinity modelling accuracy of a coastal lagoon: a comparative river flow analysis of basin model vs. traditional approaches. *Journal of Coastal Research*, SI 70:586–591.

Tsihrintzis V.A., Sylaios G.K., Sidiropoulou M. and Koutrakis E.T. (2007). Hydrodynamic modeling and management alternatives in a Mediterranean, fishery exploited, coastal lagoon. *Aquacultural Engineering*, 36(3):310–324.

Umgiesser G., Ferrarin C., Cucco A., De Pascalis F., Bellafiore D., Ghezzo M. and Bajo M. (2014). Comparative hydrodynamics of 10 Mediterranean lagoons by means of numerical modeling. *Journal of Geophysical Research-Oceans*, 119(4):2212–2226.

Valentim J.M., Vaz N., Silva H., Duarte B., Caçador I. and Dias J.M. (2013). Tagus Estuary and Ria de Aveiro salt marsh dynamics and the impact of sea level rise. *Estuarine Coastal and Shelf Science*, 130:138–151.

Vaz L. (2012). *Hydrodynamic Study of the Wave Effect in the Aveiro Inlet*. MSc Thesis, University of Aveiro, 68 pp.

Vaz N., Dias J.M., Leitão P.C. and Nolasco R. (2007). Application of the Mohid-2D model to a mesotidal temperate coastal lagoon. *Computers & Geosciences*, 33(9):1204–1209.

Vaz N., Dias J.M. and Leitao P.C. (2009). Three-dimensional modelling of a tidal channel: The Espinheiro Channel (Portugal). *Continental Shelf Research*, 29(1):29–41.

Venkatram A. (2008). Computing and displaying model performance statistics. *Atmospheric Environment*, 42(28):6862–6868.

Wahl T., Mudersbach C. and Jensen J. (2015). Statistical assessment of storm surge scenarios within integrated risk analyses. *Coastal Engineering Journal*, 57(01):1540003.

Wallingford H. (2006). *R and D Outputs: Flood Riks to People: Phase 2 FD2321/TR2 Guidance Document*. Tech. Rep., Department for Environment, Food and Rural Affairs, 82 pp.

Wang H.V., Loftis J.D., Liu Z., Forrest D. and Zhang J. (2014). The storm surge and sub-grid inundation modeling in New York City during Hurricane Sandy. *Journal of Marine Science and Engineering*, 2:226–246.

Ward S.L., Green J.A.M. and Pelling H.E. (2012). Tides, sea-level rise and tidal power extraction on the european shelf. *Ocean Dynamics*, 62(8):1153–1167.

Warner J.C., Geyer W.R. and Lerczak J.A. (2005). Numerical modeling of an estuary: A comprehensive skill assessment. *Journal of Geophysical Research-Oceans*, 110(C5).

Wong P.P., Gattuso J.P., Hinkel J., Khattabi A., McInnes K.L., Saito Y. and Sallenger A. (2014). Coastal systems and low-lying areas. In *Climate Change 2014: Impacts, Adaptation, and Vulnerability. PartA: Global and Sectoral Aspects* (Field C.B., Barros V.R., Dokken D.J., Mach K.J., Mastrandrea M.D., Bilir T.E., Chatterjee M., Ebi K.L., Estrada Y.O., Genova R.C., Girma B., Kissel E.S., Levy A.N., MacCracken S., Mastrandrea P.R. and White L.L., eds.). Cambridge University Press, Cambridge, United Kingdom and New York, 361–409.

Woodworth P.L. (2010). A survey of recent changes in the main components of the ocean tide. *Continental Shelf Research*, 30(15):1680–1691.

Xu K., Ma C., Lian J. and Bin L. (2014). Joint probability analysis of extreme precipitation and storm tide in a coastal city under changing environment. *PLoS ONE*, 9(10):e109341.

Xu Z. (2002). *Ellipse Parameters Conversion and Velocity Profiles for Tidal Currents in Matlab*. Tech. Rep., Maurice-Lamontagne Institute, 24 pp.

Yang Z.Q., Wang T.P., Voisin N. and Copping A. (2015). Estuarine response to river flow and sea-level rise under future climate change and human development. *Estuarine Coastal and Shelf Science*, 156:19–30.

Yasuda T., Nakajo S., Kim S., Mase H., Mori N. and Horsburgh K. (2014). Evaluation of future storm surge risk in East Asia based on state-of-the-art climate change projection. *Coastal Engineering*, 83:65–71.

Zhang W., Ruan X.H., Zheng J.H., Zhu Y.L. and Wu H.X. (2010). Long-term change in tidal dynamics and its cause in the Pearl River Delta, China. *Geomorphology*, 120(3-4):209–223.

Zhang Y. and Baptista A.M. (2008). SELFE: A semi-implicit eulerian-lagrangian finite-element model for cross-scale ocean circulation. *Ocean Modelling*, 21(3-4):71–96.

Zhang Y.L., Baptista A.M. and Myers E.P. (2004). A cross-scale model for 3D baroclinic circulation in estuary-plume-shelf systems: I. Formulation and skill assessment. *Continental Shelf Research*, 24(18):2187–2214.

Zheng F., Westra S., Leonard M. and Sisson S.A. (2014). Modeling dependence between extreme rainfall and storm surge to estimate coastal flooding risk. *Water Resources Research*, 50(3):2050–2071.